

Annual Report 1992

Institute of Nuclear and Hadronic Physics

Editors: Dr. F. Dönau
Dr. H. Prade

Redaction: Dr. W. Enghardt
Dr. K. Möller
Dr. J. Mösner
Dr. G. Winter
Dr. R. Wunsch

Preface

This is the first annual report of the Institute of Nuclear and Hadronic Physics (IKH) which was founded within the Research Center Rossendorf Inc. at the beginning of 1992. The report summarizes the research activities, the results and the progress achieved in the first year.

The major goal of the IKH is fundamental research directed to the study of properties of the atomic nucleus and its constituents as well as of the behaviour of the nucleonic system in high energetic nucleus-nucleus collisions. The present scientific profile as described earlier in more detail in the previous annual report (FZR 92-9) is dominantly determined by the participation in several national or international research projects. Therefore, the cooperation with colleagues from outside is of vital importance for the scientific work in our institute.

With this respect we gratefully acknowledge the close and fruitful collaboration with our partners in Germany and abroad as well as the financial support of several groups in the IKH provided by the Ministry for Research and Technology (BMFT), the German Research Community (DFG), the GSI Darmstadt and the KFA Jülich. (The support of these institutions is indicated by using the letters "B", "D", "G", "K", respectively, after the title of the corresponding contributions.)

Fortunately, during the last year the connection between the Institute of Nuclear and Hadronic Physics and the Department of Physics at the Technical University Dresden (TUD) has become deeper, especially by the vocation of Prof. Hartmut Backe (presently at University Mainz) as director of the IKH and professor at the Department of Physics of the TUD, but also by enlarged participation of our scientists in teaching at the Technical University.

Harald Prade

CONTENTS

	PAGE
I. Summary	1
II. Results of Research and Development	9
1. Theoretical Nuclear Physics	11
1.1. Scientific contributions	
Quark production in a chemical off-equilibrium gluon plasma	13
Dilepton radiation from non-equilibrated parton matter produced in ultra-relativistic heavy-ion collisions	14
Low-mass dilepton emission from an expanding superdense pion gas	15
Estimates of dielectron production in pp and pd reactions at 1 - 2 GeV	16
On the nuclear structure function F_2^A : moments $M_n(F_2^A)$ and kinematics beyond $x = 1$	17
Estimates of η and η' production in pp and pd reactions near thresholds	18
Curvature effects in the bubble free energy during the confinement transition	20
Properties of ρ - and ω -mesons in dense and hot nuclear matter near the critical pion mode softening	21
Simulation of velocity correlations between intermediate mass fragments in nuclear disassembly reactions at 150 A MeV bombarding energy	22
Effects of flow on the velocity correlations of fragments in nuclear disassembly reactions	23
Multifragmentation of gold projectiles studies within the BUU approach	24
Non-statistical fluctuations in the velocity distribution of intermediate heavy-ion collisions	25
On size and shape of the average meson fields of the semibosonized Nambu & Jona-Lasinio model	27
COM corrections of the semibosonized Nambu & Jona-Lasinio model for interacting quarks	28

Production of spin $s=3/2$ strangeness $S = -2$ cascade particles Ξ^* in (K^-, K^+) reactions on nuclei	29
Tilted cranking	30
Tilted cranking classification of multiband spectra	31
M1-bands near ^{198}Pb	32
Intruder bands and neutron-proton interaction	33
Rotational population patterns in heavy-ion two particle transfer reactions between even-even thorium nuclei	34
Rotation-induced transition from superfluid to normal phase in mesoscopic systems: ^{168}Yb and adjacent nuclei	35
Chaotic behavior in rotating warm nuclei	36
Classical phase-space structure of the single-particle motion in cranked potentials	37
Loss of spectroscopic information due to strong external coupling	38
Formation of a new order	40
Resonance states in excited systems	42
New semiclassical results for the baker map	44
Correlation dynamics in nuclear matter and Landau's kinetic equation	45
Mixing of pp- and ph-effects in the relaxation of the one-body density	47
The role of collisions and long-range correlations in the damping of collective motion	49
Collisional and collective aspects in the formation of two-body correlations	51
Shapes of Na clusters	53
Molecular dynamics (MD) simulations of GRID experiments	54
1.2. Abstracts of publications	56
2. Experimental Medium Energy Physics	61
2.1. Scientific contributions	
Test of the start detector system for the investigation of the pp-bremsstrahlung with the COSY time-of-flight spectrometer (TOF)	63

Simulation of the proton-proton-bremsstrahlung at the COSY-TOF-spectrometer	65
Calibration of the Rossendorf COSY-TOF-startdetector	67
Program for calculation of relativistic two and three body kinematics and its application for the investigation of the proton-proton-bremsstrahlung	69
Characterization of δ -electrons, generated in the COSY-TOF-spectrometer	71
Production of K^- mesons in proton-induced reactions	73
Simulation of K^+ -production measurements at the 0° facility	75
2.2. Abstracts of publications	77
3. Experimental Nuclear Spectroscopy	79
3.1. Scientific contributions	
A three-quasiparticle band in ^{81}Rb	81
DCO analysis of γ transitions in ^{83}Br and ^{85}Rb	82
Medium-spin states of negative parity in ^{85}Rb	83
Shell model study of ^{85}Kr	84
The odd-mass valence mirror nuclei $^{113}_{50}\text{Sn}_{63}$ and $^{145}_{63}\text{Eu}_{82}$	86
Yrast spectroscopy in the $N=82$ nucleus ^{142}Nd	87
3.2. Abstracts of publications	89
4. Experimental Heavy Ion Physics	91
4.1. Scientific contributions	
Status of the 4π -fragment spectrometer FOBOS	93
Nuclear reactions at the coulomb barrier induced by ^{84}Kr (4.3 AMeV) on ^{116}Sn and ^{118}Sn	95
Model independent balance analysis of fission fragments produced by $^{40}\text{Ar} + ^{194}\text{Pt}$ at energies of 5.5 AMeV and 10 AMeV	97
Extension of the ARGUS phoswich array by a FOBOS gas-detector module and test of the FOBOS data-acquisition system	99
Yields for IMF-production of the reaction $^{32}\text{S}(960 \text{ MeV}) + ^{197}\text{Au}$	100

Velocity correlations of intermediate mass fragments produced in central collisions of Au + Au at E = 150 A MeV	101
Simulations of velocity correlations using the statistical multifragmentation model	103
Entropy and isotopic ratios in light nuclear systems- a comparison between QSM and CRACKER	105
Statistical properties obtained from isotopic yield ratios	107
Simulation with GEANT	109
4.2. Abstracts of publications	110
5. Technical and Methodic Developments	113
5.1. Experimental technique	
A winding machine for the manufacturing of multi wire detectors	115
Process control of the wire winding machine	116
Some aspects of the vacuum system for the start detector device in the COSY-TOF-spectrometer	118
A laser based test system for the COSY-TOF-spectrometer	120
Status of the evacuation and gas supply system of FOBOS	122
The scintillator shell of the FOBOS 4π array	124
Particle identification in solid-state detectors by exploiting pulse-shape information	125
A start and anti halo detector for operation in magnetic field environment	127
Progress report on the drift chamber HELTRON The endflanges and the combs	129
Improvement of the tracking detector for the ALADIN facility	131
5.2. Data acquisition and electronics	
The status of the data acquisition system at the 0° facility	132
Test of photomultipliers for the 0° facility at COSY	134
Development of data acquisition electronics for FOBOS	136
Complete test of the BRAGG digital processor BDP 5385	137

5.3.	Positron emission tomography	
	Results of in-beam PET imaging experiments at the fragment separator of the GSI Darmstadt	138
	On the spatial distribution of positron-emitting nuclei generated by relativistic light ion beams in organic matter	140
	A flexible double head BGO positron camera	142
	Two different BGO detector modules for use in light ion tumour therapy	144
	A simple and fast reconstruction algorithm suitable for on-line range measurements by means of PET in light ion tumour therapy	146
5.4.	Abstracts of publications	148
III.	Publications and Talks	149
1.	Publications and Conference Contributions	151
2.	Lectures and Seminars	161
3.	Talks of visitors	171
IV.	Personnel	177

I. Summary

SUMMARY

of the research activities

Theory

Theory of nuclear and subnuclear degrees of freedom

The analysis of recent and future heavy-ion reactions demands an extensive elaboration of methods for describing non-equilibrium processes. This has been done by applying transport models to evaluate the correlation of intermediate mass fragments measured at GSI. The data were analysed in cooperation with experimental groups in order to extract information on the space-time structure of the hot source undergoing the multifragmentation process. The parton equilibration was studied to predict the rate of dilepton production from CERN energies up to RHIC and LHC energies. The investigation of the behaviour of mesons in hot and dense nuclear matter was started aiming to calculate the dielectron yield in elementary hadronic reactions.

A variational method for determining the average meson fields of the Nambu & Jona-Lasinio model was introduced which allows for removal of the center-of-mass motion and projection of the correct spin and isospin. The study of hypernuclei was extended to nuclei with excited cascade particles.

High-spin phenomena

In preparing new theoretical tools for the investigation of nuclear phenomena at high spin by means of the EUROBALL detector system a computer code realizing the "Tilded Cranking Theory" for realistic cases has been developed and it is ready for common application. Experimental spectra and transition rates were successfully analyzed by means of such a model. In cooperation with the LBL Berkeley the disappearance of the pairing correlation induced by the nuclear rotation and its consequences to excitation spectra and two-nucleon transfer-reactions were studied.

Adapting methods from nuclear structure theory the shapes of Na metal clusters in the mass range $A = 10 \dots 300$ were calculated in cooperation with the JINR Dubna.

Dynamics of open quantum systems

The selforganization of an open quantum mechanical system was studied on the basis of a realistic nuclear model. As a critical measure the information entropy was calculated as a function of the coupling to the environment. The spectroscopic redistribution taking place in the atomic nucleus at the transition from low to high level density was investigated by means of a simple S-matrix model. A hierarchical trapping effect and instability points similar to bifurcation points were observed. In cooperation with the Weizmann Institute semiclassical studies of periodically driven open quantum systems were performed.

Dynamics of nuclear fluctuations

A non-perturbative and consistent treatment of short- and long-range correlations was achieved for large-amplitude density fluctuations and the damping of giant resonances which includes ground state correlation and memory effects. The application to nuclear matter has clarified the relation to Landau's kinetic equations for Fermi-liquids.

Experimental Medium Energy Physics

COSY-TOF-Group

The Rossendorf COSY-TOF-Group participates in designing and constructing the Time-of-Flight Spectrometer TOF, which after completion shall be one of the basic experimental facilities at the external beam of the COSY cooler ring. In 1992 the main effort of the group was directed to the final setup and various test runs of the TOF-Start-Detector System needed for the $pp\gamma$ experiment (COSY proposal #9) which will be the first one scheduled after commissioning of the COSY machine in April 93. The activities in 1992 included:

- completion of the start detector vessel, design and construction of the start detector part of the TOF laser test system
- test of start detector modules with 3.5 GeV/c pions at CERN
- mounting and adjusting of the hollow light guides in the start detector vessel
- test of the performance of the detector and of its data acquisition system by irradiation with a β source.

Most of this work were done in the newly built detector laboratory of our institute. The methodical developments were continuously assisted and optimised by simulation calculations using an appropriate adaption of the CERN GEANT code. These computer simulations included the investigation of the performance of the start detector as well as the TOF spectrometer as a whole.

0° Facility group

For experiments in which the internal beam of COSY at Jülich will be used the so-called 0° Facility is under construction. Ejectiles from hadronic or nuclear reactions can be separated from the circulating COSY beam by means of three dipole magnets and their angular and momentum distribution will be analysed. Within the international user collaboration gathered for this facility at COSY the FZR project group participates in the preparation of the physical program, takes responsibility for the implementation of the data acquisition system and builds up specific detector components:

This group participated in the elaboration of two proposals accepted by the PAC at COSY. In the planning of the experiment "Subthreshold Production of K^- Mesons" the FZR is responsible for a "Letter of Intend". Calculations were carried out in order to predict the cross sections and to optimize the detector arrangement.

The data acquisition system of the 0° Facility is expected to provide the future standard structure for the data acquisition of all planned COSY experiments. The current activities in this direction include:

- implementation of the basic configuration.
- developments of software for common application and global data structures, development and testing of Fastbus modules, developments of the logging and reporting system.

Further, for the practical installation of the scintillation detector a large number of photomultipliers were tested and the voltage divider unit was optimized. In close cooperation of the detector laboratories in the FZR and the GSI the construction of a wire chamber was started in December 1992 which will be preceding prototype of larger chambers needed later on.

Experimental Nuclear Structure Physics

The spectroscopy group participates in the international EUROBALL cooperation which is realizing the various phases (I-III) of this gamma-ray spectrometer of unprecedented quality. Phase III will incorporate second generation composite detectors like the CLUSTER detectors which are expected to fill one the backward quadrant of the 4π EUROBALL array. Each CLUSTER consists of seven encapsulated Ge detectors in a common cryostat. They are surrounded by a common BGO escape-suppression shield formed by 18 BGO scintillators. The German groups of the EUROBALL collaboration will provide 6 of the 15 CLUSTER detectors for EUROBALL III. Two of them will be completed under the responsibility of the FZR group. Accordingly, the preparation for the installation of the CLUSTER detectors was the central subject of the methodical work done within this group which included the setup of the data acquisition system as well as the construction of mechanical mounting. In parallel, a number of experiments were performed within the OSIRIS collaboration concerning investigations of high-spin states in nuclides of the mass-80 region and in light tin isotopes. These studies aimed to learn about the following issues

- Break-up of the $N=50$ and $Z=50$, correspondingly, "inert" configurations in semi-magic nuclei.
- Search for oblate deformation
- The role of proton-neutron interaction
- New high-spin isomers and their decay properties

Heavy Ion Physics

HI reactions in the energy range 10 to 100 MeV/u

The completion of the 4π fragment spectrometer FOBOS at the U400M in the JINR Dubna has been continued. In 1992 the main progress achieved in building up the FOBOS spectrometer is the following:

- Mechanical completion of nearly all of the 30 double-grid avalanche counters (DGAC) all 30 Bragg ionisation chambers. Several DGAC's went into operation.
- Mounting and test of the complex evacuation and gas supply including of the corresponding automatic handling.
- Completion of the data acquisition system. The test at VICKSI (HMI) demonstrated the capability of accumulating up to 1.200 multi-parameter events/sec.
- Installation and test of a data analysis software package.
- Combination of the FOBOS gas detector module with the ARGUS spectrometer (HMI) for the experiment ^{32}S (960 MeV)+Au at VICKSI.

Several experiments were performed with the FOBOS detector test stand "mini-FOBOS" at the U400 accelerator in Dubna to measure the identification properties and dynamic ranges of the FOBOS modules, to analyse fission fragments after complete and incomplete fusion and to obtain cross-sections for subbarrier fusion and fission.

HI reactions in the energy range 0.1 to 1 GeV/u

The activities of the group were determined by the cooperation with the FOPI and the ALADIN collaboration at the GSI Darmstadt. The principal goal of the FOPI collaboration is the investigation of central and semi-central collisions of very heavy systems (Au+Au). The spectrometer ALADIN serves mainly for studies of intermediate mass fragment (IMF) formation in collisions of very heavy projectiles on light target nuclei. Both detector systems have been used in combination with other detection facilities (LAND, TAPS). The work in 1992 can be summarized as follows:

- Contributions for realising the phase II of the FOPI spectrometer.
- Contributions for improving the ALADIN spectrometer.
- participation on measurements at the SIS accelerator.
- evaluation of previously measured Au+Au reaction data.

Some results are listed below:

The two endflanges and the combs for the read-out wires of the large drift chamber HELITRON have been produced and delivered to GSI. A new start- and antihalo detector system for FOPI which has been produced, tested and installed in cooperation with KP I of the GSI. This setup operated successfully during the Au+Au experiments at 1 AGeV and 0.4 AGeV in Dec. 92.

The evaluation of the previous Au+Au data at 0.1, 0.15 and 0.25 AGeV has been continued aiming to establish velocity correlations between IMF's. The new quality of event characterization allowed us to perform a more rigorous comparison with model calculations.

The TP-MUSIC III chamber at ALADIN was supplemented by us with 18 multiwire proportional counters. In this combination the charge detection threshold could be reduced up to minimum charge of $Z=3$.

Experimental Technique

Detector laboratory

The detector laboratory the built up of which finished in autumn 1992 provides all experimental groups in the IKH an appropriate technical basis. This laboratory having an area of altogether 320 m² is especially equipped for the preparation of large gasfilled multi-wire chambers. For that purpose a new wire winding machine was built in Rossendorf, which allows us to manufacture wire electrodes up to a maximum size of 2×3 m².

During 1992 the following tasks were realized in the detector lab:

- preparation of the two endflanges of the HELITRON detector
- Assembling and test of the TOF-Start-detector system for COSY
- Building up of a set-up for testing avalanche counters of the FOBOS spectrometer
- Development of a position sensitive BGO detector for in-beam PET experiments
- Construction and test of a 4-axis robot system to simulate a cylindrical PET camera appropriate for in-beam experiments

The latter tasks concerns the activities of the PET group within the detector lab. In-beam PET experiments at the GSI Darmstadt using the Rossendorf HIDAC positron camera as

well as BGO detectors have demonstrated that tomograms of implanted distributions of positron emitting ions can be obtained and that the PET imaging of β^+ -active secondary nuclear fragments may provide a tool for on-line therapy control.

Computer network

Concerning the computational facilities further improvements were achieved during 1992 by extending the capacity of the common network of the IKH and the Institute of Ion Beam Physics Material Research which includes now 30 VAX and DEC stations.

II. Results of Research and Development

1. Theoretical Nuclear Physics

Quark production in a chemical off-equilibrium gluon plasma ^B

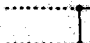
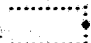
B. KÄMPFER^{a,b}, O.P. PAVLENKO^{a,c}

^a*Forschungszentrum Rossendorf e.V., Institut für Kern- und Hadronenphysik*

^b*Institut für Theoretische Physik (KAI e.V.), TU Dresden*

^c*Institute for Theoretical Physics, Kiev*

Perturbative cross sections for gluon-gluon scattering are larger than the ones for quark-quark or quark-gluon interactions. This fact might imply that in ultrarelativistic heavy-ion collisions a gluon plasma is created with a few quarks admixed [1]. Present parton cascade models [2] support such a picture. Since some of the proposed primordial quark-gluon plasma probes, such as direct photons and dileptons, measure mainly the quark distribution it seems to be necessary to refine the standard estimates for the local equilibrium quark-gluon plasma [3,4] by more detailed calculations of the quark species evolution.

We rely on a transport model of coupled Boltzmann type equations for quarks and gluons, and assume thermal equilibrium of both species. Quark pairs are created in binary collisions by lowest-order α_s processes like  and , while the inverse reactions create gluons (gluon/quark propagators - dotted/full lines). The corresponding t-channel reactions do not change the particle numbers, but maintain the thermal equilibrium. With standard cross sections [5] we derive the rate equations for the parton number $n(\tau)$ and gluon weight $x(\tau)$ (τ is the proper time)

$$\partial_\tau n = -\alpha n/\tau, \quad \partial_\tau x = nR(\tau)(\beta(1-x)^2 - x^2) \quad (1)$$



$$R(\tau) = \frac{\pi\alpha_s^2}{24m^2} \left(\frac{m}{T(\tau)}\right)^5 I(m, T), \quad I(m, T) = \int_2^\infty dz W(z)\sigma(z)K_1\left(\frac{mz}{T(\tau)}\right),$$

$W(z) = (1 - 4z^{-2})^{1/2}$, $\sigma(z) = (1 + 4z^{-2} + z^{-4})\text{arth}W - (7 + 31z^{-2})W/8$, $\beta = 4/9$, $\alpha = 1$ for the Bjorken scenario. Their solution is

$$n(\tau) = n_0 \left(\frac{\tau_0}{\tau}\right)^\alpha, \quad x(\tau) = \frac{(\beta + \sqrt{\beta})A_+ - \varphi(\tau)(\beta - \sqrt{\beta})A_-}{(\beta - 1)(A_+ - \varphi(\tau)A_-)}, \quad (2)$$

$$A_\pm = (\beta - 1)x_0 - \beta \pm \sqrt{\beta}, \quad \varphi(\tau) = \exp\left\{\tau_Q \left(\left(\frac{\tau}{\tau_0}\right)^{1-\alpha/3} - 1\right)\right\}$$

With the unique screening mass $m = \sqrt{\frac{2\pi\alpha_s}{3}}T$ at given temperature T one gets characteristic values of τ_Q which indicate a rather long time for quark cooking. After $\tau/\tau_0 \approx 3\tau_Q^{-1}$ the quarks would be approximately in chemical equilibrium.

We estimate the photon production via quark - anti-quark fusion  and Compton-like processes  and find minor changes in the rate for hard photons as long as the initial weight of quarks in the plasma is $x_0 = x(\tau_0) \leq 0.85$, otherwise the primordial production in lowest order is suppressed. Analog statements also apply for the dilepton rate. Cross features of charm production are moderately affected by the time dependence of the parton species. This is since $gg \rightarrow c\bar{c}$ and $q\bar{q} \rightarrow c\bar{c}$ processes are nearly equal in thermalized parton matter (in contrast to strangeness production).

REFERENCES:

- [1] E.V. Shuryak, Phys. Rev. Lett. 68 (1991) 3270
- L. van Hove, S. Pokorski, Nucl. Phys. B86 (1975) 243
- [2] K. Geiger, Phys. Rev. D46 (1992) 4965
- [3] J. Kapusta et al., Phys. Rev. D44 (1991) 2774
- [4] B. Kämpfer, O.P. Pavlenko, Phys. Lett. B289 (1992) 127
- [5] H.M. Georgi et al., Ann. Phys. 114 (1978) 273

Dilepton radiation from non-equilibrated parton matter produced in ultra-relativistic heavy-ion collisions ^B

B. KÄMPFER^{a,b}, O.P. PAVLENKO^{a,c}

^a*Forschungszentrum Rossendorf e.V., Institut für Kern- und Hadronenphysik*

^b*Institut für Theoretische Physik (KAI e.V.), TU Dresden*

^c*Institute for Theoretical Physics, Kiev*

Dilepton yields from a thermally and chemically equilibrated quark-gluon plasma have been considered by many authors. It turns out that the yield depends strongly on the initial temperature and formation time of the plasma (cf. also [1]). Therefore one should expect that the pre-equilibrium state, where parton are yet off equilibrium, is also a intense source of lepton pairs. Indeed, among the very first hard parton collisions there are also such ones which produce dileptons in the Drell-Yan (DY) process. The DY yield is estimated to mask completely the thermally produced pairs in present relativistic heavy ion collisions at CERN-SPS. At very high bombarding energies, as envisaged in the RHIC and LHC projects, however, there are expectations to observe dileptons from dense parton matter. At these energies the parton evolution is predicted to be described mainly by perturbative QCD.

To follow the thermal equilibration process of the parton matter towards quark-gluon plasma we use a linearized Boltzmann type transport model for the parton distribution function $f(\vec{p}_\perp, y, \tau)$

$$p^i \partial_i f = -\tau_{rel}^{-1} u^i p_i (f - f_{eq}), \quad (1)$$

$$f_{eq} = [\exp\{(u^i p_i)/T\} + s]^{-1}, \quad \int d^3 p p^0 f = \int d^3 p p^0 f_{eq}. \quad (2)$$

with the solution for predominant longitudinal evolution

$$f(p_\perp, \xi, \tau) = e^{-\phi(\tau)} [f_0(p_\perp, \xi_0) + \int_{\tau_0}^{\tau} \frac{d\tau'}{\tau_{rel}(\tau')} f_{eq}(p_\perp, \xi', \tau') e^{\phi(\tau')}], \quad (3)$$

where $f_0 = f(\tau_0)$ is the initial distribution at proper time τ , and $\phi(\tau) = \int_{\tau_0}^{\tau} d\tau'' \tau_{rel}^{-1}(\tau'')$ indicates that the relaxation time is implicitly time dependent. (The characteristics are $\tau \text{ sh } \xi = \tau_0 \text{ sh } \xi_0 = \tau' \text{ sh } \xi'$. Due to the scaling symmetry the velocity u^i is fixed. The parameter T in f_{eq} is determined by the condition of fit (2).)

Relying on chemical equilibrium we calculate the dilepton yield per space-time and momentum volume element

$$\frac{dN}{d^4 x d^4 Q} = \int \frac{d^3 p_1}{(2\pi)^3} \frac{d^3 p_2}{(2\pi)^3} f(x, p_1) f(x, p_2) v \sigma(M^2) \delta^4(Q - p_1 - p_2) \quad (4)$$

for the quark - anti-quark fusion (v - relative velocity of fusing partons, σ - fusion cross section with a lepton pair in exit channel).

As initial distribution we use [2] $f_0(p_\perp, \xi) = \mathcal{N}_0 \delta(\xi) \exp\{-p_\perp^2/K\}$, and $s = 0$. With these ingredients we find that even for very fast equilibration the dileptons carry much memory from the initial stage of the parton matter. In line with recent results [3] the calculated dilepton yield from off-equilibrium partons exceeds the DY contribution at RHIC energies. Therefore, unless strong non-perturbative QCD processes are operative, the dileptons seem to probe mainly the pre-equilibrium dense parton matter.

REFERENCES:

- [1] B. Kämpfer, O.P. Pavlenko, Phys. Lett. B255 (1991) 503
- [2] B. Kämpfer, O.P. Pavlenko, Phys. Lett. B289 (1992) 127
- [3] K. Geiger, J.I. Kapusta, preprint Minnesota (October 1992)

Low-mass dilepton emission from an expanding superdense pion gas^B

B. KÄMPFER^{a,b}, P. KOCH^c, AND O.P. PAVLENKO^{a,d}

^a*Forschungszentrum Rossendorf e.V., Institut für Kern- und Hadronenphysik*

^b*Institut für Theoretische Physik (KAI e.V.), TU Dresden*

^c*Institut für Theoretische Physik, Universität Regensburg*

^d*Institute for Theoretical Physics, Kiev*

We study the space-time evolution of dense, non-equilibrium pion matter, formed in the midrapidity region in relativistic heavy-ion collisions, in the frame work of a Boltzmann type transport model which includes effects from Bose statistics. The collision term is handled with in relaxation time approximation with density-dependent relaxation time. The pion number is conserved, since inelastic collisions are ineffective at given energy density. Starting from an initially supersaturated pion gas with a large positive effective chemical potential we find that this pion chemical potential stays approximately constant during the evolution, i.e., due the rapid expansion the partial equilibrium is maintained.

As a consequence such a scenario leads to an increased dilepton yield between the kinematical threshold for muon pair production via pion annihilation and the ρ, ω bump [1]. Depending on the lifetime of the dense hadron matter system formed in relativistic heavy ion collisions this component can be observed above the background of muon pairs from resonance decays (dashed line in Fig. 1; full line -sum of all contributions). Preliminary experimental data [2] seem indeed to indicate an enhanced yield when comparing proton-nucleus and nucleus-nucleus collisions (cf. Fig. 2).

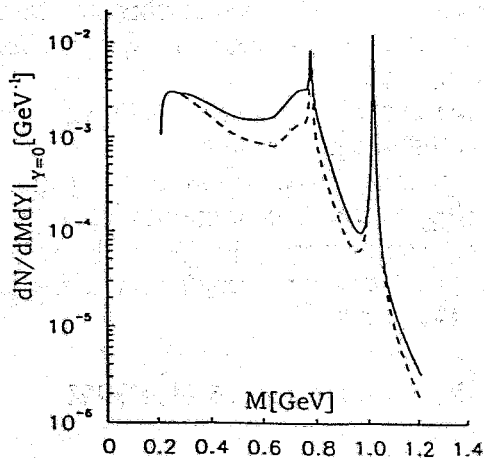


Fig. 1: The di-muon yield as function of the invariant mass for initial temperature 200 MeV and freeze-out temperature 160 MeV. The chemical potential, which parametrizes the chemical and thermal off-equilibrium, is 120 MeV throughout the evolution. These values fit also the hadron spectra.

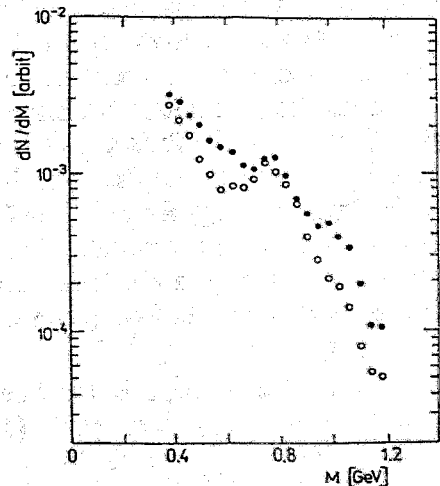


Fig. 2: The preliminary experimental results from Ref. [2]. The data are normalized in the ϕ region on a factor 3. heavy dots - S + W, circles - p + W at 200 AGeV.

REFERENCES:

- [1] B. Kämpfer, P. Koch, O.P. Pavlenko, Proc Int. Workshop Nuclei & Nuclear Excitations, Hirschegg 1993, (Ed.) H. Feldmeier; FZR-93-0x, submitted to Phys. Rev. C
- [2] U. Gerlach, Proc. Quark Matter 1991, Nucl. Phys. A544 (1992) 109c

Estimates of dielectron production in pp and pd reactions at 1 - 2 GeV^B

B. KÄMPFER^{a,b}, A.I. TITOV^c, E.L. BRATKOVSKAYA^c

^aForschungszentrum Rossendorf e.V., Institut für Kern- und Hadronenphysik

^bInstitut für Theoretische Physik (KAI e.V), TU Dresden

^cJINR Dubna, Lab. Theoretical Physics

Dielectrons represent one of the promising signals which probe directly dense and hot nuclear matter produced in heavy-ion collisions at intermediate energies. Since the electron pairs are created in various elementary reactions, one needs a reliable description of these elementary reaction channels to unfold dielectron spectra and to get the wanted signal of highly excited nuclear matter.

We have improved our previous estimates of dielectron production cross sections in elementary nucleon-nucleon subprocesses and applied them in pp and pd reactions at 1 and 2 GeV [1]. In contrast to other calculations we here rely on the vector dominance model as guiding principle for the hadron-photon interaction. Reaction channels and propositions considered are: (i) Bremsstrahlung: It is calculated within an approach which resembles the soft-photon approximation, however, uses exact kinematics. The essential point is a off-shell suppression taken from a relativistic oscillator quark model. In the pd reaction both the pp and pn bremsstrahlung contribute, i.e. the usual destructive interference in pp reactions is not operative here.

(ii) Δ Dalitz decays: In addition to the standard approach we include the M_{Δ} dependence in the cross section $\sigma_{NN \rightarrow N\Delta}$, as follows directly from a one-boson exchange model. In this subprocess we also include the vector dominance formfactor in the $\Delta N \gamma$ vertex.

(iii) η Dalitz decays: We use the usual eta decay rate with eta production cross section as calculated in the one-boson exchange model [2] and parameters fitted to the few experimental data. (Note that with respect to the recent SATURNE measurements on η production [3] a puzzling situation arises for the unexpected large pn cross section).

(iv) Fermi motion: To mimic the momentum distribution of nucleons in the deuteron we use the wave function of the Paris potential with additional short-range correlations.

Numerical results are displayed in Fig. 1 and discussed in Ref. [1]. Note that the present approach gives an energy dependence of the ratio of σ_{pd}/σ_{pp} as seen in experiments [4].

With respect to the uncertainties in several subprocesses we now apply our approach to real-photon bremsstrahlung in the same reactions in order to get supplementary informations by comparison with new data from planned experiments at COSY.

REFERENCES:

[1] B. Kämpfer, A.I. Titov, E.L. Bratkovskaya, FZR-92-04, Phys. Lett. B301 (1993) 123

[2] T. Vetter et al., Phys. Lett. B263 (1991) 153

[3] E. Chiavassa et al., poster session at INPC Wiesbaden 1992

[4] G. Roche, PCCF RI 92-08

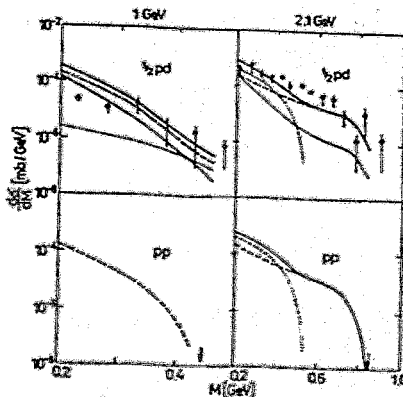


Fig. 1: The cross section of dielectron production in the pp (lower panels) and pd reactions (upper panels) at 1 GeV (left panels) and 2.1 GeV (right panels) proton energy (heavy full line - sum of all contributions, dashed/dotted/thin lines - Δ/η /bremsstrahlung contributions). The experimental data (dots, [4]) are for p ^9Be collisions scaled by $A_{^9\text{Be}}^{-2/3}$. Arrows indicate the kinematical limits in pp reactions.

On the Nuclear Structure Function F_2^A :
Moments $M_n(F_2^A)$ and Kinematics beyond $x = 1$ ^B

L.P. Kaptari^a, A.Yu. Umnikov^a and B. Kämpfer^{b,c}

^aJINR Dubna, Lab. Theoretical Physics

^bForschungszentrum Rossendorf e.V., Institut für Kern- und Hadronenphysik

^cInstitut für Theoretische Physik (KAI e.V.), TU Dresden

An analysis of the behaviour of nuclear structure functions F_2^A at large x , and its moments M_n^A at large n has been performed within two theoretical approaches: (i) the QCD-motivated Q^2 -rescaling model and (ii) the operator product expansion method within an effective meson-nucleon theory which is prompted by nuclear physics. While in the typical "EMC region" $x = 0.1 - 0.7$ various models can explain the data (see Fig. 1), near $x \sim 1$ significant deviations arise. Our theoretical estimates of nuclear structure function at $x \geq 1$ are in a good agreement with existing data (see Fig. 2, [1]). The moments, derived from experimental data, are found to depend essentially on the behaviour of the respective structure function beyond $x = 1$. A relation between the Q^2 -rescaling parameter ξ_A and nuclear averages, i.e., mean kinetic energy and chemical potential of nucleons, as well as a dependence of ξ_A on n are established.

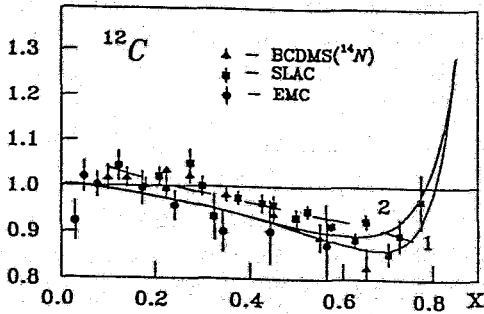


Fig. 1: The ratio of the carbon and isoscalar nucleon structure functions. Solid curves are results of our model (1 - the OPE analysis within the meson-nucleon model; 2 - the old x -rescaling formulae). The dashed line uses the original Q^2 -rescaling model. Experimental data are taken from ref. [2]. For further details consult [1].

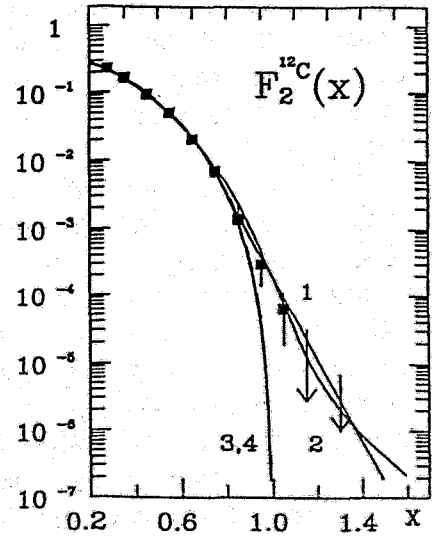


Fig. 2: The absolute value of the carbon structure function. Curves 1,3 - fits of the carbon structure function [1], curve 2 - the present approach with Fermi motion and boundness effects taken into account in the spectral function, curve 4 - our fit of the isoscalar free nucleon. Experimental data are taken from ref. [3].

REFERENCES:

- [1] L.P. Kaptari, A. Yu. Umnikov, B. Kämpfer, FZR-92-07, Phys. Rev. D (1993) in press
- [2] J. Ashman et al., Phys. Lett. B202, 603 (1988);
R.G. Arnold et al., Phys. Rev. Lett. 52, 727 (1984)
- [3] G.I. Smirnov, Proc. X-th Conf. High Energy Physics Problems,
World Scientific, Singapore (1991), p.215

Estimates of η and η' production in pp and pd reactions near thresholds^B

B. KÄMPFER^{a,b}, H. MÜLLER^a, A.I. TITOV^c

^a*Forschungszentrum Rossendorf e.V., Institut für Kern- und Hadronenphysik*

^b*Institut für Theoretische Physik (KAI e.V.), TU Dresden*

^c*Laboratory for Theoretical Physics, JINR Dubna*

Nowadays there are several theoretical models at hand for calculating meson production cross sections in elementary reactions, say pp or pn. Effective baryon-meson field theories [1,2] or Nambu - Jona-Lasinio type models, which are inspired by the quark picture of hadrons, or string models which extended towards the intermediate energy range can be used. Also statistical phase space models have been proven useful in estimating particle production rates over a wide range of energies and particle species [3].

Concerning the η meson there are a few older [4] and recent [5] measurements which can be used to fix model parameters. Precision measurements are planned for near future [6]. These measurements will test the reliability of the mentioned models in the sensible threshold region. Also reactions at complex targets (the simplest obviously being the deuteron) are envisaged [6], where secondary interactions with surrounding nucleons are to be investigated. In particular the η' is considered as interesting meson due to possible exotic quark content. The motivation of such investigations is to get more insight in the quark structure of hadrons and fundamental properties of strong interaction. However, in case of complex targets one meets the problem of the internal motion of the nucleons in the nuclear system. In particular, there is a subthreshold production to be expected, and at threshold a modification of the pd cross section is quite obvious, i.e., $\sigma_{(pd \rightarrow \eta X)} \neq \sigma_{(pp \rightarrow \eta X)} + \sigma_{(pn \rightarrow \eta X)}$.

In Fig. 1 we present results of the elementary η production cross section in pd reactions which rely on an effective Lagrangian which includes N and N₁₅₃₅^{*} baryons (p, n are different) and ρ, ω, η, π mesons as well. The parameters are fixed to get approximately in plane-wave approximation for one-boson exchange the measured pp cross sections [4]. Our results are in virtual agreement with the recent approach [1], however, slightly underestimate near-threshold data [4]. Probably, the parametrization [7] gives an optimal reproduction of the pp data. Our model predicts $\sigma_{pn} \approx 2.5\sigma_{pp}$, which is at variance with the claim of Ref. [5] to have a factor 8. We use the estimated elementary cross sections to calculate the η production in pd reactions basing our considerations on a realistic deuteron wave function ψ_d obtained within the Paris potential model $\sigma^{pd \rightarrow \eta X}(s, p) = \int (\sigma^{pp \rightarrow \eta X}(p, p') + \sigma^{pn \rightarrow \eta X}(p, p')) |\psi_d(\vec{p}')|^2 d\vec{p}'$, where \vec{p}' is the relative momentum in the deuteron. The internal nucleon motion in the deuteron is important near and below the η threshold. We also include short range correlations which describe simultaneous interaction of the proton with a correlated two-nucleon cluster in the deuteron wave function with a 5% probability. Observe the considerable cross section below the pp threshold. The short range correlations are important below 1.1 GeV proton energy. Different elementary cross sections of Refs. [1,2,7] result also in very different predictions far below the threshold. This behavior may be used to discriminate between the different models. Note that above 1.5 GeV nuclear effects are negligible.

Fig. 2 displays the prediction of the statistical phase-space model. The relative probability of populating a definite channel is calculated as the product of the Lorentz-invariant phase-space factor with the square of an empirical matrix element (for details see Ref. [3]). All channels allowed by conservation of internal quantum numbers are taken into account. Comparing the two Figures we find a remarkable agreement of the predictions of the two different models.

In the statistical approach complete events are generated, and we can look for the other reactions products. Near the threshold there is a large probability that the produced η is accompanied by a ${}^3\text{He}$, and at higher energies by a deuteron. These channels are energetically preferred compared to channels containing three nucleons.

Another interesting point is the question to which extent the η is produced via the N_{1535}^* resonance. As shown in Fig. 2 (thin curve) η production via N_{1535}^* seems to be negligible in the threshold region and is also at higher energies of minor importance. This is in contrast with the above one-boson exchange model.

Within the same approach we predict as a guideline for future experiments at planned maximum COSY energy 2.5 GeV the η' production cross section as $3 \mu\text{b}$ in pp and $55 \mu\text{b}$ in pd interactions.

REFERENCES:

- [1] T. Vetter et al., Phys. Lett. B263 (1991) 153
- [2] J.M. Laget et al., Phys. Lett. B257 (1991) 254
- [3] H. Müller and K. Sistemich, Z. Phys. A344 (1992) 197
- [4] CERN-HERA 84-01, Geneva 1984, "Compilations of cross sections III"
- [5] Chiavassa et al., poster at INPC Wiesbaden 1992, and internal reports
- [6] D. Bour et al., COSY Proposal "Study of η and η' production and interaction"
- [7] A. de Paoli et al., Phys. Lett. B219 (1989) 194

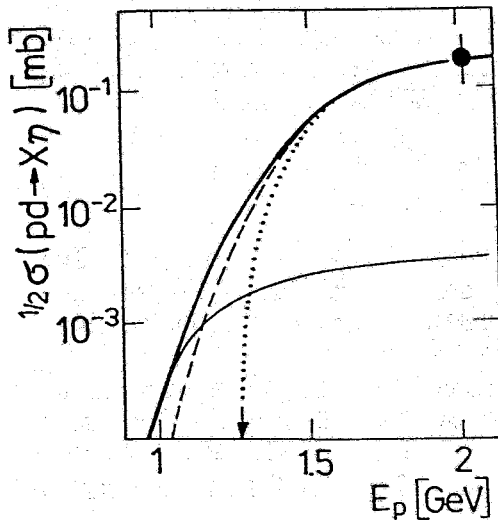


Fig. 1: $\frac{1}{2}\sigma_{pd}$ as function of the proton's kinetic energy according to the effective one-boson exchange model (for details consult text). The data point is for pp reaction [4]. dotted/dashed/thin/heavy lines - $\frac{1}{2}(\sigma_{pp} + \sigma_{pn})$ / corrected with deuteron wave function/ contribution of short-range correlations/ sum of all contributions.

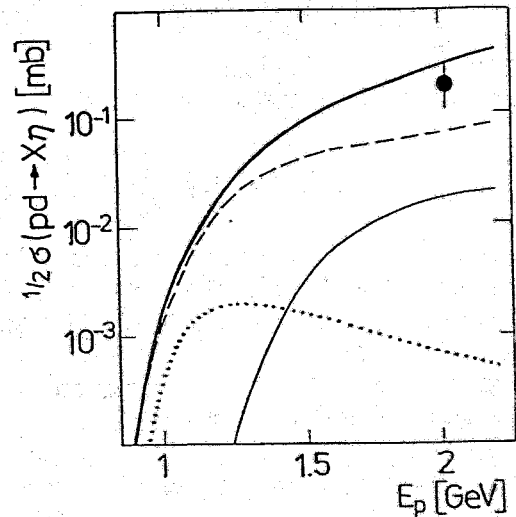


Fig. 2: The same as in Fig. 1 but for the statistical phase-space model. dotted/dashed/thin/heavy lines - associated production of ${}^3\text{He}$ / associated production of d/ η production via N_{1535}^* / sum of all contributions

Curvature effects in the bubble free energy during the confinement transition^B

L.L. JENKOVSKY^a, B. KÄMPFER^{b,c}, V.M. SYSOEV^a

^a*Institute for Theoretical Physics, Kiev*

^b*Forschungszentrum Rossendorf, Institut für Kern- und Hadronenphysik*

^c*Institut für Theoretische Physik (KAI e.V.), TU Dresden*

The recent lattice SU(3) gauge theory studies of the plane interphase between confined and deconfined matter point to rather small values of the surface tension σ_∞ [1]. This observation initiated investigations of the surface tension of finite bubbles [2]. In an expansion of the surface tension in powers of the bubble radius R , $\sigma(R) = \sigma_\infty(1 - 2\delta/R \dots)$ the next-to-leading order term is determined by the curvature δ . Obviously, if δ is sufficiently large then the curvature term dominates the free energy of bubbles or droplets in same range of R . This is supported by calculations of the free energy of finite droplets of quark-gluon plasma and finite bubbles of hadron matter in bulk plasma within a MIT bag model like approach [3].

In the framework of a phenomenological theory of first-order phase transitions, the bubble creation rate I at temperature T is usually written in the form $I = I_0 \exp\{-\Delta F/T\}$, where I_0 is the pre-exponential factor, cf. [4]. The change of the free energy due to the presence of a bubble is $\Delta F = \frac{4\pi}{3}R^3\Delta p + 4\pi R^2\sigma(R)$, with Δp as pressure difference of both phases. For $\sigma(R) = \sigma_\infty(1 - 2\delta/R)$, i.e., the Tolman approximation, the authors of Ref. [3] find that the free energy looks as displayed in Fig. 1. (In addition there might appear also the case of barrier free bubble growth due to $\Delta F < 0$ for all values of R within some region of δ). However it should be noted that the Tolman approximation is only a first-order correction, which holds at $\delta/R \ll 1$. The minimum at R_0 appears at $\delta/R > 1$ when $\delta > 0$.

According to the present state of the art of lattice calculations it is difficult to determine accurately $\sigma(R)$. Therefore one should resort to more general arguments. In a recent study [5] we used for the surface tension the Gibbs-Tolman-Koenig-Buff (GTKB) expression

$$\sigma(R) = \sigma_\infty \exp\left\{ \int_\infty^R dr \frac{(2\delta/r^2)[1 + (\delta/r) + (\delta^2/3r^2)]}{1 + (2\delta/r)[1 + (\delta/r) + (\delta^2/3r^2)]} \right\}. \quad (1)$$

In the approximation $\delta = \text{const}$ one recovers the usual behaviour as displayed in Fig. 2. The barrier $\Delta F(R_c)$ and the critical bubble radius R_c however are modified due to the curvature term δ . Therefore the estimates in Ref. [4] for the time evolution of the confinement transition need some refinement.

We have studied different approximations to eq. (1) and find that the prediction [3] of the unusual foam of micro-bubbles with radii R_0 depends sensitively on the surface tension at small R and might turn out as artifact of several approximations.

The possible supercooling of deconfined plasma and superheating of confined matter within the validity of eq. (1) now becomes asymmetric [5].

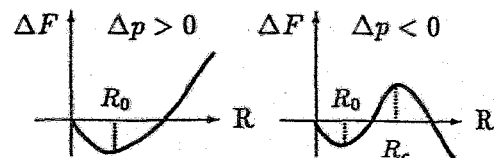


Fig. 1: Sketch of the free energy as function of the bubble radius for the Tolman approximation of the bubble surface tension.

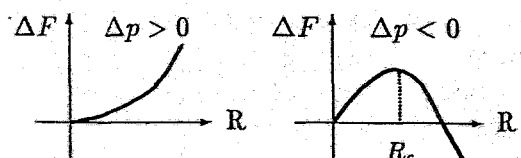


Fig. 2: As in Fig. 1 but for the surface tension according to the GTKB formula.

REFERENCES:

- [1] K. Kajantie et al. Nucl. Phys. B333 (1990) 100
- [2] K. Kajantie et al. Phys. Lett. B286 (1992) 125
- [3] I. Mardor, B. Svetitsky, Phys. Rev. D44 (1991) 878
- [4] J. Kapusta, L.P. Csernai, Phys. Rev. Lett., Phys. Rev. D in press
- [5] L.L. Jenkovsky, B. Kämpfer, V.M. Sysyov, ITP-92-51E

Properties of ρ - and ω -mesons in dense and hot nuclear matter near the critical pion mode softening^B

G.G. BUNATIAN^a, B. KÄMPFER^{b,c}

^aJINR Dubna, Lab. Neutron Physics

^bForschungszentrum Rossendorf e.V., Inst. für Kern- und Hadronenphysik

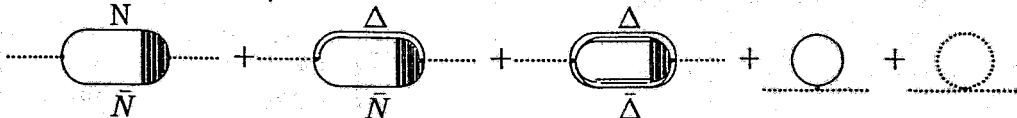
^cInstitut für Theoretische Physik (KAI e.V.), TU Dresden

Chiral symmetry arguments and QCD sum rules predict a universal mass shift of hadrons in dense and hot nuclear matter. In contrast, detailed many-body hadron interaction models show a more subtle and non-uniform behaviour of the hadron self-energies. Due to the di-electron decay modes of vector mesons there is the possibility to measure directly the changes of ρ, ω -mesons in the course of heavy-ion collisions. The HADES project at SIS in GSI represents a dedicated experiment to accomplish this goal.

In a recent paper [1] the propagators of ρ - and ω -mesons in nuclear matter have been analyzed. Due to the strong coupling to pions in $\rho\pi\pi$, $\omega\pi\pi$, $\rho\rho\pi$ etc. vertices, the ρ, ω -meson properties depend sensitively on the behaviour of the pionic mode. Relying on previous investigations of the pion propagator in nuclear matter, we elucidate the main features of the ρ - and ω -meson behaviour in dense and hot nuclear matter in the asymptotic case near the critical pion mode softening. We find that under such conditions the ρ -meson mode becomes stiffer, while the ω -meson mode softens. The widths of both the ρ, ω -mesons increase significantly and become essentially greater than the ones of free mesons.

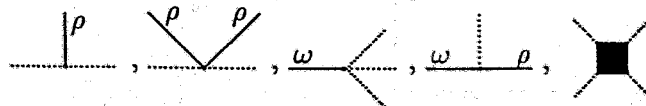
Relying on the hypothesis that these properties extrapolate down to slightly compressed and excited nuclear matter one should expect a larger (smaller) ρ (ω)-mass and a vanishing of the ρ, ω -peaks due to increasing widths.

Our pion polarization operator, which enters the pion propagator $\mathcal{D}(\xi, \vec{k}, n, T) = (\xi^2 - \vec{k}^2 - 1 - \Pi(\xi, \vec{k}, n, T))^{-1}$, is represented by $\Pi(\omega, \vec{k}, n, T) =$

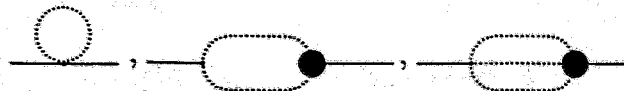


(solid/double/dotted lines: nucleon/ Δ /pion propagators. The dot denotes the irreducible πNN , $\pi\Delta N$ and $\pi\pi NN$ interactions. The hatched area is the full vertex in nuclear matter.)

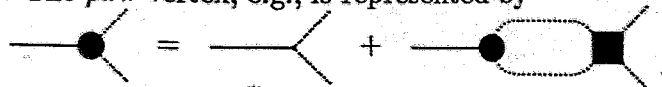
The propagator incorporates the pion mode softening at large nucleon densities and temperatures. In this limiting case it can be parametrized conveniently. Then one can easily select the dominant contributions in the ρ, ω -propagators. We include the interactions



and self-energies



where the heavy dot denotes the full reducible $\pi\pi\rho$ or $\pi\pi\pi\omega$ interaction (heavy lines: vector meson propagators). The $\rho\pi\pi$ vertex, e.g., is represented by



In the present limit, processes like $\omega \rightarrow \rho \omega$ can be neglected. The very details can be found in Ref. [1].

REFERENCES:

[1] G.G. Bunatian, B. Kämpfer, FZR-92-08, submitted to Nucl. Phys. A

Simulation of Velocity Correlations between Intermediate Mass Fragments in Nuclear Disassembly Reactions at 150 A-MeV Bombarding Energy^B

B. HEIDE AND H.W. BARZ

Forschungszentrum Rossendorf, Institut für Kern- und Hadronenphysik

In heavy ion collisions at 150 A-MeV bombarding energy the measured two-particle velocity distribution function reveals a bump-like structure. In order to extract informations from this function we worked out a statistical model based on both the percolation model and the classical equations of motion, which is easy to handle with.

With respect to our model, in the nuclear fragmentation scenario the formation of an equilibrated source should take place, followed by a phase transition which causes multifragmentation. The resulting mass spectrum is described in the framework of the percolation model (cf. [1]). Finally, we assume that, after the break-up, only the Coulomb interaction is important and we solve the Newton equations for this force. Three parameters determine our model: radial flow, break-up density and temperature. The two-particle correlation function is defined as $R(v) = \Sigma Y(v) / \Sigma Y_{mix}(v)$, where v is the scaled relative velocity (see ref. [2]), $Y(v)$ is the coincidence yield of two fragments, $Y_{mix}(v)$ denotes the so-called mixed yield by taking one of the two fragments from another event and the sum is performed over all intermediate-mass fragment combinations fulfilling certain selection criteria.

In Fig.1 we represent our theoretical results for the case where one fragment has the charge number 3 and the other one has a charge number between 4 and 7. Further, we utilized a break-up density of $0.14n_0$ (n_0 is the ground state density), a radial flow of 0.5 MeV and a temperature of 2 MeV, which might be too low but gives a good agreement with the experimental data [3] shown in Fig.2.

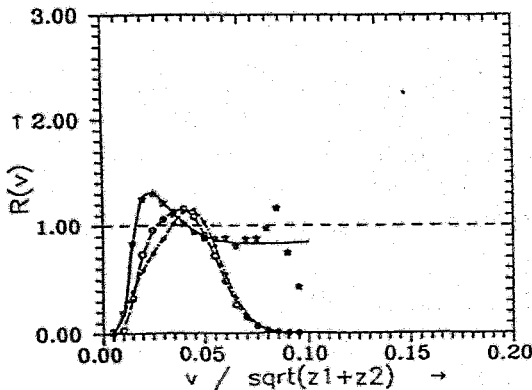


Fig.1 Correlation function R (solid line) for collisions of Au on Au at 150 A-MeV as a function of the scaled relative velocity v . The dashed line shows the true velocity distribution whereas the dash-dotted line refers to the mixed velocity distribution.

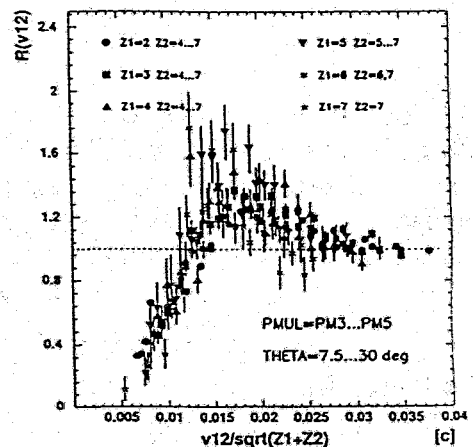


Fig.2 Experimental data of the correlation function for several charge combinations taken from ref. [3].

REFERENCES:

- [1] X. Campi, J. Phys. AL 19 (1986) 917
- [2] Y.D. Kim et al., Phys. Rev. C 45 (1992) 387
- [3] B. Kämpfer et al., "Proceedings of the International Workshop on Gross Properties of Nuclei and Nuclear Excitations XX", Hirschegg, Austria, 1992, p. 67, ISSN 0720-8715

Effects of Flow on the Velocity Correlations of Fragments in Nuclear Disassembly Reactions^B

H.W. BARZ^{1,2}, B. HEIDE², H. SCHULZ³ AND K. SNEPPEN³

¹ KAI Berlin, e.V. im Institut für Kern- und Hadronenphysik, Forschungszentrum Rossendorf e.V.

² Institut für Kern- und Hadronenphysik, Forschungszentrum Rossendorf e.V., O-8051 Dresden

³ The Niels Bohr Institut, Blegdamsvej 17, 2100 Copenhagen, Denmark

Fragment-fragment correlation has recently been studied in collisions of $Au + Au$ between $150 A \cdot MeV$ and $600 A \cdot MeV$ [1,2]. In these reactions a copious production of about 10 IMFs takes place. The correlation function shows a bump-like structure for relative velocities of $v_{rel} = .06c$ which points to interesting dynamical effects at the break-up stage of the fragmenting system.

To demonstrate that this behaviour of the correlation is associated with an overall transverse motion of the fragmenting system we combine the statistical multifragmentation model and the Boltzmann-Uhling-Uhlenbeck (BUU) approach. The correlation function is defined by the average ratio $C_2 = F_{12}/F_{12mix}$ of the two particle distributions F_{12} in a single event and of two different (mixed) events. By means of the BUU calculation we determine the size, the excitation energy and the collective velocity of the source. During its fragmentation the randomly directed transverse velocity changes the mixed distribution function leading to a peak of the correlation function C_2 . In our exploratory investigation we consider only the projectile like source the fragments of which are detected in forward direction. We sample events with impact parameters between $3fm$ and to $7fm$ simulating semi-central collisions. The resulting function C_2 for the correlations of two Li fragments shows a peak in the expected region. The height of the peak diminishes if radial flow is present (see dash-dotted line). This clearly indicates that the spread in the transverse momentum has far reaching consequences.

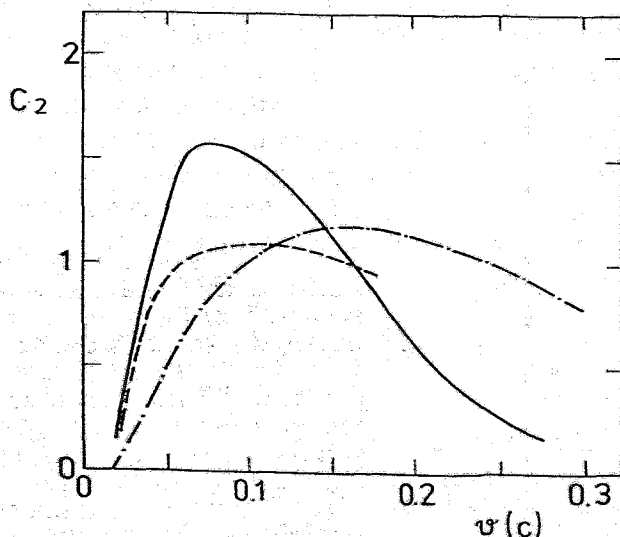


Fig. 1. Correlation function C_2 for Li fragments produced in semi-central collisions of Au on Au at $150 A \cdot MeV$ per nucleon as a function of the relative velocity v without (solid line) and with (dash-dotted line) radial flow of $5 MeV$ per nucleon. The dashed line shows the correlation without flow using an angle cut of 12 degrees.

REFERENCES:

[1] J.P. Alard et al., Phys. Rev. Lett. 69(1992)889

[2] B. Kämpfer, R. Kotte, J. Mösner, W. Neubert, D. Wohlfahrt for FOPI-collaboration, see this report

Multifragmentation of Gold Projectiles Studied within the BUU Approach ^B

H.W. BARZ¹, W. BAUER², J.P. BONDORF³, A.S. BOTWINA⁴, R. DONANGELO⁵, H. SCHULZ³ AND K. SNEPPEN³

¹ KAI Berlin, e.V. im Institut für Kern- und Hadronenphysik, Forschungszentrum Rossendorf e.V., Postfach 19, O-8051 Dresden

² NSCL Michigan University, East Lansing, MI 48824, USA

³ The Niels Bohr Institut, Blegdamsvej 17, 2100 Copenhagen, Denmark

⁴ Institute for Nuclear Research, 117312 Moscow, Russia

⁵ Instituto de Fisica, Universidade Federal do Rio de Janeiro, 21945 Rio de Janeiro, Brazil

It is now a well established fact that there is a regime where copious production of intermediate mass fragments (IMFs) heavier than α particles takes place. Especially the data of the collision of gold nuclei on various target nuclei at $600 A \cdot \text{MeV}$ taken by the GSI group [1] show a universal behaviour compatible with the idea of the fragmentation of an equilibrated system.

Using the statistical multifragmentation model the properties (mass number, excitation energy) of the equilibrated sources could be extracted by comparing to the data[1]. To understand the equilibration process the reaction was studied by a Boltzmann-Ühling-Uhlenbeck (BUU) approach which is expected to provide reliable results for the evolution process until shortly before the fragmentation sets in. Carrying out the BUU calculations we analysed the regions with densities larger than a certain critical density, chosen to be between 0.05 and 0.2 times normal nuclear matter density. In a time intervall less than 50 fm/c a large number of nucleons are spilled off and these nucleons carry away most of the excitation energy. The remnant system remains for a relatively long time span. The break-up conditions required by the analysis with the statistical multifragmentation model are compatible with the BUU results and are reached after a time of around 70-90 fm/c (see fig.1 for details).

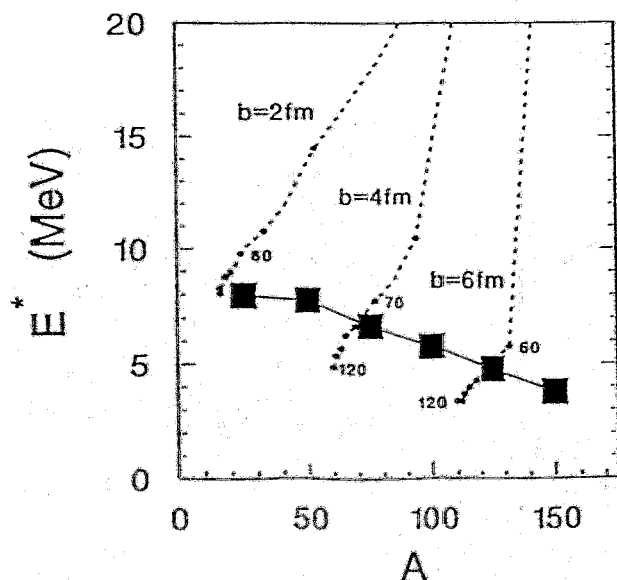


Fig. 1. Evolution of the mass number A and excitation energy E^* of the cooling remnant of the Au on Cu collision according to the BUU model for three different impact parameters (dashed lines). The numbers indicate the times in fm/c and the full squares indicate the break-up conditions needed to explain the data by the statistical model.

REFERENCES:

[1] J. Hubele et al., Phys. Rev. C46(1992)R1577; P. Kreuz et al., GSI preprint 92-23(1992)

Non-Statistical Fluctuations in the Velocity Distribution of Intermediate Heavy-Ion Collisions^B

B. HEIDE

Forschungszentrum Rossendorf e. V., Institut für Kern- und Hadronenphysik

Nuclear matter under extreme conditions is a highly complex system. Besides multifragmentation one expects new phenomena at intermediate beam energies. The structures of these new phenomena may be better studied in the framework of fractal geometry than in usual calculations. Therefore, we make use of the method of intermittency, first introduced by Bialas and Peschanski [1, 2] at ultra relativistic heavy-ion collisions, in order to get some informations from the velocity distribution of fragments produced in nuclear disassembly reactions at 150 A-MeV bombarding energy.

We simulate the velocity distribution by means of a so-called hybrid model consisting of both the BUU model and the Copenhagen model. The result is represented in fig.1a. The agreement with the (not normalized) experimental data [3], shown in fig.1b, should be sufficient for our purpose, i.e. for the study of non-statistical fluctuations.

The practical implementation of the method of intermittency is straightforward: one computes the scaled factorial moments F_i of the normalized distribution

$$F_i = \frac{1}{M^{i-1}} \cdot \frac{\langle \sum_{m=1}^M k_m \cdot (k_m - 1) \cdot \dots \cdot (k_m - i + 1) \rangle}{\langle \sum_{m=1}^M k_m \rangle^i}$$

(cf. [2]) and puts the logarithm of these moments versus the logarithm of the bin sizes Δy . There are several ways of defining F_i . We make a remark to this point in connection with our results. If there exists a power-law dependence of the moments on the bin size

$$F_i \propto (\Delta y)^{-\alpha_i}, \quad (*)$$

then a straight line arises in the plot mentioned above and one can estimate the intermittency exponent α_i as the gradient of the log-log graph. From (*) it follows immediately $F_i(a\Delta y) \propto a^{-\alpha_i} F_i(\Delta y)$, i.e. the system shows self-similarity at various resolutions. In the theory of fractals, F_i is called a measure and α_i is the dimension of the corresponding set (here taken as velocity interval). The dimension of the set describes in some way its topological properties.

Now, we turn to our results. In fig.1a the length d is the characteristic interval over which the distribution changes substantially. As seen from fig.1c the fifth scaled factorial moment is nearly independent for $\Delta y \ll d$. One also sees instabilities for $\Delta y \gg d$. Between these two regions, the curve increases linearly and shows intermittency or non-statistical fluctuations. In contrast, the graph in fig.1d which corresponds to the widely used formula

$$F_i = \frac{\langle \sum_{m=1}^M k_m \cdot (k_m - 1) \cdot \dots \cdot (k_m - i + 1) \rangle}{\sum_{m=1}^M \langle k_m \rangle^i}$$

has a different behaviour and does not clearly reveal intermittency. Hence, the formula for the F_i has to be determined very carefully. Finally, we have calculated the scaled factorial moments of a normalized distribution which refers to only one impact parameter of 5.3 fm, i.e. we exclude the mixing of different types of fragmentation events, without (fig.1e) and with (fig.1f) evaporation. We infer from fig.1c and fig.1e that event mixing does not affect the intermittency pattern. From fig.1e and fig.1f, it is seen that the α_i are approximately proportional to $i \cdot (i - 1)$, whereat this law is better fulfilled in the case with evaporation (as expected).

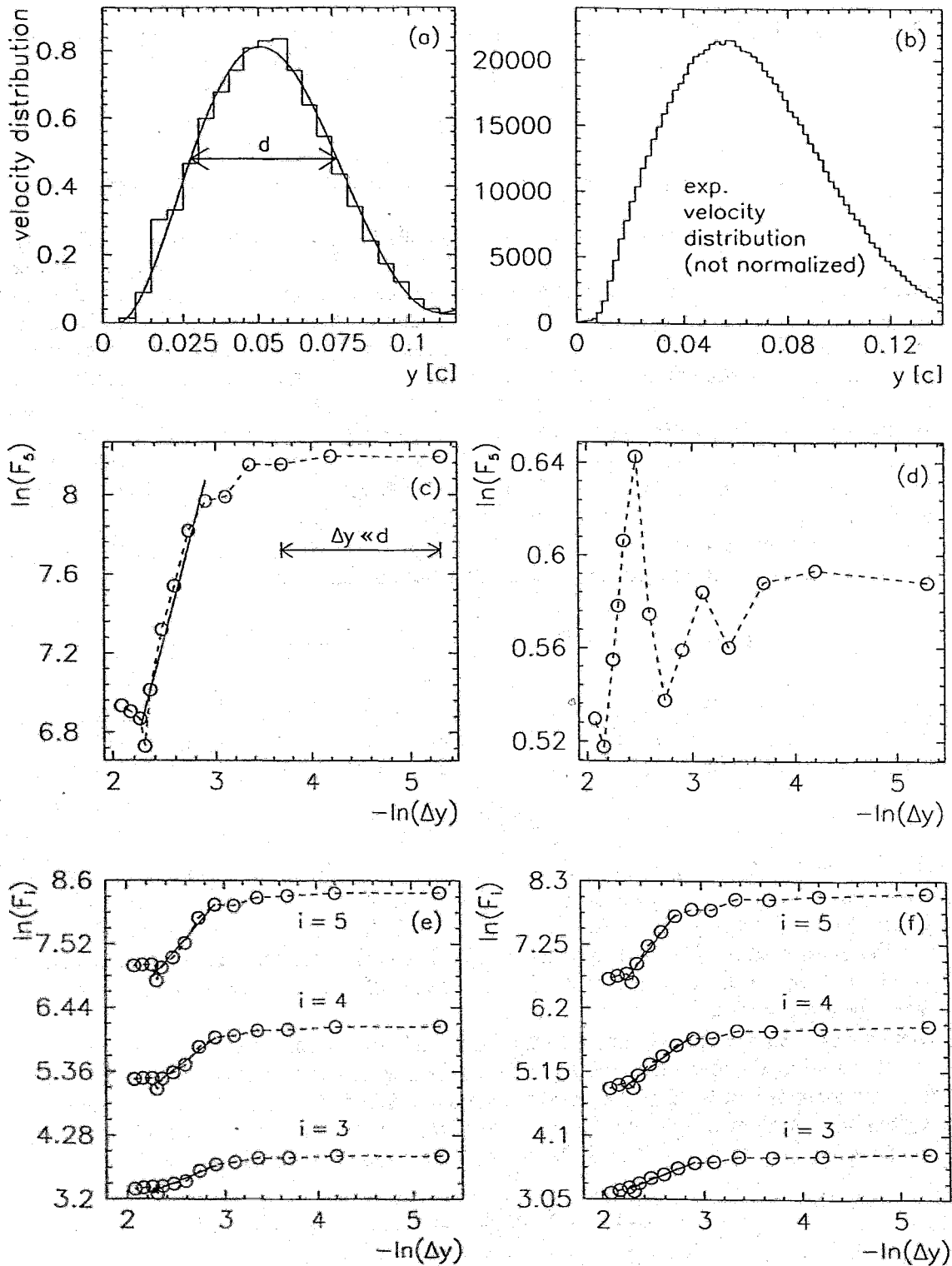


Fig.1 Velocity distributions and scaled factorial moments of various rank ($i = 3, 4, 5$). Solid lines are fits.

REFERENCES:

- [1] A. Bialas and R. Peschanski, Nucl. Phys. B273 (1986) 703-718.
- [2] A. Bialas and R. Peschanski, Nucl. Phys. B308 (1988) 857-867.
- [3] R. Kotte, private communication.

On Size and Shape of the average meson fields of the semibosonized Nambu & Jona-Lasinio model^B

R. WÜNSCH¹, K. GOEKE², TH. MEISSNER³

¹ *Institut für Kern- und Hadronenphysik, Forschungszentrum Rossendorf e.V., Postfach 19, O-8051 Dresden, Germany*

² *Institut für Theoretische Physik II, Ruhr-Universität Bochum, W-4630 Bochum, Germany*

³ *Institute for Nuclear Theory, University of Washington, HN-12 Seattle, WA 98195, USA*

We have considered a two-flavor Nambu & Jona-Lasinio model in Hartree approximation involving scalar and pseudoscalar-isovector quark-quark interaction [1]. The resulting chiral fields, which minimize the corresponding effective action, have been restricted to a spherical hedgehog shape and to the chiral circle. Such fields can be described by a single scalar profile function $\Theta(r)$. The sea contribution to the energy and to the average fields have been regularized within the proper-time schema. The corresponding cut-off energy Λ is one of the parameters of the model. Interaction strength G , vacuum amplitude σ_V of the σ field, constituent quark mass M and current quark mass m are additional parameters. The number of free parameters of the model can be reduced to a single one by means of the vacuum equation of motion, the PCAC hypothesis, and by identifying the Feynman amplitude of the weak pion decay, calculated in one-loop approximation, with its experimental value [1]. Solitonic field configurations with baryon number $B = 1$ have been found for quark masses $M \gtrsim 350 \text{ MeV}$ corresponding to $\Lambda \gtrsim 1.85 M$ and $G \gtrsim 38 M^{-2}$. The relation between valence and sea-quark contribution to any observable like mean square radii \bar{r} , axial-vector coupling strength g_A and nucleon-delta mass-splitting Δm , depend on the cut-off Λ and hence on the constituent quark mass M . While for small quark masses the observables are mainly determined by the valence-quark contribution, the sea contribution dominates at larger masses. At $M \gtrsim 725 \text{ MeV}$ ($\Lambda \lesssim M, G \gtrsim 44 M^{-2}$), the valence quark level dips into the Dirac sea and the soliton is completely determined by the properties of the Dirac sea. So the calculated observables exhibit a considerable dependence on the regularization parameter.

We have self-consistently determined the average mesonic fields and were surprised to find that the profile function is nearly independent on the regularization parameter in despite of the varying contribution of valence- and sea-quark contributions.

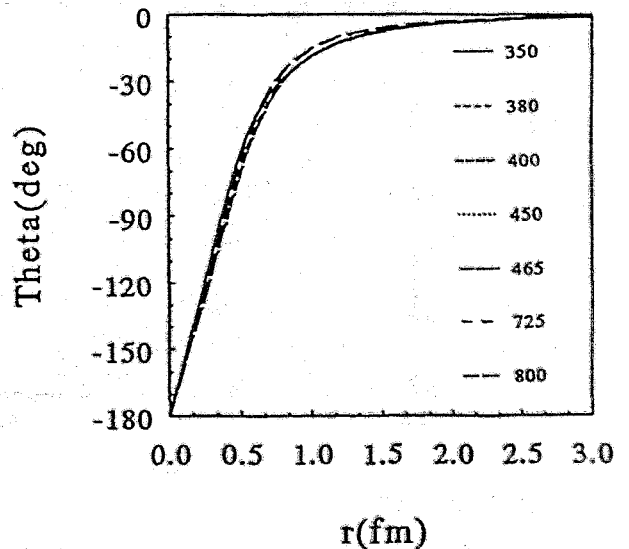


Abb.: Self-consistently determined profile functions $\Theta(r)$ for current quark-masses between $M = 350 \text{ MeV}$ and $M = 800 \text{ MeV}$.

REFERENCES:

- [1] Th. Meissner and K. Goeke *Nucl. Phys. A*524 (1991) 719

COM Corrections of the semibosonized Nambu & Jona-Lasinio Model for Interacting Quarks^B

M. SCHLEIF¹ AND R. WÜNSCH²

¹ *Institut für Theoretische Physik, TU Dresden, Zellescher Weg 1c, O-8020 Dresden, Germany*

² *Institut für Kern- und Hadronenphysik, Forschungszentrum Rossendorf e.V., Postfach 19, O-8051 Dresden, Germany*

We consider a two-flavor (u,d) Nambu & Jona-Lasinio model [1] for low and medium energy hadron physics with nonlinear scalar and pseudoscalar-isovector quark-quark interaction. The pure fermionic model can be converted into an equivalent effective meson-quark model by means of standard path integral methods. Within an appropriate regularization scheme meson and quark fields can be determined self-consistently (e.g. [2]). We restrict the mesonic fields to both the chiral circle and to spherical hedgehog configurations and assume them to be classical and time-independent [3]. Within these restrictions quark and meson energies are a functional of the mesonic profile function $\Theta(r)$ alone. Nucleons can be described by fields with a profile function varying from $|\Theta| = \pi$ at the origin to $\Theta = 0$ at $r \rightarrow \infty$. Instead of calculating the mesonic fields self-consistently we approximate the profile function by the ansatz

$$\Theta(r) = \begin{cases} -\pi \left(1 - \frac{r}{2R}\right) & \text{if } r \leq R_m \\ b \frac{1+m\pi r}{r^2} e^{-m\pi r} & \text{if } r \geq R_m \end{cases}, \quad (1)$$

which is quite close to the self-consistent profile and has the correct asymptotic behaviour at $r \rightarrow 0$ and $r \rightarrow \infty$. The radius R is the only parameter and controls the size of the mesonic fields. The quantities R_m and b are uniquely determined by the condition that the profile function and its derivative has to be smooth at the matching point R_m .

The bosonisation of the quark-quark interaction suffers, as every mean field approximation, from the presence of center-of-mass motions (COM). To study its influence we have calculated the energy accounting for this unphysical degree of freedom and compared with the total energy of the nucleon as described by the model (see fig. below). The difference between both full lines demonstrates the influence of the center-of-mass motion and the stabilizing effect of its exclusion.

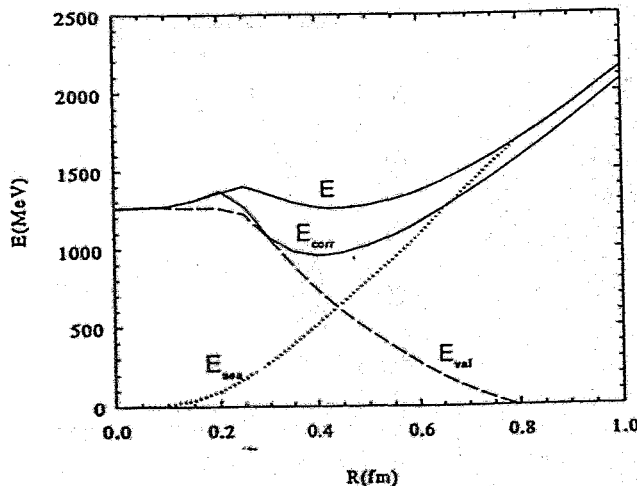


Figure: Energy (E_{val}) of the valence quarks, the sea quarks (E_{sea}), and the total energy (E) for the profile function (1) in dependence on the size parameter R . The COM-corrected total energy (E_{corr}) is shown additionally. The curves have been calculated with proper-time regularization parameter $\Lambda=636.7$ MeV, which corresponds to a constituent quark mass of 400 MeV.

REFERENCES:

1. J. Nambu, G. Jona-Lasinio *Phys. Rev.* 122 (1961) 345; 124 (1961) 246
2. H. Reinhardt and R. Wünsch *Phys. Lett.* B215 (1988) 577; B230 (1989) 93
3. Th. Meißner, K. Goeke *Nucl. Phys.* A524 (1991) 719

Production of spin $s=3/2$, strangeness $S = -2$ cascade particles Ξ^* in (K^-, K^+) reactions on nuclei^B

R. WÜNSCH¹ AND S. KREWALD²

¹ *Institut für Kern- und Hadronenphysik, Forschungszentrum Rossendorf e.V.,
Postfach 19, O-8051 Dresden, Germany*

² *Institut für Kernphysik, Forschungszentrum Jülich, W-5170 Jülich, Germany*

We have extended our investigation of nuclei with strange ingredients to the hypernucleus with the most stable *excited* baryon, the cascade particle Ξ^* . Corresponding experimental evidence has been found recently [1].

We follow the standard description of nuclear reactions with medium-energy, elementary projectiles in distorted wave impulse approximation (DWIA). The experimental findings seem to favor an one-step process $p(K^-, K^+)\Xi^{*-}$ on a bound proton of the target nucleus. According to DWIA the hypernuclear production cross-section can be factorized into the cross section of the elementary reaction on a free nucleon and an effective nucleon number of the target nucleus taking into account the binding of both the protons in the target nucleus and the produced hyperon in the final hypernucleus. Usually one takes the elementary cross section from the experiment and calculates the effective nucleon number by means of nuclear model. It is given by the matrix element of the transition operator describing the conversion of a proton into a cascade particle with the nuclear initial and the hypernuclear final states. While the transition operator for the production of a spin $s=1/2$ baryon has a well known structure, consisting of a spin-flip and a non spin-flip term, very little is known about the production of spin $s=3/2$ baryons.

The production of excited cascade particles may be a suitable example for the general study of the production of $s=3/2$ baryons. The relative stability ($\Gamma \sim 10 \text{ MeV}$) of the excited cascade particle, in comparison to excited nucleons and to the Δ resonance, allows a quite detailed study of the energy dependence of that process.

Evaluating lowest-order Feynman diagrams we have derived a $p(K^-, K^+)\Xi^{*-}$ transition operator. The t -channel exchange of a single meson can be excluded, since a $S = -2$ meson has not yet been observed. We consider the s - and u -channel contributions with an intermediate, neutral, $S = -1$ hyperon. They turn out to have a simple structure in collinear geometry (momentum transfer parallel to the projectile momentum): $T = F(p, m_Y) S_z \sigma_z$, where S_z is the spin transition operator and σ_z is the spin operator projected onto the direction of the momentum transfer. The factor $F(p, m_Y)$ determines the energy dependence of the reaction and depends on the momentum p of the projectile and on the mass m_Y of intermediate baryon. While the projectile momentum is well defined in the reaction, one has to sum over all possible intermediate baryon. The factor F exhibits a strong resonant behaviour, and one can restrict the number of intermediate particles to hyperons with a mass in the vicinity of the resonance energy.

REFERENCES:

- [1] T. Iijima et al. *KEK Preprint 92-4* (1992)

Tilted Cranking

S. FRAUENDORF

Forschungszentrum Rossendorf e. V., Institut für Kern- und Hadronenphysik

After working out the theoretical basis in the j-shell model [1], a full Tilted Cranking computer code was set up [2], which bases on the widely used CSM code. The rotating deformed field is described by the Nilsson hamiltonian h , which may include monopole pairing. The direction of the rotational axis, which is assumed to lie in one of the planes defined by the principal axes of the deformed potential, is calculated by minimizing the energy of a quasiparticle configuration $|\omega, \vartheta\rangle$ with respect to the tilting angle ϑ .

$$h' = h - \omega(\sin\vartheta j_1 + \cos\vartheta j_3), \quad h'|\rangle = E'|\rangle, \quad E'(\omega, \vartheta) \rightarrow \min \quad (1)$$

The deformation of the potential and the pairfield can be calculated from the ordinary selfconsistency relations considering h' as the meanfield approximation to the Pairing + QQ-hamiltonian. Each configuration $|\omega\rangle$ describes a rotational band. If the tilting angle ϑ is found to be equal to 90° the rotational axis is a principal one. These Principal Axis Cranking (PAC) solutions describe $\Delta I = 2$ bands, whose levels are interconnected by E2-transitions. If ϑ differs from 0° or 90° the rotational axis is tilted. These Tilted Axis Cranking (TAC) solutions describe $\Delta I = 1$ rotational bands, whose levels are interconnected by strong M1-direct and E2-crossover transitions.

The multitude of rotational bands above the yrast line is interpreted as configurations of quasiparticles in a potential that rotates uniformly about an axis that is differently oriented for each band. The orientation of the rotational axis turns out to be a very useful semiclassical concept to classify rotational bands at high spin. The TAC theory permits to calculate both the energies and the intraband E2- and M1- transition probabilities on a microscopic basis. Since TAC is formulated as a completely microscopic meanfield theory one may study the interplay of the orientation of the angular momentum with other degrees of freedom, like e. g. the triaxiality or the pair correlations.

The results of recent high spin experiments on ^{174}Hf , ^{179}W , $^{166,167}\text{Yb}$ and $^{199,200}\text{Pb}$ have been interpreted using the TAC code. Some results are discussed in the accompanying contributions. All data were obtained with the state of art multidetector γ -ray arrays (OSIRIS, NORDBALL, HERA). In such experiments always a number of rotational bands is observed, which becomes even larger for the more powerfull new arrays (GASP, EUROGAM) and is expected to grow dramatically for the arrays under construction (GAMMASHERE, EUROBALL). The TAC turned out to be a versatile tool to interpret these rich band structures. The simple picture of a nucleus rotating about an axis, whose orientation depends on the quasiparticle configuration appeals to intuition gained in classical physics. The TAC code is written in a userfriendly way and equipped with easy to use plotting facilities. It runs on VAX with DIGITAL GKS plotting software.

REFERENCES:

- [1] S. Frauendorf, T. Bengtsson, Int. Symp. on Future Directions in Nuclear Physics, Strasbourg 1991, AIP Con. Proc. 259, p. 223

Tilted Cranking Classification of Multibandspectra

S. FRAUENDORF

Forschungszentrum Rossendorf e. V., Institut für Kern- und Hadronenphysik

In the Tilted Cranking approach [1] rotational bands are interpreted as independent particle configurations rotating uniformly about an axis that may be tilted with respect to the principle axes of the deformed potential by the angle ϑ . The orientation is found by minimizing for each conf. the energy $E'(\vartheta, \omega) = \langle h - \omega(\sin\vartheta j_1 + \cos\vartheta j_3) \rangle$ with respect to ϑ . The fig. shows as an example $Z=72$ and $N=102$. We use for h the Nilsson hamiltonian. For the neutron system zero pairing is assumed. Each minimum at $\vartheta > 0$ represents a cut through a rotational band at the frequency ω , the spin I and the energy $E' = E - \omega I$. The slope of $E'(\omega)$ is equal to $-I$. The minima at $\vartheta = 90^\circ$ are the PAC solutions. They have good signature and represent $\Delta I = 2$ bands. Most minima are TAC solutions. Since the signature is not conserved they correspond to $\Delta I = 1$ bands. Bands with the following structure are found: PAC: 1 : $\pi 0^+ \nu 0^+$, TAC : 2 : $\pi 0^+ \nu 6^-$, 3 : $\pi 8^- \nu 12^+$, 4 : $\pi 8^- \nu 10^-$, 5 : $\pi 0^+ \nu 7^+$, 6 : $\pi 8^- \nu 6^-$, 7 : $\pi 0^+ \nu 0^-$, 8 : $\pi 0^+ \nu 3^+$, 9 : $\pi 0^+ \nu 3^-$, where the notation $\langle j_3 \rangle^\pi$ (rounded to integers) is used.

The strongly deformed ^{174}Hf has no preferential orientation of angular momentum, whereas the less deformed ^{163}Er prefers an orientation around 90° [3]. The semimagic nuclei $^{198,199}\text{Pb}$ have very small deformation but show regular bands oriented around an angle 45° [1,4]. Considering the classical moments of inertia of the deformed density distributions such a behavior is quite surprising. It shows that quatal effects determine the orientation of angular momentum.

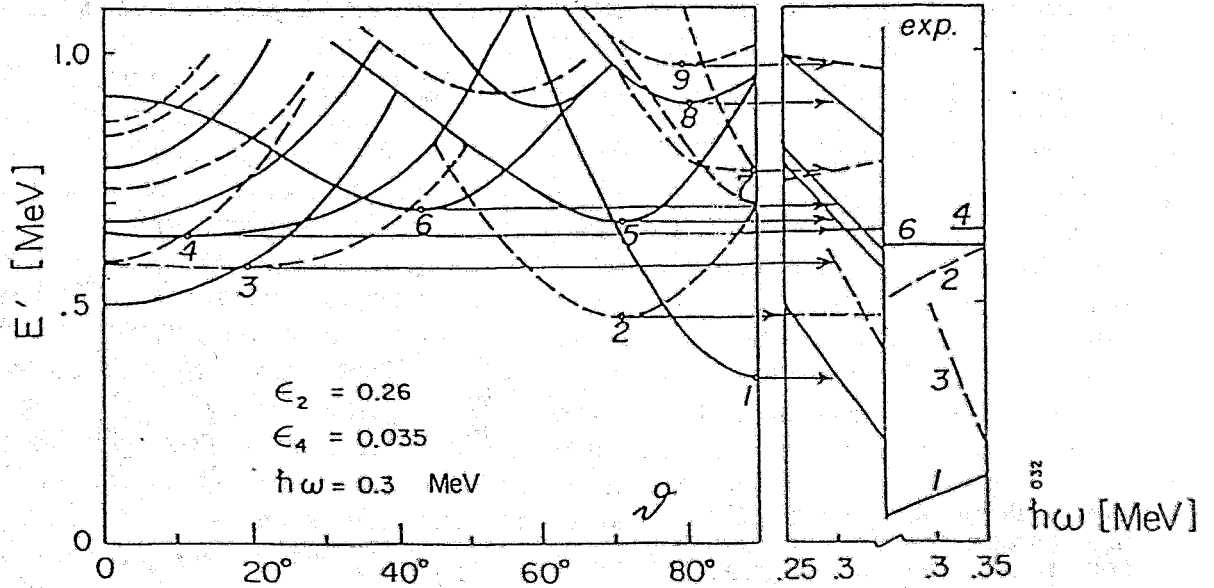


Fig. 1 Total routhians in ^{174}Hf as functions of the tilting angle ϑ (left) and the excitation spectrum as function of the frequency ω (right). Full lines indicate positive dashed negative parity. The energy zero is chosen such that the calculated band 4 agrees with the experimental ones [2]. All slopes are reduced by $I = 16\hbar$.

REFERENCES:

- [1] S. Frauendorf, Nucl. Phys. A, in print
- [2] N. Gjorup et al. Nucl. Phys. to be published
- [3] A. Brokstedt et al. Nucl. Phys. to be published
- [4] G. Baldsiefen et al. Nucl. Phys. to be published

M1-Bands near ^{198}Pb

S. FRAUENDORF

Forschungszentrum Rossendorf e. V., Institut für Kern- und Hadronenphysik

The recently discovered $\Delta I = 1$ -bands in the light Pb nuclei (c.f. e.g. [2]) are peculiar examples of TAC solutions. The figure illustrates the geometry of the high spin orbitals near the Fermi level. The relevant proton states are $h_{9/2}$ and $i_{13/2}$, which are reached by exciting protons across the $Z=82$ gap. Their density distribution looks like a torus. They drive the nucleus towards oblate shape maximizing the overlap with the proton orbit. This coupling is of DAL (deformation aligned) type. The neutron orbitals are $i_{13/2}$ holes. Their density distribution is a sphere (full $i_{13/2}$ shell) minus a torus resulting in the dumbbell like shape. It has maximal overlap with the oblate density distribution when the angular momentum stands perpendicular to the symmetry axis corresponding to RAL (Rotational Aligned) coupling. When the nucleus does not rotate (band head) \vec{i}_π is oriented along the 3-axis and \vec{i}_ν along the 1-axis. Moving up the band, most of the angular momentum is gained by gradually tilting \vec{i}_π and \vec{i}_ν towards \vec{J} . The two vectors rotate around \vec{J} with the inertial forces balancing the counter forces generated by the decreasing overlap with the deformed field. There is an apparent inertia $\mathcal{J}^{(2)} = \frac{dJ}{d\omega} > 0$. It is called "Quantal Inertia", since it originates from the reorientation of \vec{i}_π and \vec{i}_ν , whose absolute value of angular momentum is frozen by the quantization of the single particle motion. The calculated total values of $\mathcal{J}^{(2)}$ lie between 10 and 20 $\hbar^2 \text{MeV}^{-1}$ close to the observed ones. Only about 7 $\hbar^2 \text{MeV}^{-1}$ of the total value is collective, the rest is quantal.

The described mechanism is a new type of rotation, which is expected in weakly deformed nuclei, when the high spin proton level are of particle type and the high spin neutron levels are of hole type, or vice versa. It is characterized by:

- Regular $\Delta I=1$ -sequences with a low but rather constant $\mathcal{J}^{(2)}$
- Large BM1-values of several to ten μ_N^2
- Small BE2-values

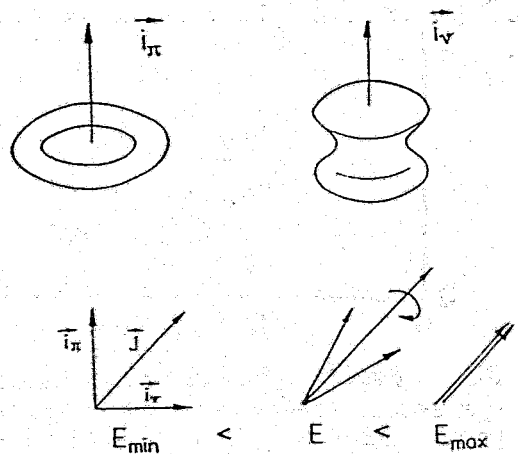


Fig. 1 Density distribution of the high j -proton and high j -neutron hole orbitals. The vector diagrams show how the orbitals couple with increasing angular momentum.

REFERENCES:

- [1] S. Frauendorf, Nucl. Phys. A, in print
 [2] G. Baldsiefen, U. Birkental, H. Huebel, N. Nenoff, B. V. Thirumala Rao, P. Willsau, J. Heese, H. Kluge, K. H. Maier, R. Schubart, S. Frauendorf, Phys. Lett., B 298 (1993) 54

Intruder Bands and Neutron-Proton Interaction

R. WYSS², W. SATULÄ³ AND F. DÖNAU¹

¹ *Institut für Kern- und Hadronenphysik, Forschungszentrum Rossendorf e.V.*

² *Manne Siegbahn Institute, S-10405 Stockholm, Sweden*

³ *Department of Mathematical Physics, Lund Institute of Technology
P.O. Box 118, S-22100 Lund, Sweden*

Rotational band structures in odd- A nuclei built on particle-like or hole-like intruder orbitals display experimentally an unexpected behaviour of the rotational alignment when comparing with the systematics predicted by the Cranked Shell Model (CSM). Considering such a band in ^{163}Lu , for instance, where the odd proton occupies the $i_{13/2}$ orbital, the typical jump of the spin alignment (backbend) should occur in a critical frequency region according to the predicted change of the neutron Yrast configuration from the vacuum ($0qp$) to a two quasiparticle ($2qp$) excited state. In fact the backbending is not observed when the odd proton fills an intruder orbital but otherwise it appears for non-intruder bands in the same nucleus as well as it is seen for the adjacent even neighbour ^{162}Yb . Various attempts failed to explain this effect in the framework of the CSM by a decent variation of the pairing and deformation parameters. Since this feature exists systematically in several mass regions for rotational bands where an odd particle is combined to an aligning configuration of particles with opposite isospin it is suggestive to consider a residual neutron-proton interaction as possible source of this effect. In our study a schematic quadrupole-quadrupole force ($Q \cdot Q$) was applied to describe the $1qp - 3qp$ configuration mixing which adds up to the rotational interaction determining the band crossing in the CSM. By taking quadrupole operators Q in doubly-stretched coordinates the self-consistency of the shape can be approximately conserved. Qualitatively, the effect of such a residual interaction may be sizeable for intruder orbitals because both the quadrupole moment and the quasiparticle occupation factor ($uu' - vv'$) are large for a low Ω -intruder particle. The simple $Q \cdot Q$ force introduces a configuration dependence to both the crossing frequency and the $0qp-2qp$ interaction which is not present in the standard mean field description. Intruder configurations give rise to a 'residual quadrupole moment' which leads to a shift of the band crossing frequency. The simple $Q \cdot Q$ gives insight into the mechanism of the band interaction but it does not quantitatively account for the observed anomalies of intruder like configurations. The main conclusions can be summarized as follows:

- Intruder configurations are classified by particle like occupation and a quadrupole moment different from the core nucleus.
- The n-p interaction may become as important as the like particle interaction. The interaction terms oscillate differently in phase as a function of the chemical potential.
- If the odd particle occupies an intruder state, the crossing frequencies with the two-qp aligned state will in general increase.
- The experimental extension towards more neutron deficient nuclei is needed for more systematic studies of the n-p interaction along isotopic chains.

Rotational Population Patterns in Heavy-ion Two Particle Transfer Reactions between Even-even Thorium Nuclei

S. Y. CHU^a, R. DONANGELO^b, S. FRAUENDORF^c, J. O. RASMUSSEN^a, Y. SHIMIZU^c AND M. A. STOYER^d

^a Lawrence Berkeley Laboratory, Berkeley, CA 94720, USA

^b Universidade Federal do Rio de Janeiro, Rio de Janeiro, Brazil

^c Forschungszentrum Rossendorf e. V., Institut für Kern- und Hadronenphysik

^d Physics Department, Kyushu University 33, Fukuoka 812, Japan

^e Lawrence Livermore National Laboratory, Livermore, CA 94551, USA

The energies of the lowest several bands in $^{230,232,234}\text{Th}$ and the neutron pair transfer strength distributions between them are calculated by diagonalizing the matrix of p-h configurations in six proton and six neutron Nilsson levels coupled to a rigid rotor as well as by means of Cranked HFB + RPA approximation. Sudden-approximation methods are applied to estimate pair transfer population patterns in $^{206}\text{Pb}+^{232}\text{Th}$ reactions. Although the two approximation schemes are rather different, the pair transfer strength distributions are remarkably similar, as illustrated in fig. 1. Around spin $20\hbar$ or frequency $\hbar\omega = 0.2$ MeV the static neutron pairing goes to zero. This transition is accompanied by a branching of the transfer strength from the yrast band into many excited bands. The spreading of the strength indicates that there is no individual pair vibrational band, like the pair addition and pair subtraction vibrational states observed in the vicinity of ^{208}Pb . The change of the strength distribution is reflected by a fragmentation of the pair transfer cross section into excited bands. Thus, COULEX combined with two particle transfer provides an experimental signal for the destruction of pairing by rotation, which is complimentary to the evidence from the experimental energies [2].

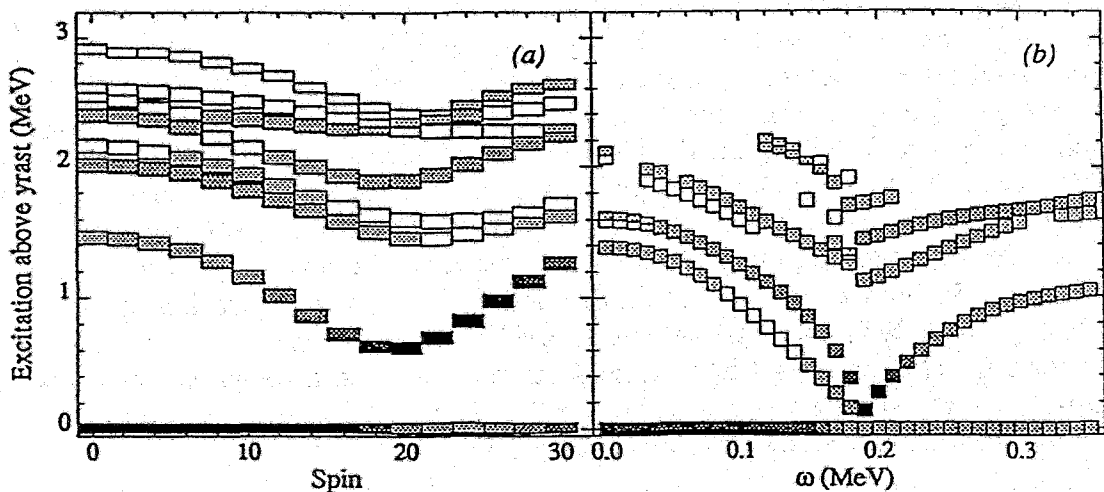


Fig. 1 Gray-scale plots of two neutron pair transfer strengths ($I \rightarrow I$ transitions) from yrast levels in ^{232}Th to states in ^{230}Th , (a) using particle rotor and (b) using CHFHB+RPA methods.

REFERENCES:

- [1] S. Y. Chu, R. Donangelo, S. Frauendorf, J. O. Rasmussen, Y. Shimizu and M. A. Stoyer, Proc. of Symp. on Nucl. Phys. of our Times, Sanibel Island, Florida, USA, Nov. 1992
- [2] J.R.B.Oliveira, S.Frauendorf, M.A.Deleplanque, R.M.Diamond, F.S.Stephens, C.W.Beausang, Phys. Rev. C, rapid com., in print and contribution to this report.

Rotation-Induced Transition from Superfluid to Normal Phase in Mesoscopic Systems: ^{168}Yb and Adjacent Nuclei

J.R.B.OLIVEIRA^a, S.FRAUENDORF^b, M.A.DELEPLANQUE^a, R.M.DIAMOND^a,
F.S.STEPHENS^a, C.W.BEAUSANG^a, J.E.DRAPER^c, C.DUYAR^c, E.RUBEL^c, J.A.BECKER^d,
E.A.HENRY^d, N.ROY^d

^a Nuclear Science Division, Lawrence Berkeley Laboratory USA,

^b Forschungszentrum Rossendorf e. V., Institut für Kern- und Hadronenphysik

^c University of California, Davis, USA

^d Lawrence Livermore National Laboratory USA, Livermore

Due to the small number of correlated particles it is difficult to find clear experimental signatures for the rotation induced transition from the paired to the unpaired state in a nucleus. Specific changes, which appear in the excitation spectrum of the rotational bands when the static pairfield goes to zero, may signal this transition. The Cranked Shell Model is used to calculate the rearrangement of the excitation spectrum of some Yb nuclei. The close correspondance between the calculated and measured band spectra demonstrates that above the frequency of $\hbar\omega=0.35$ MeV the static neutron pairing has disappeared.

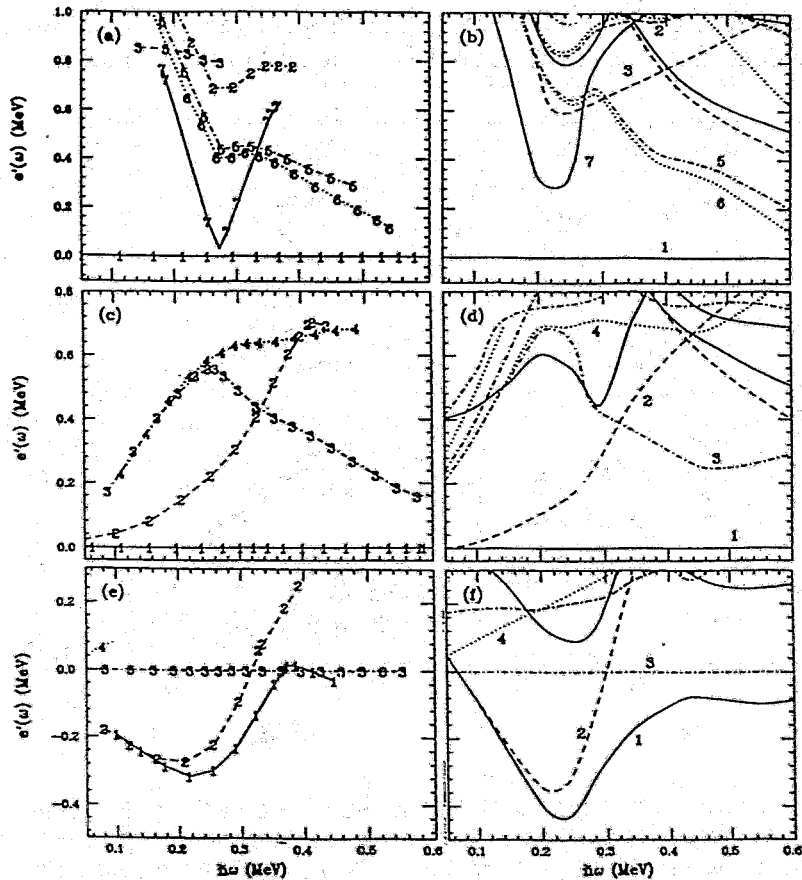


Fig. 1 Experimental (left) and calculated (right) relative routhians for ^{166}Yb (upper p.), ^{167}Yb (middle p.) and ^{169}Yb (lower p.). Below $\hbar\omega=0.2$ MeV strong and above $\hbar\omega=0.4$ MeV zero static pairing is assumed.

REFERENCES:

- [1] J.R.B.Oliveira, S.Frauendorf, M.A.Deleplanque, R.M.Diamond, F.S.Stephens, C.W.Beausang, Phys. Rev. C, rapid com., in print

Chaotic Behavior in Rotating Warm Nuclei

M. MATSUO^a, T. DØSSING^b, B. HERSKIND^b, S. FRAUENDORF^c, E. VIGEZZI^d, R. A. BROGLIA^{b,d}

^aYukawa Institute for Theoretical Physics, Kyoto University, Kyoto 606-01, Japan

^bNiels Bohr Institute, University of Copenhagen, DK-2100 Copenhagen Ø, Denmark

^cForschungszentrum Rossendorf e. V., Institut für Kern- und Hadronenphysik

^dINFN Sezione di Milano, via Celoria 16, 20133 Milano, Italy

Fluctuations associated with stretched E2 transitions from high spin levels in nuclei around ¹⁶⁸Yb are investigated by a cranked shell model (CSM) extended to include residual two-body interactions. In the CSM without the residual interaction the gamma-ray energies behave like random variables and the energy spectra show the Poisson fluctuations. With two-body residual interaction included, the pattern of dominant E2 transitions within unmixed rotational bands is still valid up to around 600 keV above yrast, in good agreement with experiments. At higher excitation energy, the transitions begin to branch out as a consequence of the band mixing. A gradual onset of rotational damping emerges. At 1.8 MeV above yrast, complete damping is observed with GOE type fluctuations for both energy levels and transition strengths (Porter-Thomas fluctuation). The onset of chaos depends on the order of the multipoles of the interaction. The SDI (high multipoles) accounts for the experimental evidence on rotational damping, whereas the P+QQ (only low multipoles) fails.

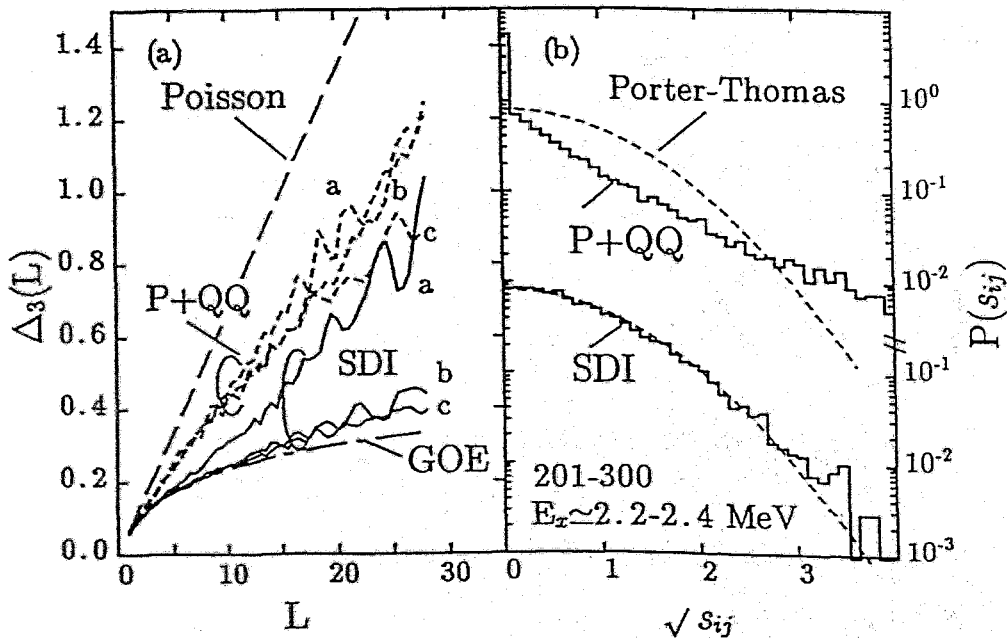


Fig. 1 The Δ_3 statistics of energy level fluctuations (a) and the normalized E2 strength distribution (b) calculated by CSM including residual interactions. The curves a,b,c in (a) refer to the first, second and third group of 100 levels, respectively, whereas (b) refers to the second group.

REFERENCES:

- [1] M. Matsuo, T. Døssing, B. Herskind, S. Frauendorf, Nucl. Phys. , subm.
- [2] M. Matsuo, T. Døssing, B. Herskind, S. Frauendorf, E. Vigezzi, R. A. Broglia, Nucl. Phys., in print

Classical Phase-Space Structure of the Single-Particle Motion in Cranked Potentials

J. REIF

Forschungszentrum Rossendorf, Institut für Kern- und Hadronenphysik

The phase-space structure of the three-dimensional single-particle motion in a cranked Buck-Pilt potential of lemniscatoidic shape has been investigated. The cranking (x -) axis is assumed to be perpendicular to the symmetry (z -) axis [1]. The deformation of the finite-depth potential is characterized by the parameter δ which ranges from 1 to 0, covering a family of shapes between a single sphere and two touching spheres, respectively. The calculation of classical single-particle trajectories in the rotating system has been performed for fixed rotational frequencies ω of clockwise as well as counterclockwise rotation about the x -axis. The chosen initial conditions realize a single-particle momentum with a fixed z -component, a y -component equal to zero, and a positive x -component corresponding to the considered binding energy.

The phase-space structure has been investigated in terms of Poincaré surfaces of section (PSS), the mean value of the maximal positive Ljapunov exponents, and the chaotic fraction of phase space as a function of the cranking frequency.

The analysis of the PSS has shown that, due to the inertial forces, a chaotic motion is produced gradually for the whole available phase space if the rotational frequency is increased. The clockwise rotation with the collective angular momentum and the x -component of the initial single-particle angular momentum oriented in opposite directions turns out to be most effective in generating a transition from regular to chaotic motion.

In order to characterize the single-particle motion as a function of ω in a more quantitative manner the chaotic volume μ of the phase space has been determined by making use of maximal Ljapunov exponents which are calculated for 350 trajectories [2]. The chosen initial conditions represent the whole available phase space. The chaotic volume μ as a function of ω is shown in Fig.1. The chaotic volume increases with growing ω . For necked-in potentials ($\delta=0.6$) a saturation value of $\mu \approx 1$ (fully chaotic phase space) is achieved already for a very low value of ω . For weakly deformed potentials ($\delta=0.9, 0.8$) an oscillatory structure is superimposed, the relative minima of which indicate a relative stabilization of regular orbits for certain ratios of the single-particle and collective frequency. This behaviour is different for clockwise and counterclockwise rotation of the potential.

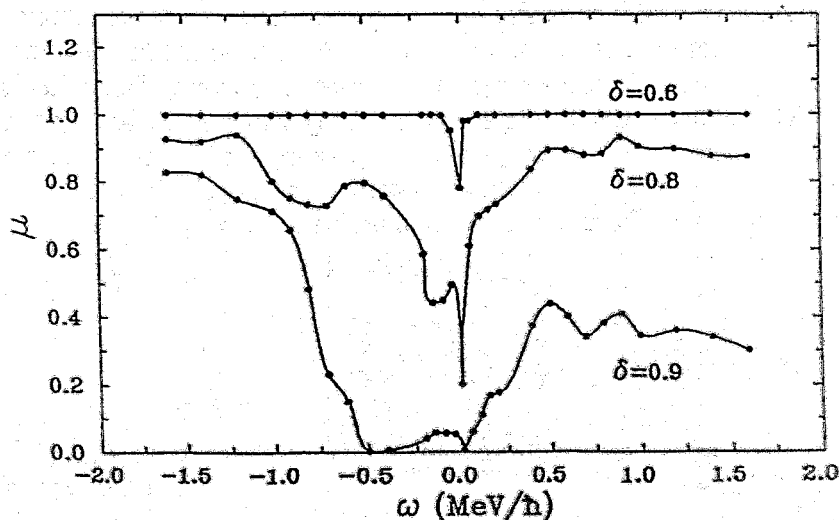


Fig.1 Chaotic volume μ as a function of the frequency ω for various deformation parameters δ .

REFERENCES:

- [1] J. Reif et al., *J. Phys. A: Math. Gen.* **25** (1992) L115
- [2] B. Milek et al., *Z. Phys.* **A339** (1991) 231

Loss of Spectroscopic Information due to Strong External Coupling^{DW}

W. ISKRA¹ M. MÜLLER AND I. ROTTER²

Forschungszentrum Rossendorf, Institut für Kern- und Hadronenphysik

¹ On leave of absence from Soltan Institute for Nuclear Studies,
00-681 Warszawa, Poland

² also Technische Universität Dresden, Abteilung Physik,
O-8027 Dresden, Germany

The properties of the atomic nucleus are investigated from the point of view of selforganization. The model used in the present calculations is the continuum shell model [1,2] which describes the nucleus as an open quantum mechanical system embedded in the continuum of decay channels (subspace P). That leads to a nonlinear Schrödinger equation with an effective Hamiltonian $H_{QQ}^{eff} = QHQ + QHPG_P^{(+)}PHQ$, which describes the system in the subspace of bound states $Q = \sum_R |\phi_R^{SM}\rangle \langle \phi_R^{SM}|$, and energy dependent, complex eigenvalues $\tilde{E}_R = \bar{E}_R(E) + \frac{i}{2}\tilde{\Gamma}_R(E)$. The transition from low to high level density is investigated as a function of the coupling strength between the discrete nuclear states $|\phi_R^{SM}\rangle$ and the environment of decay channels $|\xi_E^{c(+)}\rangle$

$$W_{RR'}^{ex} = \sum_c \int dE' \langle \phi_R^{SM} | \alpha^{ex} V^{res} | \xi_{E'}^{c(+)} \rangle \frac{1}{E^{(+)} - E'} \langle \xi_{E'}^{c(+)} | \alpha^{ex} V^{res} | \phi_{R'}^{SM} \rangle . \quad (1)$$

A redistribution inside the nucleus takes place in a small region around some critical value of the coupling strength α^{ex} . The rearrangement is investigated in detail in [2]. It takes place in the nuclear system if the level density is so large that the distance between the resonances is comparable with their widths, on the average.

In order to illustrate the redistribution, the imaginary parts $\frac{1}{2}\tilde{\Gamma}_R$ of the complex eigenvalues of the effective Hamiltonian H_{QQ}^{eff} are calculated as a function of the coupling strength α^{ex} in the case of two open decay channels and shown in Fig. 1. As long as α^{ex} is small, the widths of all modes increase with increasing coupling strength α^{ex} between bound and continuous states. Beyond some critical value α_{cr}^{ex} , the widths of most modes *decrease* with increasing coupling strength while in some cases they *increase very slowly* ("trapping"). In contrast to this, the widths of some modes – their number is equal to the number of open decay channels – *increase very quickly* with increasing coupling strength α^{ex} from the very beginning. Here the influence of the environment is perceptible. As a result, the widths of the trapped modes are much smaller than those of the two fast modes for $\alpha > \alpha_{cr}$.

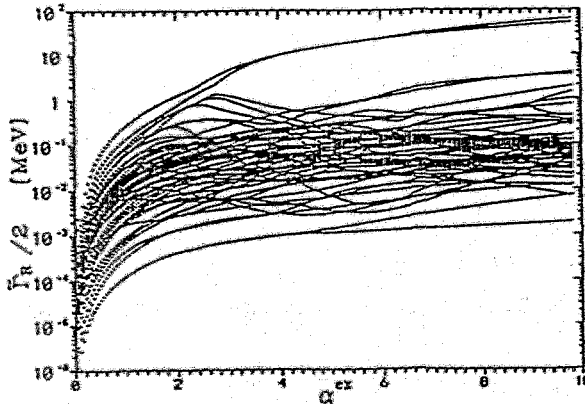


Figure 1

The imaginary part of the complex eigenvalues $\tilde{E}_R = \bar{E}_R - \frac{i}{2}\tilde{\Gamma}_R$ versus α^{ex} . The calculations are performed at $E = 34.7$ MeV for $N = 70$ resonance states and $K = 2$ open decay channels.

In Fig. 2, the widths $\tilde{\Gamma}_R$ are shown as a function of the energy E_{cm} of the system for $\alpha^{ex} = 2$ and 6. The position of the inelastic threshold is at $E_{cm} = 6.3$ MeV (Fig. 2a,b) and shifted to 30.0 MeV (Fig. 2c,d). The $\tilde{\Gamma}_R^J$ depend smoothly on energy with the exception of threshold effects. The influence of the inelastic threshold on the widths can be seen at all α^{ex} (Fig. 2c,d). The pictures show clearly the appearance of one broad mode below the inelastic threshold at large α^{ex} , while there are two broad modes as soon as two channels are open. It is interesting to see that the one broad mode below the inelastic threshold is not among the two broad modes above the threshold. This result illustrates very nicely that the original spectroscopic information of a state is not decisive for the question whether a mode becomes trapped or relevant.

Summarising the rearrangement proceeds in such a manner that the spectroscopic information on the resonance states which is relevant at low level density is *lost* at high level density. As a result of the redistribution, the effective number of degrees of freedom is reduced at the time and energy scale characteristic of the system. Only a few unstable modes become relevant for describing the decay process and their number is exactly equal to the number of open decay channels. In other words, the environment imprints its properties into the system.

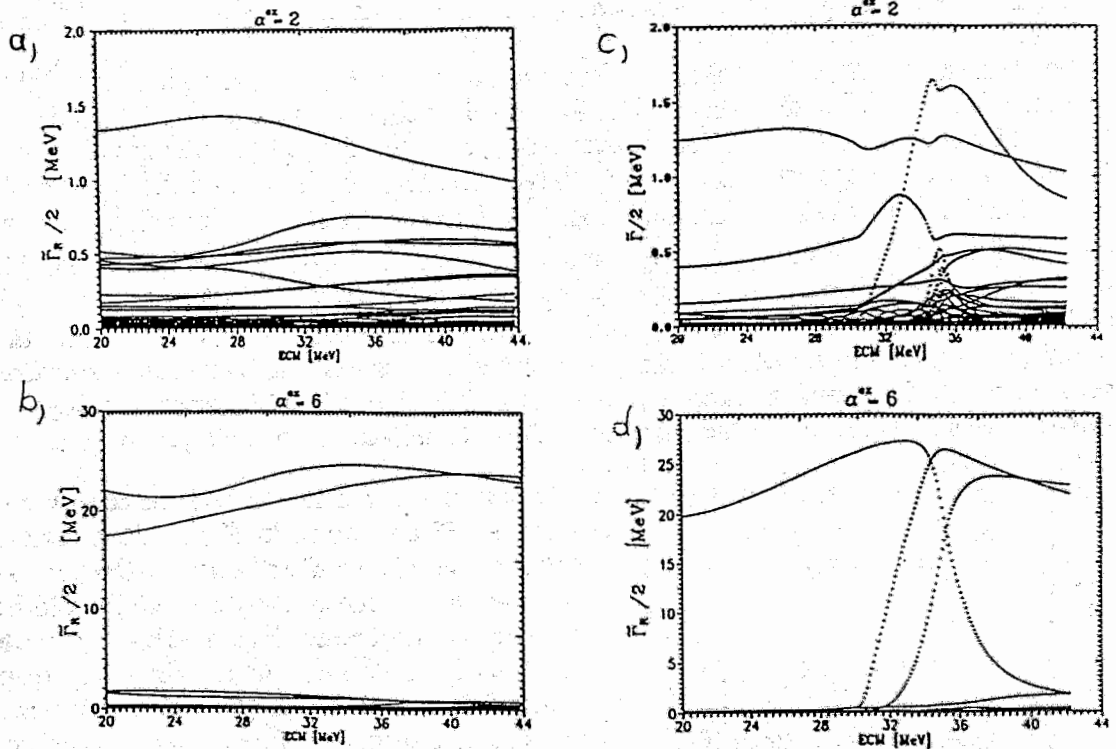


Fig.2 The imaginary part $\frac{1}{2}\tilde{\Gamma}_R$ of the complex eigenvalues \tilde{E}_R versus the center-of-mass energy E of the system ($E_R = E + 12.1$ MeV) for $\alpha^{ex} = 2$ (2a,c) and 6 (2b,d). The second channel opens at 6.3 MeV (2a,b) and at 30.0 MeV (2c,d), respectively ($E=34.7$ MeV, 70 resonances, 2 channels)

REFERENCES

- [1] I. Rotter, Rep. Progr. Phys. 54, 635 (1991) and references therein
- [2] W. Iskra, M. Müller, I. Rotter, "Selforganization in the nuclear system I: The slaving principle"; to be published

Acknowledgment: The present investigations are supported by the Deutsche Forschungsgemeinschaft (Ro 922/1) and by the Bundesministerium für Forschung und Technologie (WTZ X081.39).

Formation of a New Order^{DW}

W. ISKRA¹ M. MÜLLER AND I. ROTTER²

Forschungszentrum Rossendorf, Institut für Kern- und Hadronenphysik

¹ On leave of absence from Soltan Institute for Nuclear Studies,
00-681 Warszawa, Poland

² also Technische Universität Dresden, Abteilung Physik,
O-8027 Dresden, Germany

Systems described by non-linear equations are expected to be selforganized. Their properties are determined by the interplay between internal stability and interaction with the environment. The evolution of a system can be traced best by investigating its behaviour near instability points in dependence on some control parameter [1]. Here the systems which were described by classical methods are shown to form stable modes together with a few unstable modes. The unstable modes determine the behaviour of the system while the stable ones are suppressed ("slaving principle"). By that, the complexity of the system is reduced. Further, the information entropy increases, in this case, up to a certain maximal value as a function of the increasing control parameter ("maximal information entropy principle") [1].

In an open quantum mechanical nuclear system, one can also differentiate between stable and unstable modes [2]. Here the full Hamiltonian $H = H_0 + V$ is diagonalised in the subspace of bound states. Therefore the corresponding differential equation becomes nonlinear [2] and describes an open system embedded in the environment of decay channels. That leads to an effective, nonhermitian Hamiltonian $H_{QQ}^{eff} = QHQ + QHG_P^+HQ$ with complex, energy-dependent eigenvalues $\bar{E}_R = \bar{E}_R + \frac{i}{2}\bar{\Gamma}_R$ and complex eigenstates $\bar{\phi}_R$. In this relation Q is the projector to the bound state part ($Q = |\phi_R^{SM}\rangle\langle\phi_R^{SM}|$) of the Hilbertspace $Q + P = 1$ and P to the environment of scattering functions. The second term in H_{QQ}^{eff} represents the coupling to the continuum which is changed in the present calculation by means of a control parameter α^{ex} . The residual interaction is written as $V^{ex} = \alpha^{ex} \cdot V$ in order to study the evolution of the system under the influence of the environment of scattering states.

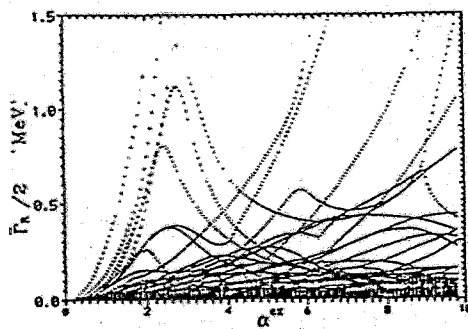


Figure 1

The imaginary part of the complex eigenvalues $\bar{E}_R = \bar{E}_R - \frac{i}{2}\bar{\Gamma}_R$ versus α^{ex} . The calculations are performed at $E = 34.7 \text{ MeV}$, $N = 70$ resonance states and $K = 2$ open decay channels.

The widths $\bar{\Gamma}_R$ as a function of the control parameter α^{ex} are shown in Fig. 1. At a certain value $\alpha_{cr}^{ex} \approx 2.6$, a redistribution in the nucleus takes place as a consequence of which the widths of two states (fast relevant modes) become much larger than the widths of all the other ones (trapped modes). The number of these relevant modes is exactly equal to the number of open decay channels. The picture shows, further, that the redistribution at $\alpha_{cr}^{ex} \approx 2.6$ is not the only one. At higher values of α^{ex} further redistributions take place by which broad modes of the second and third generation are created. These results illustrate the slaving principle holding in selforganizing systems.

The eigenfunctions of H_{QQ}^{eff} are $\bar{\phi}_R = \sum_{R'} \beta_{RR'} \phi_{R'}^{SM}$. In order to characterize their mixing in relation to ϕ_R^{SM} , the values $I_\beta^R = -\sum_{i=1}^N |\hat{\beta}_{Ri}|^2 \ln |\hat{\beta}_{Ri}|^2$ with $|\hat{\beta}_{Ri}|^2 = \frac{|\beta_{Ri}|^2}{\sum_i |\beta_{Ri}|^2}$ are calculated. We consider the sum $I_\beta = \sum_R I_\beta^R$ as the information entropy.

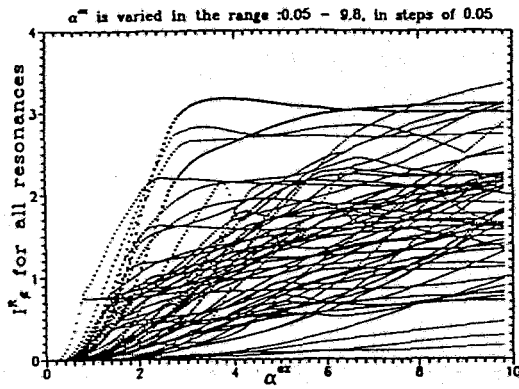


Figure 2 The mixing coefficients I_{β}^R in relation to the basic set of the shell model wavefunctions Φ_R^{SM} versus α^{ex} ($E = 34.7$ MeV, $N = 70$, $K = 2$).

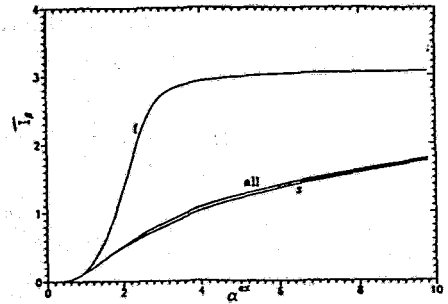


Figure 3 The mixing coefficients I_{β}^R averaged over the two broad modes (f), all 70 modes (all) and the 68 trapped modes (s) in relation to the basic set of shell model wavefunctions Φ_R^{SM} versus α^{ex} ($E = 34.7$ MeV, $N = 70$, $K = 2$).

The information entropies calculated by us, reflect all the features of the reorganization process which we observed in *Fig. 1*. At $\alpha^{ex} < 1$, the widths as well as the I_{β}^R of all states are rising with increasing α^{ex} . For larger α^{ex} but $\alpha^{ex} < \alpha_{cr}^{ex}$, the widths and the I_{β}^R of a few states increase strongly in comparison with those of the other ones. At $\alpha^{ex} \approx \alpha_{cr}^{ex}$ up to $\alpha^{ex} \approx 4$, the mixing coefficients I_{β}^R of the two relevant modes reach their maximal value and remain more or less constant as a function of α^{ex} . In correspondence to this, the two broad modes behave like isolated resonances starting from $\alpha^{ex} \approx 4$. At $\alpha^{ex} \approx 6$, a new generation of broad modes appears (*Fig. 1*). In the same region, we observe a comparably strong increase of the I_{β}^R of some trapped modes (*Fig. 2*).

In *Fig. 3* the information entropy of the unstable modes increases at the instability point much stronger than that of the stable modes. They are a signature for the driving role of the fast modes in the process of redistribution at the instability point which is formed under the influence of the environment. This is in accordance to the results of Haken [1].

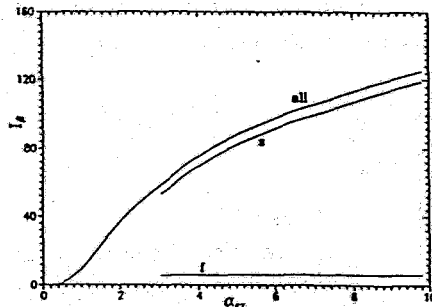


Figure 4

The information entropy I_{β} for all 70 modes (all) as well as for the relevant (f) and irrelevant (s) modes beyond the instability point, in relation to the basic set of the shell model wavefunctions Φ_R^{SM} versus α^{ex} ($E = 34.7$ MeV, $N = 70$, $K = 2$).

In *Fig. 4* it can be seen easily that I_{β} increases with increasing α^{ex} for all α^{ex} if the sum runs over all 70 states or over the 68 trapped modes. This result is in full accordance with the maximal information entropy principle. Our results confirm $I'^{max} < I^{max}$, where $I'^{max} = K \cdot \ln K$ is the information entropy of the relevant modes and $I^{max} = N \cdot \ln N$ is the information entropy of all modes. According to the formation of a new order in the system, the information entropy I' is reduced at $\alpha^{ex} > \alpha_{cr}^{ex}$ in comparison to the information entropy I for $\alpha^{ex} < \alpha_{cr}^{ex}$ where all degrees of freedom are equally important. Thus, in reaching a relevant ordered state far from thermal equilibrium, the exceeding entropy is *not* exported into the environment but diminished inside the system by creating (irrelevant) trapped modes (noise) near to thermal equilibrium.

REFERENCES

- [1] H. Haken, *Information and Selforganization*, Springer-Verlag Berlin, Heidelberg 1988
- [2] I. Rotter, *Rep. Progr. Phys.* 54, 635 (1991) and references therein

Acknowledgment: The present investigations are supported by the Deutsche Forschungsgemeinschaft (Ro 922/1) and by the Bundesministerium für Forschung und Technologie (WTZ X081.39).

Resonance States in Exited Systems^{DW}

W. ISKRA¹ M. MÜLLER AND I. ROTTER²

Forschungszentrum Rossendorf, Institut für Kern- und Hadronenphysik

¹ On leave of absence from Soltan Institute for Nuclear Studies,
00-681 Warszawa, Poland

² also Technische Universität Dresden, Abteilung Physik,
O-8027 Dresden, Germany

The transition from low to high level density in an atomic nucleus is traced as a function of the coupling strength between the discrete nuclear states and the environment of the scattering states. In an exact theory – the model used is the continuum shell model [1] – the coupling to the continuum of decay channels has to be taken into account from the very beginning. The Schrödinger equation must be solved with an ansatz containing not only the discrete states but also the scattering states. The spectroscopic properties are then described in a subspace Q of the whole function space P+Q.

The corresponding effective Hamiltonian H_{QQ}^{eff} , which describes an open quantum system, is nonhermitian and the diagonalizing transformation is not unitary but orthogonal. Its eigenfunctions $|\tilde{\phi}_R\rangle = \sum_R \beta_{RR'} |\phi_{R'}^{SM}\rangle$ ($|\phi_{R'}^{SM}\rangle$ is the usual shell model solution) and the eigenvalues $\tilde{E}_R = \bar{E}_R(E) + \frac{1}{2}\tilde{\Gamma}_R(E)$ are complex. Then it follows, that the wavefunctions $|\tilde{\phi}_R\rangle$ are not normalised with the scalarproduct. Instead it is $\langle \tilde{\phi}_R | \tilde{\phi}_R \rangle \geq 1$ and $(|\tilde{\phi}_R\rangle)^2 = 1$. Because of that, the relation between widths and partial widths reads $\tilde{\Gamma}_R = \langle \tilde{\phi}_R | \tilde{\phi}_R \rangle \sum_c |\tilde{\gamma}_{Rc}|$.

We are varying the coupling to the environment by multipling the residual interaction with a factor α^{ex} . At a critical value of the coupling strength between system and environment, a redistribution of the spectroscopic values takes place. Most states of the system become long-lived (trapped) while a few of them are distinguished by large widths. The number of these states, the widths of which are large as a result of the redistribution taking place in the nucleus, is exactly equal to the number of open decay channels [2](see Fig.1).

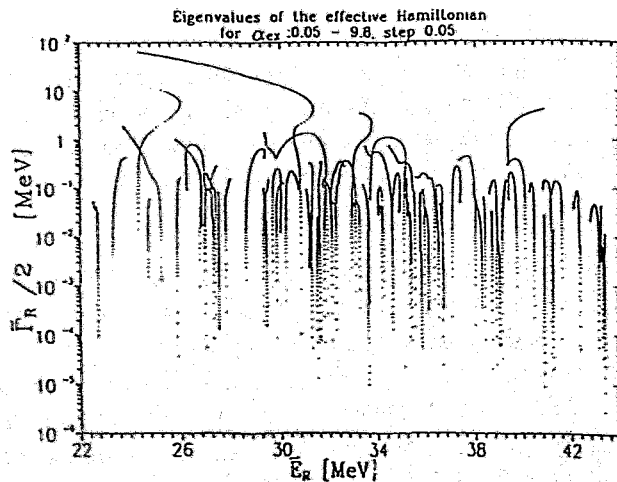


Figure 1

The complex eigenvalues of the effective Hamiltonian $\tilde{E}_R = \bar{E}_R - \frac{1}{2}\tilde{\Gamma}_R$ for α^{ex} varied from 0.05 up to 9.8 in steps of 0.05. ($E=34.7$ MeV, $N=70$ resonances, $K=2$ open decay channels).

We focus mainly on the differences in the wavefunctions of trapped and broad modes which occur, in any case, by selforganization at high level density.

In Fig. 2, $\langle \tilde{\phi}_R | \tilde{\phi}_R \rangle$ is given for all 70 resonances and different α^{ex} . As one can see from the figure, $\langle \tilde{\phi}_R | \tilde{\phi}_R \rangle$ stays always near by one, with the exception of a few comparably narrow regions of α^{ex} where redistributions in the system take place. In the first region ($\alpha^{ex} = 2 - 3$) the two broad modes separates from each other. At higher values of α^{ex} further redistributions take place, and some other "broader" modes are growing on (Fig.1), but their lifetimes remain longer than those of the first broad modes.

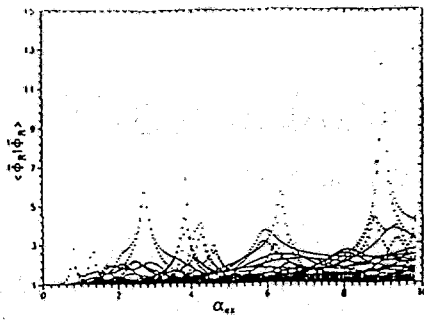
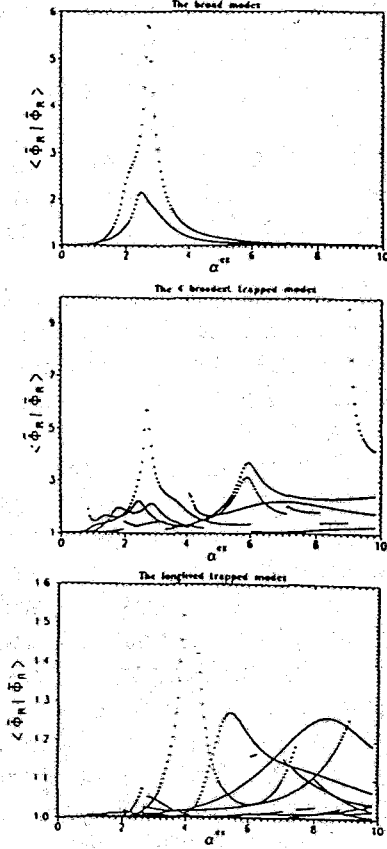


Figure 2

The $\langle \tilde{\Phi}_R | \tilde{\Phi}_R \rangle$ as a function of α^{ex} ($E=34.7$ MeV, $N=70$, $K=2$).



The dependence of $\langle \tilde{\Phi}_R | \tilde{\Phi}_R \rangle$ on α^{ex} is shown for the two fast (f) modes (Fig. 3a) as well as for some slow (s) modes (Fig. 3b,c). For the fast (broad) modes, the scalar product increases up to 6 in the critical region where the redistribution in the nucleus occurs. For larger α^{ex} , it decreases again. Below and beyond the critical region, $\langle \tilde{\Phi}_R^f | \tilde{\Phi}_R^f \rangle \approx 1$, i.e. the resonances R_f behave like usual resonances, although they *do* overlap, in the sense that the relation $\tilde{\Gamma}_R \approx \sum_c |\tilde{\gamma}_{Rc}|$ is fulfilled. This result is surely connected with the fact that the channel wavefunctions $\{\xi_E^c\}$ for different channels c are orthogonal to each other. Therefore, the large overlapping integrals $\langle \xi_E^c | \tilde{\Omega}_R^f \rangle$ suggest $\langle \tilde{\Omega}_R^f | \tilde{\Omega}_{R'}^f \rangle \approx \delta_{RR'}$, where $|\tilde{\Omega}_R \rangle = |\phi_R \rangle + \sum_c \int_{E_c} dE' \frac{1}{E-E'} |\xi_E^c \rangle \langle \xi_E^c | V | \phi_R \rangle$ is the full wavefunction for a resonance with the bound and scattering part. The wavefunctions $\tilde{\Phi}_R^s$ of the other modes show a different behaviour (Fig. 3). For most of them, $\langle \tilde{\Phi}_R^s | \tilde{\Phi}_R^s \rangle$ remains larger 1 for large α^{ex} . The "gaps" in Figs. 3b, c arise because the ordering of the resonances according to the value of their widths changes with α^{ex} . In spite of their small widths, the trapped modes do *not* behave like isolated resonances which are independent from each other. Here $\tilde{\Gamma}_R < \sum_c |\tilde{\gamma}_{Rc}|$ holds. They are correlated due to the existence of the broad unstable modes by which they are overlapped. It is worth-while to mention that such a result follows not only from the numerical calculations given in this paper but is very well known from experimental nuclear physics studies, e.g. from the isobaric analogue resonances.

Figure 3

The $\langle \tilde{\Phi}_R | \tilde{\Phi}_R \rangle$ as a function of α^{ex} for the two fast modes (3a), the four broadest trapped modes (3b) and other trapped modes (3c) ($\alpha^{in} = 1$, $E=34.7$ MeV, $N=70$, $K=2$).

As a result, the wavefunctions of the broad modes overlap strongly with the channel wavefunctions due to the large contribution of their scattering part $\tilde{\omega}_R^f$ in $\tilde{\Omega}_R^f$. They behave like isolated resonances with the exception of the region around α_{cr}^{ex} , at which the rearrangement inside the nucleus takes place (Fig. 3a) and where their wavefunctions are complex. At higher coupling strength, they repel each other. That means, they are described quite well by neglecting the trapped modes altogether. The wavefunctions of the trapped modes, on the contrary, are described well by the $\tilde{\Phi}_R$ ($\tilde{\Omega}_R^s \approx \tilde{\Phi}_R^s$).

REFERENCES

- [1] I. Rotter, Rep. Progr. Phys. 54, (1991) 635 and references therein
- [2] V.V. Sokolov and V.G. Zelevinsky, Ann. Phys. (N.Y.) 216, (1992) 323

Acknowledgment: The present investigations are supported by the Deutsche Forschungsgemeinschaft (Ro 922/1) and by the Bundesministerium für Forschung und Technologie (WTZ X081.39).

New semiclassical results for the baker map

F.-M. DITTES¹ AND U. SMILANSKY²

¹ *Forschungszentrum Rossendorf, Institut für Kern- und Hadronenphysik*

² *The Weizmann Institute of Science, Department of Nuclear Physics, 76100 Rehovot, Israel*

The traditional treatment of chaotic systems in the semiclassical approximation (SCA) is based on the consideration of periodic orbits of the corresponding classical system, and on the calculation of quantum variables like the level density $d(E)$ on the basis of Gutzwiller-like formulas:

$$d(E) \sim \sum A_p \exp(iS_p/\hbar). \quad (1)$$

Here the sum runs over all periodic orbits p , S_p denotes the classical action of the corresponding orbit, and the A_p are certain weight factors. Since the number of orbits entering eq. (1) increases exponentially with the energy resolution ΔE one is interested in, the application of eq. (1) is practically restricted to large ΔE or, correspondingly, small times.

On the other hand, it has been realized recently that, at least for certain systems, the SCA is able to describe the fine structure of the spectrum very well [1]. In particular, it has been shown that the SCA for the spectral form factor $K(t)$, defined as the Fourier transform of the two-point correlation function of the spectrum, follows the quantum predictions up to times $t > h/\bar{d}$ (\bar{d} is the mean level distance), where the discreteness of the spectrum is already important.

In order to investigate such long-time behaviour in more detail, and in particular to determine the time scale at which the SCA starts to fail, more powerful computational techniques have to be employed. One of such techniques proposed recently [2] is based on the fact, that for long periodic orbits the quantities S and A entering eq. (1) can be factorized, approximately, into contributions of shorter trajectories. This allows one to define a *semiclassical transfer operator* V which describes the evolution of the system over a given time interval (for kicked systems or maps, over one period) in terms of classical quantities, and to generate an expression equivalent to (1) by considering the traces (over phase space) of powers of this operator.

We investigated this technique on one of the simplest chaotic systems, the baker map. The latter one is defined as a mapping of the unit square onto itself: $x' = \{2x\}$, $y' = y/2 + [2x]/2$, where $\{x\}$ and $[x]$ represent the integer and fractional parts of x , respectively. The transfer operator V is given by

$$V(x, y; x', y') = \sqrt{2} \delta(x - (x' + [2y'])/2) \delta(y - (2y' - [2y'])) \exp(2\pi i L(1-x)[2x]). \quad (2)$$

Here, the expression in the exponent results from the action of classical trajectories; L denotes the inverse Planck constant: $L = 1/\hbar$, and is required to be an integer.

We studied various quantities expressed in terms of powers of V , V^n , over a wide range of n and L . In particular, we concentrated on the reliability of different finite-dimensional approximations to V . Comparing our results with those ones based on the consideration of the lowest 2^{31} periodic orbits [1], we find an excellent agreement, the computational effort increasing only *powerlike* with the required precision. This allows us to go far beyond periodic orbit calculations. In particular, for the first time we have been able to show an exponential increase of the spectral form factor $K(t)$ over a wide range of h . This indicates a breakdown of the SCA, the breakdown time t_c going like $h^{-1/2}$. We relate this effect to the existence of arbitrary fine (fractal-like) structures in the distribution of classical actions of periodic orbits.

Based on the obtained experience, a semiclassical treatment of realistic kicked systems is in progress.

REFERENCES

- [1] N. Argaman, E. Doron, J. Keating, A. Kitaev, M. Sieber and U. Smilansky, preprint WIS-92/73/Sept-PH, submitted to *Phys. Rev. Lett.*
- [2] E. B. Bogomolny, *Nonlinearity* 5 (1992) 805

Correlation Dynamics in Nuclear Matter and Landau's Kinetic Equation^D

A. PFITZNER AND H. HOFMANN¹

*Forschungszentrum Rossendorf, Institut für Kern- und Hadronenphysik
¹ Technische Universität München, Physik Department*

Properties of infinite systems for excitation energies at the Fermi surface (low temperature) and small momentum transfer q (long-wavelength limit) are successfully described by Landau Fermi liquid theory. For a generalisation of this approach (cf. [1]) it is of interest to relate it to microscopic theories for nuclear matter. In particular, it is tempting to recover Landau's equation from time-dependent density matrix theory (TDDM) and to relate, e.g. the damping of zero sound in liquid ${}^3\text{He}$ to the damping of giant resonances in nuclei. Landau's (Fourier-transformed) kinetic equation reads

$$(\omega - v_p q) \delta\rho(p, q, \omega) + v_p q \frac{\partial n_p}{\partial \epsilon_p} \left[\sum_{p'} f_{pp'} \delta\rho(p', q, \omega) + \delta U \right] = iI(\delta\rho). \quad (1)$$

Here, $\delta\rho(p, q, \omega) = \rho(p, q, \omega) - n_p$ is the deviation of the one-body density from global equilibrium [2], ϵ_p the quasi-particle energy, $v_p = \frac{\partial \epsilon_p}{\partial p}$, and $f_{pp'}$ are the Landau forces. $I(\delta\rho)$ is a collision term, usually taken in relaxation time approximation $I(\delta\rho) \approx -\tau_{rel}^{-1} \delta\rho^{le}$, with $\delta\rho^{le}$ the deviation from local equilibrium. In (1), memory effects are neglected. The mean-field part of (1) is completed by an external perturbation δU in view of the study of response functions [2].

In the small-amplitude limit of TDDM the one-body equation $i\delta\dot{\rho} - [h(\rho^0), \delta\rho] - [\delta h + \delta U, \rho^0] = tr_{(2)}[v, \delta C]$ is coupled with the equation for the deviation $\delta C = C - C^0$ of the two-body correlation function from the ground state correlations C^0 . For nuclear matter we apply a plane-wave single-particle basis $|p\rangle$, leading to a quantum-kinetic equation for $\delta\rho(p, q, \omega) = \langle p+q/2 | \delta\rho(\omega) | p-q/2 \rangle$. For a first guess it is sufficient to solve the equation for $\delta C(t)$ in Born approximation, neglecting ground state correlations. In the resulting collision term we omit the q -dependence for simplicity. For small q , the final one-body equation may be cast into the form

$$\begin{aligned} (\omega - \Delta_p(\omega) - qv_p) \delta\rho(p, q, \omega) + q v_p \frac{\partial n_p}{\partial \epsilon_p} \sum_{p'} [(v(0) - v(p-p')) \delta\rho(p', q, \omega) + \delta U] \\ \approx -i \frac{1}{\tau_p(\omega)} \delta\rho(p, q, \omega) - \sum_{p'} M(p, p', \omega) \delta\rho(p', q, \omega). \end{aligned} \quad (2)$$

Here, $v(0) - v(p-p')$ is the Fourier-transformed HF potential at $q=0$. The energy shift Δ_p and the life time τ_p originate from the decay of a particle $|p+q/2\rangle$ and a hole $|p-q/2\rangle$ into $2p-1h$ and $2h-1p$ states and correspond to contributions from the respective self-energies in Green's function formalism. In particular, we find

$$\begin{aligned} \tau_p(\omega)^{-1} \approx \pi \sum_{kk'} |v(p-k')|^2 (n_k \bar{n}_{k'} \bar{n}_{p+k-k'} + \bar{n}_k n_{k'} n_{p+k-k'}) \cdot \\ \cdot \{ \delta(\omega + \Delta\epsilon(p, k, k')) + \delta(\omega - \Delta\epsilon(p, k, k')) \}, \end{aligned} \quad (3)$$

with $\bar{n} = 1 - n$ and $\Delta\epsilon(p, k, k') = \epsilon_p + \epsilon_k - \epsilon_{k'} - \epsilon_{p+k-k'}$. The last term on the r.h.s. of (2) describes the coupling with $2p-2h$ -intermediate states via exchange and interference processes (cf. [3]). The imaginary part of $M(p, p', \omega)$ prevents the description of the damping

by a common relaxation time τ_{rel} .

Eq. (2) is a generalisation of (1) in so far as it retains the memory of the system. This shows up in the ω -dependence of $\Delta_p(\omega)$, $\tau_p(\omega)$ and $M(p, p', \omega)$. In contrast to this, the Landau forces $f_{pp'}$ as well as the collision term (or τ_{rel}) in (1) are assumed to be ω -independent. The additional ω -dependence in (2) complicates the pole-behaviour of the density-density response function defined by $\chi = \frac{-\delta n(q\omega)}{\delta U}$, with $\delta n(q\omega) = \sum_p \delta \rho(p, q, \omega)$. The basic structure of χ as used in [2] is retained only if the sum

$$\sum_p [\omega - \Delta_p(\omega) - q v_p + i/\tau_p(\omega)]^{-1} (q v_p \frac{\partial n_p}{\partial \epsilon_p} v(p-p') - M(p, p', \omega)) := F(p', q, \omega) \quad (4)$$

may be replaced by an average with respect to p' , $F(p', q, \omega) \approx \langle F(q\omega) \rangle$. In this case we obtain an expression which resembles the response function in [2],

$$\chi(q, \omega) \approx \frac{\kappa(q, \omega) \chi^0(q, \omega)}{1 + \kappa(q, \omega) v(0) \chi^0(q, \omega)},$$

$$\kappa(q, \omega) = \frac{1}{1 - \langle F(q, \omega) \rangle}, \quad (5)$$

with $\chi^0(q, \omega) = \sum_p q v_p \frac{\partial n_p}{\partial \epsilon_p} [\omega - \Delta_p(\omega) + q v_p + i/\tau_p(\omega)]^{-1}$ the response function without Landau forces. Obviously, the ω -dependence of χ^0 is more complicated than that of the "unperturbed" response function χ_{00}^0 given in [2].

REFERENCES:

- [1] H. Heiselberg, C.J. Pethick, D.G. Ravenhall, Phys. Rev. Lett. 61 (1988) 818
- [2] H. Hofmann, D. Kiderlen, I. Tsekhmistrenko, Z. Phys. A 341 (1992) 181
- [3] A. Pfitzner, W. Cassing, this report

Mixing of pp- and ph-effects in the relaxation of the one-body density

A. Pfitzner

Forschungszentrum Rossendorf, Institut für Kern- und Hadronenphysik

One-body propagation in a strongly interacting many-body medium is controlled by two-body correlations C , according to $i\dot{\rho} - [h(\rho), \rho] = \text{tr}_2[v, C]$. The equation of motion for C is given in [1]. A rigorous integration of the equation, comprising pp (ladder)- as well as ph (loop) contributions, is extremely complicated by the appearance of diagrams containing combinations of ladders and loops. To account approximately for this mixing we propose the following scheme. First of all we specify different types of correlations by their labels [1]. By inspection of the one-body equation we observe that only special correlations \hat{C} couple with ρ , in particular doorway correlations and 2p-2h-amplitudes. The evolution of \hat{C} is determined by "propagating" correlations, e.g. $C^{pp} = C_{pppp}$ and $C^{ph} = C_{phph}$ which, in their turn, couple again with \hat{C} . This mutual internetting is truncated neglecting \hat{C} in the equations for C^{pp} and C^{ph} , which is supported by the argument of different time-scales on the one- and two-body level [2]. Neglecting one of the channels in the equation for \hat{C} allows for a straightforward integration and yields, e.g., a system of coupled equations for ρ and C^{ph} [2]. In the general case, this elimination of \hat{C} is only possible switching from the usual space of 4-label operators to a 6-label space. This way, ρ , C^{pp} and C^{ph} are coupled with each other, but now the respective equations of motion contain effective in-medium interactions comprising loop-ladder combinations.

For illustration we consider the relaxation of occupation numbers $n_\alpha = \rho_{\alpha\alpha}$, as induced by $\hat{C} = C_{phpp}$, in the HF-basis, $\hat{h}|\alpha\rangle = \epsilon_\alpha|\alpha\rangle$, and apply the Markov limit. With the effective interactions \hat{G} and G (see below), the uncorrelated two-body density $\rho_{20} = A(\rho\rho)$ and $\dot{h}(\rho) = t + \text{tr} \text{Re} \hat{G} \rho$ the equation for $n_\alpha(t)$ reads

$$\begin{aligned}
 i\dot{n}_\alpha \simeq & \alpha \{ [\hat{h}(\rho), \rho] \} |\alpha\rangle + i \sum_3 \langle \alpha 3 | [\text{Im} \hat{G}(\epsilon_\alpha), \rho_{20}]_+ | \alpha 3 \rangle - \\
 & \sum_3 \langle \alpha 3 | [G(\epsilon_\alpha) g^{pp}(\epsilon_\alpha + \epsilon_3), (\rho_{20} + C^{pp})^+ (v^\pm)^+] | \alpha 3 \rangle - \\
 & \sum_{1,2,3,2',3'} \{ G^a(\epsilon_\alpha)_{\alpha 3,12} g_{23}^{ph}(\epsilon_\alpha - \epsilon_1) C_{23',32'}^{ph} v_{12',\alpha 3'}^\perp + \\
 & v_{\alpha 3,12}^\perp C_{23',32'}^{ph} g_{2',3'}^{ph}(\epsilon_\alpha - \epsilon_1) G^a(\epsilon_\alpha)_{12',\alpha 3'}^+ \} \quad (1)
 \end{aligned}$$

The blocking operators Q^\pm and Q^\perp defining $v^\perp = Q^\perp v^a$ and $v^\pm = Q^\pm v$ are explained in [3]. The first term of (1) describes propagation in the renormalised mean field. The 2. term has the structure of a loss term, which becomes evident using the relation $\text{Im} \hat{G} = \hat{G} Q^\pm \text{Im} g \hat{G}^\pm$, with g the usual mean-field propagator. Both terms are exclusively generated by the doorway correlation \hat{C} . The correlations $C^{pp}(t)$ and $C^{ph}(t)$ control the evolution in the pp- and ph-channel. The 3. term constitutes a generalised gain term as can be verified by using a proper stationary solution $C^{pp}(t) \simeq C^{pp}(\rho(t))$. The last term contains the ph-correlations responsible for density fluctuations [2]; it may be expressed in terms of collective RPA-phonons.

At first glance, we have achieved a separation of the channel contributions in the one-body equation (1). However, the mixing of pp- and ph-effects is hidden in the effective interactions $\hat{G} = v \hat{\Omega}$ and $G = v \Omega$. The Moeller operators $\hat{\Omega}$ and Ω are 6-label operators,

e.g. $G_{\alpha\beta\alpha'\beta'}^a = \sum_{123} v_{\alpha 3, 12}^a \Omega_{123, \alpha'\beta'\beta}$. By way of example, we present the integral equation for Ω by diagrams in Fig. 1 for the case of summing first ladders, then loops.

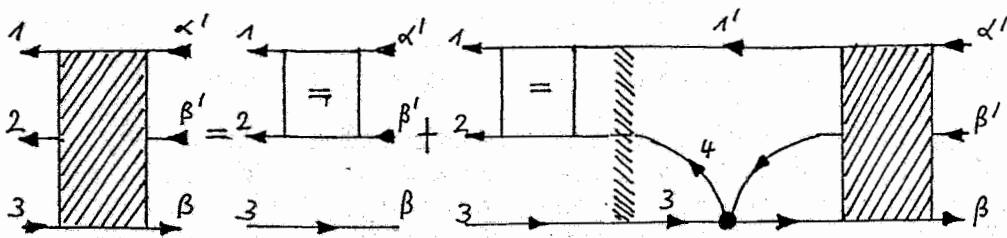
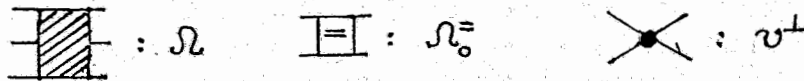


Fig 1 Equation for Ω summing loops after summing ladders by Ω_0^{\equiv}



The 4-label box represents the pp-scattering Moeller operator Ω_0^{\equiv} which follows $\Omega_0^{\equiv} = 1 + g^{pp}v = \Omega_0^{\equiv}$ and defines the Brueckner G-matrix $G_0^{\equiv} = v\Omega_0^{\equiv}$. The shaded region between this box and the ph-interaction v^{\perp} indicates the position of a (diagonal) 6-label propagator $\hat{g}(\omega)_{1'34} = [\omega^{(+)} + \epsilon_3 - \epsilon_{1'} - \epsilon_4]^{-1}$. The operator $\hat{\Omega}$ is related with Ω by $\Omega = \hat{\Omega}\Omega_0^{\perp}$, where Ω_0^{\perp} integrates the ph-channel similar as Ω_0^{\equiv} does for the pp-channel. We recover, in the stationary limit $C^{pp}(\rho(t)) = (\Omega_0^{\equiv} - 1)\rho_{20}$, current approximations, namely (i) first order perturbation theory with $\Omega_0^{\equiv} = 1$, $C^{ph} = 0$ and \hat{C} calculated in Born approximation, and (ii) time-dependent G-matrix theory with $v^{\perp} = 0$ or $\Omega_0^{\perp} = 1$ which yields $\hat{G} = G$ and in addition, $G = G_0^{\equiv}$, because Ω reduces to Ω_0^{\equiv} (see Fig.1).

REFERENCES:

- [1] W. Cassing, A. Peter A. Pfitzner, this report, p.
- [2] A. Pfitzner, L. Muenchow, P. Maedler, Phys. Letters B 218, 295 (1989)
- [3] W. Cassing, A. Pfitzner, Z. Phys. A342,161 (1992)

The Role of Collisions and Long-Range Correlations in the Damping of Collective Motion^{DBG}

A. PFITZNER W. CASSING¹

Forschungszentrum Rossendorf, Institut für Kern- und Hadronenphysik,

¹Institut für theoretische Physik, UNI Giessen

Damping of nuclear excitations allows to study collective motion in competition with incoherent decay mechanisms. In particular giant resonances are a favourite subject for experimental and theoretical efforts in this context.

Usually, collective and incoherent (or collisional) aspects of nuclear motion are attached to long- and short-range correlations respectively. However, the complicated dynamics of these correlations, as described by the hierarchy of time-dependent density-matrices [1], does not allow to disentangle them straightforwardly. We therefore tackle this problem in two steps, guided by the structure of the microscopic equations:

- 1.) We sum up ladders separately, this way accounting for short-range correlations; they care for a renormalisation of the mean field and for instantaneous in- medium two body collisions.
- 2.) We sum up loops to account for long-range correlations; they are operative in between the collisions and, in particular, responsible for ground-state correlations. They are modelled by antisymmetrised collective phonons according to $C \approx A(ff)$, where \hat{f} follows a RPA-like equation [2]. The resulting renormalised equation for the one-body density ρ comprises, in addition to the Brueckner G-matrix collision term, a phonon-particle coupling. Linearisation with respect to $\delta\rho(t) = \rho(t) - \rho^0$ and $\delta f(t) = f(t) - f^0$ and elimination of $\delta f(t)$ provides (i) coupled equations for the stationary solutions ρ^0 and f^0 which describe the correlated ground state, and (ii) an equation for $\delta\rho$ which reads in an arbitrary s.p.-basis $|\alpha\rangle$ [3]

$$i\delta\dot{\rho}_{\alpha\alpha'} - [\bar{h}(\rho^0), \delta\rho]_{\alpha\alpha'} - [\delta\bar{h}, \rho^0]_{\alpha\alpha'} = \delta I_{\alpha\alpha'}^{coll} + I^0(\delta\rho)_{\alpha\alpha'} + \int_0^t dt' \sum_{\gamma\gamma'} M_{\alpha\gamma'\alpha'\gamma}(t-t')\delta\rho_{\gamma\gamma'}(t'). \quad (1)$$

Short-range correlations show up in the renormalised mean field \bar{h} and the linearised collision term δI^{coll} . The long range correlations produce a coupling I^0 with the ground state correlations $C^0 = A(f^0 f^0)$ as well as a memory term originating from induced correlations $\delta C(t) = A(f^0 \delta f(t) + \delta f(t) f^0)$.

The secular equation corresponding to the l.h.s. of (1) is a renormalised RPA-equation with eigenvalues Ω_ν and eigenstates $\xi_{\alpha\alpha'}^\nu$. In the HF-limit, the labels (α, α') reduce to (p,h)- or (h,p)-states.

We introduce collective states ν by the amplitudes $a_\nu(t) = \sum_{\alpha\alpha'} \xi_{\alpha\alpha'}^{\nu*} \delta\rho_{\alpha\alpha'}(t)$, with $\xi_{\alpha\alpha'}^\nu = (n_{\alpha'} - n_\alpha)^{-1} \xi_{\alpha\alpha'}^\nu$, derive an equation of motion for $a_\nu(t)$ using (1) and study solutions $a_\nu(t) \propto \exp(-i\omega_\nu - \Gamma_\nu/2)t$. The resulting equations for widths Γ_ν and positions ω_ν may be cast into the form

$$\Gamma_\nu \approx \Gamma_\nu^{coll} + \Gamma_\nu^0 + \Gamma_\nu^{mem}(\omega_\nu), \quad \omega_\nu \approx \Omega_\nu + \Delta\omega_\nu. \quad (2)$$

The shift $\Delta\omega_\nu$ stems from the real part of the r.h.s. of (1). The spreading width Γ_ν separates into three parts according to the three mechanisms discussed after (1). Collisional damping Γ_ν^{coll} couples the (ph)- subspace to the 2p-2h- intermediate states, whereas Γ_ν^0 may couple (ph)- with more complex states via annihilation of a 2p- 2h- state spontaneously created by

ground state correlations $C_{pp,hh}^0$ (see fig.1). Γ_{ν}^{coll} and Γ_{ν}^0 , in their turn, separate into decay, exchange and interference (see fig.2) contributions. At variance to Γ_{ν}^{coll} and Γ_{ν}^0 , the memory term in (2) comprises intermediate phonons χ^{μ} (see fig.3). These phonons model the induced correlations δC and control the memory-time of the system.

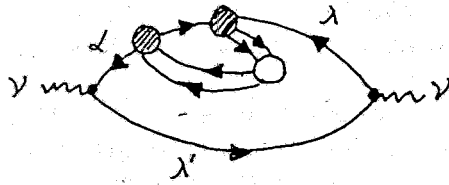


Fig. 1 Particle decay with ground-state correlations

⊗ : G-matrix

○ : correlation C^0

γ wavy line : phonon-particle vertex

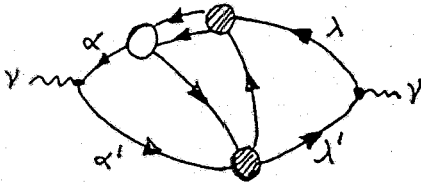


Fig. 2 Interference contribution with ground-state correlations

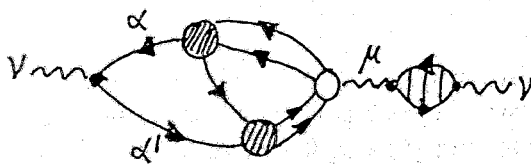


Fig. 3 Contribution from the memory term

O^{μ} : $\delta C^{\mu} = A(f^0 \chi^{\mu} + \chi^{\mu} f^0)$

γ wavy line : phonon-phonon coupling

REFERENCES:

- [1] W. Cassing, A. Pfitzner, Z. Phys. A 337 (1990) 175
- [2] W. Cassing, A. Peter, A. Pfitzner, Nucl. Phys. A in print
- [3] A. Pfitzner, W. Cassing, submitted for publication

Collisional and Collective Aspects in the Formation of Two-Body Correlations^{BG}

W. CASSING¹ A. PETER¹ AND A. PFITZNER

Forschungszentrum Rossendorf, Institut für Kern- und Hadronenphysik

¹ *Institut für Theoretische Physik, Universität Giessen*

The interplay between single-particle (or collisional) and collective motion is still a fundamental and fascinating problem in nuclear dynamics. Representative for the first type of motion are Brueckner G-matrix theories, and for the second type RPA-approaches. They are usually related to short- and long-range correlations, respectively.

The coupled equations of motion for the one-body density, $i\dot{\rho} = [h(\rho), \rho] + tr_{(2)}[v, C]$, and for the two-body correlations C have rendered a suitable basis for a consistent description of these correlations. In an arbitrary s.p.-basis $|\alpha\rangle$, the 2-body equation reads

$$i\dot{C}_{\alpha\beta\alpha'\beta'} = \langle \alpha\beta | [v(\rho)^{\pm}, A(\rho\rho)] | \alpha'\beta' \rangle + \langle \alpha\beta | [1 * h(\rho) + h(\rho) * 1, C] | \alpha'\beta' \rangle + \langle \alpha\beta | [v(\rho)^{\pm}, C] | \alpha'\beta' \rangle + A(\alpha\beta)A(\alpha'\beta') \sum_{\gamma\gamma'} v(\rho)_{\alpha\gamma\alpha'\gamma'}^{\perp} C_{\gamma\beta\gamma'\beta'}. \quad (1)$$

The driving term (1. contribution) cares for a formation of correlations irrespective of the initial conditions. The 2. term describes mean-field propagation. The in-medium interactions $v^{\pm} = Q^{\pm} \cdot v$ and $v^{\perp} = Q^{\perp} \cdot v$ are selective to pp(hh)- and ph(hp)-states, respectively [1]. Their alternative connection with C may be viewed as the source for alternative kinds of motion. To disentangle their effects on the dynamics we apply three approaches: (i) Born approximation generated by the first 2 terms of (1), (ii) time-dependent G-matrix theory including the 3. term (TDGMT or pp-channel), and (iii) including the last instead of the 3. term (RPA or ph-channel). The importance of the respective channel is studied by means of the evolution of propagating correlations $C_{pppp}, C_{hhhh}, C_{pphh}$, doorway correlations C_{ppph}, C_{phhh} , and the "2p-2h-amplitude" C_{pphh} which is related to a spontaneous creation of 2p-2h-states.

The coupled equations for ρ and C are solved within an oscillator basis for a system of 16 nucleons, starting with a HF-distribution for ρ .

To exhibit the sensitivity of the approaches (i)-(iii) with respect to the range of the bare interaction v , the calculations are performed for a Yukawa-potential comprising a long-range part, as well as for a short-range contact force. For calculational details see [2].

The formation of correlations sets in with a rapid increase of C_{pphh} , irrespective of the approach and the range of v . This is shown for TDGMT in Fig.1 and 2. Remarkable enough it turns out that this type of correlations is almost completely generated by the Born term, - in contrast to the remaining correlations. This initial formation of C_{pphh} opens phase-space for the other correlations to become operative. A common feature is that C_{hhhh} remains small in any case. The pp-correlations C_{pppp} are clearly favoured by short-range forces (compare Fig.1 and 2), whereas C_{pphh} is favoured by the Yukawa-potential.

Instructive is the amount of correlations produced in the different channels. This is demonstrated for the doorway- and ph-correlations in case of the more realistic Yukawa-potential. Whereas in TDGMT, all correlations remain negligible (see Fig.3), we observe a considerable formation of correlations in the ph-channel (Fig.4).

We conclude that (1) the ph-channel dominates for systems close to the ground state, and (2) short-range forces control the pp-channel and herewith 2-body collisions, whereas long-range forces control the ph-channel and herewith collectivity. Although this confirms intuitive expectations, the study of other systems and initial conditions is desirable.

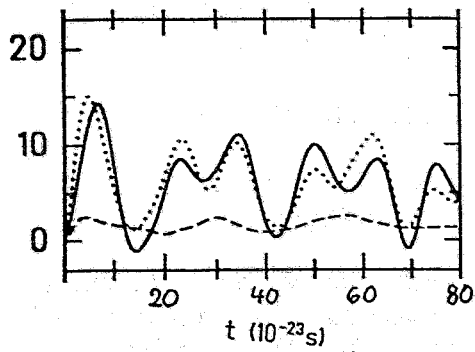


Figure 1
Formation of correlations in the pp-channel in case of δ -force ($v_0 = -220 \text{ MeV}$)

— C_{pppp}
 --- C_{hhhh}
 ... C_{pphh}

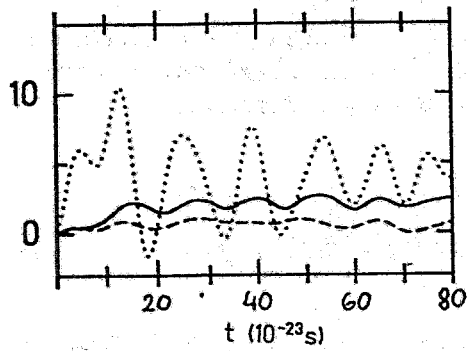


Figure 2
The same as Fig. 1, but with a Yukawa force ($v_\pi = -3.4 \text{ MeV}$, $v_\omega = 19.0 \text{ MeV}$)

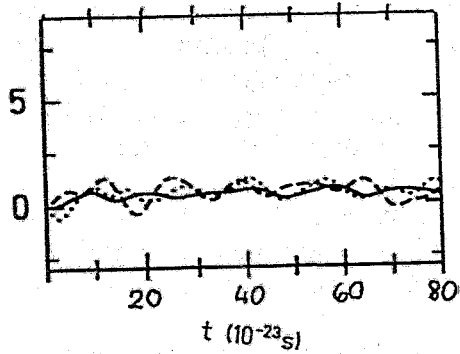


Figure 3
Formation of correlations with the Yukawa force in the pp-channel

— C_{phph}
 --- C_{phhh}
 ... C_{pphh}

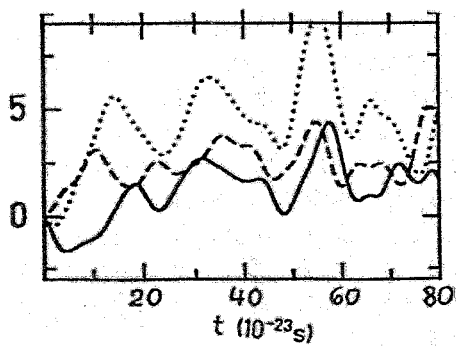


Figure 4
The same as Fig. 3, but in the ph-channel (RPA)

REFERENCES:

- [1] W. Cassing, A. Pfitzner, Z. Phys. A342,161 (1992)
- [2] A. Peter, W. Cassing, A. Pfitzner, GSI annual report 1992

Shapes of Na Clusters

S. FRAUENDORF^a, V. V. PASHKEVICH^b

^a *Forschungszentrum Rossendorf e. V., Institut für Kern- und Hadronenphysik*

^b *Laboratory for Theoretical Physics, Joint Institute for Nuclear Research Dubna, Russia*

Micro clusters consisting of several hundred alkali metal atoms are systems that show a number of remarkable similarities to nuclei. The application of methods developed in nuclear theory to clusters permits a deeper understanding of different aspects of nuclear and cluster structure. At the same time, the study of the similarities and the differences between clusters and nuclei will help to develop the general theory of mesoscopic systems, which draws increasing attention from the point of view of conceptual understanding and practical application.

The shell correction method has been adapted to study the shape of Na clusters [1]. The shapes of cluster in the range of 10 to 310 atoms have been calculated. Similar to nuclei strong quadrupole and hexadecapole deformations are found between the magic clusters 8, 20, 40, 58, 92,, which are spherical. The predicted axis ratios correlate well with the splitting of the plasmon resonances (analog to the GDR in nuclei), measured recently [2]. Stable octupole deformations are predicted for the clusters at the beginning of each shell. The calculated monomer and dimer separation energies show clear evidence for the deformations, which is born out by the experimental evaporation rates and formation abundancies.

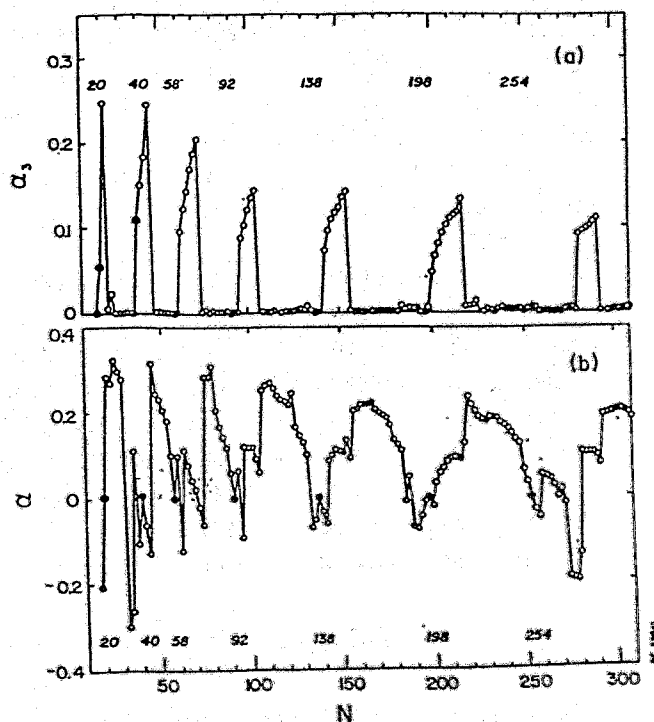


Fig. 1 Quadrupole (α) and octupole (α_3) deformations of Na clusters with N atoms.

REFERENCES:

- [1] S. Frauendorf, V. V. Pashkevich, *Z. f. Physik D*, in print
- [2] J. Pedersen et al., *Z. f. Physik D*, in print

Molecular Dynamics (MD) simulations of GRID experiments^B

K.-H. HEINIG* AND D. JANSSEN

*Institut für Ionenstrahlphysik und Materialforschung

Forschungszentrum Rossendorf e. V., Institut für Kern- und Hadronenphysik

Full MD calculations are the most realistic method to simulate the slowing down of low-energy ions in solids through atom-atom collisions [1]. The basic idea of the MD calculations is that the positions and velocities of both the low-energy ion and the target atoms are calculated by numerical integration of Newton's equations of motion. In ref. [1] we used this method to investigate ion implantation phenomena.

Very recently, we applied our MD method to simulate γ -lines of recoiling excited nuclei [2], which are measured by the γ -ray induced Doppler-broadening (GRID) method [3]. In the GRID method a recoiling excited nucleus is produced by the emission of a primary γ -ray of energy E_p from the compound nucleus after thermal neutron capture. When the recoiling nucleus decays further by the emission of the secondary γ -ray of energy E_γ , the measured Doppler shift ΔE_γ of E_γ depends on the velocity $v(t)$ of the recoiling atom at the time t after the emission of E_p and the angle θ under which E_γ is observed relative to the recoil direction, i. e. $\Delta E_\gamma = E_\gamma \beta(t) \cos \theta$, where $\beta(t) = v(t)/c$ and c is the velocity of light.

The Doppler broadened γ -line contains information on the lifetime of the nuclear state and/or the stopping power of the recoiling atom in the solid. However, in general it is not possible to reproduce the measured γ -profile and to extract the lifetime of the nuclear state without a theoretical description of the collisions between the recoiling and the lattice atoms. Several procedures of theoretical analysis are currently applied to the GRID data, the most appropriate MD method has been employed by Kuronen [4]. Improved lifetimes of excited nuclear states and first experimental information on the interatomic interaction potential in the energy range of a few 100 eV have been obtained.

Up to now an isotropic target has been assumed [4]. In ref. [5], for polycrystalline titanium measured lineshapes are compared with lineshapes calculated by the MD method. The smooth shapes of the line profile allow the fit of one quantity at best, in the actual case the lifetime of the nuclear state. If another interatomic interaction potential is taken for the MD simulation, the fit gives a modified lifetime. To fit both, lifetime and potential, for a transition a more structured lineshape or a series of lineshapes is necessary but not available by this procedure.

Recently, we predicted for the first time γ -lineshapes for single crystals [2]. Up to now no experiments have been carried out for single crystals [6]. We use

$$I(\Delta E_\gamma) = \frac{1}{\tau} \sum_i \int_0^\infty dt e^{-t/\tau} \delta(E - E_\gamma - \frac{v_i(t)n}{c} E_\gamma), \quad (1)$$

where $\Delta E_\gamma = E - E_\gamma$. Our more general formula (1) contains the direction of the spectrometer axis n (with respect to the crystal axis) and all velocity vectors $v_i(t)$ of the recoiling atoms i . Using our MD code, we simulate for the nuclear reaction $^{28}\text{Si}(n, \gamma) ^{29}\text{Si}$ the profile of the Doppler-broadened γ -line of the secondary γ -transition with $E_\gamma = 2.43 \text{ MeV}$ and $\tau = 10 \text{ fs}$, where the Doppler-broadening comes from the primary γ -decay with $E_p = 6.05 \text{ MeV}$.

In our MD simulations, the recoil atoms start from a lattice point into 3000 randomly distributed directions. The slowing down of the recoils is calculated using a finite cell of 960 atoms with periodical boundary conditions. The crystal structure is of diamond type.

After each time step t_j at the Doppler shift $\Delta E_\gamma = v_i(t_j)n/c$ the value $P_j = e^{-t_j/\tau}$ has been added to the intensity $I(\Delta E_\gamma)$. This procedure is equivalent to the calculation of $I(\Delta E_\gamma)$ corresponding to eq. (1).

Our theoretical prediction proves that considerably improved GRID experiments can be carried out with monocrystalline samples. Then different crystal alignments lead to different lineshapes with a pronounced structure (see Fig. 1). These lineshapes contain sufficient information to fit several quantities (e. g. lifetimes, potential) in one experiment. Fig. 1c demonstrates that even small differences in potentials should be measurable in the energy region $50 \text{ eV} < E_\gamma < 1 \text{ keV}$, where other methods fail to give good results. After the reconstruction of the research reactor at the ILL Grenoble our proposed experiments will be carried out [6]. The new ultra-high-resolution gamma spectrometer GAMS5 should even allow to determine the location of impurities in a host crystal.

This work was supported in part by the Bundesministerium für Forschung und Technologie under Grant No. 211-5291-03-HE3ROS.

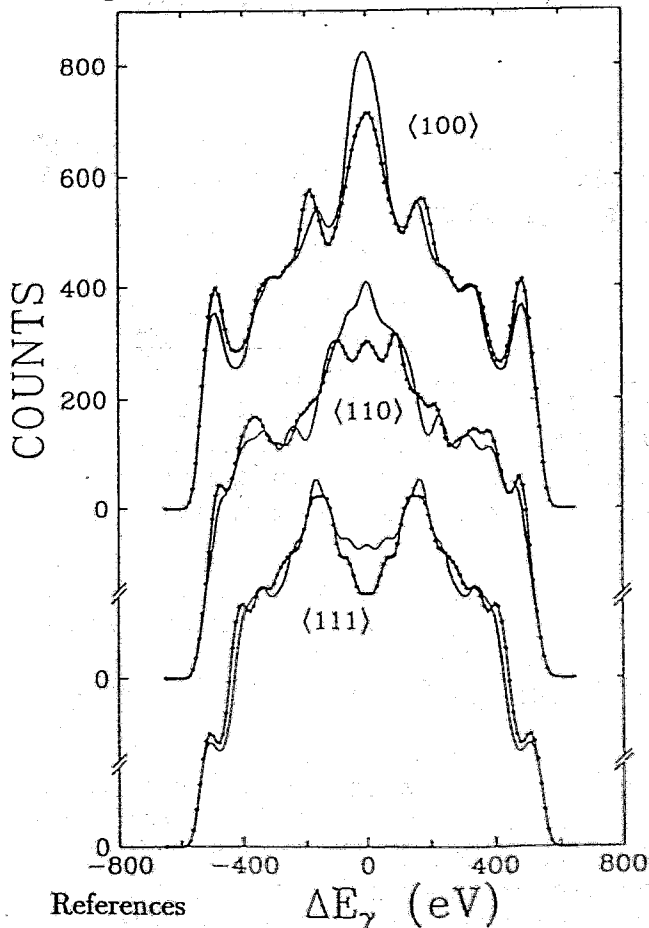


Fig. 1: Examples for Doppler-broadened lineshapes due to the slowing down of recoils in monocrystalline silicon. The Doppler-broadened lineshapes are predicted by our MD simulations for the secondary γ -decay with $E_\gamma = 2.43 \text{ MeV}$, $\tau = 10 \text{ fs}$, where the recoils are produced by the primary γ -decay with $E_p = 6.05 \text{ MeV}$ following the nuclear reaction $^{28}\text{Si}(n, \gamma)^{29}\text{Si}$. The structure in the lineshape reflects the dependence of the slowing down process of recoils on the recoil direction in the crystal. The temperature dependence is small, here we present results for $T = 0^\circ \text{K}$ only. Different alignments between the spectrometer axis and the crystal orientation give different lineshapes. The universal potential (marked line) and the Moliere potential (thin line) result in different line shapes. Such differences should be experimentally resolveable.

References

- [1] K.-H. Heinig and D. Stock, to appear in *Nucl. Instr. and Meth.*;
D. Stock and K.-H. Heinig, MRS Fall Meeting, Symposium A *Beam-Solid Interactions: Fundamentals & Applications*, Boston, USA, Nov. 30 - Dec. 4, 1992, contr. paper A7.11.
- [2] K.-H. Heinig and D. Janssen, in: *Workshop on Applications of High Resolution Gamma Spectroscopy in Studies of Atomic Collisions and Nuclear Lifetimes*, Grenoble Oct 5-7, 1992, eds. H.G. Börner, J. Jolie, M. Pendlebury, and S. Ulbig, Inv. contr.; to appear in *Phys. Letters*.
- [3] H.G. Börner, J. Jolie, F. Hoyle, S.J. Robinson, M.S. Dewey, G.L. Green, E.G. Kessler, R.D. Deslattes, *Phys. Lett. B*215 (1988) 45;
J. Jolie, S. Ulbig, H.G. Börner, K.P. Lieb, S.J. Robinson, P. Schillebeeckx, E.G. Kessler, M.S. Dewey, G.L. Greene, *Europhys. Lett.* 10 (1989) 231.
- [4] A. Kuronen, *J. Phys. G*3 (1991) 11;
A. Kuronen, J. Keinonen, H.G. Börner, J. Jolie, and S. Ulbig, *Nucl. Physics A*549 (1992) 59.
- [5] A. Kuronen, *J. Phys. Condens. Matter* 3 (1991) 1363.
- [6] H.G. Börner, private communication

First observation of a crossing of oblate dipole bands in the $A = 200$ region
(Physics Letters B298 (1993) 54)

G. Baldsiefen, U. Birkental, H. Hübel, N. Nenoff, B.V. Thirumala Rao, P. Willsau, J. Heese, H. Kluge, K.H. Maier, R. Schubert and S. Frauendorf

Abstract: High-spin states in ^{199}Pb were populated in the $^{186}\text{W}(^{18}\text{O},5n)$ reaction at a beam energy of 94 MeV. The analysis of the γ -ray coincidences revealed a new oblate rotational band of strong dipole transitions which shows a pronounced backbending. The connection between this band and the normal spherical states is established. Thus, spin and excitation energy of an oblate collective band in the Pb isotopes are determined for the first time. The backbending is interpreted as a crossing of bands with different numbers of aligned $i_{13/2}$ neutrons.

Particle production during inflationary reheating
(International Journal of Modern Physics A, Vol. 7 (1992) 2033)

M. Basler and B. Kämpfer

Abstract: A possible reheating mechanism in inflationary universe models is studied in some detail. Results are presented of numerical investigations of particle creation and corresponding reheating within a self-coupled scalar field model. By using the method of Hamiltonian diagonalization attention is devoted to the time development of the process and its parameter dependence. The effect of particle production is found to depend strongly on the anharmonicity of the potential around its minimum and on the amplitude of the oscillations of the scalar background field.

Pion-pion cross section in a dense and hot pionic gas
(Physics Letters B275 (1992) 19)

H.W. Barz, G. Bertsch, P. Danielewicz and H. Schulz

Abstract: We examine the in-medium scattering cross section in a dense and hot pionic gas. We show that the increase of the scattering rate associated with the Bose occupancy factors is largely compensated by a drop in the cross section, when medium effects on the pionic cross section are consistently taken into account. Implications for calculating the pion spectrum at low transverse momentum, in ultrarelativistic heavy ion collisions, are discussed.

Mechanism for nuclear disassembly of the Ar + Th and Pb + Au systems at intermediate energies

(Physical Review C46 (1992) R42)

H.W. Barz, J.P. Bondorf, C.H. Dasso, R. Donangelo, G. Pollarolo, H. Schulz and K. Sneppen

Abstract: We show that the neutron multiplicities observed in the reaction ^{40}Ar on ^{232}Th at incident energies between 27 and 77 MeV per nucleon are consistent with the predominantly binary character of the collision process. The most violent encounters lead to excitation energies of several MeV per nucleon, sufficiently high to crack the colliding nuclei into many small fragments. We also give the neutron multiplicity and decay pattern for the reaction ^{208}Pb on ^{197}Au at 29 MeV per nucleon, for which some preliminary data are available.

Fluctuations and intermittency in multifragmentation processes

(Physical Review C45 (1992) R2541)

H.W. Barz, J.P. Bondorf, R. Donangelo, I.N. Mishustin, H. Schulz and K. Sneppen

Abstract: Nuclear multifragmentation processes may show features such as intermittency that signal scale-invariant properties of fluctuations in the fragment distributions. We test this behaviour using several models and show that intermittency may be caused by a combination of finite-size effects and the mixing of fragmentation events corresponding to different initial conditions.

Thermalization of mesons in ultrarelativistic heavy-ion reactions

(Physics Letters B287 (1992) 40)

H.W. Barz, P. Danielewicz, H. Schulz and G.M. Welke

Abstract: The Boltzmann equation with bosonic factors in the collisions integral is solved for an expanding gas of mesons modelling the central rapidity region of central ^{16}O on Au collisions at 200 GeV/nucleon. The employed in-medium π - π scattering-amplitude is derived from a Bethe-Goldstone equation. Mean field effects are not included. In a purely pionic scenario thermalization explains the experimentally observed low- p_{\perp} peak in the pion spectra if a hadronization time of ~ 4.5 fm/c is assumed. Inclusion of the mesonic resonances reduces the effects of statistics and a much shorter hadronization time of ~ 1 fm/c is needed to describe the data.

Self-consistent truncation of the BBGKY hierarchy on the two-body level
(Z. Phys. A342 (1992) 161)

W. Cassing and A. Pfitzner

Abstract: We present a coupled set of equations for the one-body density matrix and the two-body correlation function consistent with trace relations and conservation laws which provide an extension of correlation dynamics on the two-body level. The additional interaction terms are discussed in the context of time-dependent G-matrix theory and NQCD and studied numerically by one-dimensional calculations for colliding finite fermion systems.

Nonexponential decay of a stochastic one-channel system
(Phys. Rev. A45 (1992) 701)

F.-M. Dittes, H.L. Harney and A. Müller

Abstract: A general formula is presented that expresses the temporal evolution of compound systems. It connects the time dependence of the density matrix with the energy dependence of the scattering matrix. Using results of random matrix theory, we then study the decay behaviour of stochastic compound systems with arbitrary coupling between bound states and decay channels. As an example we consider the case of one open channel and prove a nonexponential decay law for all times that asymptotically is of the form $t^{-3/2}$.

Quenched proton-neutron coupling in $h_{11/2}$ high spin states of ^{128}Ba
(Physics Letters B274 (1992) 149)

S. Frauendorf, W. Lieberz, D. Lieberz, P. von Brentano and A. Gelberg

Abstract: Analyzing experimental E2-branching ratios in terms of a three level model coupling matrix elements between the 10^+ states of the ground band and the neutron and proton S-bands are estimated. The coupling matrix element between the two S-bands is found to be less than about 3 keV, which upper limit includes the errors.

Time evolution of chaotic quantum systems

(Ann. Phys. 220 (1992) 159)

H.L. Harney, F.-M. Dittes and A. Müller

Abstract: We consider a quantum system which is open in the sense that a number of metastable states are coupled to a set of decay channels. A solution of the time dependent Schrödinger equation is developed that allows us to describe both the excitation and the decay process. Assuming the excitation to be practically instantaneous, the decay is studied in detail for systems which have a random Hamiltonian or - what is closely related - behave chaotically. The decay function is worked out in a form amenable to numerical evaluation with standard techniques. For several instructive special cases, it is evaluated in closed analytical form. It turns out to be generally neither exponential nor independent on the way by which the system was excited. It is exponential and independent of the excitation only if a large number of decay channels are present. If only one channel is open, the decay function is asymptotically proportional to $t^{-3/2}$.

Hierarchical trapping of resonance states at high level density

(Phys. Rev. C47 (1993))

W. Iskra, I. Rotter and F.-M. Dittes

Abstract: On the basis of a simple S -matrix model we show that at high average level density, local fluctuations in the density of states of an open quantum mechanical system create locally a few broad resonance states together with a larger number of narrow (trapped) ones. The widths of the broad states are of the order of the length which characterizes the local fluctuations in the spectrum. They serve as a background for the narrow "finestructure resonances". If the spectrum shows a hierarchical fluctuation pattern in energy, this behaviour repeats on all energy scales. From these results, we conjecture that the well-known intermediate structures in nuclei at high level density, described by the doorway mechanism, are formed due to such a trapping effect.

Dilepton radiation from non-equilibrated parton matter produced in ultra-relativistic heavy-ion collisions

(Physics Letters B289 (1992) 127)

B. Kämpfer and O.P. Pavlenko

Abstract: Dilepton radiation from parton (quark-gluon) matter, produced in ultrarelativistic nucleus-nucleus collisions, is calculated within a kinetic theory approach in order to study non-equilibrium effects. We investigate (i) the approach towards equilibrium in early collisions stages and (ii) the departure from a supposed equilibrium stage due to the subsequent longitudinal expansion. Independent of the details of the parton equilibration process the continuum dilepton rates from quark fusion in deconfined matter are found to exceed the Drell-Yan background in the J/ψ region at RHIC and LHC energies. The appearance of higher mass dileptons depends on the degree of thermalization.

The soliton of the effective chiral action in a heat-kernel expansion
(Ann. Physik 1 (1992) 106)

B. Kämpfer and H. Reinhardt

Abstract: It is shown that the heat-kernel expansion (rather than the gradient expansion) of the effective chiral action of the quark loop yields in next-to-leading (i.e., fourth) order an effective low-energy Lagrangian which possesses stable soliton solutions. The baryon number-one soliton solution of this effective chiral Lagrangian is found numerically.

Scale invariance and the stability of a hedgehog soliton
(Physics Letters B299 (1993) 183)

Th. Meissner, G. Ripka, R. Wünsch, P. Sieber, F. Grümmer and K. Goeke

Abstract: We show that a scale invariant chiral action proposed not long ago prevents the recently discovered collapse of the hedgehog soliton off the chiral circle calculated with a proper time regularized Nambu-Jona-Lasinio action. The soliton calculated with the scale invariant action turns out to be close to the chiral circle and hence has properties which are very similar to those of the chiral quark loop. Its mass obeys the Ioffe formula.

Unified description of quasi-free and resonant processes of hypernuclear production and decay
(Czech. J. Phys. 42 (1992) 1061)

R. Wünsch

Abstract: We review a unified description of resonant and quasi-free hypernuclear production reactions on the basis of the continuum shell-model. Both reaction mechanisms are considered as boundary cases of the same process. We apply the model to the (K^-, π) and to the (π, K^+) reaction on light target nuclei. Particular attention is given to the consequences of the shallow hyperon-nucleus potential. Hypernuclear disintegration by baryon emission is considered as transition from the bound to the unbound part of the configurational space.

2. Experimental Medium Energy Physics

Test of the Start Detector System for the Investigation of the pp-Bremsstrahlung with the COSY Time-of-Flight Spectrometer (TOF)^{B,K}

P. MICHEL, A. SCHÜLKE, K. MÖLLER, A. SCHAMLOTT, B. NAUMANN, L. NAUMANN

*Forschungszentrum Rossendorf, Institut für Kern- und Hadronenphysik
and the COSY-TOF Collaboration*

In the previous annual report a concept of a start detector was presented for the measurement of the pp-bremsstrahlung by means of the COSY TOF-spectrometer.

The final version of this start detector is shown in fig.1. Additionally to some preliminary tests of the performance of the hollow light guides described in the previous annual report the components of the start detector were tested under realistic conditions using minimally ionizing particles (3.5 GeV/c pions) in a test measurement in the T 11 test area at CERN.

The following main properties of the start detector were to be investigated by the tests:

- the local variation of the light output amplitude in dependence on the place where the detected particle hits the trapezium-like plastic scintillator
- the gap width between neighbouring scintillator segments
- the average time resolution for minimally ionizing particles

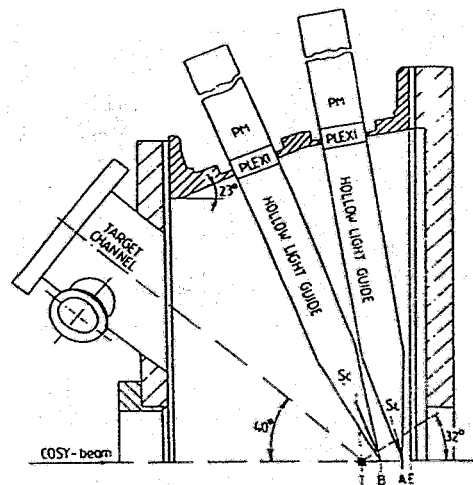


Fig.1 Start detector for the investigation of pp-bremsstrahlung (Sc=scintillator T=target position)

The set-up for the test measurements is shown in fig.2. Here P and E are two identical test modules consisting of two neighbouring start detector segments each.

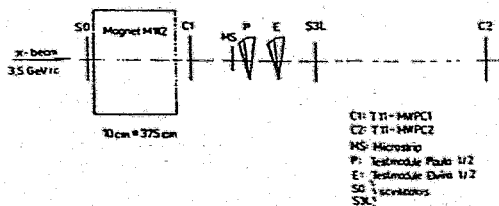


Fig.2 Experimental set-up for the test of the start detector components P and E

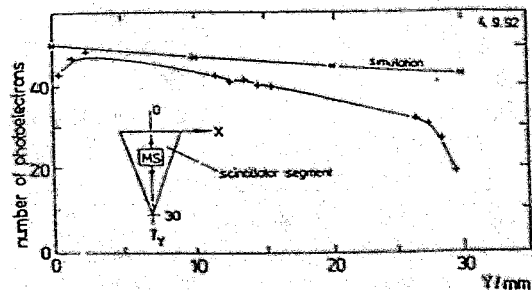


Fig.3 Local efficiency variation of the scintillator segments

In a first test run the local variation of the light transmission efficiency of a start detector segment was determined by scanning the trapezium-like scintillator segment with a microstrip detector system (MS) consisting of two crossed $24 \times 200 \mu\text{m}$ microstrip detectors.

The result of the efficiency measurement is presented in fig.3. An analogous result as shown in fig.3 was obtained for the X-direction perpendicular to the Y-direction.

Apart from an overall decrease of the light intensity with Y increasing there is an intensity decrease in the border regions of the scintillator segment. The general trend of an intensity decrease with Y increasing can be reproduced at least qualitatively by light transmission simulation calculations using the LIGUI code. An exact reproduction of the behaviour of the light transmission efficiency is not possible because the LIGUI code takes into account only the light transport in the hollow light guides whereas the transport of the light in the scintillator elements is not included into the code.

In a second test measurement the gap width was determined between neighbouring scintillator segments using again the microstrip detector system. The logical scheme for measuring the gap width is presented in fig.4. The result is shown in fig.5.

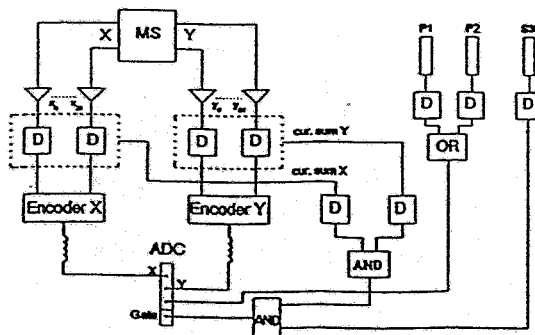


Fig.4 Electrical arrangement for measuring the gap between neighbouring scintillator segments

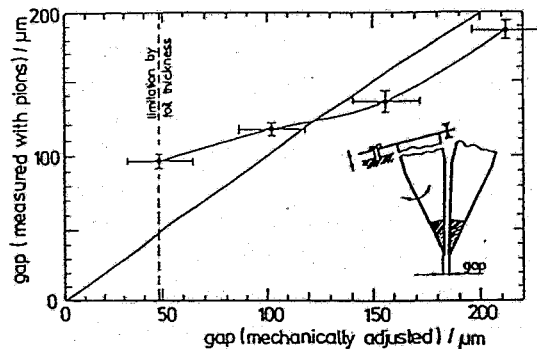


Fig.5 Gap measurement with pions

From fig.5 one can infer that the minimum gap "felt" by the particles amounts to $100 \mu\text{m}$ whereas the minimum mechanically adjustable gap is $48 \mu\text{m}$. This minimum mechanical gap width is determined by the thickness of the mylar foils between neighbouring scintillator elements.

For larger gap sizes the "particle measured" gap nearly coincides with the mechanically adjusted gap.

To determine the time resolution of the start detector for minimally ionizing particles the time of flight was measured between the two identical modules P and E (s. fig.2).

In the electrical set-up to determine the time of flight constant fraction discriminators were used. The measured time spectrum is shown in fig.6. From the time resolution $\Delta t(\text{FWHM}) = 780 \text{ ps}$ in fig.6 one obtains the value $\Delta t/\sqrt{2} = 550 \text{ ps}$ (FWHM) for the time resolution of a single module.

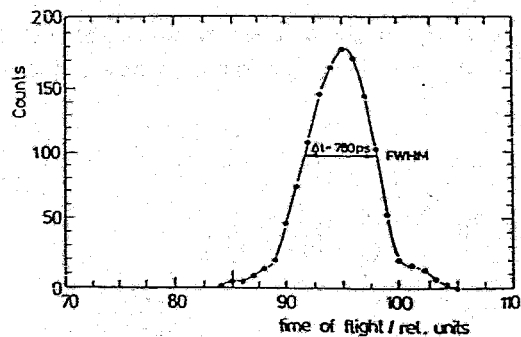


Fig.6 Time of flight spectrum measured between the identical test modules P and E

We would like to thank our colleagues from the COSY-group at the University of Erlangen for the support in performing the measurements at CERN.

SIMULATION OF THE PROTON-PROTON-BREMSSTRAHLUNG AT THE COSY-TOF-SPECTROMETER^{B,K}

B. NAUMANN, P. MICHEL, K. MÖLLER, L. NAUMANN, A. SCHAMLOTT AND A. SCHÜLKE

Forschungszentrum Rossendorf, Institut für Kern- und Hadronenphysik

Monte-Carlo simulations have been performed to help in designing the start detector as a part of the whole COSY-TOF-Spectrometer for the Proton-Proton-Bremsstrahlung measurements. The simulations have been carried out using the Monte-Carlo program GEANT3 [1]. The COSY-TOF-Spectrometer [2] is represented by a structure of geometrical volumes. Each volume is characterized by a set of tracking medium parameters, which includes references to the materials filling the volumes. The simulated events have been generated with the Monte-Carlo phase space program FOWL [3]. Using GEANT3 utilities the tracking of the reaction products through the experimental setup has been controlled for each event. In a first experiment with the TOF-Spectrometer a reduced stop detector device will be used consisting of the end-cap only. The geometrical structure of this spectrometer is shown in Fig.1.

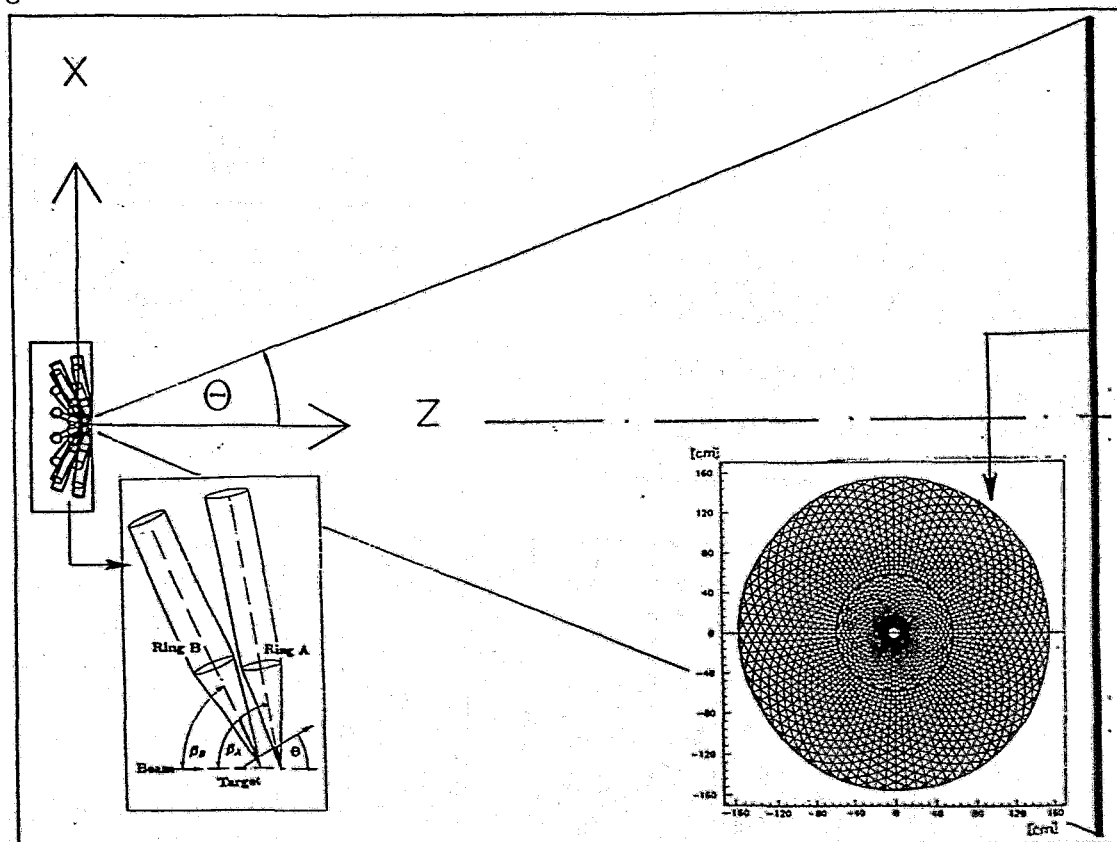


Fig.1 Schematic view of the detector arrangement used for the simulations ($\theta \approx 22^\circ$)

The liquid hydrogen target and the start detector are placed inside a vacuum vessel. The start detector consists of a start (A) and a veto (B) ring each with 16 trapez-like plastic scintillators surrounded by hollow light guides. The end-cap consists of the Ring and the Quirl three layer scintillator hodoscopes. The distance between start and stop detectors was chosen to be 3.7 meters. The aim of the presented calculations was to consider the influence of air along the proton flight paths for different physical mechanisms. There are three cases:

- A - energy loss and multiple scattering in detectors, construction materials and the air along the flight path;
- B - energy loss and multiple scattering in detectors and construction materials, the flight path is evacuated;
- C - tracking without energy loss and multiple scattering.

The incident beam momentum for all calculations was 0.8 GeV/c. Only events were accepted, where the two outgoing protons in the start as well as in the stop detector had been registered. Low energetic protons are stopped along the path length for about 10% of the events, photons with high CMS energy however are detected if the start and the stop detectors are placed in air instead of vacuum (see Figs.2-4).

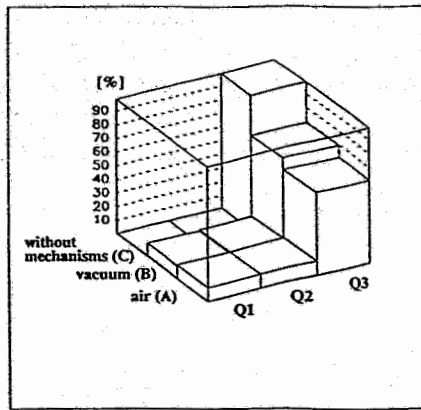


Fig.2 Event statistics in the end-cap hodoscope layers normalized to case C
 Q1 - one proton was stopped in the first layer;
 Q2 - one proton was stopped in the second layer;
 Q3 - both protons passed through the third layer.

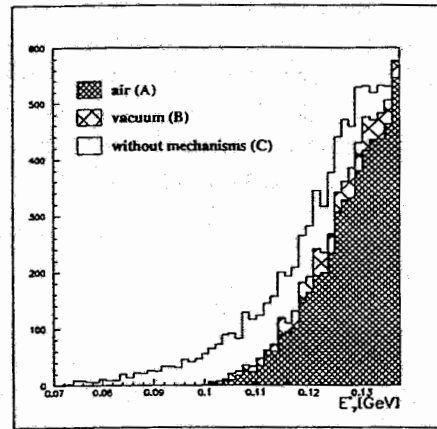


Fig.3 CMS photon energy in dependence on event counts after the third end-cap hodoscope layer (Q3)

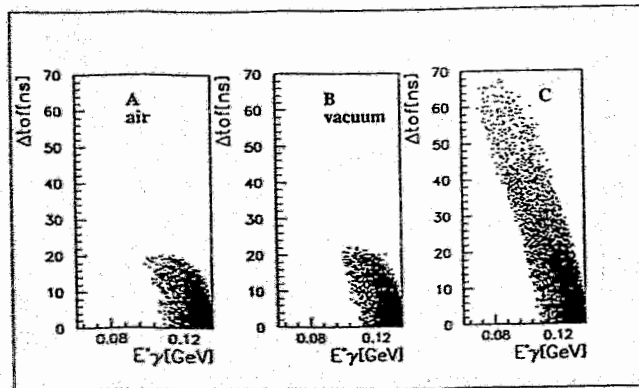


Fig.4 CMS photon energy in dependence on the difference of the time of flight between the outgoing protons after the third end-cap layer (Q3)

REFERENCES:

- [1] R.Brun et al., GEANT3, CERN data handling division, 1987, DD/EE/84-1
- [2] IKP Annual Report 1991, KFA Jülich(1992) 3-7
- [3] General Monte-Carlo Phase-Space Program FOWL, CERN Program Library W505, 1972

CALIBRATION OF THE ROSSENDORF COSY-TOF-STARTDETECTOR^{B,K}

A. SCHÜLKE, P. MICHEL, K. MÖLLER, A. SCHAMLOTT, B. NAUMANN, L. NAUMANN

*Forschungszentrum Rossendorf, Institut für Kern- und Hadronenphysik
and the COSY-TOF Collaboration*

The concept of the Rossendorf start detector developed for the COSY-Time-of-Flight-Spectrometer TOF is described in [1,2]. The detector system has been designed and constructed in the years 1991/1992 and is now being tested.

To fully use the distinguished properties of the COSY-ring (emittance $\approx 1\pi$ mm mrad, momentum resolution $\Delta p/p \approx 10^{-4}$) the start detector has to meet severe requirements concerning the geometrical precision

- small distance (our choice: 4 cm) between the target position and the start detector to minimize start time dispersion
- small "beam hole" in the start detector (our choice: 1 mm radius) to get maximum angle acceptance in forward direction

In Fig.1 part of the array is shown of the 2×16 scintillator segments (ring A and ring B). In the first experiment (measurement of the $pp\gamma$ -bremsstrahlung / COSY proposal #9) the B-ring will be operated as a veto counter to reject events arising from the elastic pp -scattering. To avoid loss of veto particles a small overlap between neighbouring segments is required whereas for ring A a small gap between the segments is tolerable. Also between ring A and ring B a small overlap is required to make sure that even for finite size targets each ejectile is registered at least by one of the two rings (except for a small loss of detection efficiency due to the gaps of ring A). These considerations result in a scintillator segment geometry shown in Fig.2.

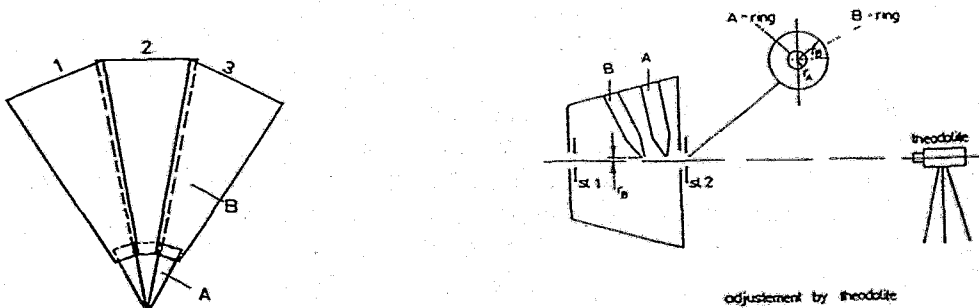


Fig.1 Arrangement of scintillators in the start detector

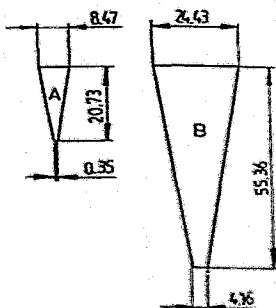


Fig.2 Geometry of the A- and B-scintillator-segments

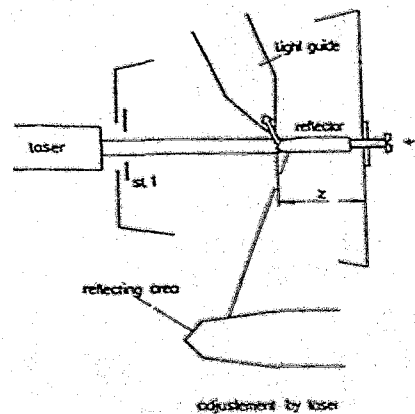


Fig.3 Adjustment arrangement for positioning of the light guides

The light pulses from the scintillator segments are transmitted to the photomultipliers by hollow light guides (length 30 cm) described in paper [3]. The hollow light guides are attached to the detector vessel by an adjustable three-point suspension mechanism. The adjustment has to be performed with high precision (in the order of one tenth of a mm) to meet the geometrical requirements mentioned above.

The mechanical adjustment proceeded in three steps:

1. At first a fictive beam axis was defined in the detector vessel and a theodolite was adjusted to this axis. After that the hollow light guides were adjusted symmetrically to this axis using a cross wire sight in front of the light guides additionally to the theodolite. So the "beam hole" was fixed with an accuracy of 0.1 mm.
2. To adjust the angle between the beam axis and the symmetry axis of the hollow light guides a laser beam was used (Fig.3). The hollow light guides must be adjusted that way that the direction of the laser beam reflected from the pin shown in Fig.3 coincides with the symmetry axis of the light guides. This can be controlled by observing the laser light spot at the position of the PM.
3. In a third step the overlap was determined between the segments of ring B as well as between the segments of ring A and ring B. To this aim a ^{90}Sr β -source (≈ 50 kBq) was used. In an electronical set up (Fig.4) the coincidence efficiency was determined which is a measure of the geometrical overlap of the segments. Additionally the energy loss ΔE of the β -particles as well as the hit pattern of the events was determined by the data taking system. A suitable 2-dimensional matrix representation of the hit pattern is shown in Fig.5. One can measure three types of correlation pattern: B-B, A-A, B-A. For the first two types the main diagonals of the matrices contain the single events whereas the diagonals adjacent to the main diagonal contain the two-fold coincidences. By comparing the number of coincidences of neighbouring channels with the number of single events the geometrical overlap can be calculated. According to this result a geometrical readjustment can be performed if necessary.

The accuracy of measuring the overlap between neighbouring scintillator segments is limited to about 10% since additionally to the true coincidences corresponding to the geometrical overlap there are background coincidences originating from scattering of the source electrons on the foils of the hollow light guides.

To improve the accuracy of the result it is intended to remeasure the overlap at the Rossendorf cyclotron using 13 MeV protons.

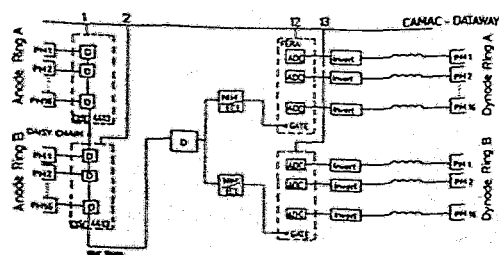


Fig.4 Electronical arrangement for measuring the coincidence efficiency

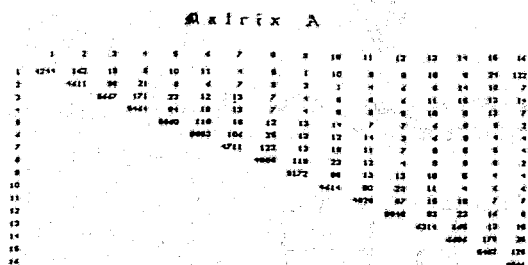


Fig.5 Example of a coincidence array

REFERENCES:

[1] P. Michel et al., Annual Report 1991 FZR 92-09, 48
 [2] P. Michel et al., this Annual Report
 [3] P. Michel et al., Mikrowellen & HF Magazin 18 (1992) 170

A PROGRAM FOR CALCULATION OF RELATIVISTIC TWO AND THREE BODY KINEMATICS AND ITS APPLICATION FOR THE INVESTIGATION OF THE PROTON-PROTON-Bremsstrahlung^{B,K}

B. NAUMANN, L. NAUMANN, P. MICHEL, K. MÖLLER, A. SCHAMLOTT AND A. SCHÜLKE

Forschungszentrum Rossendorf, Institut für Kern- und Hadronenphysik

The program AFKINE [1] was developed to investigate two and three body kinematics for the spectrometer design of planned experiments with relativistic particles. The program provides possibilities to calculate in an analytical way or to simulate the phase space by a Monte-Carlo method. AFKINE has been written in FORTRAN and is available at the CONVEX and the RISC 6000 machines of the Research Centre Rossendorf Inc.

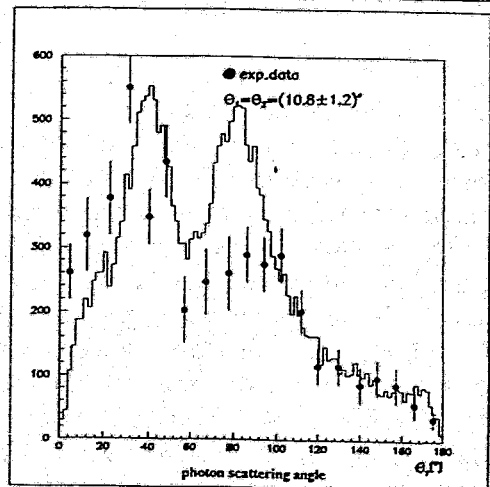
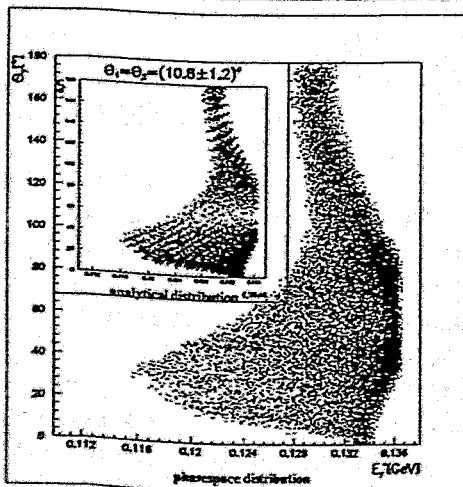
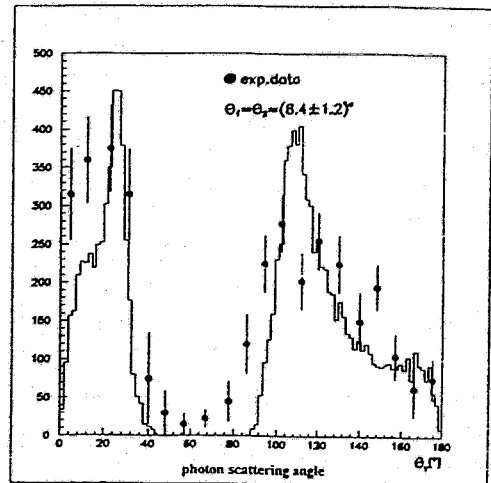
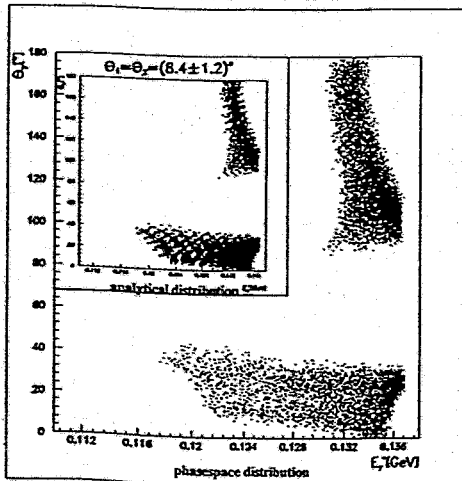
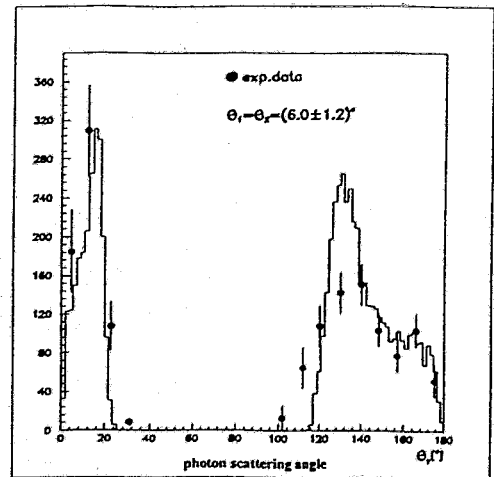
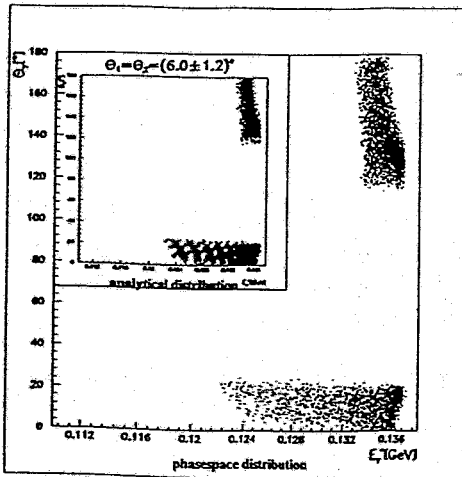
Input parameters for nuclear reactions are names of participating particles and values of incident beam momenta. Output parameters are scattering angles, momenta and total energies of reaction products in the Laboratory (LS) and in the Centre of Mass Systems (CMS). The results are stored in an event data structure (n-tuple) which can be analysed by help of the CERN Program PAW [2].

The formule for analytic calculations are based on Kajantie and Byckling [3]. Discrete input values for LS scattering angles and momenta ranges of reaction products are given by the user. Kinematically allowed regions for an investigated nuclear reaction can be inferred. The phase space calculations are based on the General Simulation program FOWL of the CERN Program Library [4]. The events are generated according to Lorenz-invariant phase space. It is possible to store the results of this type of calculation for either the full phase space or the detectable phase space of a given experimental setup.

To demonstrate calculations with the program AFKINE we used the Bloomington data [5] for the Proton-Proton-Bremsstrahlung at incident beam energy $E_{beam} \simeq 280$ MeV, where the outgoing protons were scattered symmetrically ($\Theta_1 \simeq \Theta_2$). The angle of noncoplanarity was constrained by trigger conditions to $\Psi \leq 70^\circ$. The results are shown in the figure.

On the left-hand side of the figure analytical calculations have been compared with phase space distributions for the LS photon scattering angle in dependence on the CMS photon energy. The analytical shape gives an exact information on the location of the kinematically allowed regions. For the evaluation of detector efficiencies it is necessary to calculate the detectable phase space distributions of the reaction products. In this case the CPU time for the event accumulation strongly depends on the given solid angle and can be substantially larger than for analytical calculations. In the chosen example 3 and 12 events per second have been accumulated with phase space calculations for $\Theta = (6.0 \pm 1.2)^\circ$ and $\Theta = (10.8 \pm 1.2)^\circ$ respectively. Approximately 4500 events per second have been stored with analytical calculations.

At the right-hand side of the figure the LS scattering angle distribution of high energetic photons from phase space calculations has been compared with the Bloomington data [5]. The shapes of the calculations were normalized arbitrarily. The normalization gives a good agreement of all three distributions, so it seems that this data can be interpreted using phase space kinematics.



Photon LS scattering angle in dependence on the CMS photon energy

Comparison of the Bloomington data for differential cross section with our phase space calculations

REFERENCES:

- [1] B. Naumann "AFKINE - users guide", in preparation
- [2] PAW The Complete Reference Version 1.07, CERN Program Library Q121, Geneva, 1989
- [3] E. Byckling and K. Kajantie "Particle kinematics", London, 1973
- [4] General Monte-Carlo Phase-Space Program FOWL, CERN Program Library W505, 1972
- [5] B.v. Przewoski et al., Phys. Rev. C, 45,(1992) 2001

CHARACTERIZATION OF δ -ELECTRONS, GENERATED IN THE COSY-TOF-SPECTROMETER^{B,K}

B. NAUMANN, L. NAUMANN, P. MICHEL, K. MÖLLER, A. SCHAMLOTT AND A. SCHÜLKE

Forschungszentrum Rossendorf, Institut für Kern- und Hadronenphysik

The COSY-TOF-Spectrometer [1] consists of a large number of scintillation counters inside a huge vacuum tank. The generation of δ -electrons by particle beams crossing matter is well known [2] and spectrometers with magnetic dipoles or lenses bend them out of the solid angle for particle registration [3]. The COSY-TOF-Spectrometer does not contain magnetic fields, so that the δ -electrons could be registered in this setup. For discussion of background it is necessary to analyse the influence of the δ -electrons on the scintillation counter signals because the energy loss of relativistic electrons and protons is in the same order of magnitude. The considerations start with kinematical calculations of proton-electron elastic scattering. Fig.1 shows the connection between proton and electron scattering angles in the lab-system. The incident beam momentum varies from 0.8 to 1.8 GeV/c. All protons are strongly aligned in the beam direction ($\Theta^p \leq 0.032^\circ$) outside of the scintillation counter area, whereas the δ -electrons are distributed up to 90° in the forward hemisphere.

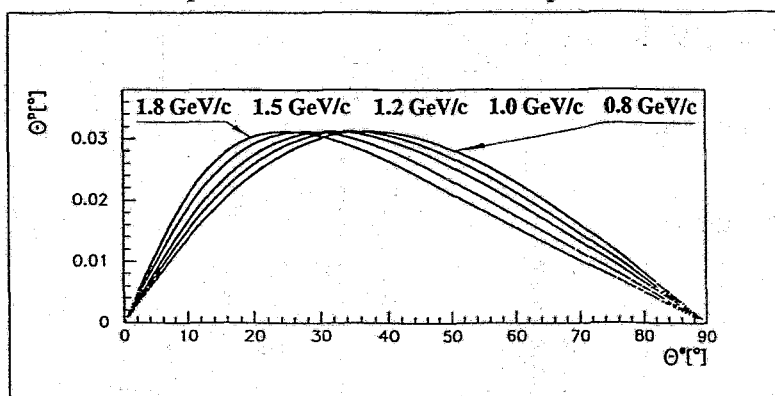


Fig.1 Connection of scattering angles for elastic p-e scattering in the lab-system at various beam momenta.

For electrons the kinetic energy in dependence on the scattering angle is shown in fig.2a. Energy loss and radiation length of the electrons for a first experiment version of the TOF-Spectrometer, where the start-stop flight path will be one meter in air have been calculated with an algorithm given by Katz and Penford [4].

The sequence of the materials, seen by the electrons, which were generated in the middle of the target is given in the following table:

layer	material	thickness [mm]	TOF-Spectrometer component	Label
1	liquid hydrogen	4.5	target	LH ₂
2	scintillator	0.5	start detector	start
3	air	1000.0	flight path	air
4	scintillator	5.0	stop detector	Q ₁
5	scintillator	5.0	stop detector	Q ₂
6	scintillator	5.0	stop detector	Q ₃

The energy loss of δ -electrons for each layer and the complete material sequence are demonstrated in figs.2b and 2c. In conclusion one can say, that most δ -electrons, generated in the target by beam protons with incident momentum $P_{beam} \leq 1.2$ GeV/c do not reach the second layer (Q₂) of the stop detector for the material composition given in the table. That means, they can be discriminated by trigger conditions, which demand a coincidence of the start with two stop signals.

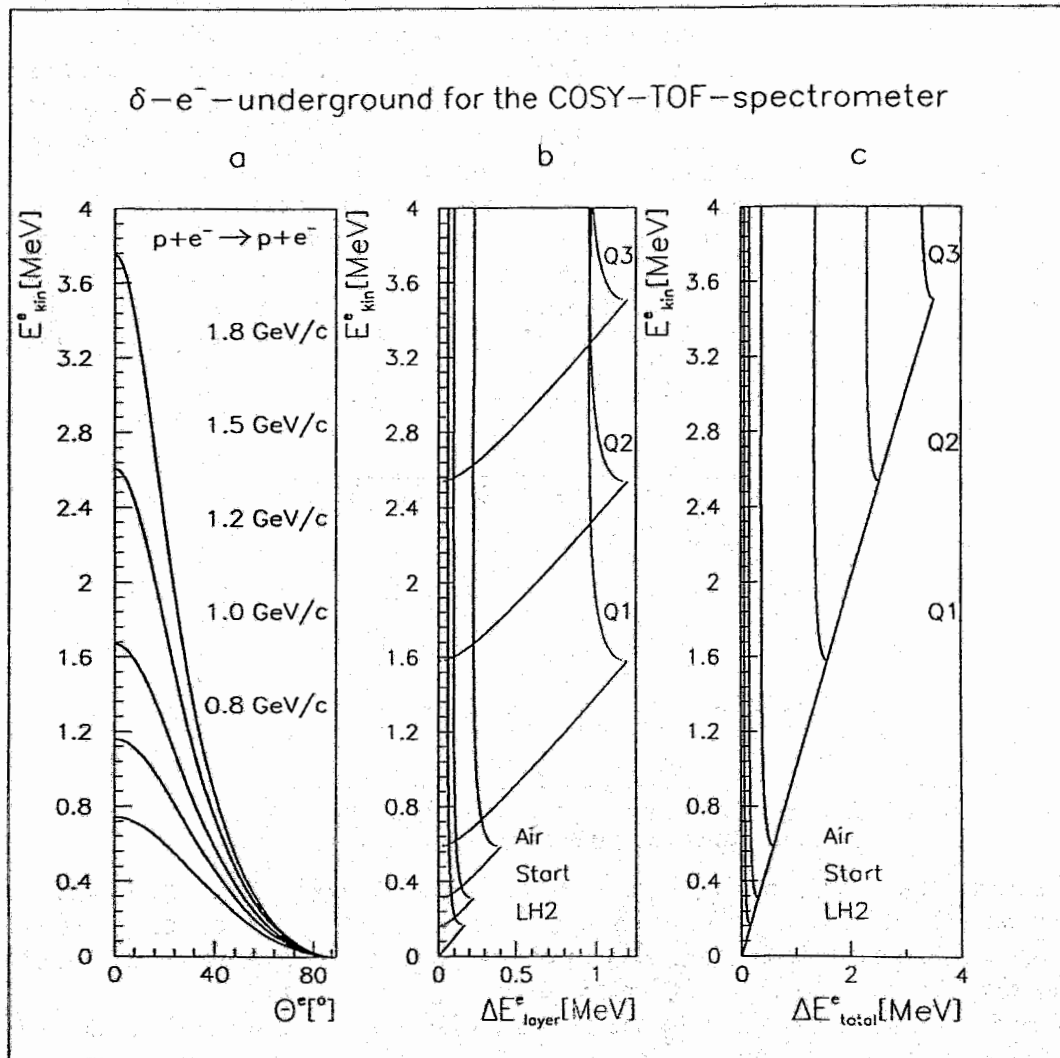


Fig.2 Kinematical parameters and energy loss for δ -electrons in the TOF-Spectrometer

REFERENCES:

- [1] IKP. Annual Report 1991, KFA Jülich (1992) 3-6
- [2] Review of Particle Properties, Phys. Lett. B239 (1990) 108
- [3] K. Michaelian et al., Phys. Rev. D, 41,(1990) 2689
- [4] Katz and Penford, Rev. Material Properties 24 (1952) 28

PRODUCTION OF K^- MESONS IN PROTON-INDUCED REACTIONS^B

H. MÜLLER

Forschungszentrum Rossendorf, Institut für Kern- und Hadronenphysik

The production of particles in proton-nucleus (pA) reactions at energies below the corresponding threshold for free nucleon-nucleon interactions is a typical cooperative nuclear phenomenon. The K^- channel is especially interesting, because due to strangeness conservation each K^- is accompanied by a K^+ meson and the produced mass amounts to nearly 1 GeV. This value is considerably larger than in the case of pion or K^+ production.

In a recent paper [3] subthreshold production of K^+ mesons has been considered in the framework of the modified phase-space model. Here, these investigations are extended to the production of K^- mesons. There are no data for K^- production, neither for elementary proton-proton (pp) nor pA interactions. Therefore, the available data for production of other meson types in the energy region of interest are confronted with model calculations with the aim to adapt the model parameters in such a way that predictions for unknown channels become possible. The results are shown in Figures 1-3, where the majority of the data is well reproduced.

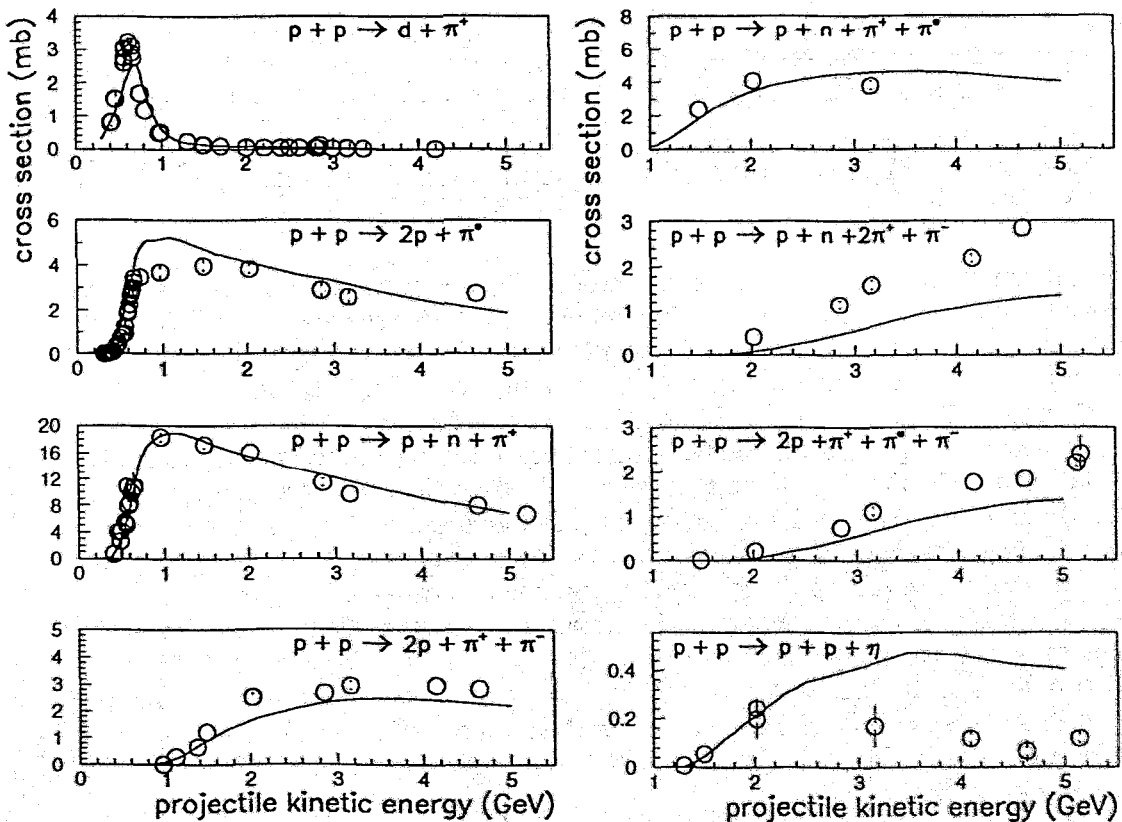


Fig.1 Energy dependence of the cross section for pion production. Data from Ref. [1].

Fig.2 Energy dependence of the cross section for pion and η production. The two preliminary data points for η production at 1.3 and 1.5 GeV are taken from Ref. [2].

For the deuterium target the region between the pd threshold at 1.7 GeV and the pp threshold at 2.5 GeV is the subthreshold region, which can be populated only via nuclear effects. The Fermi motion of the nucleons is taken into account by applying the Paris deuteron wave function to describe the momentum distribution of the spectator in quasi-free collisions. The

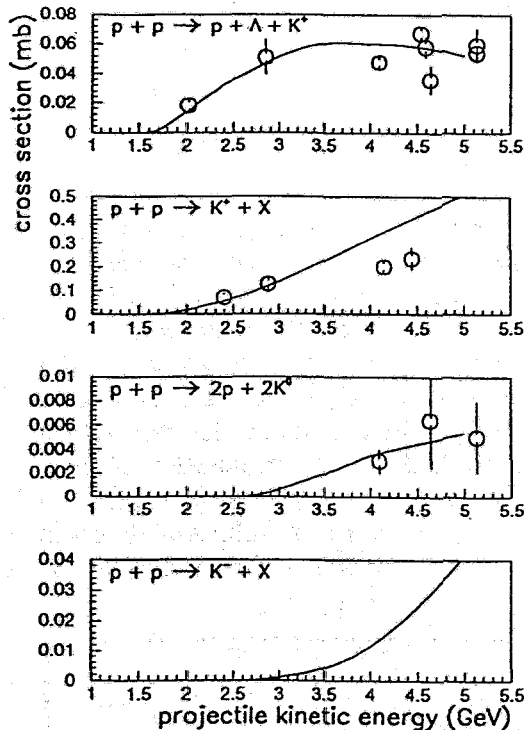


Fig.3 Energy dependence of the cross section for channels with strangeness production. Data from Ref. [1].

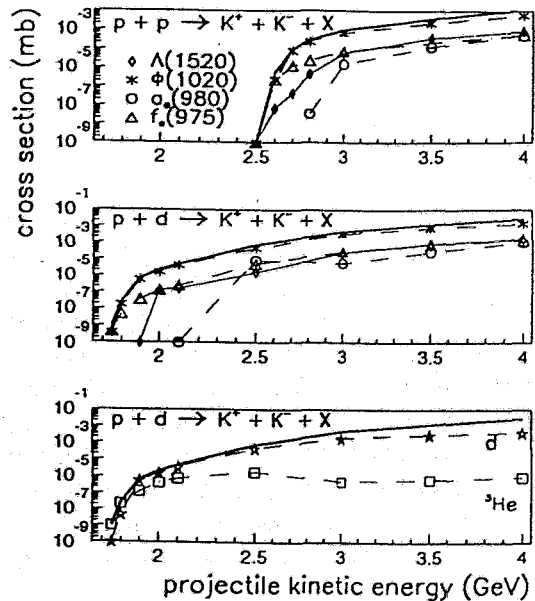


Fig.4 Energy dependence of the cross section for inclusive production of K^+K^- pairs in pp and pd reactions. In the upper two figures the the partial cross sections for K^+K^- production via resonances, and in the lower figure the cross section for associated production of light fragments are plotted.

Fermi motion of the nucleons is taken into account by applying the Paris deuteron wave function to describe the momentum distribution of the spectator in quasi-free collisions. The other principal reaction mechanism is called cluster excitation and includes all processes with both nucleons of the deuteron participating in the interaction. Such a cluster of nucleons is treated as an entity, which interacts in the same way as a hadron.

From the calculation presented in the lower part of Fig. 4 it can be expected that up to about 100 MeV above the threshold there is a large probability that the produced K^+K^- pair is accompanied by a ${}^3\text{He}$, while at higher energies the deuteron becomes the dominating particle. The production of the $K\bar{K}$ pair consumes so much energy that no energy is left for the relative motion of the remaining particles, and bound states are favoured.

The $K\bar{K}$ pair may be created directly or via resonances. However, the nature of the involved resonances is not well established at present. This concerns especially the $f_0(975)$ and the $a_0(980)$ resonances. In agreement with the latest particle review [1] these two resonances are treated as usual $q\bar{q}$ quark-model states. But for the estimate of the total cross sections this uncertainty is not so important, because K^+K^- production via the $\Phi(1020)$ meson yields the main contribution (see Fig. 4).

The planned 0° facility [4] at COSY is well suited for investigating subthreshold K^- production, and the calculated cross sections may serve as a basis for estimating the expected counting rates.

REFERENCES:

- [1] V. Flamino et al., Preprint CERN-HERA 84-01 (Geneva 1984)
- [2] E. Chiavassa et al., Sixièmes Journées d'Études Saturne (Mont Sainte Odile, 1992)
- [3] H. Müller and K. Sistemich, Z. Phys. A344 (1992) 197
- [4] W. Borgs et al., COSY Proposal #18 (1991)

Simulation of K^+ -Production Measurements at the 0° Facility^B

M. BÜSCHER^a, S. DSHEMUCHADZE^b, H. MÜLLER^b, CHR. SCHNEIDERREIT^b

^a *Forschungszentrum Jülich, Institut für Kernphysik*

^b *Forschungszentrum Rossendorf, Institut für Kern- und Hadronenphysik*

For the planned measurement of subthreshold K^+ production (COSY-Proposal Nr.18 [1]) an efficient first-level trigger is necessary in order to select the rare K^+ events from the background of pion and proton events. In Fig. 1 the expected spectra of protons, π^+ and K^+ mesons from the interaction of 1.5 GeV protons with carbon are plotted.

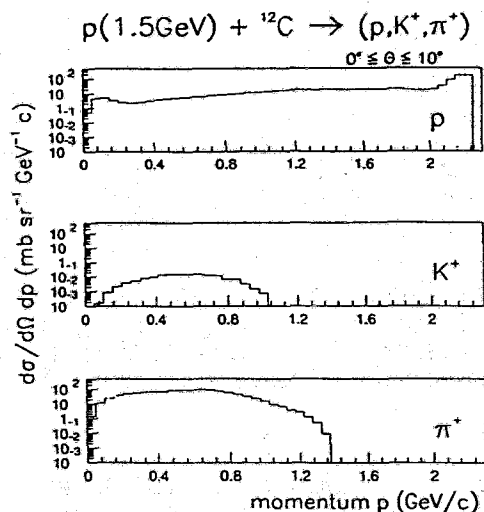


Fig.1 Calculated differential cross sections for the production of protons, π^+ and K^+ mesons from the reaction $p + {}^{12}\text{C}$ at 1.5 GeV incidence energy.

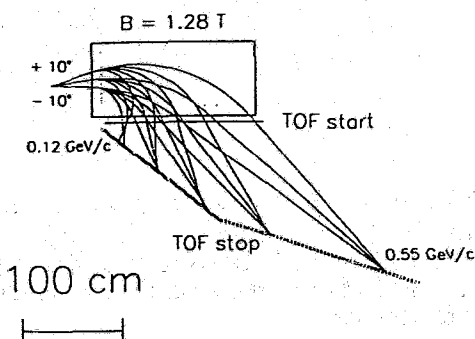


Fig.2 Schematic view of the detector arrangement used for the calculations. The 30 start counters have a width of 5 cm, while the width of the 32 stop counters varies between 7 cm and 15 cm.

In the momentum region around 0.5 GeV/c the ratio of the differential cross sections for K^+ , proton and π^+ production is about $K^+ : p : \pi^+ = 1 : 10^2 : 10^3$. It should be stressed, however, that measurements also at energies below 1 GeV are planned. Due to the strongly decreasing K^+ cross section the relation between kaons and the other charged particles becomes then even worse.

The above estimate of the expected cross sections is carried out in the framework of the modified phase space model [2], which is implemented in such a way that complete events are generated. These events are used as input for the CERN program GEANT in order to simulate the response of the detector arrangement, which is shown in Fig. 2. This is a simplified version of the arrangement suggested in the proposal with the multiwire chambers omitted, since they will not be used for the first-level trigger. There are 30 start scintillation detectors placed near the magnet and 32 stop detectors positioned in the vicinity of the focal plane. A fast first-level trigger will use time-of-flight and ΔE information from these detectors to suppress the unwanted pion and proton events. Here we concentrate ourselves on the time-of-flight measurement. Particles ejected in the angular acceptance region $\Theta < 10^\circ$ of the magnet may pass through different start counters on their ways to a definite stop counter. Therefore, in the fast trigger the time-of-flight information from all these possible combinations of start and stop detectors must be analysed.

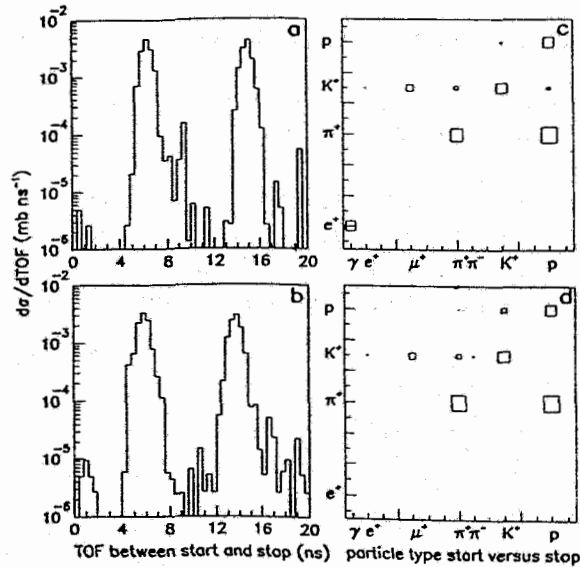


Fig.3 Time-of-flight spectra from hits in stop detector Nr. 25 combined with hits in a) start detector Nr. 14 and b) Nr. 18. The right hand part of the figure shows the particle types which cause the hits in the corresponding start and stop detectors for events in the time-of-flight interval of c) 8-10.5 ns and d) 7-9.5 ns. The dimensions of the boxes are proportional to the intensities.

In order to give an impression of the expected results we show in Fig. 3 as an example the time-of-flight spectra arising from combining hits either in start counter Nr. 14 or Nr. 18 with hits in the stop counter Nr. 25. For the time resolution of the photomultiplier a value of 0.65 ns FWHM is assumed.

We see the expected structure of the spectra with two pronounced peaks around 5 and 15 ns arising mainly from pions and protons. In between the K^+ peak is much smaller and in the Fig. 3a better separated from the pion peak than in Fig. 3b. In a next step windows in the time-of-flight spectra are chosen such that practically no K^+ events are lost. Now we scan the events which lie in the time windows indicated in the capture of Fig. 3 and look what kind of particles have made the hits in the start and stop detectors. The result is shown in the right hand part of the figure. Besides the true events where the hit in the start and in the stop detector has been caused by the same kaon there are other events originating either from kaons which decay before they reach the stop detectors or from different particles which hit the start and stop detector accidentally within the selected time interval. The portion of the true kaon events amounts to 23 % and 3.5 % for the two investigated detector combinations. These numbers can be considered as an optimistic estimate of the trigger efficiency which can be reached on the basis of the time-of-flight information. At lower incidence energies, however, the number of kaons drastically decreases and the trigger becomes less efficient. Therefore, the first-level trigger must be improved by combining the time-of-flight with the ΔE information and using a more complicated structure of the stop detectors including veto and Čerenkov counters to suppress the pions. Appropriate simulations are under preparation.

REFERENCES:

- [1] W. Borgs et al., COSY Proposal Nr. 18, 1991
- [2] H. Müller, Z. Phys. A339 (1991) 409

Subthreshold production of K^+ mesons and the fragmentation of the target nucleus

(Z. Phys. A344 (1992) 197)

H. Müller, M. Büscher and K. Sistemich

Abstract: The interplay between subthreshold K^+ -production and the fragmentation of the target nucleus is considered in proton-nucleus interactions at projectile energies between 0.8 and 1 GeV. Inclusive data for the production of K^+ mesons and of fragments are well described in the framework of the modified phase space model. For a coincidence measurement between K^+ mesons and fragments the model predicts a decrease of the relative yield of intermediate mass fragments by about four orders of magnitude. This strong decrease is a consequence of energy-momentum conservation, because at subthreshold energies a second endothermic process like multifragmentation can hardly proceed simultaneously with the K^+ production. A K^+ meson is, therefore, expected to be accompanied by a heavy target residue, which is so weakly excited that it may evaporate a few nucleons but cannot decay into fragments. Due to the large energy and momentum transfer in this process the strength of the predicted effect is supposed to be sensitive to the details of the reaction dynamics.

3. Experimental Nuclear Spectroscopy

A Three-Quasiparticle Band in ^{81}Rb

H. ROTTER^{1,2}, J. DÖRING³, L. FUNKE⁴, L. KÄUBLER^{1,5}, R. SCHWENGER¹, G. WINTER¹

¹Forschungszentrum Rossendorf, Institut für Kern- und Hadronenphysik

²Arbeitsbeschaffungsverein Rossendorf

³Department of Physics, Florida State University, Tallahassee, Florida, USA

⁴Ingenieurgesellschaft IAF Dresden

⁵KAI im Forschungszentrum Rossendorf

The investigation of high-spin states in ^{81}Rb was earlier started by bombarding a NH_3Br target of natural isotopic abundance with 27 MeV α -particles from the Rossendorf cyclotron [1]. Especially, a level sequence built on top of the 2636 keV level was established by these experiments. The investigation of ^{81}Rb was completed by measuring the angular distribution of the γ -rays emitted from a Na^{79}Br target (enriched to 98.6%) during the α -particle bombardment. The angular distribution coefficients of the transitions depopulating the 2697 keV state to levels with well-known spin and parity (see fig. 1) allow us to fix the spin value of the initial state to 17/2. Among the intraband transitions the 61 keV transition with $A_2 = -0.21(2)$ appears clearly to be a dipole transition, whereas for the peaks at 300 keV and 430 keV being complex due to unresolved dipole transitions from ^{81}Rb and ^{81}Kr , respectively, only some total of A_2 values can be given. Similar negative-parity 3qp bands have been found, e.g., in the neighbouring isotopes ^{83}Rb and ^{79}Rb (refs. [2] and [3], resp.) as well as in the adjacent isotones ^{79}Br and ^{83}Y (refs. [4] and [5], resp.). A plot of the aligned angular momentum I_x as a function of the rotational frequency reveals for the 3qp band in ^{81}Rb a similarly large value of I_x as for the negative-parity 3qp bands, e.g., in ^{79}Br and ^{83}Y (see fig. 2). Such a large alignment suggests that the negative-parity 3qp band in ^{81}Rb involves at least one $g_{9/2}$ proton, while one of the unpaired neutrons is due to the $g_{9/2}$ shell and the other one can be attributed to the negative-parity orbits $p_{1/2}$, $p_{3/2}$ and/or $f_{5/2}$.

REFERENCES:

- [1] W. Wagner et al., Annual report 1988, ZfK-667(1989) 28
- [2] W. Gast et al., Phys.Rev.C22(1980)469
- [3] J. Döring et al., to be published
- [4] R. Schwengner et al., NPA486(1988)43
- [5] C.J. Lister et al., Z.Phys.A329(1988)413

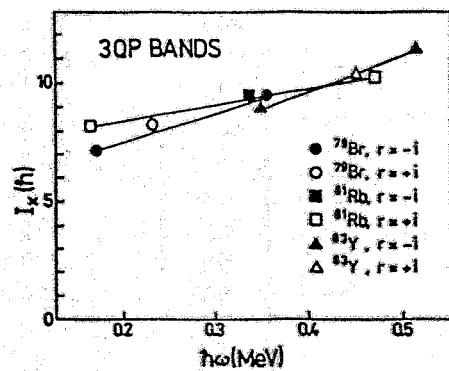
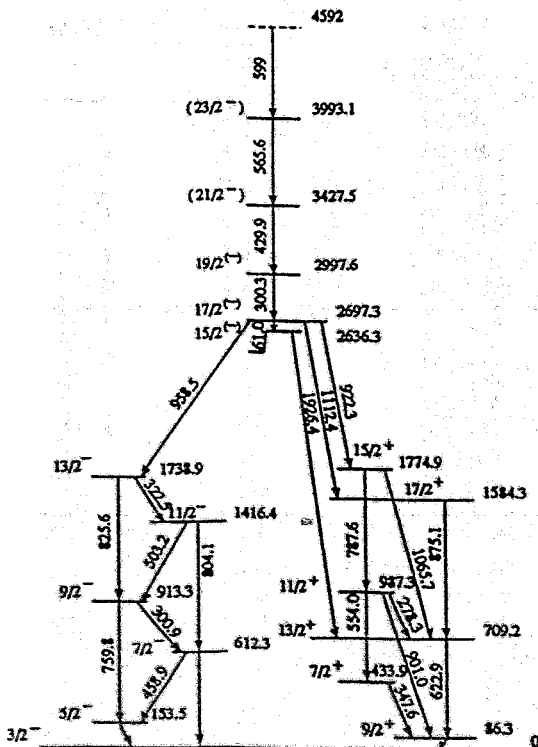


Fig. 2 Aligned angular momentum I_x of negative-parity 3qp bands in ^{79}Br , ^{81}Rb and ^{83}Y as a function of the rotational frequency $\hbar\omega$

Fig. 1 Partial level scheme of ^{81}Rb displaying the deexcitation of the 3qp band as obtained in the $(\alpha, 2n)$ reaction

DCO Analysis of γ Transitions in ^{83}Br and ^{85}Rb

R. SCHWENGER¹, G. WINTER¹, R. WIROWSKI², N. NICOLAY²,
P. VON BRENTANO² AND W. ANDREJTSCHIEFF³

¹*Forschungszentrum Rossendorf, Institut für Kern- und Hadronenphysik*

²*Institut für Kernphysik der Universität zu Köln*

³*Institute for Nuclear Research and Nuclear Energy, Sofia, Bulgaria*

In experiments with multidetector arrays the analysis of directional correlations of γ rays from oriented states (DCO) is applied to deduce the multipole order of the γ rays and the spins of the emitting states. The DCO ratio is defined as $R_{DCO} = W(\theta_1, \theta_2, \phi)/W(\theta_2, \theta_1, \phi)$, where $W(\theta_1, \theta_2, \phi)$ denotes the intensity of a transition γ_2 measured in a detector at the angle θ_2 relative to the beam, gated by a transition γ_1 measured in a detector at θ_1 . The quantity ϕ is the angle between the two planes opened by the respective target-detector axis and the beam axis [1]. The intensity $W(\theta_2, \theta_1, \phi)$ describes the reverse case arising from an exchange of the angles or of the gating and observed transition. A ratio of $R_{DCO}=1$ is obtained if the transitions γ_1 and γ_2 have equal multipole order and are stretched transitions.

The nuclei ^{83}Br and ^{85}Rb have been investigated in coincidence experiments with the detector array OSIRIS CUBE at the tandem accelerator in Köln [2,3]. In order to deduce DCO ratios the γ - γ coincidence data were sorted into 8 E_{γ_1} - E_{γ_2} matrices that correspond to each detector combination with $\theta_1=45^\circ$, $\theta_2=90^\circ$, $\phi=90^\circ$. Further 8 matrices were created from γ - γ - α coincidence events. Coincidence spectra were extracted by setting gates on certain peak and background intervals in the $(45^\circ, 90^\circ)$ and the transposed $(90^\circ, 45^\circ)$ matrices. To use the full statistics all 8 spectra related to a certain peak or background gate at one angle combination were corrected for the energy-dependent efficiencies of the gating and the spectrum detector and were added up. DCO ratios were then obtained from peak intensities in the background-corrected sum spectra. Based on these values several spin assignments for new levels in ^{83}Br and ^{85}Rb could be made. Examples of DCO ratios are given in table 1.

Table 1: DCO ratios in ^{83}Br and ^{85}Rb

	E_{γ_1} (keV) ¹⁾	E_{γ_2} (keV)	$R_{DCO} =$	$L_{\gamma_1}^{1,2)}$	$L_{\gamma_2}^{2)}$	$(I_i - I_f)_{\gamma_2}$
	gate	analysed peak	$\frac{I_{\gamma_2}(90^\circ, 45^\circ, 90^\circ)}{I_{\gamma_2}(45^\circ, 90^\circ, 90^\circ)}$			
^{83}Br	356	225	0.95(5)	1	1	1
	356	572	1.02(6)	1	1	1
	356	1260	1.32(11)	1	2	2
	609	225	0.59(5)	2	1	1
	609	636	0.53(17)	2	1	1
	609	1064	0.95(6)	2	2	2
^{85}Rb	228	192	0.97(4)	1	1	1
	228	436	1.56(6)	1	1	0
	228	779	1.64(5)	1	2	2
	779	192	0.61(3)	2	1	1
	779	1014	1.04(3)	2	2	2
	779	1365	0.50(3)	2	1	1

¹⁾ Transition with known multipole order and spin difference of initial and final state.

²⁾ Multipole order: Transitions with $L = 1$ can include admixtures of $L = 2$.

REFERENCES:

- [1] A. Krämer-Flecken et al., Nucl. Instr. Meth. A275 (1989) 333
- [2] R. Schwengner et al., Annual report 1991, FZR 92-09 p. 37
- [3] G. Winter et al., contribution to this report

Medium-spin States of negative Parity in ^{85}Rb

G. WINTER, R. SCHWENGNER, W. ANDREJTSCHEFF[◇] AND H. PRADE
Forschungszentrum Rossendorf, Institut für Kern- und Hadronenphysik
[◇]*Institute for Nuclear Research and Nuclear Energy, Sofia*

R. WIROWSKI, N. NICOLAY AND P. VON BRENTANO
Institut für Kernphysik der Universität zu Köln

In connection with our in-beam experiments for the study of high-spin states in $^{85,86}\text{Kr}$ via the bombardment of ^{82}Se with 32 MeV ^7Li ions [1,2] new $\gamma\gamma$ coincidence data have also been obtained for the nucleus ^{85}Rb that is formed after the emission of four neutrons from the compound system. Using the 6 detector arrangement OSIRIS-CUBE at the tandem accelerator in Cologne approximately 3×10^8 coincidence events have been collected. In order to derive information on the directional correlations of coincident γ rays from oriented nuclei (DCO ratios) these data have been sorted in a total matrix and also in different submatrices according to the observation angles of the detectors involved.

As a result of this study a new group of medium-spin states in ^{85}Rb has been established that de-excite mainly to the $9/2^+$ isomer but also to the $5/2^-$ ground state. Due to the decay pattern observed we assign tentatively negative parity to most of the new states. In the previous level scheme [3] only two negative-parity states of spin $I \geq 9/2$ were known, $19/2^-$ and $21/2^-$, and interpreted as the coupling of a proton in the $p_{3/2}$ or $f_{5/2}$ orbital, respectively, to the 8^+ two neutron-hole excitation.

The new levels may arise from the excitations of three protons within the negative-parity subshell ($f_{5/2} p_{3/2}$) and the two neutron holes might be coupled to 0^+ , 2^+ or 4^+ . At higher excitation energy two protons may occupy the $g_{9/2}$ orbital while a third remains in the lower lying negative-parity orbitals.

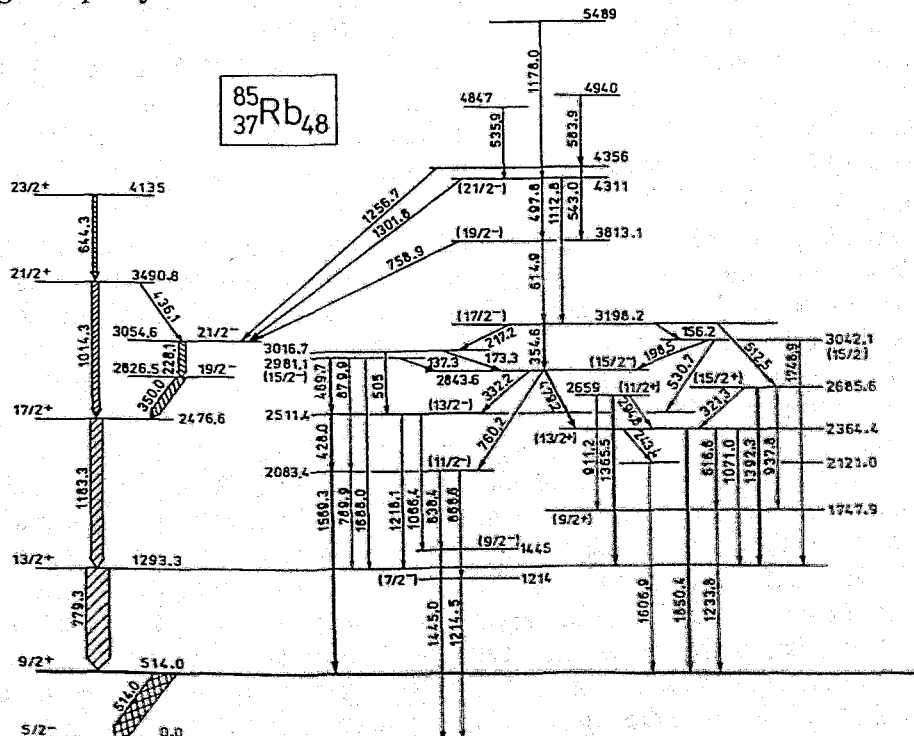


Fig. 1. Part of the level scheme of ^{85}Rb showing the decay of the new medium-spin states.

REFERENCES:

- [1] G. Winter et al. *Z. Physik A343* (1992) 369
- [2] G. Winter et al. *Z. Physik A344* (1992) 229
- [3] G. Winter et al. *Z. Physik A334* (1989) 415

Shell Model Study of ^{85}Kr

J. REIF, G. WINTER

Forschungszentrum Rossendorf, Institut für Kern- und Hadronenphysik

H. GRAWE, R. SCHUBART

Hahn-Meitner-Institut Berlin, Bereich Schwerionenphysik

Recently, high-spin states in the $N=49$ nucleus ^{85}Kr were investigated via in-beam spectroscopy, and a new sequence of states built on the $17/2^+$ μs isomer with excitation energies up to 4.8 MeV and tentative spins up to $(23/2)$ was established [1]. A tentative assignment of the configuration $\nu 0g_{9/2}^9 \pi (0g_{9/2}^1 1p_{3/2}^3$ or $0f_{5/2}^5)$ was proposed [1] to the new levels.

In order to verify this conjecture shell model calculations have been carried out employing the code RITSSCHIL [2]. For the calculation of states with $J \geq 9/2$ it has been assumed that the energy levels up to 5 MeV can be described by coupling one neutron hole in the $0g_{9/2}$ orbital to the proton system. In the Kr nuclei the Fermi level in the proton system is close to the $1p_{3/2}$ or $0f_{5/2}$ orbitals, and the high-j orbital $0g_{9/2}$ comes into play at high excitation energies. Therefore the model space has been generated out of active $0f_{5/2}$, $1p_{3/2}$, $1p_{1/2}$, $0g_{9/2}$ proton (π) and $0g_{9/2}$ neutron (ν) orbitals relative to a ^{68}Ni core. The effective interaction in the proton shells has been taken from the work by Ji et al. [3]. For the $\pi\nu$ -interaction connecting the $\pi(1p_{1/2}, 0g_{9/2})$ and $\nu 0g_{9/2}$ orbitals the data given by Gross et al. [4] have been used. The matrix elements of the $\nu\nu$ -interaction for the $0g_{9/2}$ orbital have been assumed to be equal to the $T=1$ component of the $\pi\nu$ -interaction given in [4]. For the $(\pi 0f_{5/2}, \nu 0g_{9/2})$ residual interaction the matrix elements proposed by Li et al. [5] have been applied. The remaining two-body matrix elements have been calculated with the modified surface delta interaction using the strength parameters $A_{T=1}=A_{T=0}=0.35\text{MeV}$. The single-particle energies relative to the ^{68}Ni core have been derived from the single-particle energies of the proton orbitals with respect to the ^{78}Ni core [2] and from the neutron single-hole energy of the $0g_{9/2}$ orbital relative to the ^{88}Sr core [3]. The transformation of these single-particle energies with respect to the ^{68}Ni core has been performed on the basis of the residual interactions given above. The obtained values are, in MeV, $\epsilon_{f_{5/2}}^\pi = -9.806$, $\epsilon_{p_{3/2}}^\pi = -9.733$, $\epsilon_{p_{1/2}}^\pi = -3.023$, $\epsilon_{g_{9/2}}^\pi = -1.226$, $\epsilon_{g_{9/2}}^\nu = -6.583$.

Following Ji et al. [3] a truncation of the proton model space has been used where at most four protons are allowed to occupy the $0g_{9/2}$ shell, and no restrictions are assumed for the other considered proton orbitals. The coupling of the neutron hole excitation in the $0g_{9/2}$ shell to this restricted proton space yields a model space which has dimensions up to 10000. The result of the calculation of level energies is shown in Fig. 1 together with the experimentally observed levels. The excitation energies of all experimentally known yrast states with $I^\pi \geq 9/2^+$ or $I^\pi > 15/2^-$ are well reproduced in the calculation. In particular, the small energy separation observed between the $13/2^+$ and $17/2^+$ yrast levels is also predicted by the shell model. The analysis of the calculated wave functions reveals that the $11/2^+$, $13/2^+$ or $15/2^+$, $17/2^+$ states are predominantly formed by coupling the neutron hole to the lowest 2^+ or 4^+ states of the proton system, respectively, as indicated by the dashed lines in Fig. 1. Similarly, the $15/2^-$, $17/2^-$, and $19/2^-$, $21/2^-$ states result mainly from the coupling of the neutron hole to the 5^- and 6^- proton states, respectively. The lowest 7^- proton state dominates in the wave function of the $23/2^-$ level. Because the main components of the wave functions of the 5^- and 6^- , 7^- levels are given by the configurations $(f_{5/2}^4, p_{3/2}^3, g_{9/2}^1)$, $(f_{5/2}^6, p_{3/2}^1, g_{9/2}^1)$ and $(f_{5/2}^5, p_{3/2}^2, g_{9/2}^1)$, respectively, the shell model predicts the proposed configuration $\nu 0g_{9/2}^9 \pi (0g_{9/2}^1 1p_{3/2}^3$ or $0f_{5/2}^5)$ [1] to the states on top of the $17/2^+$ isomer.

In addition, $B(E2)$ values have been calculated using effective charges of 1.35e and 0.35e for protons and neutrons, respectively. The value $B(E2, 13/2^+ \rightarrow 9/2^+) = 2.06$ W.u. is in agreement with the experimental value of $2.8 \pm_{0.3}^{0.4}$ W.u. [6] whereas the value $B(E2, 17/2^+ \rightarrow 13/2^+) = 0.56$ W.u. is too small compared to the experimental result of $B(E2, 17/2^+ \rightarrow 13/2^+) = 3.8 \pm 1.8$ W.u. [7].

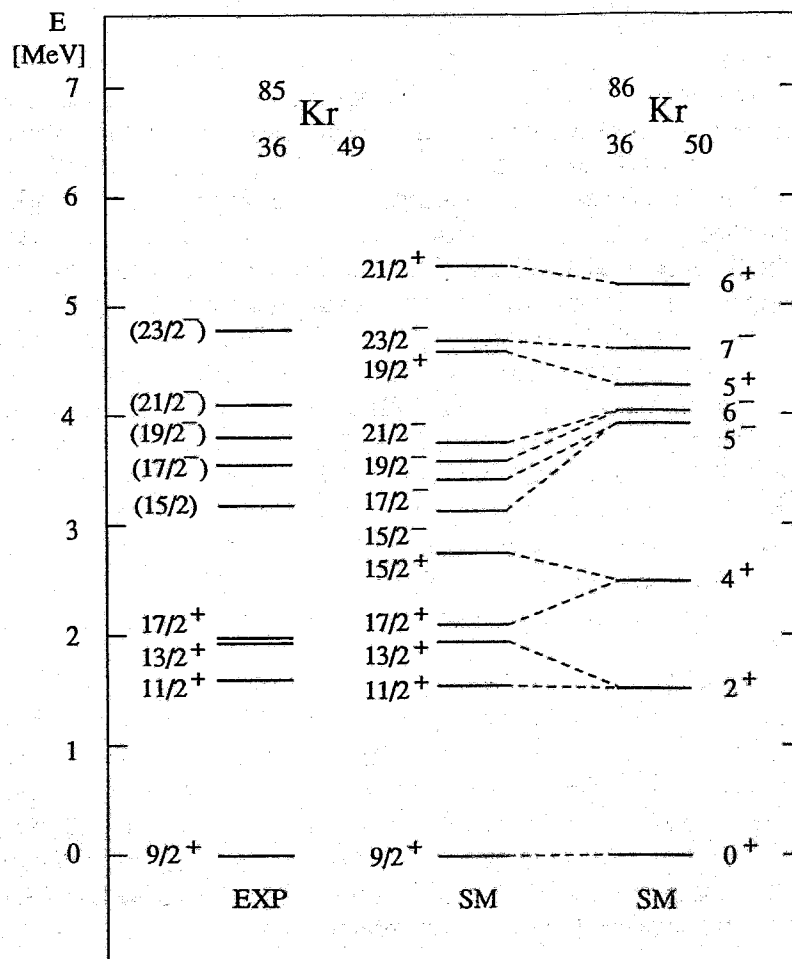


Fig.1 Comparison of experimental (column 1) and calculated (column 2) level energies of ^{85}Kr . Out of the calculated levels only the yrast states with $I^\pi \geq 9/2^+$ or $I^\pi \geq 15/2^-$ are shown. The calculated level energies of the lowest states of the $Z=36$ proton system (^{86}Kr) are shown in the third column. For each calculated energy level in ^{85}Kr , the proton state coupling dominantly to the neutron-hole excitation is indicated by a dashed line.

REFERENCES:

- [1] G. Winter et al., Z. Phys. A344 (1992) 229
- [2] D. Zwarts, Comput. Phys. Commun. 38 (1985) 565
- [3] X. Ji et al., Phys. Rev. C 37 (1988) 1256
- [4] R. Gross et al., Nucl. Phys. A267 (1976) 25
- [5] P. C. Li et al., Nucl. Phys. A469 (1987) 303
- [6] A. E. Zobov et al., Reports on 36. Conference on Nuclear Spectroscopy and Nuclear Theory, Kharkov (1986) 72
- [7] G. Winter et al., Z. Phys A332 (1989) 33

The Odd-Mass Valence Mirror Nuclei $^{113}_{50}\text{Sn}_{63}$ and $^{145}_{63}\text{Eu}_{82}$ ^{B,D}

L. KÄUBLER^{1,2}, H. PRADE¹

¹Forschungszentrum Rossendorf, Institut für Kern- und Hadronenphysik
²KAI e.V. Wissenschaftlerintegrationsprogramm

Assuming ^{113}Sn and ^{145}Eu as semimagic nuclei with closed $N=50$, $Z=50$ or $Z=50$, $N=82$ cores, respectively, the 13 active neutrons or protons should occupy the same shell model orbits. Such pairs of nuclei are denoted as quasimirror nuclei [1] or valence mirror nuclei [2]. As a consequence of the charge symmetry and charge independence of the nuclear forces, shell model calculations for both nuclei using the same single-particle energies and the same residual interaction give identical results. But, for real calculations different shell model parameters for tin nuclei and $N=82$ nuclei have to be used to obtain optimal correspondence between theory and experiment (cf. the corresponding table in Ref. [1]).

As a result of our comprehensive study [3] of ^{113}Sn its experimentally observed yrast states are compared with the corresponding states in ^{145}Eu (Fig.1). Like in the hitherto compared pairs of even-even valence mirror nuclei in this region, remarkable similarities are observed. The negative-parity states with $11/2^- < J^\pi \leq 23/2^-$ have nearly the same level sequence and within 250 keV similar excitation energies. In both nuclei $25/2^+$ and $27/2^+$ states are found at nearly the same energy which should have $\nu 1h_{11/2}^2$ components. Furtheron, in both nuclei no comparable positive-parity states with $7/2^+ < J^\pi < 25/2^+$ are observed. For the $1/2^+$, $3/2^+$ and $5/2^+$ states characterized by the occupation of the $3s_{1/2}$, $2d_{3/2}$ and $2d_{5/2}$ shell model states large differences are found. On the other hand, the $11/2^-$ states based on the $1h_{11/2}$ orbit agree very well.

The observed similarities seem to be in contradiction to the different shell model parameters used for the tin and $N=82$ nuclei. To explain this discrepancy, the influence of the extra neutron core between $N=50$ and 82 in the $N=82$ nuclei has to be considered [4]. The monopole proton-neutron residual interaction, e.g., is most attractive for the similar orbits $\pi 1g_{9/2}$ and $\nu 1g_{7/2}$ causing a different behaviour of the $g_{7/2} - d_{5/2}$ splitting in tin and $N=82$ nuclei. Thus, even if the underlying single particle energies are different, the mirror similarity can persist. The comparison of ^{113}Sn and ^{145}Eu confirms the difficulty with the assumption of neutron-proton symmetry in the valence mirror nuclei.

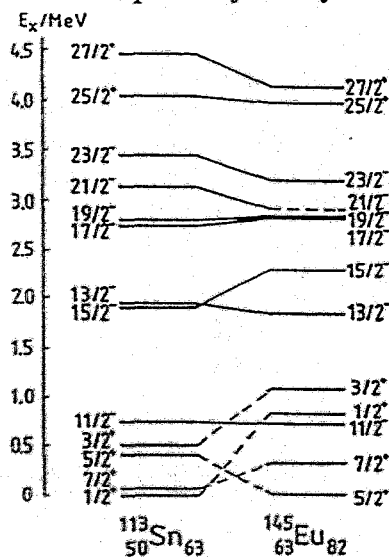


Fig. 1. Comparison of the experimentally observed yrast states in ^{113}Sn with the corresponding levels in ^{145}Eu

REFERENCES:

- [1] H. Prade et al., Nucl. Phys. A425(1984)317
- [2] R. Wirowski et al., J. Phys. G14(1988)L195
- [3] I.N. Vishnevski et al., Annual Report 1988, ZfK-667(1989)35; L. Käubler et al., Annual Report 1992, FZR 92-09(1992)34; L. Käubler et al., Book of Abstracts, Int.Nucl.Phys.Conf., Wiesbaden 1992, p. 1.2.16
- [4] R.F. Casten et al., Nucl. Phys.A514(1990)252

Yrast Spectroscopy in the N=82 Nucleus ^{142}Nd ^B

H. PRADE, J. DÖRING¹, W. ENGHARDT², L. FUNKE³, L. KÄUBLER²,
R. SCHWENGER AND G. WINTER

Forschungszentrum Rossendorf, Institut für Kern- und Hadronenphysik

¹*Department of Physics, Florida State University, Tallahassee, Florida, USA*

²*KAI im Forschungszentrum Rossendorf* ³*Ingenieurgesellschaft IAF Dresden*

R. WIROWSKI, J. YAN, P. PETKOV, A. DEWALD, A. GELBERG AND P. VON BRENTANO

Institut für Kernphysik der Universität zu Köln

In-beam studies of multiparticle excitations in the N=82 nucleus ^{142}Nd had been independently started at the same time in the former Central Institute for Nuclear Research in Rossendorf and at the University of Cologne. Preliminary results of these investigations have been published in *Zeitschrift für Physik* [1,2] and earlier annual reports [3,4].

With respect to the close collaboration between the spectroscopy groups in Cologne and Rossendorf, well established especially during the recent years, we decided to combine our earlier results up to an excitation energy of about 6 MeV, where they are overlapping, in a common final publication being in preparation.

Our major activities and results can now be summarized as follows:

Excited states of ^{142}Nd have been studied in the reactions $^{140}\text{Ce}(\alpha, 2n)^{142}\text{Nd}$, $^{139}\text{La}(^7\text{Li}, 4n)^{142}\text{Nd}$ and $^{130}\text{Te}(^{16}\text{O}, 4n)^{142}\text{Nd}$. Using in-beam spectroscopic methods energies, intensities, excitation functions, $\gamma\gamma$ -coincidences, angular distribution and linear polarization of γ -rays as well as γ -ray time distributions relative to the beam pulses have been measured at the beams of the Rossendorf cyclotron and of the tandem accelerator in Cologne.

In Fig. 1 the level scheme of ^{142}Nd as deduced from our experimental results is shown up to an excitation energy of 5747 keV and spin values up to 14 \hbar . Altogether 33 new levels have been established and for five of them nanosecond lifetimes have been determined (indicated also Fig. 1).

The experimental data on excitation energies and electromagnetic properties of even-parity ^{142}Nd levels are compared with predictions of the spherical shell model. Odd-parity states of ^{142}Nd are interpreted in terms of a particle-core coupling approach by coupling one $1h_{11/2}$ proton to $\pi = +1$ shell-model states in ^{141}Pr .

As shown in [3] the experimental level energies are generally predicted a bit too small, while the sequence and the spacings of the levels are well reproduced. A similar good agreement between theoretical and experimental values was found with respect to the half-lives, branching and mixing ratios. Thus, it can be stated, that the shell-model approach applied in the present studies is capable of describing the mean features of positive- and negative-parity states up to an excitation energy of 5.5 MeV.

REFERENCES:

- [1] H. Prade et al., *Z. Physik* A328 (1987) 501
- [2] R. Wirowski et al., *Z. Physik* A347 (1988) 509
- [3] H. Prade et al., Annual report 1987, ZfK-638 (1988) 25
- [4] H. Prade et al., Annual report 1988, ZfK-667 (1989) 36

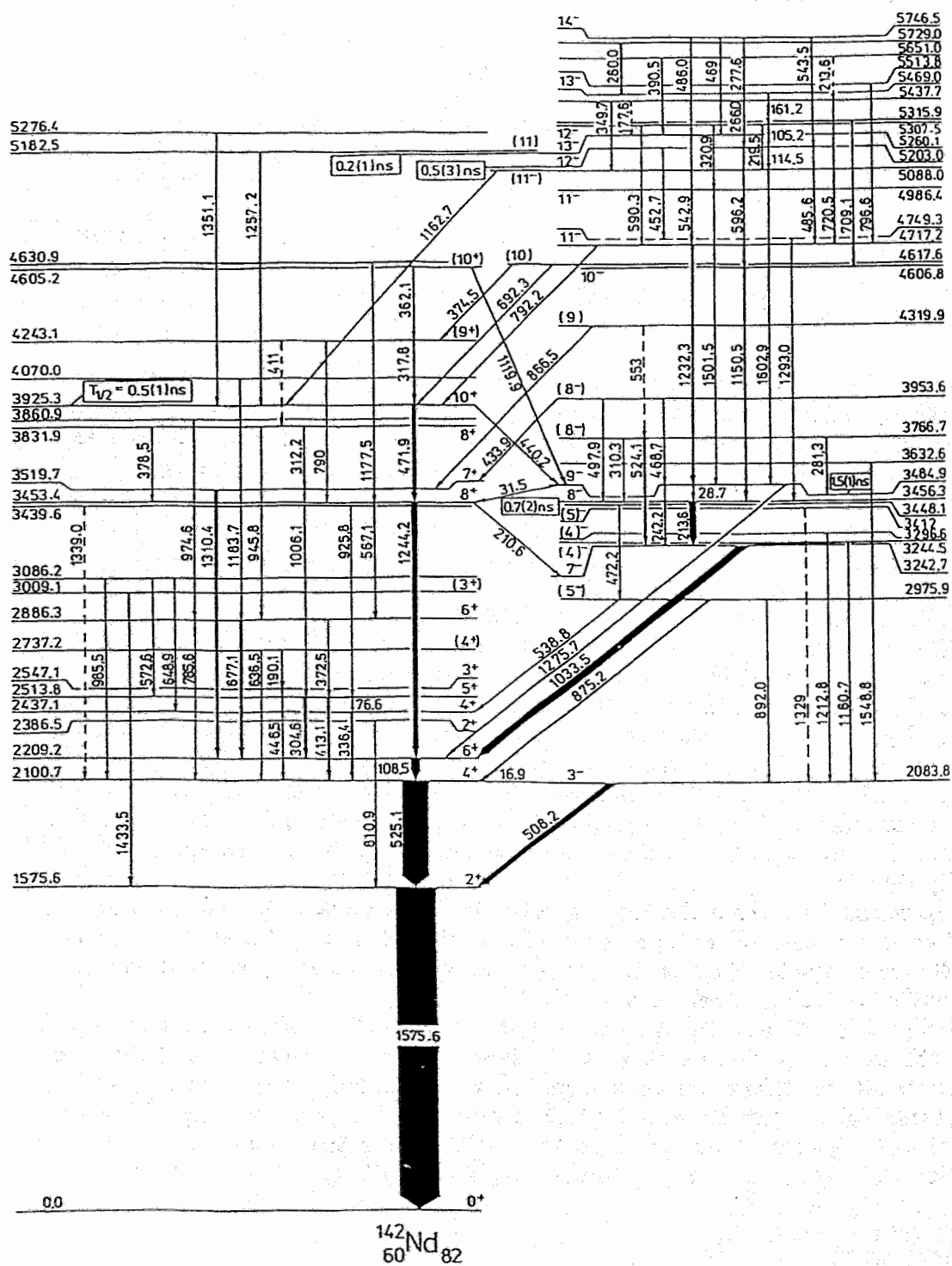


Fig. 1: Level scheme of ^{142}Nd as obtained in the present investigations. The width of the arrows is proportional to the γ -ray intensity observed in the $(\alpha,2n)$ reaction with 27 MeV α -particles.

Evidence for new isomers and band structures in ^{80}Rb
(Physical Review C46 (1992) R2127)

J. Döring, G. Winter, L. Funke, B. Cederwall, F. Lidén, A. Johnson, A. Atac, J. Nyberg, G. Sletten and M. Sugawara

Abstract: Excited states in the doubly odd nucleus ^{80}Rb have mainly been studied via the $^{68}\text{Zn}(^{19}\text{F},\alpha 3n)$ reaction at 72 MeV beam energy utilizing the NORDBALL detector system. The level scheme has been extended up to a (15^+) state at 4446 keV excitation energy. In the low-spin region seven new isomers with lifetimes in the nanosecond region have been found. In addition, a 6^+ isomer with a half-life of the order of μs has been identified at an excitation energy of 494.4 keV. For the level sequence built on this isomer positive parity is suggested and the states are ascribed to the intruder two-quasiparticle configuration $(\pi g_{9/2} \otimes \nu g_{9/2})$ and collective excitations.

Classical phase-space structure of the single-particle motion in cranked potentials
(J. Phys. A25 (1992) L115-L120)

J. Reif and R. Reif

Abstract: The phase-space structure of the single-particle motion in three-dimensional cranked Buck-Pilt potentials of lemniscatoidic shape has been investigated in terms of Poincaré surfaces of section, the mean value of positive maximal Ljapunov exponents, and the chaotic fraction of phase space as a function of the rotational frequency. Due to the rotation a partial regularization of the particle motion was found for certain values of deformation and frequency.

A new sequence of high-spin states built on the $17/2^+$ isomer in ^{85}Kr
(Z. Phys. A344 (1992) 229)

G. Winter, L. Funke, R. Schwengner, H. Prade, R. Wirowski, N. Nicolay, A. Dewald and P. von Brentano

Abstract: High-spin states in ^{85}Kr have been studied via in-beam spectroscopy by bombarding a ^{82}Se target with 32 MeV ^7Li ions. Since ^{85}Kr is only formed with a small relative cross section proton- γ - γ coincidence techniques have been applied to enhance the γ rays of ^{85}Kr , even with respect to those of ^{86}Kr , in the measurements. A new sequence of high-spin states with excitation energies up to 4.8 MeV and tentative spins up to $(23/2)$ has been established on top of the $17/2^+$ μs isomer. A tentative assignment of the configuration $\nu g_{9/2}^{-1} \pi (g_{9/2} p_{3/2}^{-1} \text{ or } f_{5/2}^{-1})$ to the new levels is proposed.

The half-life of the 1437 keV $11/2^-$ state in ^{97}Mo
(Z. Phys. A342 (1992) 145)

L.G. Kostova, W. Andrejscheff, L.K. Kostov, L. Funke, E. Will and A.I. Vdovin

Abstract: Using the (α, n) reaction, the half-life of the first $11/2^-$ level in ^{97}Mo has been determined as $T_{1/2}(1437.0 \text{ keV}) = 2.5 \pm 0.3 \text{ ns}$ by means of the pulsed beam method. The experimentally obtained $B(M2)$ value between the $h_{11/2}$ and $g_{7/2}$ configurations in ^{97}Mo has been satisfactorily described within the quasiparticle-phonon model using $g_s^{eff} = 0.6 g_s^{free}$. Similar calculations and comparisons with experimental data have been performed also for $^{95,99}\text{Mo}$ as well as for ^{99}Ru and ^{101}Pd .

High-spin states in the $N = 50$ nucleus ^{86}Kr
(Z. Phys. A343 (1992) 369)

G. Winter, L. Funke, R. Schwengner, H. Prade, R. Wirowski, N. Nicolay, A. Dewald and P. von Brentano

Abstract: High-spin states in the $N = 50$ nucleus ^{86}Kr have been investigated via the $^{82}\text{Se}(^7\text{Li}, p2n)$ reaction using 32 MeV ^7Li ions. In order to suppress γ -rays arising from pure neutron evaporation the measurements of angular distributions and relative excitation functions of the γ -rays as well as γ - γ coincidences have been performed in particle- γ coincidence modes. Levels with excitation energy up to 7.9 MeV and tentative spins up to (12) have been established. On the basis of systematics tentative assignments of shell model configurations are proposed.

4. Experimental Heavy Ion Physics

Status of the 4π -Fragment Spectrometer FOBOS ^B

H.-G. ORTLEPP^{1,2}, M. ANDRASSY^{1,2}, G.G. CHUBARIAN¹, M. DANZIGER^{1,3},
L. DIETTERLE^{1,2}, A.S. FOMICHEV¹, P. GIPPNER^{1,2}, C.-M. HERBACH^{1,2}, A.I. IVANENKO¹,
I.V. KOLESOV¹, A. MATTHIES^{1,2}, D. MAY^{1,2}, YU. TS. OGANESSIAN¹,
YU. E. PENIONZHKEVICH¹, V.N. POKROVSKIJ¹, G. RENZ^{1,2}, L.A. RUBINSKAJA¹,
V.E. SHUCHKO¹, O.V. STREKALOVSKIJ¹, V.V. TROFIMOV¹, V.M. VASKO¹, K. HEIDEL²,
K.D. SCHILLING², W. SEIDEL², H. SODAN⁴, W. WAGNER², H. FUCHS⁵, D. HILSCHER⁵,
H. HOMEYER⁵, W.V. OERTZEN⁵, G. PAUSCH^{5,6}, P. ZIEM⁵

¹Joint Institute for Nuclear Research, Dubna

²Forschungszentrum Rossendorf e. V. ³Technische Universität Dresden

⁴Zentralinstitut für Kernforschung Rossendorf

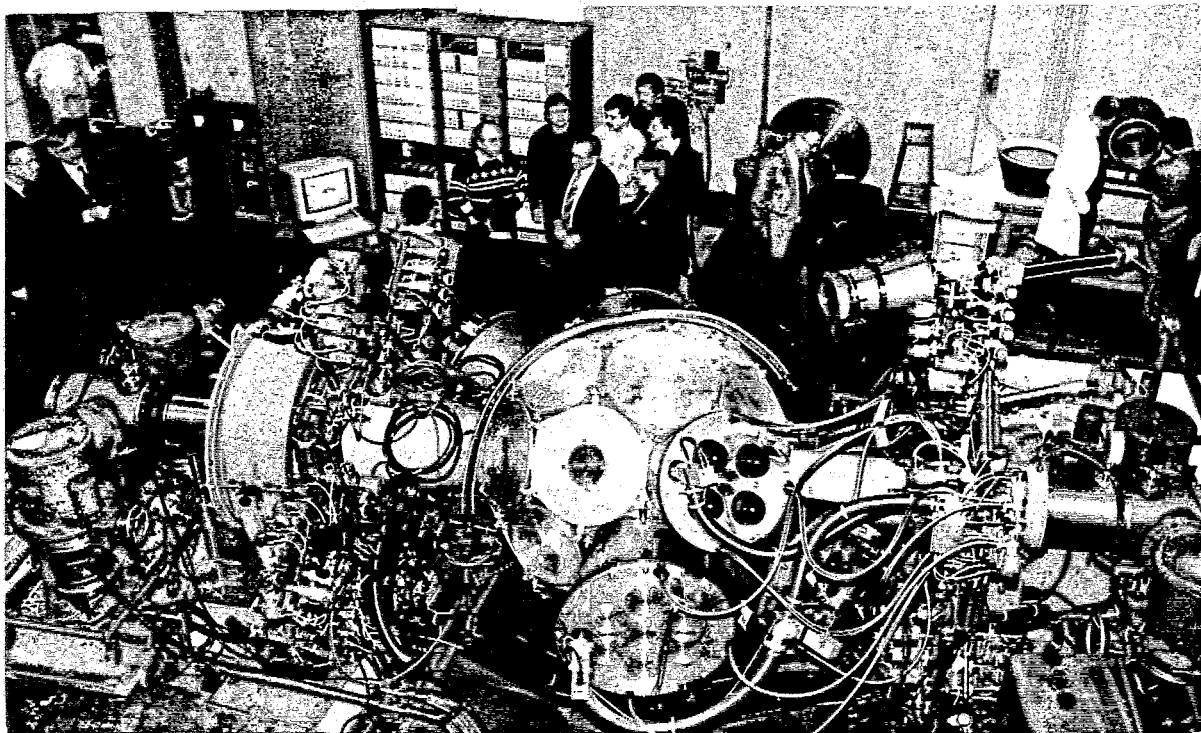
⁵Hahn-Meitner-Institut Berlin ⁶Freie Universität Berlin

The FOBOS spectrometer is intended for heavy ion reaction studies in the bombarding energy range of 10...100 A MeV [1-3]. In its final stage it will consist of a "gas ball" of 30 position-sensitive avalanche counters (DGAC) and 30 axial "Bragg" ionization chambers (BIC) behind them. A shell of 210 CsI(Tl) scintillation counters surrounds the gas ball. As forward detector, the ARGUS phoswich array [4] is planned to be used.

At present (February 1993), the components for 25 DGAC's are completed, 9 DGAC's are assembled and tested with an alpha source. Most of the BIC components have been delivered and are being assembled. All photomultipliers and the first 37 CsI(Tl) crystals have been obtained, remaining construction elements of the 210 scintillation counters are to be delivered soon. All pumps, valves, flow and pressure control units of the evacuation and gas supply system are mounted and checked for leaks [5]. The whole system equipped with 6 modules is now in the test phase. A basic software for control and diagnosis has been written. In 1992, further equipment for the front-end electronics has been received. 6 DGAC + BIC channels as well as the first-level trigger are prepared for experiments. The software for the data transfer from CAMAC via VDB-bus, an Eurocom-6 VME station and Ethernet to a VAX computer has been developed and implemented into the HOOPSY data acquisition system [6]. The whole system has been applied successfully in an experiment at VICKSI [7]. This new hard- and software enabled us to increase the data accumulation rate up to 1200 multi-parameter events per second. For the data analysis, a work station has been installed in Dubna where the OLYMP system [8] is running. Simulation and analysis procedures taking into account the geometry and individual properties of the FOBOS detectors have been further developed. The response to binary fission and multifragmentation has been simulated in order to study problems of acceptance, double hits and others. Trajectory calculations have been performed in order to simulate the proximity effect in the IMF (intermediate mass fragment) emission and the influence of the FOBOS geometry on the measurement of relative velocities. During 1992, experiments with gas-filled detector modules at the "mini"-FOBOS set-up, installed at the U-400 heavy ion cyclotron in Dubna, have been continued. Some results concerning near-barrier reaction cross sections (4.3 A MeV ⁸⁴Kr on ¹¹⁶Sn and ¹¹⁸Sn) and fission after incomplete fusion (10 A MeV ⁴⁰Ar on ¹⁹⁴Pt) are presented in contributions [9,10]. The independent mass determination based on the TOF-E method for each detected reaction product - one of the basic design features of FOBOS - enabled the data analysis without any additional assumptions. The interactive data analysis procedure [3], which takes into account all energy losses the particle suffers before reaching the sensitive volume of the

ionization chamber, has been further improved. Systematic errors and limitations of this method as well as their influence on momentum balances have been studied. If the full dynamic range is covered, the overall mass uncertainty (σ) does not exceed 2 amu for IMF's and 5 amu for FF's (fission fragments). For narrow ranges it becomes about twice better. In an 21 A MeV ^{20}Ne on ^{232}Th experiment, backward emitted FF's leaving the target with only 0.35 A MeV have been detected with an estimated mass resolution of 8%. IMF's up to ^{26}Fe have been resolved with regard to Z applying our digital Bragg peak spectroscopy method [11].

Prototypes of the large-area (\varnothing 200mm) CsI(Tl) crystals [12] of the FOBOS scintillator shell have been tested successfully in Dubna and at GANIL. The energy resolution and the identification capacity achieved practically correspond to the best literature data obtained so far with small crystals.



REFERENCES:

- [1] H.-G. Ortlepp et al., Report ZfK-734 (Rossendorf, 1990)
- [2] H.-G. Ortlepp et al., Proc. Int. Conf. on New Nuclear Physics with Advanced Techniques, Ierapetra, Crete, Greece, 1991 (World Scientific, 1992) 302
- [3] Annual report 1991 (FZ Rossendorf, Institute for Nuclear and Hadronic Physics) FZR 92-02 (1992) 51-66; also in: H.-G. Ortlepp and K.D. Schilling (eds.), Report FZR 92-11 (Rossendorf, 1992)
- [4] W. Terlau et al., Report HMI 482 (Berlin, 1990) 93
- [5] G. Renz et al., this Annual report
- [6] G. Roeschert et al., Bericht HMI 436 (Berlin, 1986)
- [7] G. Pausch et al., this Annual report
- [8] K.-P. Eckert et al., OLYMP User's Manual, Report HMI (Berlin, 1986)
- [9] C.-M. Herbach et al., this Annual report
- [10] H.-G. Ortlepp et al., this Annual report
- [11] H.-G. Ortlepp and A. Romaguera, Nucl. Instr. Meth. A 276 (1989) 50
- [12] W. Wagner et al., this Annual report

**Nuclear Reactions at the Coulomb Barrier
Induced by ^{84}Kr (4.3 A MeV) on ^{116}Sn and ^{118}Sn ^B**

C.-M. HERBACH^{1,2}, M. ANDRASSY^{1,2}, G.G. CHUBARIAN¹, P. GIPPNER^{1,2},
A. MATTHIES^{1,2}, H.-G. ORTLEPP^{1,2}, G. RENZ^{1,2}, K.D. SCHILLING²

¹ *Joint Institute for Nuclear Research, Dubna*

² *Forschungszentrum Rossendorf e.V.*

In the course of testing the detectors of the 4π -fragment spectrometer FOBOS [1], the reactions ^{84}Kr on ^{116}Sn and ^{118}Sn have been investigated at the U-400 cyclotron of the JINR Dubna with an incident beam energy slightly above the Coulomb barrier. Two gas-filled detector modules were coupled to the reaction chamber at the angles of $\vartheta_1 = 45^\circ$, $\varphi_1 = 270^\circ$ and $\vartheta_2 = 45^\circ$, $\varphi_2 = 90^\circ$ with respect to the beam axis and covered apertures of $\Delta\vartheta_1 = \pm 13.4^\circ$ and $\Delta\vartheta_2 = \pm 16.9^\circ$. Each of the modules consists of a position-sensitive double-grid avalanche counter (DGAC) and a Bragg ionization chamber (BIC) behind it. Whereas the elastic projectile scattering at the lighter target ingredients (Al, O etc.) is effectively suppressed by the kinematics, this geometry has a high acceptance for elastically scattered recoils (ESR) as well as for reaction products (RP) emitted from an intermediate system. In order to obtain start signals for the time-of-flight measurements independently for both detector modules, two small parallel-plate avalanche counters (PPAC) were positioned near the target.

The calculation of particle mass and emission energy is based on the analysis of the time-of-flight (TOF) and of the residual energy (EBIC). Thereby, an iterative procedure [2] considers the large amount of energy loss of the charged particles that have to pass through 7 mylar foils with a total areal density of 1.7 mg/cm^2 before they reach the BIC volume. The resulting mass resolution for the scattered Kr and Sn of $\text{FWHM} = 8 \text{ amu}$ is dominated by the experimental resolutions $\text{FWHM}(\text{TOF}) = 0.5 - 0.7 \text{ ns}$ and $\text{FWHM}(\text{EBIC}) = 2 - 5 \text{ MeV}$. According to the VIOLA systematics [3], the RP events differ from those of ESR in a reduced TKE what corresponds to a decrease of the relative velocity (VREL) of the associated particles (from 2.9 cm/ns to about 2.45 cm/ns) and a shift to smaller folding angles by about 5° . However, resulting from the angle straggling of $2^\circ - 4^\circ$, an overlap of the RP exists within the polar detection angle distribution $\vartheta_2 - \vartheta_1$, especially within the region of ESR events with higher ^{84}Kr energies.

The RP identification was performed by data analysis with the ATHENE code [4]:

1. Random coincidences and events from higher-energetic ^{84}Kr projectiles are discriminated by windows within the TOF-EBIC plots.
2. Only those events are considered that fulfill the coplanarity condition for binary events ($\varphi_2 = \varphi_1 - 180^\circ$) within $\pm 2.5^\circ$.
3. Events with reduced TKE are selected within the $\text{TOF}_2 - \text{TOF}_1$ plot.
4. After data sorting by the restrictions above, a window is created within the $\vartheta_2 - \vartheta_1$ distribution, which contains the RP events and a strongly reduced ESR portion.
5. The remaining events are concentrated in a TKE - VREL plot within two separated groups (fig.1).

The efficiency of this procedure is demonstrated in the $\vartheta_2 - \vartheta_1$ distribution: Whereas the selection window is extended widely into the ESR region of the unsorted data (fig.2), the finally selected events are located homogeneously inside the window without any sharp break-off at the boundary (fig.3).

Total cross sections have been deduced from the RP/ESR ratios (fig.4). Unfortunately, the beam energy in the present experiment is known only within an uncertainty of about $\pm 15 \text{ MeV}$. However, using the parametrization from ref. [5] to estimate the fusion cross section, the value at the upper limit of 250 mb agrees with our data. The total RP

cross sections concerning the reactions at ^{116}Sn and ^{118}Sn differ from each other in the ratio of about 5 to 1. The analysis of the RP mass distributions (fig.4) in dependence on the folding angle $\vartheta_1 + \vartheta_2$ indicates that this behaviour is correlated with an additional reaction component, which produces fragment masses nearby those of Kr and Sn.

A corresponding component was not found for the ^{118}Sn measurement. By sorting the selected events of the ^{116}Sn runs by the additional requirement $\vartheta_1 + \vartheta_2 < 90^\circ$, the mass distribution of the remaining events becomes more flat but is still more extended and contains about twice the intensity of the RP from ^{118}Sn .

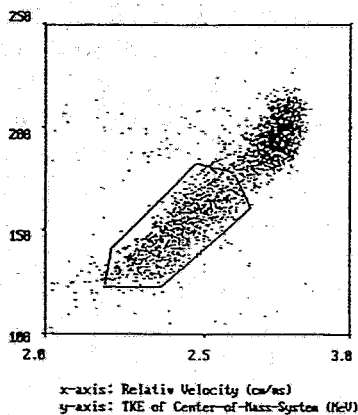


Fig.1 Final RP identification at ^{116}Sn runs by TKE - VREL analysis

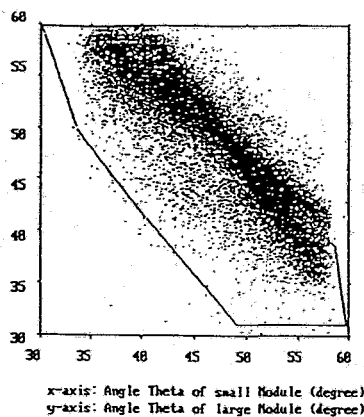


Fig.2 $\vartheta_2 - \vartheta_1$ plot containing all coincidences from ^{116}Sn runs

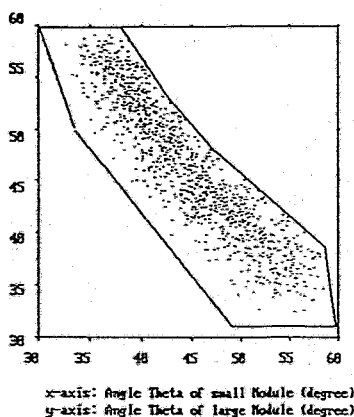


Fig.3 $\vartheta_2 - \vartheta_1$ containing the identified RP from ^{116}Sn runs

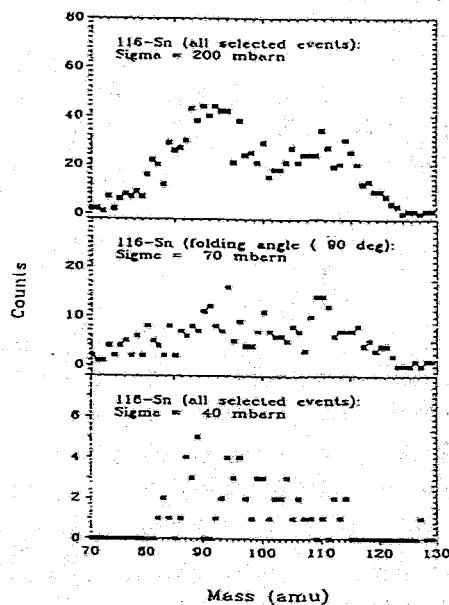


Fig.4 Mass distributions of RP (see text)

REFERENCES:

- [1] H.-G. Oertlepp et al., Proc. Int. Conf. on New Nuclear Physics with Advanced Techniques, Ierapetra, Crete, Greece, 1991 (World Scientific, 1992);
see also: Report FZR 92-11 (Rossendorf, 1992) 3
- [2] C.-M. Herbach, H.-G. Oertlepp, Annual report 1991 (FZ Rossendorf) FZR 92-09 (1992) 56
- [3] V.E. Viola, Nucl. Data Sect. A1 (1966) 391;
V.E. Viola et al., Phys. Rev. C31 (1985) 1550
- [4] C.-M. Herbach, C. Umlauf, Annual report 1991 (FZ Rossendorf) FZR 92-09 (1992) 61
- [5] W.W. Wilcke et al., Atomic Data and Nucl. Data Tables 25 (1980) 391

Model Independent Balance Analysis of Fission Fragments Produced by $^{40}\text{Ar} + ^{194}\text{Pt}$ at Energies of 5.5 AMeV and 10 AMeV ^B

H.-G. ORTLEPP^{1,2}, M. ANDRASSY^{1,2}, G.G. CHUBARIAN¹, P. GIPPNER^{1,2},
C.-M. HERBACH^{1,2}, A. MATTHIES^{1,2}, G. PAUSCH³, G. RENZ^{1,2}, K.D. SCHILLING²

¹ Joint Institute for Nuclear Research, Dubna

² Forschungszentrum Rossendorf e.V. ³ Freie Universität Berlin

Experimental investigations concerning the fission of heavy systems after incomplete fusion are often based on the measurement of the fission fragment folding angle. Most of the experimental data are successfully interpreted within the frame of the naive Massive Transfer Model (MTM): The whole excitation energy is deposited into the fused nucleus. The nucleons of the projectile that are not coupled to the compound system cannot take part in the momentum and energy transfer.

However, the direct experimental determination of the masses and velocity vectors of the fission fragments event by event allows to analyse the data independently from the MTM. On average, the velocities are not influenced by the neutron emission, and the fission fragment mass ratios are equal before and after evaporation. With these assumptions, the fission after incomplete fusion can be described as a sequential process. Within the frame of a pure kinematical picture, the correlation between the mass and the momentum transfer can be studied and the number of evaporated neutrons can be estimated as a measure of the excitation energy deposited [1].

Our measurements have been performed at the heavy ion cyclotron U-400 of the JINR Dubna by bombarding ^{194}Pt with ^{40}Ar at incident energies of 5.5 AMeV and 10 AMeV. From the two large gas-filled modules of the Mini-FOBOS set-up [2,3], that were positioned under the angles of $\vartheta_1 = 105^\circ$, $\varphi_1 = 270^\circ$ and $\vartheta_2 = 45^\circ$, $\varphi_2 = 90^\circ$ with respect to the beam axis, for each of the recorded fragments the time-of-flight (TOF), the residual energy (EBIC) and the detection position (X,Y) were derived. The start signal was generated by a small parallel-plate avalanche counter, which has been positioned near the target and covered the cone of the forward module. In order to detect the remaining part of the projectile after incomplete fusion, an additional small avalanche counter was placed into the reaction chamber under an angle of $\vartheta_3 = 20^\circ$, $\varphi_3 = 270^\circ$. The mass and the emission energy were calculated for each single fission fragment independently by the TOF-EBIC analysis [4].

Qualitatively, our data agree with the results obtained in similar experiments [5,6]: At 5.5 AMeV the fission always occurs after complete fusion, but at 10 AMeV the recorded events accumulate into two groups corresponding to a large and a small momentum transfer. These two groups are well separated in fig.1, where the total momentum $\vec{P} = \vec{p}_1 + \vec{p}_2$ is shown with its component parallel to the beam P_z and the transverse P_y -coordinate ($\varphi = 90^\circ$ in the definition of our lab. system). Compared to the estimated experimental resolutions of $\text{FWHM}(P_z) \approx \text{FWHM}(P_y) \approx 500 \text{ MeV}/c$, the widths of the measured distributions displayed in fig.1 are more than a factor of 2 larger resulting from neutron evaporation and transverse momentum transfer.

The mass and the momentum transfers (fig.2) were calculated for each of the fission events individually. While the mean total fragment mass (fig.3) was determined to be 207 ± 5 amu and 217 ± 5 amu (10 AMeV, neutron evaporation corrected) for the above two groups of momentum transfer, the mean values of the mass as well as the momentum transfer for the corresponding two event groups amount to 40 % and 80 %, respectively (fig.2). (Note that the response of our set-up at 10 AMeV bombarding energy decreases drastically for momentum transfers near 100 %). Generally, the direct proportional correlation as predicted by the MTM is confirmed. For about 2 % of the accumulated events, a third particle was detected. In correspondence with the position of the additional forward detector, the P_y -component of these events turns out to be positive.

For the measurement at 10 A MeV, the mean values of the relative fission fragment velocity v_{rel} result in 2.31 ± 0.15 cm/ns (2.46) and 2.51 ± 0.15 cm/ns (2.61) concerning the event groups with small and large momentum transfer (fig.4). The values in brackets are estimates using the VIOLA systematics [7]. The mean number of evaporated neutrons deduced event by event from the mass, energy and momentum conservation was compared with the estimates of the MTM using the TKE from [7]. Our respective experimental values of 3 ± 6 and 9 ± 6 are smaller than the theoretical estimates by about 6 units. However, although it seems to be difficult to obtain the predicted absolute values, the difference of the neutron numbers between the two groups is reproduced correctly. This is of particular importance for the analysis of events with higher multiplicities, where the folding angle method cannot be applied, namely to possess a filter of excitation energy.

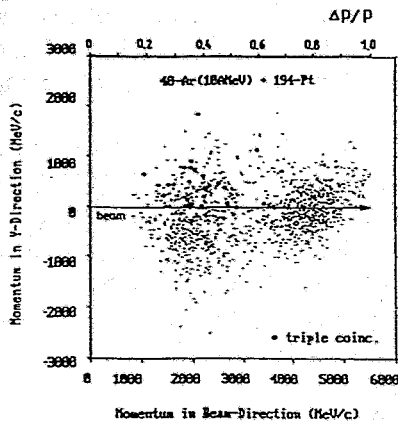


Fig.1 Total fragment momentum distribution

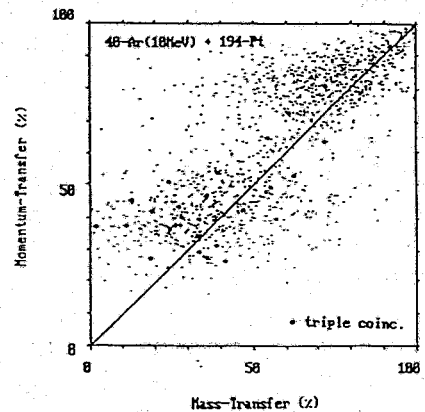


Fig.2 Mass and momentum transfer correlation

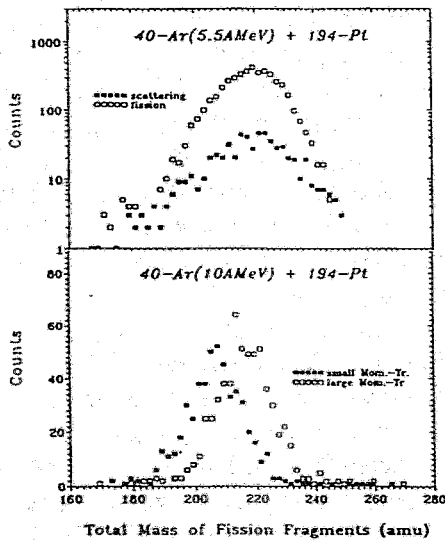


Fig.3 Total fragment mass distribution

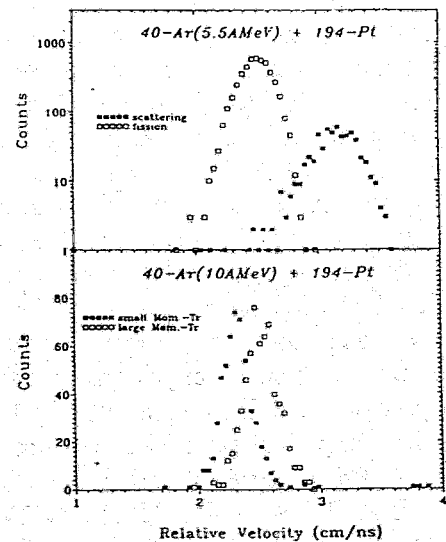


Fig.4 Relative velocity of fission fragments

REFERENCES:

- [1] E.C. Polacco et al., Phys.Lett. B146 (1984) 29
- [2] M. Andrassy et al., Annual report 1991 (FZ Rossendorf) FZR 92-09 (1992) 58
- [3] H.-G. Ortlepp et al., Annual report 1991 (FZ Rossendorf) FZR 92-09 (1992) 59
- [4] C.-M. Herbach, H.-G.Ortlepp,-Annual report 1991-(FZ Rossendorf) FZR 92-09 (1992) 56
- [5] M. Fatyga et al., Phys.Rev.Lett. 55 (1985) 1376
- [6] U. Jahnke et al., Report HMI-B 463 (Berlin, 1988)
- [7] V.E. Viola, Nucl.Data Sect. A1 (1966) 391;
V.E. Viola et al., Phys. Rev. C31 (1985) 1550

Extension of the ARGUS Phoswich Array by a FOBOS Gas-Detector Module and Test of the FOBOS Data-Acquisition System ^B

G. PAUSCH¹, J. KRÜGER², W. SEIDEL², W. WAGNER²,
C.-M. HERBACH³, A. MATTHIES³, H.-G. ORTLEPP³, W. SHUCHKO³, W. TROFIMOV³,
H. FUCHS⁴, H. HOMEYER⁴, G. RÖSCHERT⁴, A. TUTAY⁴, P. ZIEM⁴
A. BUDZANOWSKI⁵, A. SIWEK⁵, L. ZRODŁOWSKI⁵

¹Freie Universität Berlin, ²Forschungszentrum Rossendorf e.V.,

³Joint Institute for Nuclear Research, Dubna, ⁴Hahn-Meitner-Institut Berlin,

⁵Institute of Nuclear Research, Krakow

An experiment carried out in 1991 at VICKSI⁷ showed that the detection of intermediate-mass fragments (IMF) at backward angles is an efficient trigger to study processes with high energy dissipation in heavy-ion collisions where lighter projectiles are incident on heavy target nuclei [1]. It is interesting to analyse mass, velocity, and angular distributions of projectile residues in coincidence with such IMF or in coincidence with binary fission products (f) where the excitation energy of the target-like or incompletely fused system can be estimated from the folding angle.

To prepare a corresponding experiment for the system $^{32}\text{S}(960 \text{ MeV}) + ^{197}\text{Au}$ (which has already been studied at the HMI [2]), we extended and modified the ARGUS multidetector set-up [3]:

1. A prototype [4] of the FOBOS detector modules [5], consisting of a position-sensitive doublegrid avalanche counter (DGAC) and a Bragg ionization chamber (BIG) of 24 cm depth, was mounted at $\langle \theta_{\text{Lab}} \rangle = 123^\circ$. For this purpose a new backward hemisphere for the ARGUS reaction chamber was constructed and assembled in Krakow.
2. Eleven of the phoswich detectors in the horizontal plane were replaced by silicon detectors of 450 to 1000 μm thickness. A registration of energy and time-of-flight then allows to measure mass distributions of IMF (slow projectile residues) and fission fragments at selected forward angles.

A test run was carried out in Dezember 1992, using the VME-based data-acquisition system which had been developed for the FOBOS detector [6]. We obtained a maximum data acquisition rate of ≈ 1200 events/s with ≈ 25 parameters/event on average. An estimate based on few hours of data collection with a $500 \mu\text{m}/\text{cm}^2$ Au target results in a ff coincidence rate of ≈ 4000 per hour including all possible pairs of silicon detectors (folding angles up to 138°) and in a ff coincidence rate between BIC and one of the silicon detectors of ≈ 700 per hour (folding angles larger than 117°) which should be sufficient to analyse the properties of projectile residues as a function of the dissipated energy.

REFERENCES:

- [1] G. Pausch et al., Annual Report 1991, HMI-Bericht 497(1992)83
- [2] C. Schwarz et al., Phys. Lett. B279(1992)223
- [3] W. Terlau et al., Annual Report 1989, HMI-Bericht 482(1990)93
- [4] A. Matthies et al., Annual Report 1987, ZfK-638(1988)98
- [5] H.-G. Ortlepp et al., Proc. Intern. Conf. on New Nuclear Physics with Advanced Techniques, Ierapetra, Crete, Greece, 1991
- [6] P. Ziem et al., Jahresbericht 1991, FZR. 92-09(1992)66

Yields for IMF-Production of the Reaction $^{32}\text{S}(960 \text{ MeV})+^{197}\text{Au}$ ^B

J. KRÜGER¹, G. PAUSCH², W. SEIDEL¹, W. WAGNER¹

¹Forschungszentrum Rossendorf e.V., ²Freie Universität Berlin

In order to study the production of intermediate mass fragments (IMF) in the reaction $^{32}\text{S}(960 \text{ MeV})+^{197}\text{Au}$ [1], a prototype [2] of the FOBOS-detector modules (FM) [3] had been mounted under a backward angle of 123° to the ARGUS-multidetector array [4].

The yields of IMF measured with the BRAGG ionization chamber (BIC) (covering a solid angle of 37 msrad) amounted to 1% of the registered total reaction yield. Fig.1 shows the charge spectrum of selected particles, that were stopped within the BIC and gave their full BRAGG-peak signal (SP). High energetic IMF penetrating the BIC (FP) as well as low velocity particles not reaching their BRAGG-peak maximum are neglected. Values of IMF production yields, for SP and FP are shown in fig.2.

The charge resolution is sufficient to separate adjacent charges from He up to Ar with a precision better than 0.3 charge units. The detection threshold of the avalanche counter of the FM leads to a suppression of energetic light IMF, whereas the detection efficiency for heavier IMF is suggested to be 100%. The decrease of yields for higher Z-values is in correspondence with the mass distribution [5].

Further conclusion needs in an efficiency correction for the avalanche counter of FM; investigations of this item are also of great importance for FOBOS experiments.

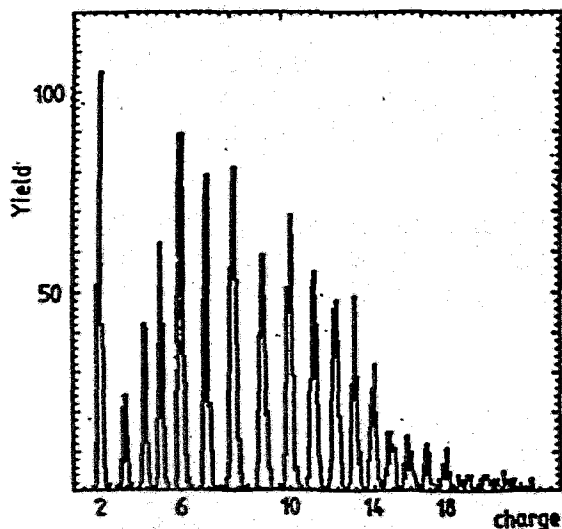


Fig. 1. Charge spectrum (see text)

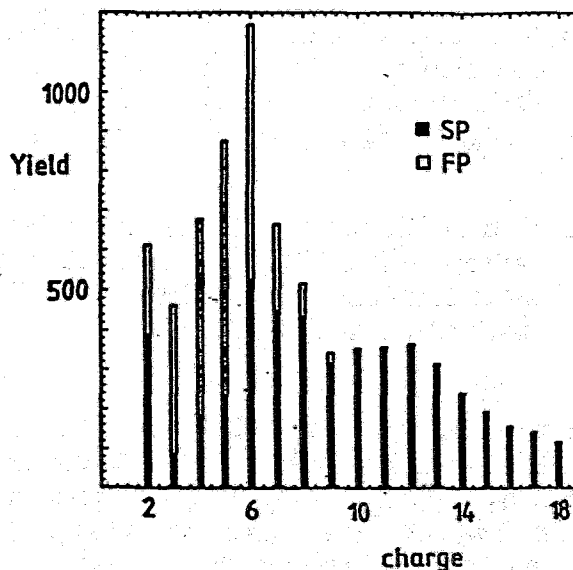


Fig. 2. Yields for SP from BRAGG-peak analysis and FP identified by time-of-flight analysis

REFERENCES:

- [1] G. Pausch et al., this Report .
- [2] A. Matthies et al., Annual Report 1987, ZfK-638(1988)98
- [3] H.-G. Ortlepp et al., Proc. Int. Conf. on New Nuclear Physics with Advanced Techniques, Ierapetra, Crete, Greece, 1991
- [4] W. Terlau et al., Annual Report 1989, HMI-482(1990)93
- [5] G. Pausch et al., Annual Report 1991, HMI-497(1992)83

**Velocity correlations of intermediate mass fragments produced
in central collisions of Au + Au at $E = 150 \text{ A} \cdot \text{MeV}^B$**

B. Kämpfer¹, R. Kotte, J. Mösner, W. Neubert, D. Wohlfarth
Forschungszentrum Rossendorf, O-8051 Dresden, PF 19, Germany
and the FOPI collaboration

GSI Darmstadt, Univ. Heidelberg, CRN Strasbourg, LPC Clermont-Ferrand, INFN
Florence, IPNE Bucharest, CRIP Budapest, Univ. Mainz, ITEP and IAE Moscow,
IEP Warsaw, RBI Zagreb

Nuclear intensity interferometry supplies informations on disassembling excited nuclear matter produced in heavy ion collisions. The space-time structure of the source which emits the reaction products can be explored by analyzing velocity correlations. In the final state intermediate or heavy fragments mainly obey Coulomb interaction. The Coulomb repulsion hinders the proximity of such fragments in momentum space. Therefore, the appearance of small velocity differences of neighbouring fragments is suppressed, in particular for small and/or short-living sources.

Here we present experimental data and first interpretations of velocity correlations of intermediate mass fragments (IMF) in central Au + Au collisions at beam energy $E = 150 \text{ A} \cdot \text{MeV}$. The data were taken by the high-granular, azimuthally symmetric component "outer plastic wall" of the FOPI detector system [1] at the heavy ion synchrotron SIS of GSI Darmstadt. For more informations on event characteristics and one-body IMF observables see refs. [2,3]. Let be $Y_{12}(\vec{v}_1, \vec{v}_2)$ the coincidence yield of IMF pairs with charges $Z_{1,2}$ and velocities $\vec{v}_{1,2}$. Then the two-particle correlation function is defined as

$$1 + R_{12}(\vec{v}_1, \vec{v}_2) = \mathcal{N} \frac{\sum_{\text{events,pairs}} Y_{12}(\vec{v}_1, \vec{v}_2)}{\sum_{\text{events,pairs}} Y_{12,\text{mix}}(\vec{v}_1, \vec{v}_2)}, \quad (1)$$

where the subscript "mix" means event mixing. \mathcal{N} is a normalization factor fixed by the requirement to have the same number of true and mixed pairs. The correlation function (1) is projected onto the hypersurface $v_{12} = |\vec{v}_{12}| = |\vec{v}_1 - \vec{v}_2|$. Displaying $1 + R$ vs. $v_{red} \equiv v_{12}/\sqrt{Z_1 + Z_2}$, instead vs. v_{12} , we find that different charge combinations result in rather similar curves [4]. This scaling, predicted in ref. [5] and first verified experimentally in ref. [7], is used in what follows. Fig. 1 displays our experimental results for all events in multiplicity bins PM3 (17 - 24), PM4 (25 - 32) and PM5 (≥ 33). In the region $v_{red} < 0.02c$ the mutual Coulomb repulsion causes the pronounced Coulomb hole. Additionally, we find an enhancement of correlations at $v_{red} \sim 0.025c$ (see squares in Fig. 1). When rotating all events into a unique reaction plane the enhancement vanishes (see dots in Fig. 1). This indicates the importance of the reaction plane and carefully determined event mixing conditions. Therefore, the correlation function (1) seems to be affected strongly by the directed flow.

In order to understand the experimental results and their global dependences we run different simulation codes (including detector filter). The interpretation mainly relies on calculations of the Coulomb trajectories of the charged particles which are initially randomly (non-overlapping and with minimum surface distance 1 fm) distributed in a sphere of radius R with a Maxwellian velocity distribution characterized by a temperature T . A collective radial expansion, with linear velocity profile $v(r) = (r/R)v_{surf}$, is superimposed on the random thermal initial motion. After Coulomb evolution the source is boosted in longitudinal (to account for the *cms* motion) and randomly in transverse direction (to mimic transverse directed flow). For central events the temperature T and the radial expansion velocity v_{surf}

¹also: Institut für Theoretische Physik (KAI e.V.), TU Dresden, O-8027 Dresden, Mommsenstr. 13, Germany

can be fixed by fitting the observed dependence of the average energy per nucleon on fragment mass ($A=2Z$ assumed) $E/A = (E/A)_{flow} + (3T/2)/A$ [3,7]. The transverse boost v_{\perp} is the main variable for reproducing the enhanced correlations observed at $v_{red} \sim 0.025c$. A systematic analysis of the directed flow [7] shows that not more than 1 MeV per nucleon resides in the collective transverse motion. This restricts the maximum transverse boost velocity to $v_{\perp} < 0.05c$. We find then optimum agreement with the data with a parameter set for central events :

$$R = 16 \text{ fm}, T = 35 \text{ MeV}, v_{surf} = 0.20 c, v_{\parallel} = 0.27 c, v_{\perp} = 0, \quad (2)$$

and with another set for the superposition of central and semicentral events in PM3 - PM5 (with a reduced radial expansion, with an average source velocity half between midrapidity and projectile velocity, and with some sideward directed flow included) :

$$R = 15 - 20 \text{ fm}, T = 35 \text{ MeV}, v_{surf} = 0.10 c, v_{\parallel} = 0.40 c, v_{\perp} = 0.05 c. \quad (3)$$

With the 2nd set of parameters we reproduce the correlation functions with and without regarding the reaction plane (see Fig. 1).

The present simulations point to rather short life times and seem to be compatible with the picture of fast (instantaneous) multifragmentation. Even we rely on an instantaneous break-up, the particles need some time to leave the volume bounded by R . According to the initial velocity and spatial distribution this translates to a source decay time being less than 100 fm/c. Note that our tentative data interpretation indicates an expansion effect: the extracted source radius is substantially larger than a $2A_{Au}$ system at nuclear saturation density.

REFERENCES:

- [1] A. Gobbi et al. (FOPI collaboration), Nucl. Instrum. and Methods A324 (1993) 156
- [2] J.P. Alard et al. (FOPI collaboration), Phys. Rev. Lett. 69 (1992) 889,
cf. also GSI scientific report GSI-92-1, p. 25 -36
- [3] S.C. Jeong and J. Randrup (FOPI collaboration), to be submitted to Phys. Rev. Lett.
- [4] B. Kämpfer, R. Kotte, J. Mösner, W. Neubert, D. Wohlfarth (FOPI collaboration), Proc. Int. Workshop, Hirschegg (1992), p. 67, (ed.) H. Feldmeier
- [5] Y.D. Kim, R.T. de Souza, C.K. Gelbke, W.G. Gong, S. Pratt, Phys. Rev. C45 (1992) 387
- [6] Y.D. Kim, R.T. de Souza, D.R. Bowman, N. Carlin, C.K. Gelbke, W.G. Gong, W.G. Lynch, L. Phair, M.B. Tsang, F. Zhu, Phys. Rev. C45 (1992) 338
- [7] N. Herrmann for the FOPI collaboration, invited talk at Int. Nucl. Phys. Conf., July 26th - Aug. 1st, 1993, Wiesbaden, Germany, to appear in Nucl. Phys. A

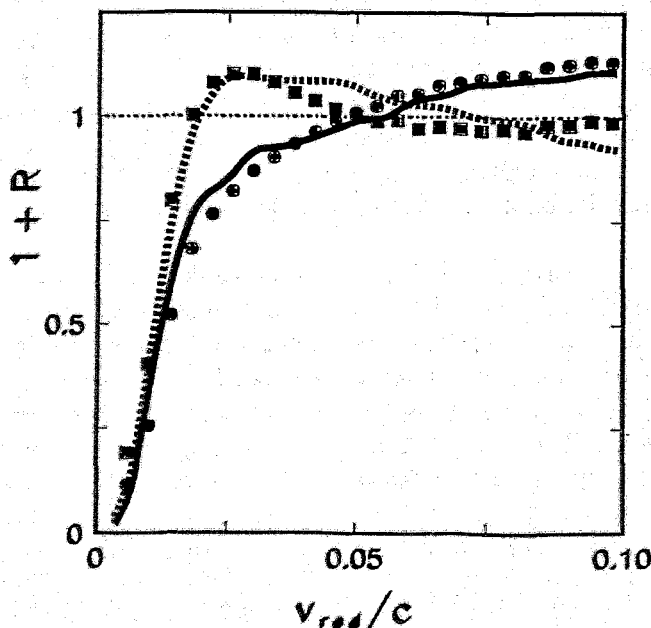


Fig. 1: Correlation function (1) of IMFs from an admixture of central and semicentral events PM3 - PM5 (squares). The dots are for the same events, however the events are rotated into a unique reaction plane before determining the mixed event yield. Dashed (full) lines depict results of Coulomb trajectory simulations using parameter set (3) with $R = 20$ fm with (without) randomization of the transverse boost orientation. The experimental correlation function changes when selecting data from stronger centrality cuts (not displayed).

Simulations of Velocity Correlations Using the Statistical Multifragmentation Model ^B

H.W. BARZ*, B. KÄMPFER*, R. KOTTE, J. MÖSNER, W. NEUBERT, D. WOHLFARTH

*Forschungszentrum Rossendorf, Institut für Kern- und Hadronenphysik
and * KAI e.V. Berlin*

The Statistical Multifragmentation Model [1] was utilized to simulate velocity correlations of Intermediate Mass Fragments (IMF). This model considers primarily the prompt break-up process and the evaporation of secondary particles during the dynamical evolution which is governed by the Coulomb force. The code version 'CRACKER' was supplemented with an acceptance subroutine having regard to the 8 sectors of the outer plastic wall of the 4π -spectrometer at GSI [2] and read out of each of the 64 single scintillator strips of each sector. Double hits were excluded from the analysis.

Then the code 'CRACKER' as event generator was completed with a procedure which considers collective radial flow.

The charged particle multiplicity within the wall acceptance was used to find a relation between the incident beam energy and the excitation energy which is one of the free input parameters of 'CRACKER'. At $150 A \cdot \text{MeV}$ the mean multiplicity of about 25 favours an excitation energy of $E^* = 8 A \cdot \text{MeV}$. Recent BUU calculations show that the size of the source of IMF production is considerably smaller than the mass of the combined system $Au + Au$. As first approximation, the mass of the disassembling system was set to be $A_0 = 197$ what seems even somewhat overestimated.

The relative velocity distributions $Y_{12}(v_1, v_2)$ were calculated for pairs of charges with $Z_1, Z_2 \geq 3$ within an IMF multiplicity window from 2 to 7. Additional selection conditions concerning the relative angle between the velocity vectors and the rapidity of the IMFs could be introduced. An essential point is that the cuts which were applied to the generated true events must be also used for determination of relative velocities calculated by mixing two different events. Both relative velocity distributions were scaled by $\sqrt{Z_1 + Z_2}$ and they were normalized to $\int Y_{12} dv = 1$.

The goal of this study was to find out to what extent the correlation function is sensitive to physical magnitudes. The simulations show that the excitation energy in the interval from 8 to 10 MeV/u has minor influence. The same comes out for changes of about 30% in the IMF source size. In spite of the Z_1, Z_2 scaling, the correlation function was found to be sensitive to the choice of the break-up density. A change of $\Delta(\rho/\rho_0) \simeq 0.15$ causes roughly a displacement of $1.7 \cdot 10^{-3} \cdot c$ on the coordinate of the reduced velocity. Decrease in ρ/ρ_0 shifts the correlation function towards smaller reduced velocities and the ascent becomes somewhat steeper. Higher break-up densities flattens the ascent.

So far as $A_0 = 197$ is considered the collective radial flow causes a substantial change of the correlation function. It remains nearly unchanged if the flow does not exceed 1 MeV/u. Increasing flow energy flattens the ascent of the correlation function, it reaches unity above $v_{red} \simeq 0.025 \cdot c$ and the Coulomb hole becomes more filled. Results of the simulations are shown in fig.1.

REFERENCES:

- [1] J.P. Bondorf et al., Nucl. Phys. A443 (1985) 321
- [2] A. Gobbi et al., Nucl. Instr. Methods 324 (1993) 156

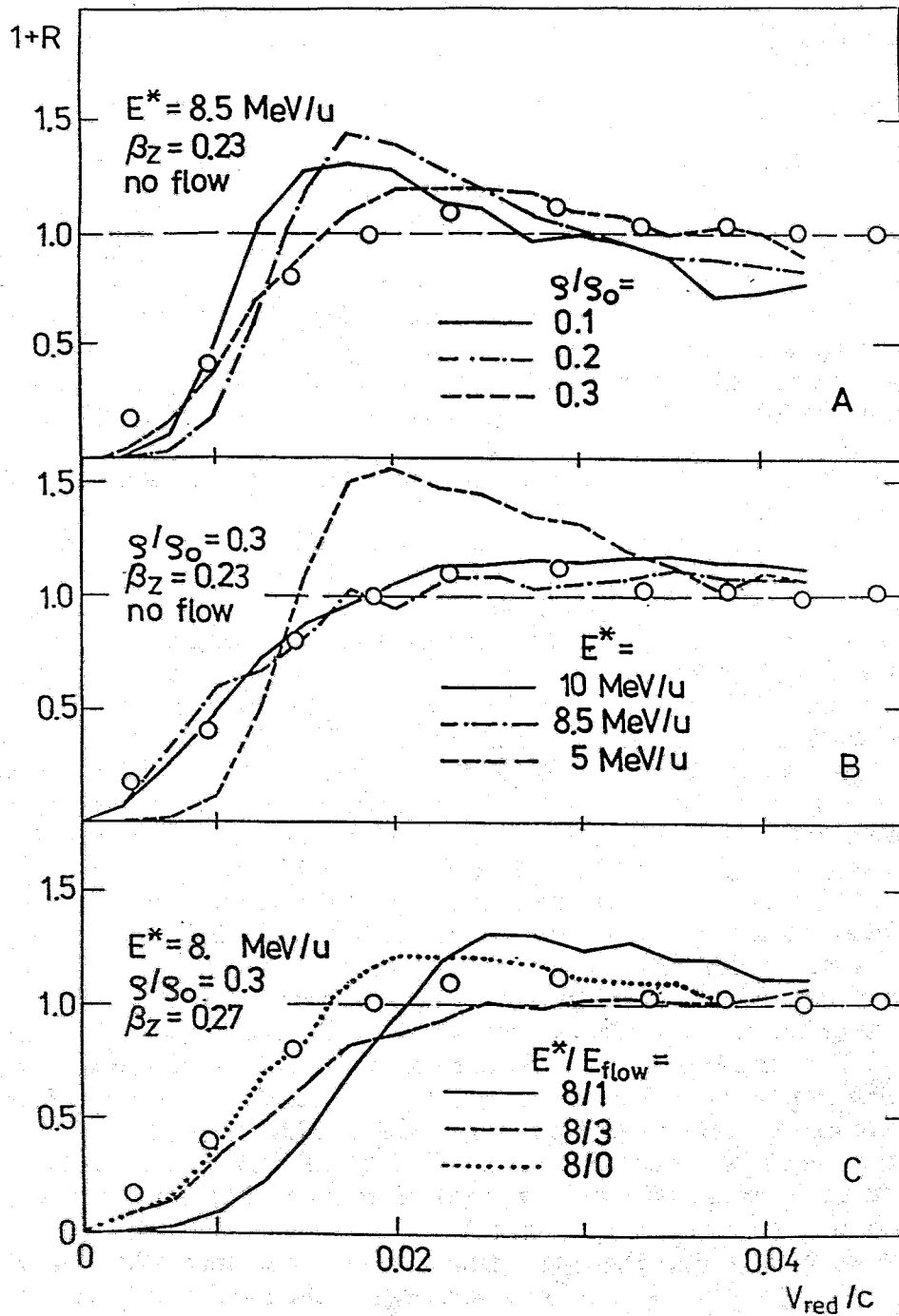


Fig.1 Correlation functions calculated with the Statistical Multifragmentation code. O - experimental data for central and semicentral events. A - dependence on the break-up density, B - influence of the excitation energy, C - influence of the radial flow.

Entropy and Isotopic Ratios in Light Nuclear Systems- a Comparison between QSM and CRACKER ^B

R. KOTTE, J. MÖSNER, W. NEUBERT, W. TRAUTMANN* AND D. WOHLFARTH

*Forschungszentrum Rossendorf, Institut für Kern- und Hadronenphysik
and * GSI Darmstadt*

In multifragmentation processes the evolution from the break-up point to the point where the final nuclear fragments are created is mainly determined by its baryonic entropy S/A . Observables which are sensitive to that magnitude are of special interest. We have learned that isotopic ratios belong to such signals [1]. In the framework of the Quantum Statistical Model (QSM), the isotopic ratios are found to be correlated to the isentropic lines as shown when both magnitudes are plotted in the temperature vs. density diagram. This behaviour is based on the dependence of the mean neutron-to-proton ratio (for fixed Z) on the baryonic entropy. Results of QSM calculations are shown in fig.1 where several disassembling nuclear systems are considered. The mentioned dependence is obviously restricted to heavy and medium weight nuclei. In light nuclei the mean N/Z -ratio does not depend on the entropy. This insensitive region includes nuclei with masses from $A \simeq 20$ to $A \simeq 50$.

In order to check the consequences we have investigated the system with $Z, N = 14$. The reason of that choice is the fact that experimental data are available for $Al + p$ in two references [2, 3]. The results of calculations are given in fig.2 which shows that lines of constant isotopic ratio ${}^7\text{-}^9\text{Li}/{}^6\text{Li}$ have another behaviour than those of isentropic lines. We believe that the method used in ref. [1] is inapplicable to that case and for nuclei in the vicinity of $A \simeq 30$. As seen from fig. 2, the experimental ratio ${}^7\text{-}^9\text{Li}/{}^6\text{Li} \approx 1.5$ would be located at unrealistic high temperatures and densities.

We turn now to the following question: Is there a general restriction or is this result only a model dependent limitation? Therefore, we have calculated the same quantities for the system $Z, N = 14$ by means of the Statistical Multifragmentation Model [4]. Realistic interactions and deexcitation of the fragments in the expansion stage are included in this model. At first, a nearly complete „phase diagram“ in temperature ($2 \text{ MeV} \leq T \leq 10 \text{ MeV}$) and reduced density ($0.1 \leq \rho/\rho_0 \leq 0.9$) has been calculated using the code version „CRACKER“. The entropies calculated by both models agree roughly only in the low density and in the low temperature regions. Starting from here, QSM predicts entropies which increase much faster with increasing temperature than those determined by „CRACKER“. Consequently, the isotopic ratios predicted by the two models are quite different. Although in the calculations with „CRACKER“ the structure of lines for constant isotopic ratio is more complicated there is still a certain region where entropy and isotopic ratio are correlated. As seen from fig. 3, this is fulfilled for temperatures above 5 MeV. Furthermore, we found that the power-law parameter τ is well correlated to the entropy S/A as shown in fig.4.

REFERENCES:

- [1] R. Wada, K.D. Hildenbrand et al., Phys. Rev.Letters 58 (1987) 1829
- [2] G.D. Westfall et al., Phys. Rev. C17 (1978) 1368
- [3] L.N. Andronenko et al., to be published in Zeitschrift für Physik
- [4] J.P. Bondorf et al., Nucl. Phys. A443 (1985) 321

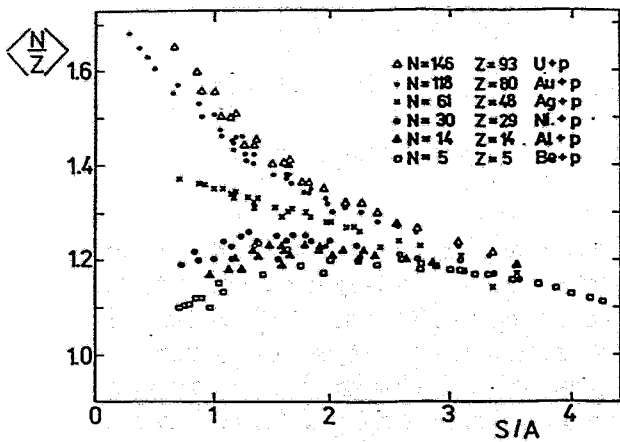


Fig.1 Calculated mean neutron-to-proton ratios for Li-isotopes produced in different collisions

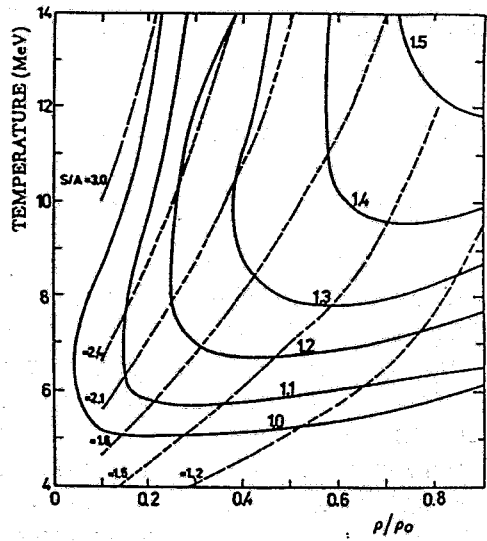


Fig.2 Lines of constant isotopic ratio ${}^7\text{-}{}^9\text{Li}/{}^6\text{Li}$ (solid lines) and isentropic lines (dashed) for $N,Z=14$

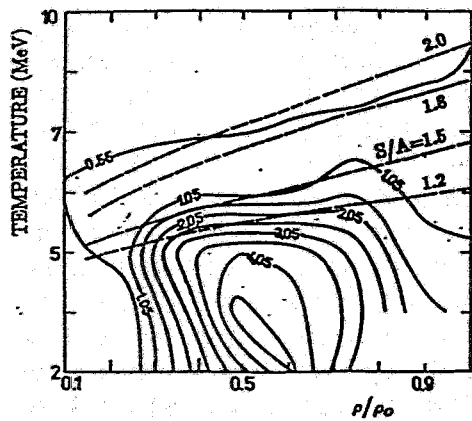


Fig.3 The same as in fig. 2 but calculated with the code CRACKER, dashed lines-entropy, solid lines- ratio ${}^7\text{-}{}^9\text{Li}/{}^6\text{Li}$.

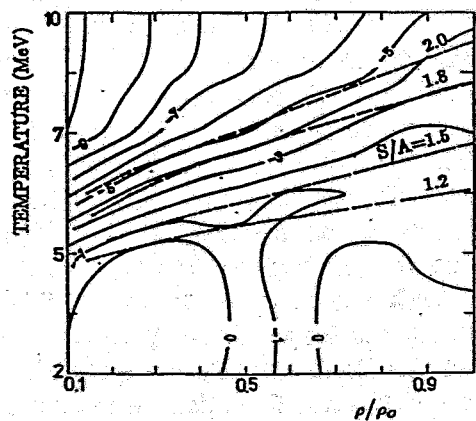


Fig.4 Power-law parameter τ for IMF's ($3 \leq Z \leq 12$) -(solid lines) and entropy-(dashed lines) as function of temperature and density.

Statistical Properties Obtained from Isotopic Yield Ratios ^B

W. NEUBERT, R. KOTTE, J. MÖSNER AND D. WOHLFARTH

Forschungszentrum Rossendorf, Institut für Kern- und Hadronenphysik

Current multifragmentation models assume that thermal equilibrium is reached before the system breaks up. The occurring intermediate mass fragments (IMF) are expected to carry information of the underlying process. We consider here properties of adjacent isotopic pairs produced in this way. In the grand canonical approach the isotopic ratio R for two neighbour isotopes $(N1, Z)$ and $(N2, Z)$ can be expressed as

$$R \sim \exp \left[\mu'_n (N2 - N1) \frac{N}{Z} \frac{1}{T} \right] \quad (1)$$

where N/Z is the neutron-to-proton ratio of the combined system target + projectile. This expression follows from the supposition that the neutron chemical potential is a linear function of the neutron-to-proton ratio.

We have analysed isotopic ratios of He, Li, Be and B obtained in inclusive measurements in order to check the above model predictions. We restricted the analysis to $p+A$ reactions [1-5] which avoid possible ambiguities due to some contributions from projectile fragmentation. Furthermore, we selected strictly such data where for the same target nucleus the yields of at least 3 isotopes are available simultaneously. Systematic errors unavoidable in analysing different experimental data should be minimized by this choice.

The compiled data are given in table 1. The yield ratios as function of the neutron-to-proton ratio were submitted to an exponential fit and the corresponding 'slope' is also listed in table 1. A first inspection shows that the slopes increase with increasing ΔN . The predicted relation

$$\text{slope}(\Delta N = 1) : \text{slope}(\Delta N = 2) : \text{slope}(\Delta N = 3) = 1 : 2 : 3 \quad (2)$$

is only roughly fulfilled.

The Quantum Statistical Model (QSM) which is basically a grand canonical one was exploited to reproduce the data. Calculations were performed for Ni, Ag, Au and U. The relation (2) was proved correct for the primordial IMF's. The influence of secondary particle emission onto the isotopic ratios was investigated within QSM in dependence on the temperature and density of the system. Densities larger than $\rho/\rho_0 > 0.3$ and temperatures $T \geq 8$ MeV lead to slope parameters which are outside of the experimental limits. In all considered cases, we found that particle emission cause an increase of the slope parameters as observed in the experimental data.

No interaction during the IMF production is taken into account so far as the QSM is considered. A more realistic description is possible by the Statistical Multifragmentation Model [6]. We used the standard parameter set, an overall excitation energy of 6 MeV/u and a break-up width of 1.2 fm. The masses of the fragmenting systems were taken from previous INC-calculations [7]. The agreement with the experimental data for Au and U could be improved by using a multiplicity-dependent break-up density. Actually, the calculated values reproduce the slope; but there are considerable deviations in the calculated absolute ratios.

Inadmissible long computation times made it impossible to calculate the low yield of ${}^6\text{He}$ so that the corresponding ratios ${}^6\text{He}/{}^4\text{He}$ and ${}^6\text{He}/{}^3\text{He}$ could not be verified. Summing up, we conclude that the presented data favour statistical IMF production.

REFERENCES:

- [1] R.E.L. Green, R.G. Korteling, K.P. Jackson Phys. Rev. C29 1806 (1984)
- [2] G.M. Raisbeck, et al.: Phys. Rev. C12 527 (1975)
- [3] E.N. Volnin, D.M. Seliverstov, E.M. Spiridenkov, et al.:
Preprint LNPI Nr. 101, Leningrad 1974
- [4] A.S. Hirsch, et al.: Phys. Rev. C29 508 (1984)
- [5] M.N. Andronenko, private communication
- [6] J.P. Bondorf, et al.: Nucl. Phys. A443 321 (1985)
- [7] L.N. Andronenko, A.A. Kotov et al.: Z.f.Physik A310 347 (1983)

		$\Delta N=1$		$\Delta N=2$			$\Delta N=3$	ref.
	N/Z	${}^7\text{Li}/{}^6\text{Li}$	${}^{11}\text{B}/{}^{10}\text{B}$	${}^8\text{Li}/{}^6\text{Li}$	${}^{12}\text{B}/{}^{10}\text{B}$	${}^9\text{Be}/{}^7\text{Be}$	${}^{10}\text{Be}/{}^7\text{Be}$	
Ni	1.03	1.00 ± 0.2	1.53 ± 0.3	\pm	\pm	0.38 ± 0.1	0.19 ± 0.1	(2)
Ag	1.271	1.14 ± 0.3	1.24 ± 0.3	0.09 ± 0.03	0.18 ± 0.1	1.05 ± 0.2	0.50 ± 0.1	(1)
Ag	1.271	1.17 ± 0.4	1.85 ± 0.6	0.18 ± 0.1	0.32 ± 0.1	1.05 ± 0.4	0.59 ± 0.2	(3)
Xe	1.04	2.65 ± 0.4	3.17 ± 0.4	0.73 ± 0.1	0.81 ± 0.1	1.81 ± 0.2	1.76 ± 0.2	(4)
Au	1.475	1.88 ± 0.6	2.69 ± 0.9	0.38 ± 0.1	0.92 ± 0.3	2.92 ± 0.9	2.62 ± 0.8	(3)
U	1.57	2.33 ± 0.5	3.54 ± 1.3	0.59 ± 0.1	1.36 ± 0.5	5.00 ± 1.8	5.43 ± 2.2	(3)
slope		1.90 ± 0.7	2.28 ± 1.2	5.39 ± 2.4	6.04 ± 1.4	4.49 ± 0.6	7.68 ± 1.0	

		$\Delta N=1$	$\Delta N=2$	$\Delta N=3$	ref.
TARGET	N/Z	${}^4\text{He}/{}^3\text{He}$	${}^6\text{He}/{}^4\text{He}$	${}^6\text{He}/{}^3\text{He} \cdot 10^{-2}$	
${}^{58}\text{Ni}$	1.0345	7.59 ± 1.13	2.00 ± 0.24	1.51 ± 0.79	(5)
${}^{64}\text{Ni}$	1.2414	9.26 ± 1.47	6.18 ± 2.52	5.72 ± 2.61	(5)
${}^{48}\text{Ti}$	1.1300	8.31 ± 1.35	3.12 ± 1.17	2.59 ± 1.1	(5)
${}^{112}\text{Sn}$	1.2157	11.65 ± 1.41	3.32 ± 1.40	3.87 ± 1.65	(5)
${}^{124}\text{Sn}$	1.451	12.05 ± 1.53	13.25 ± 3.20	15.96 ± 3.81	(5)
Ag	1.271	13.00 ± 0.65	\pm	\pm	
Ag	1.271	11.36 ± 4.00	4.43 ± 3.11	5.03 ± 1.87	(3)
Au	1.475	28.57 ± 10.6	8.85 ± 2.51	25.32 ± 10.14	(3)
U	1.570	40.00 ± 16.0	16.45 ± 4.63	65.90 ± 15.7	(3)
slope		1.36 ± 0.44	3.86 ± 0.42	6.89 ± 0.86	(3)

Table 1 Compilation of isotopic yield ratios and results of the fits.

Simulation with GEANT ^B

R. KOTTE, J. MÖSNER, W. NEUBERT AND D. WOHLFARTH

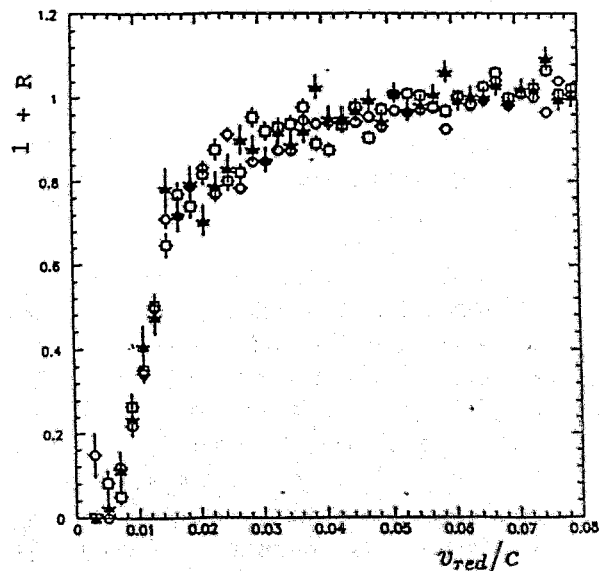
Forschungszentrum Rossendorf, Institut für Kern- und Hadronenphysik

Nowadays, many questions concerning planning, design and data analysis often can be solved only approximately by simulation because of the complexity of the interaction mechanisms or detector geometry. In a special case we studied the influence of the detector system [1] on the velocity correlations of intermediate mass fragments by Monte Carlo simulation with several event generators and the GEANT package [2]. One principal application of GEANT is the tracking of particles through the experimental setup for acceptance studies or simulation of the detector response. The simulation was carried out for the reaction Au+Au at 150 A MeV beam energy performed with the FOPI (phase 1) detector system [3] at SIS in GSI Darmstadt. The data have been analysed with the same routine of the software package [1] which has been used for the experimental runs, too.

We find, as in raw data, an enhanced coincidence yield due to multiple counting at the very small relative velocities ($v_{red} < 0.005 c$) mainly caused by secondary interactions in the scintillator strips, which can be excluded in a controlled way.

The figure shows the correlation functions of particles with nuclear charge $3 \leq Z \leq 6$ for the generator events under the following condition: a) almost without restriction (\circ), b) angular acceptance ($7^\circ \leq \delta \leq 30^\circ$) and energy thresholds (\square), complete selection by the apparatus (\blacktriangle).

The correlation function filtered by the response of the setup suffers for $v_{red} > 0.006 c$ in average few distortions if the finite resolution for velocity and charge, energy thresholds and the nearly exact geometry including dead zones are taken into account. Summarizing, acceptance and energy thresholds have minor influence on the shape (especially on the steep incline) of the correlation function.



REFERENCES:

- [1] N. Herrmann, private communication
- [2] R. Brun, et al., GEANT 3, CERN data handling division, 1987, DD/EE/84-1
- [3] A. Gobbi et al., Nucl. Instr. and Methods A324 (1993) 156

Midrapidity source of intermediate-mass fragments in highly central collisions of Au + Au at 150A MeV

(Physical Review Letters 69 (1992) 889)

J.P. Alard, Z. Basrak, N. Bastid, I.M. Belayev, M. Bini, Th. Blaich, R. Bock, A. Buta, R. Čaplar, C. Cerruti, N. Cindro, J.P. Coffin, M. Crouau, P. Dupieux, J. Erő, Z.G. Fan, P. Fintz, Z. Fodor, R. Freifelder, L. Fraysse, S. Frolov, A. Gobbi, Y. Grigorian, G. Guillaume, N. Herrmann, K.D. Hildenbrand, S. Hölbling, O. Houari, S.C. Jeong, M. Jorio, F. Jundt, J. Kecskemeti, P. Koncz, Y. Korchagin, R. Kotte, M. Krämer, C. Kuhn, I. Legrand, A. Lebedev, C. Maguire, V. Manko, T. Matulewicz, G. Mgebrishvili, J. Mösner, D. Moisa, G. Montarou, P. Morel, W. Neubert, A. Olmi, G. Pasquali, D. Pelte, M. Petrovici, G. Poggi, F. Rami, W. Reisdorf, A. Sadchikov, D. Schüll, Z. Seres, B. Sikora, V. Simion, S. Smolyankin, U. Sodan, N. Taccetti, K. Teh, R. Tezkratt, M. Trzaska, M.A. Vasiliev, P. Wagner, J.P. Wessels, T. Wienold, Z. Wilhelmi, D. Wohlfarth and A.V. Zhilin

Abstract: Charged particles have been observed in collisions of Au on Au at an incident energy of 150A MeV using a high-granularity detector system covering approximately the forward hemisphere in the center-of-mass system. Highly central collisions have been studied using a double selection criterion which combines large charged-particle multiplicities with small transverse-momentum directivities. In this class of events about one-quarter of the total nuclear charge emerges as intermediate-mass fragments with nuclear charges $Z > 2$. These fragments are centered at midrapidity and are produced with large transverse velocities.

A highly-segmented ΔE -time-of-flight wall as forward detector of the 4π -system for charged particles at the SIS/ESR accelerator

(Nuclear Instruments and Methods in Physics Research A324 (1993) 156)

A. Gobbi, J.P. Alard, G. Augustinski, Z. Basrak, N. Bastid, I.M. Belayev, Th. Blaich, P. Boccaccio, R. Bock, S. Boussange, A. Buta, R. Čaplar, C. Cerruti, R.J. Charity, N. Cindro, J.P. Coffin, M. Crouau, F. Daudon, J.F. Devin, P. Dupieux, J. Erő, Z.G. Fan, C. Fayard, P. Fintz, Z. Fodor, L. Fraysse, R. Freifelder, S. Frolov, E. Gimenez, Y. Grigorian, G. Guillaume, N. Herrmann, K.D. Hildenbrand, S. Hölbling, F. Hornecker, A. Houari, S.C. Jeong, M. Jorio, F. Jundt, J. Kecskemeti, P. Koncz, Y. Korchagin, R. Kotte, M. Krämer, C. Kuhn, A. Lebedev, I. Legrand, C.F. Maguire, V. Manko, M. Marquardt, T. Matulewicz, S. Mayade, G. Mgebrishvili, J. Mösner, D. Moisa, G. Montarou, I. Montbel, P. Morel, W. Neubert, R. Neunlist, G. Ortlepp, D. Pelte, M. Petrovici, F. Rami, W. Reisdorf, M.A. Saettel, E. Sahuc, G. Savinel, Z. Seres, D. Schüll, B. Sikora, V. Simion, S. Smolyankin, U. Sodan, M.H. Tanaka, K.M. Teh, R. Tezkratt, B. Tischler, M. Trzaska, M.A. Vasiliev, D. Vincent, P. Wagner, J. Weinert, J.P. Wessels, T. Wienold, Z. Wilhelmi, D. Wohlfarth and A.V. Zhilin

Abstract: At the SIS/ESR accelerator facility at GSI in Darmstadt the 4π -detector system FOPI is under construction at present. It is designed for the investigation of central collisions of heavy ions in the energy range up to 2 A GeV. As phase I of this detector a forward wall has been built and used in various experiments. It comprizes a total number of 764 scintillators with an additional shell of 188 thin ΔE -detectors in front of it and covers the full azimuth of the polar angles from 1° to 30° . The velocity and the nuclear charge of the fragments are determined by a combined time-of-flight and ΔE measurement.

Statistical fragmentation of Au projectiles at $E/A = 600$ MeV
(Physical Review C46 (1992) R1577)

J. Hubele, P. Kreutz, V. Lindenstruth, J.C. Adloff, M. Begemann-Blaich, P. Bouissou, G. Imme, I. Iori, G.J. Kunde, S. Leray, Z. Liu, U. Lynen, R.J. Meijer, U. Milkau, A. Moroni, W.F.J. Müller, C. Ngô, C.A. Ogilvie, J. Pochodzalla, G. Raciti, G. Rudolf, H. Sann, A. Schüttauf, W. Seidel, L. Stuttge, W. Trautmann, A. Tucholski, R. Heck, A.R. DeAngelis, D.H.E. Gross, H.R. Jaqaman, H.W. Barz, H. Schulz, W.A. Friedman and R.J. Charity

Abstract: The mean multiplicity of intermediate mass fragments (IMF) $\langle M_{IMF} \rangle$ produced by fragmentation of Au projectiles interacting with targets of C, Al, Cu, and Pb at an incident energy of $E/A = 600$ MeV is compared to predictions of statistical multifragmentation and sequential evaporation models. The initial conditions for the calculations were provided by Boltzmann-Uehling-Uhlenbeck simulations. In the high excitation energy regime where the IMF multiplicity reaches its maximum the observed universal correlation between $\langle M_{IMF} \rangle$ and the total charge Z_{bound} of projectile fragments with charges $Z \geq 2$ cannot be reproduced by a sequential evaporation code. In this regime the data are better described by statistical decay calculations which assume the formation of an expanded nuclear system and a rather fast breakup.

Correlations in multi-fragment events
(Nuclear Physics A545 (1992) 329c)

U. Lynen, P. Kreutz, J.C. Adloff, M. Begemann-Blaich, P. Bouissou, J. Hubele, G. Imme, I. Iori, G.J. Kunde, S. Leray, V. Lindenstruth, Z. Liu, R.J. Meijer, U. Milkau, A. Moroni, W.F.J. Müller, C. Ngô, C.A. Ogilvie, J. Pochodzalla, G. Raciti, G. Rudolf, H. Sann, A. Schüttauf, W. Seidel, L. Stuttge, W. Trautmann and A. Tucholski

Abstract: We have measured the multi-fragment decays of Au projectiles after collisions with C, Al, Cu and Pb targets at a bombarding energy of 600 MeV/nucleon. We have developed a series of observables that progressed in complexity. These observables were examined as a function of the violence of the collision and span the region from evaporation to total disassembly of the nuclear system. The results are compared to both nuclear statistical and percolation calculations.

The rise and fall of multifragment production in $^{197}\text{Au} + \text{C, Al, and Cu}$ reactions
at $E/A = 600$ MeV
(Nuclear Physics A538 (1992) 473c)

W. Trautmann, J.C. Adloff, M. Begemann-Blaich, P. Bouissou, J. Hubele, G. Imme, I. Iori, P. Kreutz, G.J. Kunde, S. Leray, V. Lindenstruth, Z. Liu, U. Lynen, R.J. Meijer, U. Milkau, A. Moroni, W.F.J. Müller, C. Ngô, C.A. Ogilvie, J. Pochodzalla, G. Raciti, G. Rudolf, H. Sann, A. Schüttauf, W. Seidel, L. Stuttge, A. Tucholski

Abstract: We have studied the transition from the evaporation to the vaporization regime in ^{197}Au induced reactions on C, Al, and Cu targets at a beam energy of 600 MeV per nucleon. The experiment was performed with the ALADIN forward spectrometer at SIS. We find that with increasing violence of the collision the mean multiplicity of intermediate mass fragments first increases to a maximum $\langle M_{IMS} \rangle \simeq 3.5$ and then decreases again. Calculations using the BUU model suggest that the fragmentation is governed by the energy E_{dep} deposited into the Au nucleus and that the maximum of $\langle M_{IMF} \rangle$ is reached around $E_{dep} = 8$ MeV nucleon.

5. Technical and Methodic Developments

A winding Machine for the Manufacturing of Multi Wire Detectors

M. SOBIELLA, M. FREITAG, H. HAUCK¹, J. HUTSCH, H. KRUG¹, P. MANFRASS,
J. STEPHAN¹

*Forschungszentrum Rossendorf, Institut für Kern- und Hadronenphysik,
¹ Zentralabteilung Forschungs- und Informationstechnik*

A winding machine for producing wire planes as components of nuclear and particle physics detectors has been developed. It is suited for wire planes with a maximum width of 2 m and a maximum length of a single wire of 2.7 m.

The main design criterion was to reach a high precision in wire positioning and tension. Furthermore, the construction of the machine is based on the following requirements for essential parameters:

- possible wire diameters: 10 ... 100 μm ,
- wire tension: 200 mN ... 5 N (continuously adjustable, accuracy better than 5 %),
- wire distances: 0.5 ... 20 mm, maximum error 10 μm ,
- maximum cumulated positioning error for wire planes of 2000 mm width: 250 μm .

For constructing the machine we adopted the widely used principle, where a wire plane is wound on a double auxiliary frame in a first and mounted on the detector frame in a second step. The control of the winding as well as the parameter settings are performed by means of an AT386 personal computer based process control unit. A quadro-linear table providing a range of 2090 mm is used for wire positioning, which is controlled by an optical measuring system with an accuracy of $\pm 2 \mu\text{m}$.

The wire supply unit mounted on the linear table guarantees the exact wire positioning on the winding frame as well as a constant wire tension. The latter is provided by the torque of a current-stabilized electric motor, where the wire coil is mounted on the motor axis.

The essential parameters of the winding machine as e.g. wire position accuracy and tension have been determined by means of a video microscope and a tensiometer, respectively, showing the following results:

- 1) In a first version of the wire supply unit, where the distance between the guide roller and the optical measuring system was comparatively long, we observed large periodic deviations in the wire positions, which were correlated with the pitch of the spindle of the linear table. After decreasing the distance between the roller and the measuring system the influence of the spindle guiding to wire positioning became negligible.
- 2) Furthermore, we found a wire mispositioning up to 40 μm that occurred due to vibrations of the frame of the machine. These deviations could be reduced by increasing the stiffness of the frame.
- 3) As the main reason for the positioning error of 20 μm the manufacturing tolerance of the guide roller was detected. The required accuracy of 10 μm is expected to be reached, if this roller will be replaced by a vertically mounted polished cylinder that will guide the wire from the supply to the winch.
- 4) The deviations in wire tension have been measured to be less than 2 % and meet therefore the requirements given above.

Process control of the wire winding machine

H. KRUG

Forschungszentrum Rossendorf, Zentralabteilung Forschungs- und Informationstechnik

The mechanical construction of the wire winding machine is shown schematically in fig. 1a. The control of the winding process is performed by the following important components (fig. 1b):

the driving system for the winding frame, the wire supply unit and the feedback drive for the linear positioning unit.

For the drive of the winch a reversing drive with control of the rotational speed for the geared DC-motor has been used.

The motor moment of 106 Nm is sufficient to produce the acceleration necessary for the motion of the winch with changing rotational speed. The positions of the winch is absolute measured by means of a position encoder (single turn).

The functions of the wire supply unit are to guarantee defined wire tension and an exact guidance of the wire to the winding frame. The adjustable resetting force is obtained with a current controlled reversing drive of a disk motor with a small moment of inertia. The feedback drive of the wire supply unit has been realized with a commercially available linear positioning unit combined with a high-resolution incremental length-measuring system with a position accuracy of 1 μm . All functions of the machine are controlled by a personal computer AT 386. This enables us to use a menu controlled operation providing a great flexibility of the facility. By means of the developed software wire planes of different dimensions and structures can be produce. The computer is connected via a serial interface with the feed rate control. The measured position values for the winch were read in via a parallel interface in the Gray-Code. The set-point value of the speed control for the winch drive and the current set-point value for the unwinding drive of the wire supply unit are delivered from an analog interface.

The most critical point is to control the rotational speed of the winch drive in such a way, that the acceleration of the unwinding wire coil is small enough to obtain a constant wire tension. A sinuous approach was chosen for the wire speed during a half turn of the winding frame. With respect to the geometry of the mechanical configuration the required set-point value for the speed as function of the frame position is calculated. The storage ability of the wire supply unit supports this kind of control by smoothing the wire acceleration amplitude. For starting the winding machine, the operator has to put in only the feeding, the wire tension, the average winding speed and the frame dimensions. The winding process is started and stopped in one of the two zero positions of the winch. In these positions a pick feed of half a wire distance takes place.

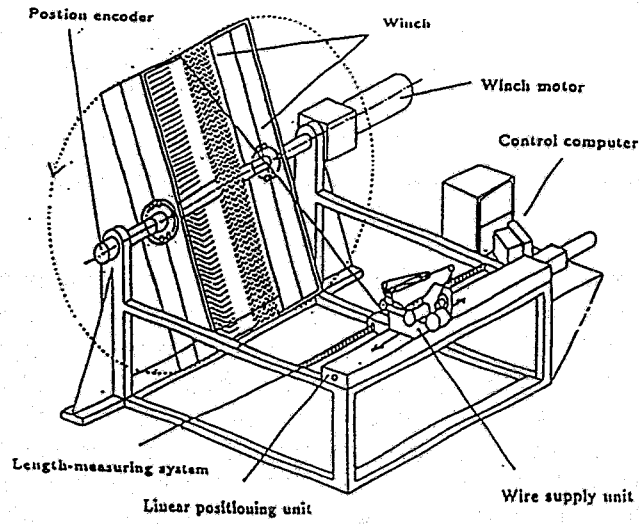


Fig. 1a

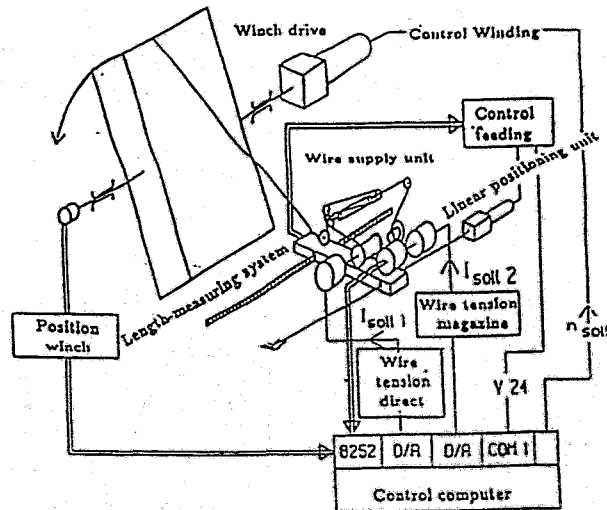


Fig. 1b

Fig. 1 Wire winding machine
 a) Mechanical Scheme
 b) Principle of control

SOME ASPECTS OF THE VACUUM SYSTEM FOR THE START DETECTOR DEVICE IN THE COSY-TOF-SPECTROMETER^{B,K}

L. NAUMANN, W. NEUMANN*, G. SCHMIDT, J. HUTSCH, P. MICHEL, K. MÖLLER,
B. NAUMANN, A. SCHAMLOTT, A. SCHÜLKE AND M. SOBIELLA

*Forschungszentrum Rossendorf, Institut für Kern- und Hadronenphysik
Zentralabteilung Forschungs- und Informationstechnik

The COSY-TOF-spectrometer [1] consists of many detectors in a vacuum tank with a volume of appr. 50 m³. Vacuum pressure less than 10⁻² mbar is necessary in precise nuclear physics experiments for elimination of such disadvantages as background production, energy loss and multiscattering along the flight path of particles. The liquid hydrogen target [2], which is positioned in the start detector vessel, requires vacuum pressure in the order of 10⁻⁵ mbar, to suppress condensation of residual gas at the target windows. Such condensates would falsify the original composition of the target material. The start detector vessel with a volume of appr. 60 l, which contains the liquid hydrogen target and 32 scintillation counters, was separated from the huge tank, because it seems difficult, to evacuate 50 m³ down to 10⁻⁵ mbar.

This separation has been achieved by a 19 μm thin Mylar foil of 600 mm diameter. In the routine working regime the pressure difference Δp between the two sides of the foil creates a small force, which does not deform the foil visibly. But if this pressure difference amounts to Δp ≥ 6 mbar, the foil touches the sensible hollow light guides [3] of the start detector, and may destroy them.

We constructed a foil holder with an integral pressure regulation mechanism, to prevent such a destruction.

The layout of the vacuum test system is shown in fig.1.

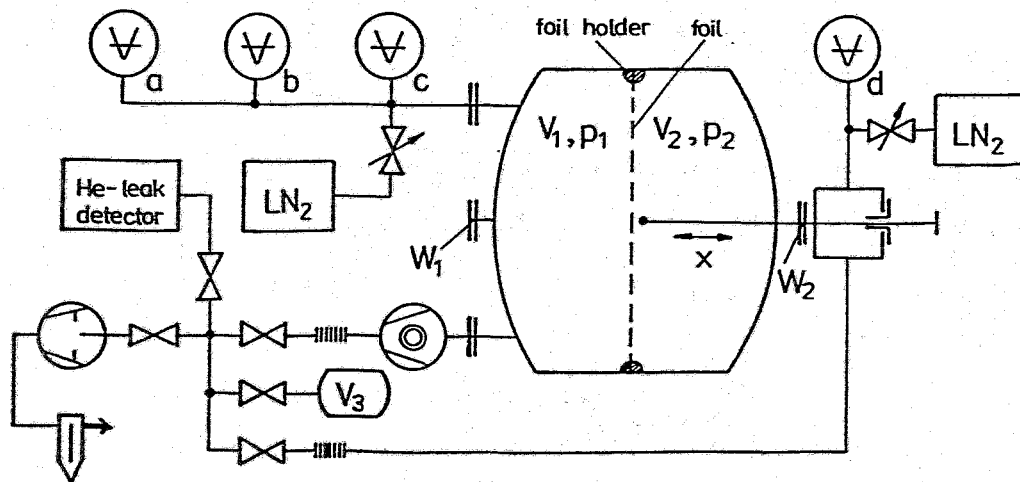


Fig.1 Layout of the vacuum test setup; working ranges of the vacuummeters [mbar]:
a) 10³ - 1; b) 1 - 10⁻⁴; c) 10⁻⁴ - 10⁻¹⁰; d) 10³ - 10⁻³;

A turbo molecule pump (400 l/s) in connection with a fore-vacuum pump creates in the start detector vessel a pressure in the order of 10^{-6} mbar, if the second window (W_2) is closed by a flange and the foil was removed.

The foil was accurately mounted between the two windows (W_1 and W_2), to test the pressure regulation mechanism. The pressure p_2 was varied by filling the volume V_2 with nitrogen (LN_2) through a precision valve. The measured ratio of the pressures p_2/p_1 in dependence of the pressure difference Δp is shown in fig.2. There three qualitative different states are seen for the pressure regulation mechanism:

- closed for $\Delta p \leq 0.04$ mbar,
- switching for $0.04 \text{ mbar} < \Delta p < 0.5$ mbar and
- open for $\Delta p \geq 0.5$ mbar.

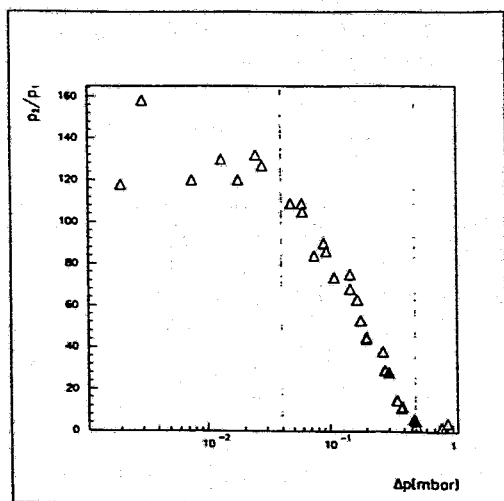


Fig.2 Working characteristic of the pressure regulation mechanism

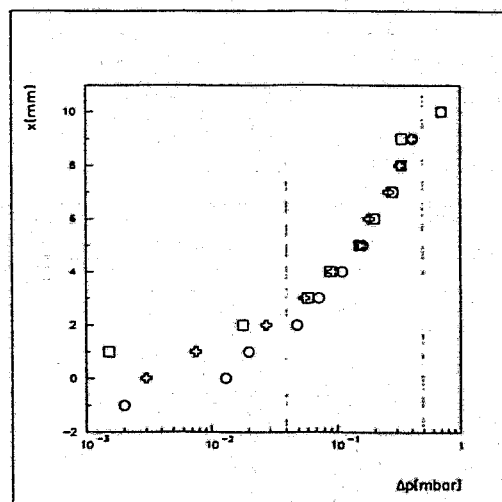


Fig.3 Mechanical deformation x of the foil in dependence on the pressure difference

The deformation of the foil has been measured simultaneously. The result is shown in fig.3. For $\Delta p \leq 0.10$ mbar the deformation is not well defined. When Δp increases, the foil expands up to $x = 10$ mm along the rotation symmetry axis of the device.

The strength of the foil was tested by shock waves of different power generated by opening volume V_3 . All tests were repeated several times and a good reproduction of all results was observed.

REFERENCES:

- [1] IKP. Annual Report 1991, KFA Jülich (1992) 3-6
- [2] V.G. Jaeckle, Diplomarbeit, KFA Jülich, Jül-2633 (1992)
- [3] P. Michel et al., Mikrowellen & HF Telecom. Magazin, Vol.18 No.3 (1992) 170

A LASER BASED TEST SYSTEM FOR THE COSY-TOF-SPECTROMETER^{B,K}

P. HERMANOWSKI, H. BRAND, S. BRAND, S. CHAMERA, H. FREIESLEBEN,
A. FRITSCHÉ, H. KOCH, J. KRUG, E. KUHLMANN, J.S. LANGE, H. MATTHÄY,
P. RINGE, A. RÖSER AND M. STEINKE

Ruhr-Universität Bochum, Institut für Experimentalphysik I

L. NAUMANN, P. MICHEL, K. MÖLLER, B. NAUMANN, A. SCHAMLOTT AND A. SCHÜLKE
*Forschungszentrum Rossendorf, Institut für Kern- und Hadronenphysik
and the COSY-TOF-Collaboration*

We describe a calibration system for routine control of approximately one thousand scintillation counters of the Time-of Flight-Spectrometer [1] at the Jülich Cooler Synchrotron as shown in fig.1. Optical test systems for calibration and control of a large number of scintillation counters from the point of signal creation inside or near the scintillator up to the data acquisition system are often used in modern spectrometers [2].

The aim of this test system is primarily to find drifts in time resolution and delay of individual detector channels, exceeding 220 ps. It is also possible, to monitor the gain drift of the PMT and the following electronics.

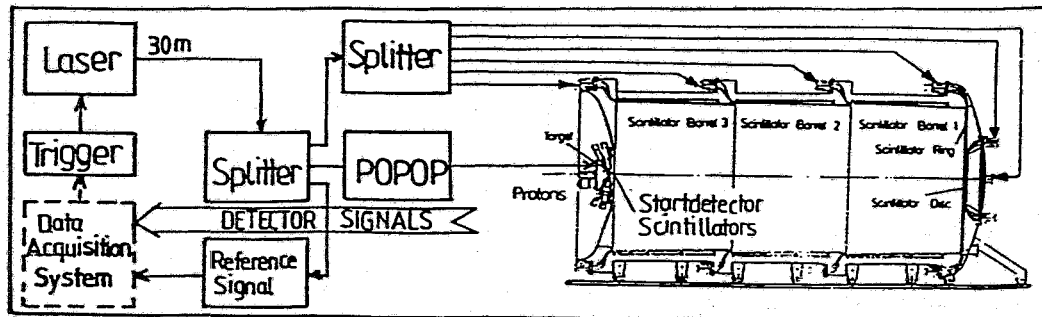


Fig.1 Layout of the laser test system for the COSY-TOF-Spectrometer

The laser is positioned 30 m away from the TOF-Spectrometer. The parameters of the laser (type Laser Photonics LN 120C) are listed in the following table:

The optical fibres (type Ceram Optec) have a quartz core of either 200 μm or 1000 μm in diameter and a quartz cladding.

Filling	N_2 ; 0.1 l/min
Wavelength	337.1 nm
Pulse FWHM	300 ps
Beam divergence	3×7 mrad
Beam size	2×3 mm ²
Pulse energy	70 μJ
Pulsing frequency	≤ 20 Hz

The attenuation for UV-light of these fibres is 80 dB/km. The divergence of the outgoing light amounts to $\pm 12^\circ$. A thick fibre of 30 m length connects the laser with a light splitting device with three outputs. One is wavelength shifted from ultraviolet to visible blue by POPOP (1,4-di-(2-(5-phenyl-oxazolyl)-benzene)) and then coupled to light guides of the start detector. The second output is used to create the reference signal for calibration and the other one is guided to the scintillation counters of the stop components of the COSY-TOF-Spectrometer.

Details of the construction of the calibration system for all 32 scintillator counters of the start detector device are shown in fig.2. A flange connector couples the light to thin fibres inside the vacuum vessel. The construction allows an easy and well defined connection of the fibre. The light intensity can be varied up to a factor of 15 by an attenuator (A), tube (B)

contains 37 fibres with polished endfaces. Each fibre is 1.5 m long and ends in a reflector head (C), which reflects the emitted light onto the light guide toward the PMT (type XP 2020).

The fibres cannot be mounted directly on the scintillators of the start detector device because of the sensitive mechanical construction of the hollow light guides [3].

For the scintillation counters in the stop detector it is possible to feed the light pulses into the scintillator of the opposite side from the PMT, such that the test includes also scintillator properties.

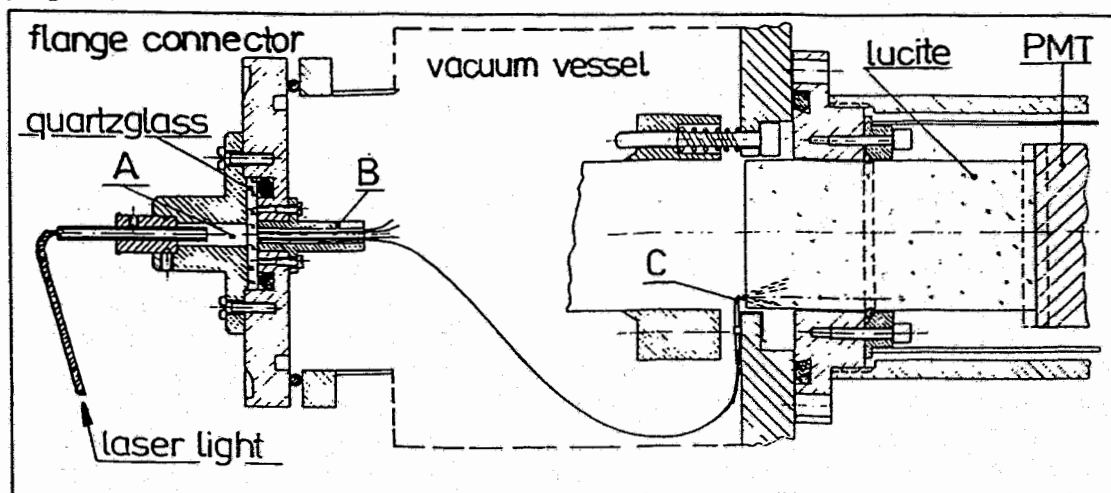


Fig.2 Test system for the start detector setup

TDC- and ADC-spectra, as shown in fig.3, demonstrate results for one start detector channel. The time spectra were taken with two identically PMT's and a constant-fraction-discriminator (Ortec 934). For the peak shape of the squares a time resolution of appr. 220 ps (FWHM) was estimated.

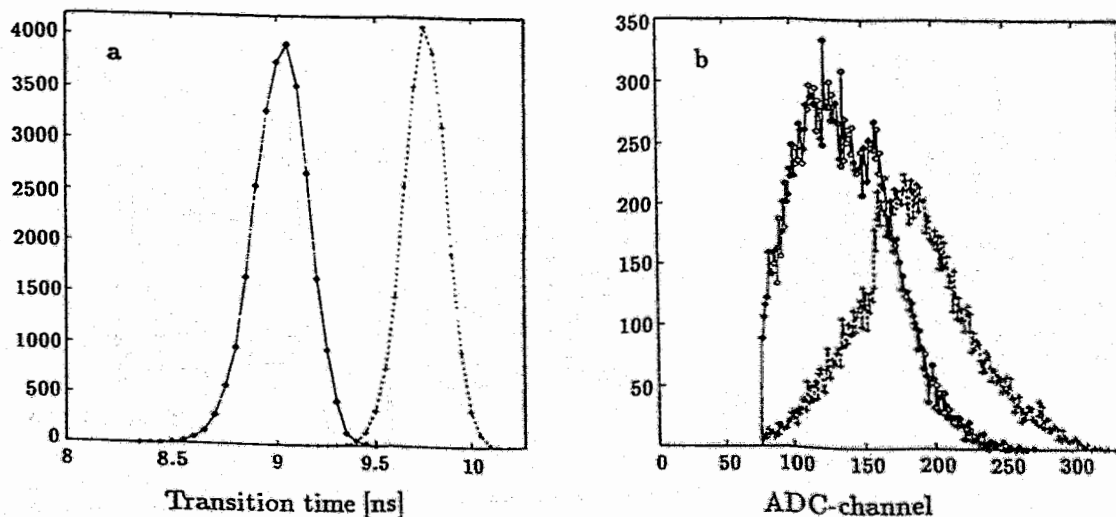


Fig.3 Start detector calibration system (\diamond - with lucite light guide; $+$ - without lucite light guide)

a: TDC-spectrum

b: ADC-spectrum

REFERENCES:

- [1] IKP. Annual Report 1991, KFA Jülich (1992) 3-6
- [2] S. Berglund, P.J. Carlson, J. Jacobson, Nucl. Instr. Meth. 190 (1981) 503
- [3] P. Michel et al., Mikrowellen & HF Telecom. Magazin, Vol.18 No.3 (1992) 170

Status of the Evacuation and Gas Supply System of FOBOS^B

G.RENZ^{1,2}, P.GIPPNER^{1,2}, C.UMLAUF^{1,2}, V.M.VASKO¹, D.MAY^{1,2}

¹Joint Institute for Nuclear Research, Dubna

²Forschungszentrum Rossendorf e.V.

The FOBOS evacuation system was successfully tested. A vacuum of $2 \cdot 10^{-6}$ Torr within the FOBOS ball has been achieved using four turbo molecular pumps. All Bragg ionization chamber cases and the manipulator for handling them were delivered from Bulgaria. All the gas flow and pressure control units including supporting valves and pumps of the gas supply system were mounted mechanically and electrically. A system for on-line gas mixing for the Bragg chambers was mounted and added to the FOBOS setup.

All these components can be controlled either manually or remotely by the SIEMENS SX automation system [1] (fig.1), which was successfully installed and tested in 1992. Basic software for process visualization on X-terminals of the changing status of the evacuation and gas supply system has been developed (fig.2). The actual pressure values can be observed at 64 different positions of the system. The valves and pumps can be switched over in a simple manner by mouse clicks only.

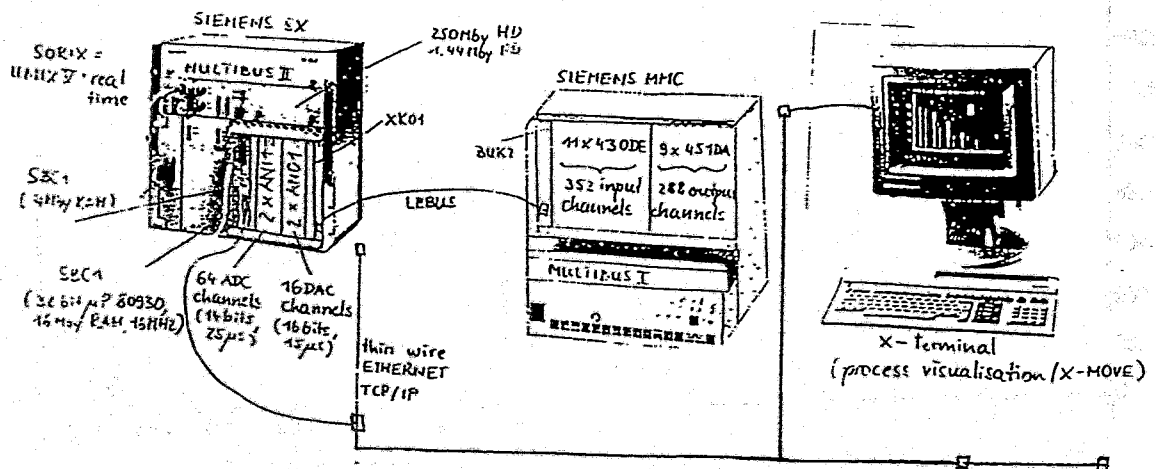


Fig.1 SIEMENS SX automation system hardware

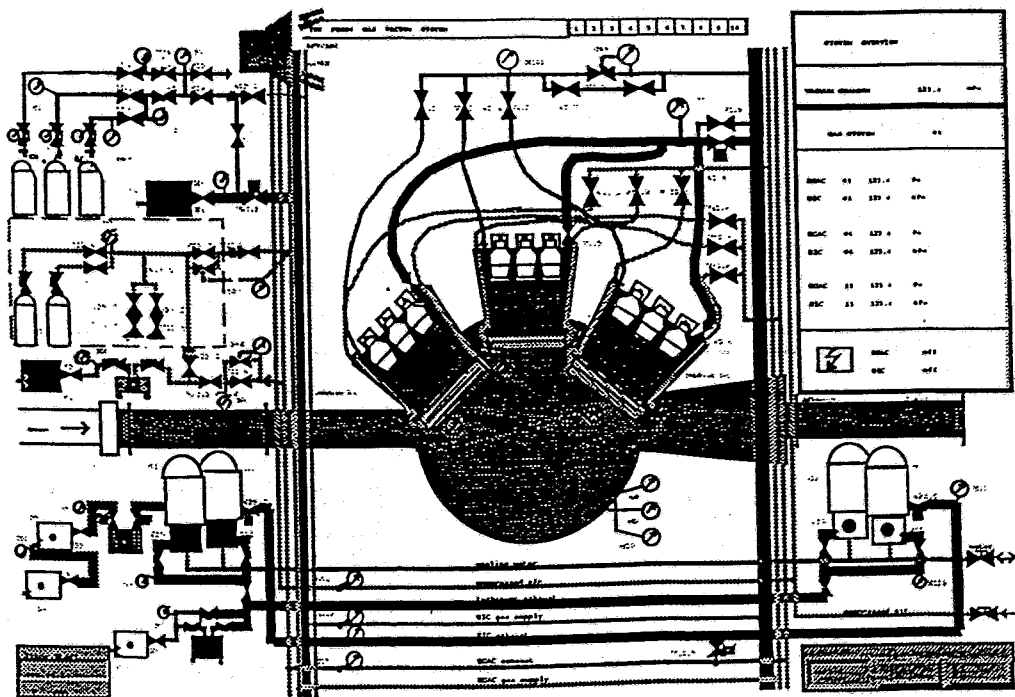


Fig.2 FOBOS process visualization X-graphic display

REFERENCES:

- [1] G. Renz, M. Andrassy, Annual report 1991 (FZ Rossendorf, Institute for Nuclear and Hadronic Physics) FZR 92-09 (1992) 64

The Scintillator Shell of the FOBOS 4π Array ^B

W. WAGNER¹, A.S. FOMICHEV², C.-M. HERBACH², A. MATTHIES²,
H.-G. ORTLEPP², O.V. STREKALOVSKIJ², V.A. VITENKO³, G. PAUSCH⁴

¹Forschungszentrum Rossendorf e.V., ²Joint Institute for Nuclear Research, Dubna,
³Chlopin Radium Institute, Sankt Petersburg, ⁴Freie Universität Berlin

The gas-filled detectors of the FOBOS array [1] are not able to registrate penetrating light charged particles (LCP). This emission of LCP, however, can give valuable insight into the reaction mechanisms which will be studied at FOBOS. Especially correlations between LCP and heavier fragments are of interest.

Therefore the gas detector of FOBOS will be surrounded by scintillation counters [2]. The CsI(Tl) scintillator shell consists of 210 hexagonal crystals (200 mm and 150 mm diameter) situated behind the Bragg ionization chambers covering them with a geometrical efficiency of 73.4 %. The number of scintillators joined together in one module is equal to seven. Scintillator thicknesses of 1.5 cm and 1 cm have been chosen for the angles $\theta = 16^\circ - 52^\circ$ and $\theta = 53^\circ - 164^\circ$ respectively.

The crystals polished at the front side and rough at the back side are coupled via hollow conical light guides to the photomultipliers of type FEU 173 ($\varnothing 150$ mm) and FEU 167 ($\varnothing 100$ mm). Efforts have been made to enhance the light collection efficiency and to avoid inhomogenities due to the large dimensions of the crystals. Typical energy resolutions for Pu alpha particles of 6-7% have been achieved.

LCP were discriminated up to $Z = 3$ by a pulse-shape inspection method [3] integrating the current pulse of the photomultiplier with the help of two charge-to-digital converters (QDC) within the time gates of $\delta t_1 = 0-400$ ns and $\delta t_2 = 1600-3600$ ns (fig. 1). The reaction shown in this example is 9.1 A MeV $^{20}\text{Ne} + ^{58}\text{Ni}$. The detector was placed at 45° with respect to the beam direction.

Data acquisition will be realized by FASTBUS electronics coupled via VSB to a VME work station.

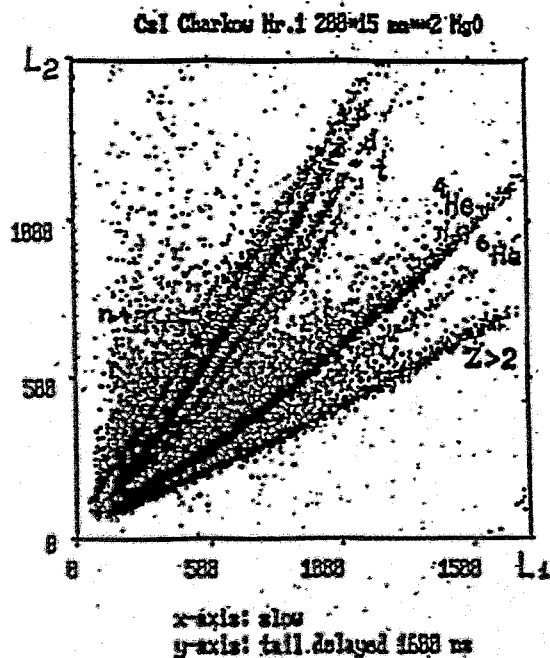


Fig. 1. Pulse-shape discrimination of light charged particles with a 15 mm thick CsI(Tl)

REFERENCES:

- [1] H.-G. Ortlepp et al., Proc. Conf. on New Nuclear Physics with Advanced Techniques, Ierapetra, Crete, Greece (1991), FZR 92-11(1992)
- [2] A.S. Fomichev et al., Preprint JINR, P15-92-50(1992), Dubna
- [3] J. Alarja et al., Nucl. Instr. and Meth., A242(1986)352

Particle Identification in Solid-State Detectors by Exploiting Pulse-Shape Information

G. PAUSCH¹, W. BOHNE², H. FUCHS², D. HILSCHER², H. HOMEYER²,
H. MORGENSTERN², A. TUTAY², W. WAGNER³

¹Freie Universität Berlin, ²Hahn-Meitner-Institut Berlin,

³Forschungszentrum Rossendorf e. V.

The shape of current signals from solid-state detectors is sensitive to the length and density of the ionization track and consequently to charge and mass of the detected ion. This effect which has already been used for particle identification (see e.g. [1,2] and refs. therein) was investigated experimentally in more detail at the VICKSI facility [3].

We irradiated various silicon detectors of 450 to 2000 μm thickness with reaction products from $^{12}\text{C}(360 \text{ MeV}) + \text{Ho}$ and $^{32}\text{S}(795 \text{ MeV}) + \text{Au}$, and scanned the current signals with a series of QDC channels. Charge samples Q_i were taken simultaneously in 16 equidistant time windows (short integration gates fixed with respect to the CFD timing signal), and stored event-by-event together with the total charge (i.e. the integral over the total pulse length which is proportional to the energy deposition E in the depleted zone of the detector) and the time-of-flight information. This method allowed an off-line analysis of $Q_i(E)$ correlations as well as a crude reconstruction of pulse-shapes using the complete sets of charge samples Q_i . The results of data analysis can be summarized as follows:

1. Particle information is present not only in the rise time, but encoded in the entire shape of the current signals (fig.1). The pulse-shapes are mainly determined by an interplay of the plasma erosion effect (see [4] and refs. therein) and charge-carrier drift times, both depending on the initial ionization density $\rho_0(x)$ and the electric field strength $F(x)$ inside the detector.
2. Correlations between charge samples Q_i and energy deposition E are suited to identify charge and - at least for lighter ions - mass numbers of the detected ions (figs. 2,3) within a limited dynamical range. The corresponding electronic technique comprises a simultaneous short- and long-gate integration of the current signals and is well known from phoswich detectors.
3. Other techniques of pulse-shape analysis, e.g. charge-balance discriminators or pulse-length detection, should also be well suited for particle identification in solid-state detectors. Maximum resolution is expected from scanning techniques (fast flash-ADC's) and an adapted arithmetic data processing.

REFERENCES:

- [1] C.A.J. Ammerlaan et al., Nucl. Instr. and Meth. 22(1963)189
- [2] J.B.A. England et al., Nucl. Instr. and Meth. A280(1989)291
- [3] G. Pausch et al., Nucl. Instr. and Meth. A322(1992)43
- [4] W. Seibt et al., Nucl. Instr. and Meth. 113(1973)317

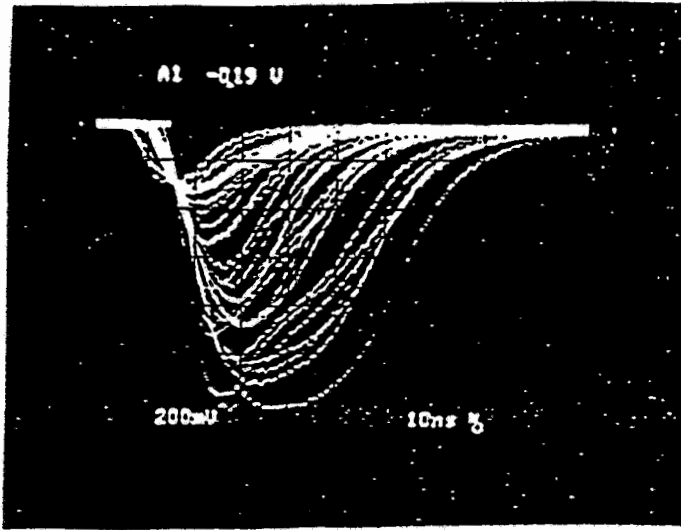


Figure 1. Current signals of a $450\mu\text{m}$ silicon detector (Inter-technique IPE 450-450-25, E-mount) irradiated with reaction products from ^{32}S (795 MeV) + Au at $\langle\theta_L\rangle = 23.5^\circ$.

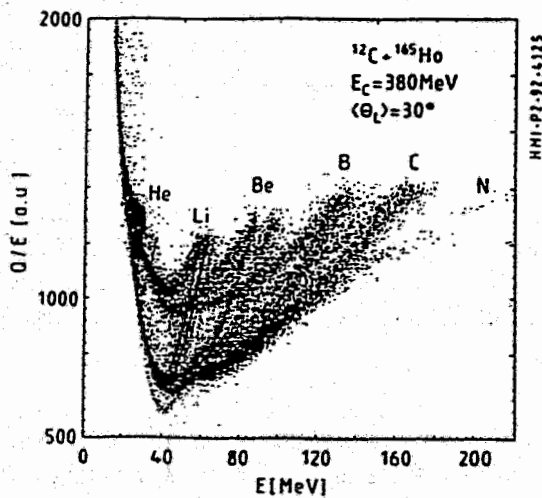


Figure 2. Particle identification for a $450\mu\text{m}$ silicon detector (Inter-technique IPE 450-450-25, E-mount) obtained with short-gate integration including the pulse tail: The y axis of this scatterplot displays a charge sample Q of the current signal (integration gate: 25 to 70 ns with respect to the start of the pulse; Q includes an arbitrary offset) normalized to the energy parameter E . Unit-mass identification up to Be isotopes was observed, and separated Z branches are visible also for particles not stopped in the detector corresponding to higher Q/E values than for stopped ions at the same energy E .

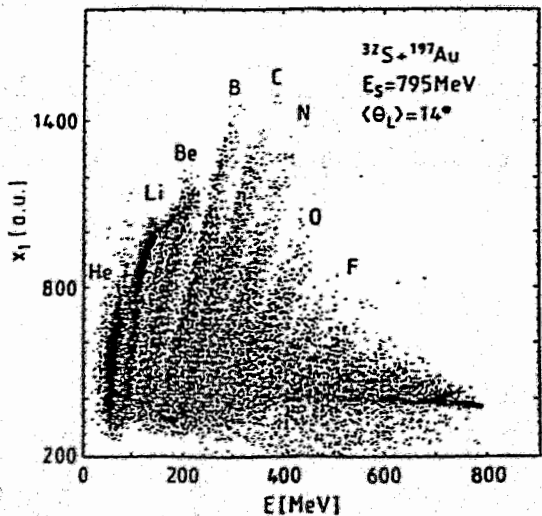


Figure 3. Scatterplot of the "charge balance" parameter X_1 versus energy E for a $2000\mu\text{m}$ silicon detector (ORTEC TA-19-100-2000, T-mount) irradiated from the rear side with reaction products from ^{32}S (795 MeV) + Au at $\langle\theta_L\rangle = 14^\circ$: X_1 represents the ratio of time integrals over the leading ($t = 0$ to 40 ns) and trailing ($t = 80$ to 160 ns) parts of the current pulse.

A Start and Anti Halo Detector for Operation in Magnetic Field Environment ^B

J. BIEGANSKY, K.D. HILDENBRAND*, R. KOTTE, J. MÖSNER,
W. NEUBERT, J. WEINERT* AND D. WOHLFARTH

*Forschungszentrum Rossendorf, Institut für Kern- und Hadronenphysik
and * GSI Darmstadt, KP1*

In 1992 the superconducting solenoid and the Central Drift Chamber of the 4π -detector facility at GSI came into operation. The corresponding start detector system requires a shield from the magnetic field to enable the usage of phototubes close to the solenoid. Different from the phase I arrangement the beam passes through a new adjustable antihalo-detector 1 and the start detector in vacuum. A $100\ \mu\text{m}$ Capton window allows the beam to leave the vacuum tube and to enter the helium bag where target and antihalo-counter 2 are located. A new start- and antihalo detector system (see fig. 1) was designed, tested and operated under beam conditions.

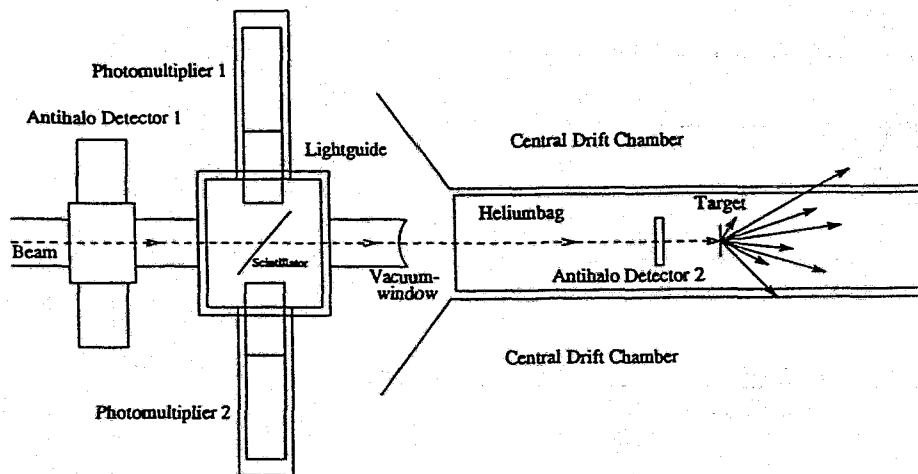


Fig.1 Schematic view of the start detector and its location
in the FOPI-detector system

The start detector consists of two shielded Phillips XP 2020 phototubes with active bases. The tubes are embedded in a threefold cylindrical shielding. The central cube and both outer screw-holdered shielding cylinders are made from soft iron type C3A1 with a carbon content less than 0.04 %. This outer shielding is followed by a second cylinder also made from soft iron. The final shielding of the PMTs is a cylinder of Mu-metal (0.8mm thick). For an assumed magnetic stray field of 0.1 T the shielding factor of this arrangement was estimated to be ≈ 6000 .

Beam particles pass through a thin ($50\ \mu\text{m}$) scintillator foil made from PILOT U with raw surface. The scintillation light is seen by the two photocathodes via plexiglass light guides which also seal the vacuum of the beam line from the PMTs.

Tests were made with an UV Laser. A time resolution of $\sigma = 80\ \text{ps}$ was achieved without magnetic field for an anode voltage of 1.5 kV. Measurements under beam conditions were carried out with 1 A-GeV Au projectiles. With applied magnetic field a time resolution of about $\sigma = 130\ \text{ps}$ was found.

The antihalo counter 2 is located in the strong magnetic field of about 0.6 T which renders more difficult to use photomultipliers to get a fast timing signal. Therefore we decided to couple the scintillators to PIN photodiodes (Hamamatsu type S 3588-03) with a sensitive area of $30 \times 3.4 \text{ mm}^2$. Each PIN photodiode was connected to a charge sensitive preamplifier type CATSA 82 which provides both energy and timing output signals.

Tests were carried out with a piece of fast scintillator material NE 104 (10 mm thick) excited with an UV Laser. Although there is only a small overlap in the wavelength of the emission spectrum of the scintillator and the spectral response of the PIN diode a sufficient signal-to-noise ratio has been observed. The pulse height could not sufficiently improved by the use of an orange scintillator which shifts the emission spectrum to larger wavelengths. Full depletion of the PIN diode is reached for a bias of 70 V. The corresponding rise time was measured to be 10 ns. The time resolution was determined against a fast scintillator coupled to a Hamamatsu PMT resulting in $\sigma = 140 \text{ ps}$.

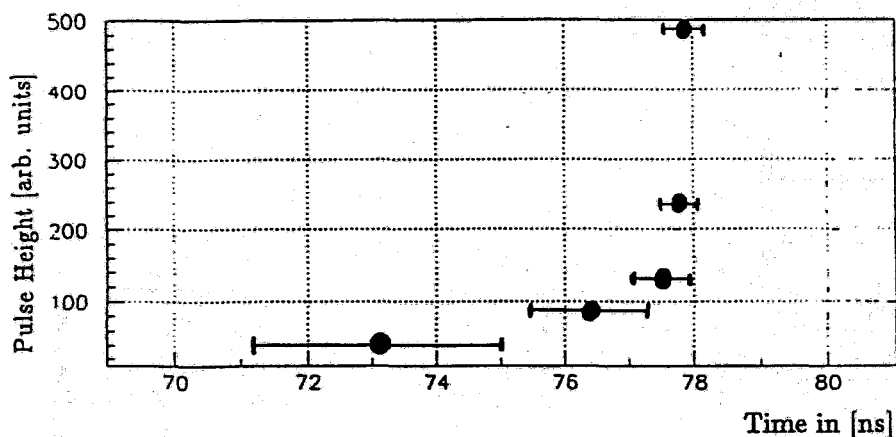


Fig.2 Walk and time resolution as function of the pulse height of the PIN-photodiode

Further tests were carried out with a 1 A-GeV U beam which provides typical signal amplitudes of 60 mV (10 ns rise time, 50 ns duration) corresponding to a typical signal-to-noise ratio of about 40. The pulse height distribution provided by the energy output of the preamplifier CATSA 82 shows a peak which corresponds to the energy loss in the scintillator and a tail extended to smaller pulse heights. The energy loss resolution for U was estimated to be $\approx 7\%$. The time resolution under beam conditions was measured against a start counter as described above. Fig. 2 shows the mean position and σ of the time peak in dependence of the pulse height obtained from the energy output of the preamplifier. For sufficient large pulse heights the time resolution was measured to be 180 ps. The measured quantities fulfill the demands made for use as fast timing signals in the beam-trigger pattern. The new start- and antihalo detector system was used successfully during the Dec. beam time of FOPI at SIS (Au+Au, 1 AGeV and 400 AMeV) in a similar manner as described in ref.[1].

REFERENCE :

- [1] A. Gobbi et al.,
Nucl. Instr. and Methods A324 (1993) 156

Progress Report on the Drift Chamber HELITRON The Endflanges and the Combs ^B

H.W. DAUES *, J. HUTSCH, R. KOTTE, J. MÖSNER, W. NEUBERT,
W. TEICH AND D. WOHLFARTH

*Forschungszentrum Rossendorf, Institut für Kern- und Hadronenphysik
and * GSI Darmstadt*

The detector HELITRON is a 24-sector cylindrical drift chamber with radially strung sense wires. It has a diameter of 2 m and a depth of 0.6 m and will be situated in the axial magnetic field of the 4π -detector system FOPI, directly downstream the Central Drift Chamber (CDC). Its design construction and characteristic data are described in refs. [1] to [3]. Here, we report on the production of the two endflanges of the chamber and that of the combs defining the positions of the sense and potential wires.

Each endflange consists of two rings of Stesalit which are hold together by 24 spokes of glasfiber strengthened epoxy resin. The spokes have been stretched by 200 N and glued into suitable rabbets in the inner and outer ring. The field defining wires of $50\ \mu\text{m}$ diameter CuBe were strung by 0.9 N and soldered on printed-circuit boards which have been glued on the rings before. The boards on the outer rings also carry the resistor chains ($25 \times 15\ \text{M}\Omega$ per sector) of the voltage dividers and the contact elements for high voltage supply. Each sector has its own connections to the cylindrical part of the chamber allowing to be powered separately.

The wire grids define the homogeneous electric field of the drift region at the end sides of the chamber. The pattern of the wires for one sector is schematically shown in fig. 1. Each sector has 50 wires parallel to the sense and potential wires, where the spacing of these field forming wires is 5 mm.

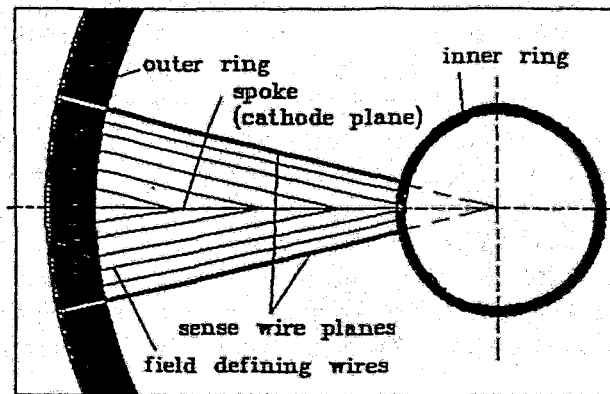


Fig.1 Schematic view of one sector of the endflange of HELITRON

We measured the misalignment of this spacing to be less than $\pm 0.04\ \text{mm}$. An overall accuracy (centrality, position of spokes etc.) of $\pm 0.2\ \text{mm}$ has been achieved by using suitable devices for production and measuring the flanges. The endflanges have been completed at the Rossendorf detector laboratory and delivered to GSI in December 1992.

The combs for the wires of the read-out plane were designed similar to that used for the CDC. It foresees a wire spacing of 5 mm and a staggering of $\pm 200 \mu m$. The shape of a comb is shown in fig. 2 schematically, where the potential wires are in the mean and the sense wires in the low or high positions. Each read-out plane consists of 58 sense ($50 \mu m$ diameter NiCr) and 59 potential wires ($100 \mu m$ diameter gold plated tungsten).

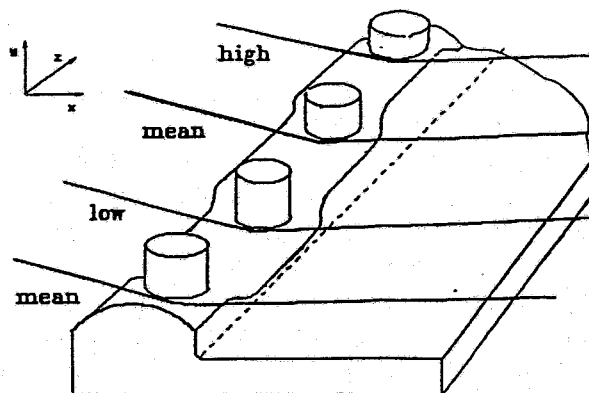


Fig.2 Schematic view of a comb of detector HELITRON

The combs have been produced by casting fluid epoxy resin *) in brass forms. Each comb was casted in several steps, where the epoxy resin was made bubble free by evacuation between the steps. For practical reasons the length of the combs was chosen to be no longer than 320 mm. Therefore, two combs have to join for each side of an anode plane. In order to test the combs a device was produced which allows to fasten two combs in parallel and to string the wires in a similar manner as in the HELITRON. By means of an optical microscope facility the coordinates (spacing and staggering) of the wires have been measured. Mean deviations of $6 \mu m$ and maximum ones of $20 \mu m$ from the average spacing and staggering values were observed. Furthermore the shrinkage has been determined for each of the 96 combs. The mean relative shrinkage value is 7×10^{-4} , but the individual values are distributed between zero and 10^{-3} , depending mainly whether the comb was tempered (in order to shorten the hardening process) or not. Therefore, for each anode plane four combs with similar shrinkage values will be used in order to avoid additional inaccuracies in track recognition later on. The combs have been produced in Rossendorf and delivered to the GSI. We thank A. Gobbi (GSI) for many helpful discussions and H.J. Benz and D. Henke (both GSI) for careful machining of the brass forms. L. Göbel is thanked for measuring the combs.

*) We used the epoxy resin Araldit CW 2215 with hardener HY 5162 from Ciba-Geigy. This epoxy resin contains „Dolomite“ (stone powder) as filler.

REFERENCES:

- [1] Z. Fodor et al., GSI Scientific Report 91-1, p. 302
- [2] H.W. Daues et al., GSI Scientific Report 91-1, p. 303
- [3] J. Erő et al., GSI Scientific Report 92-1, p. 352

Improvement of the Tracking Detector for the ALADIN Facility^B

W. SEIDEL AND T. MÖHLENKAMP

Forschungszentrum Rossendorf, Institut für Kern- und Hadronenphysik

TH. HOFMANN, W.D. KUNZE, V. LINDENSTRUTH, U. LYNEN, W.F.J. MÜLLER,
J. POCHODZALLA, H. SANN AND A. WÖRNER

GSI Darmstadt

The fragmentation of excited nuclei produced in high-energy heavy ion reactions has been a subject of considerable interest since the first multifragment events were observed in emulsion studies. The ALADIN collaboration [1] studies these questions in experiments designed to measure the decay of excited projectiles in inverse kinematics. An important component of the ALADIN spectrometer is the new Time Projection-Multiple Sampling Ionization Chamber (TP-MUSIC). This detector measures very precisely the track coordinates and the atomic numbers Z of the reaction products.

In order to reduce the detection threshold of the TP-MUSIC for minimum ionizing particles, this detector was supplemented with 18 Multiwire Proportional Counters (MWPC), which were proposed by our group [2]. First test results are shown in refs. [3-5].

The operation of the TP-MUSIC in a continuously sensitive mode can cause the unwanted formation of space charge in the drift region. This space charge is mainly due to the ions created in the amplification regions of the MWPC's.

A fraction of these ions is dropping into the drift region. In order to avoid this effect we use a gating grid in front of the MWPC [3]. Otherwise the resulting space charge can seriously distort the trajectories of drifting electrons [5].

Normally the gating grid is closed and only opened by a positive trigger decision. This operating condition prevents most of the undesired primary ionization (primary beam particles or background events) from reaching the MWPC's and effectively eliminates substantial space charge formation.

In several test runs we have checked different methods for the signal read-out electronics of the MWPC's and several trigger circuits for controlling the gating grid. An unpleasant feature on using these circuits arises from the fact that the read-out electronics of the MWPC's as well as the adjacent TP-MUSIC anodes are disturbed for about $5\mu\text{s}$ after opening the gating grid. During this period each half of the tracking detector ignores the first 25 cm of its 100 cm drift length. In this reduced drift room we have measured a resolution of $Z/\Delta Z = 31$ (Ni-beam, $E/A=650$ MeV) for the MWPC, available without distortion of the excellent Z -separation of the TP-MUSIC. Further investigation on shortening this dead time of the electronics is necessary.

REFERENCES:

- [1] A Proposal for a Forward Spectrometer at the 4π Detector, GSI-Report 88-08, 1988
- [2] W. Seidel et al., Annual report ZfK-731 (1989) 42
- [3] W. Seidel et al., Jahresbericht 1991, FZR 92-09 (1992) 73
- [4] F. Rosenberger, Diplomarbeit, Universität Frankfurt/Main, Juni 1992
- [5] M. Mang, Diplomarbeit, Universität Frankfurt/Main, Sept. 1992

The Status of the Data Acquisition System at the 0° Facility^B

N. BRUMMUND^b, S. DIENEL^a, M. DROCHNER^c, W. ERVEN^c, J. HOLZER^c,
M. KARNADI^b, H. KOPP^c, K.-W. LEEGE^a, R. NELLEN^b, W. OEHME^a,
K.-H. WATZLAWIK^b, P. WÜSTNER^c AND K. ZWOLL^c

^a *Forschungszentrum Rossendorf, Zentralabteilung Informations- und Forschungstechnik*

^b *Forschungszentrum Jülich, Institut für Kernphysik DV*

^c *Forschungszentrum Jülich, Zentrallabor für Elektronik*

The basic equipment of the Data Acquisition System for the experiments to be carried out at the 0° Facility of COSY was designed according to the recommendations of the CANU-commission [1] in 1992. In Fig.1 the components of the hardware basis are shown which are available at Rossendorf. These components were selected in collaboration between Rossendorf and Jülich (IKP-DV and ZEL) [2]. The Data Acquisition System is adaptable to different requirements of the experiments, its components are standard modules and most of them are programmable. They are arranged in a three level structure.

The experimentalist will handle his experiment fully by using an Experimental-Workstation (base level) which is connected to a local network area via Ethernet ThinWire. At present a DECstation 5000/240 is installed. In the future this can be a network of workstations and more powerful workstations for example ALPHA-workstations depending on the requests for Online Data Analysis. A VME-Crate containing 3 Fast Intelligent Controllers FIC 8232 are used in a second level of hierarchy. One of them is a complete software development system with connections to Ethernet, to a SCSI interface and a hard disk. Its operating system is OS/9. The FIC's will work as event builder or subevent reader during the experiment. The hard disk is used only for software development. The events will be stored on a magnetic tape (EXABYTE 8500C) by the event builder. In the front end area (third level of hierarchy) FASTBUS and CAMAC crates are employed. Each of the FASTBUS crates is controlled by an intelligent master called CHI. These are complete computers basing on an EPROM-resident operating system OS/9. During the experiment the FASTBUS systems are working as fast data-read-out systems. Both TDC and QDC modules (Phillips Scientific 10C6, 10C2) are scheduled to be used for the instrumentation of the side detector. For the task of experiment control and for the data acquisition from wire chambers it is planned to use CAMAC crates with VIC-A2 controllers which are able to support the VICbus. These controllers are also intelligent components basing of an EPROM-resident operating system OS/9. These crates must be equipped depending on the tasks of experiment control. It will be also possible to use these crates for the data acquisition from wire chambers and to complete them in this way.

In the field of software development for the Data Acquisition System at the 0° Facility it was decided to work in a collaboration between Jülich (ZEL, IKP-DV) and Rossendorf (FFI) to create a general solution for all experiments at COSY basing on the same or similar hardware. A general solution requires a great initial expense but we can hope that most of the experiments can be supported with only minor changes of the software. So the developed software will be better adaptable to the experimentalists requirements [3]. The modular and configurable data acquisition software will run on the UNIX-Workstation visualized by an OSF/MOTIF user interface. The CERN software tools (PAWX11, HBOOK) [5] will be implemented for the on-line data analysis. First global software modules like Data Base, Master Control, Logging- and Reporting-System are under tests [6]. For a comfortable and effective software developing also in the front-end area an OS/9-NFS-cluster system was built. All computers are connected via Ethernet on TCP/IP. We can use the possibilities

of File Transfer Program and Terminal Local Net. The CHI's and FIC's which haven't an own disk can use remote mounted disks on the workstation via Network File System. It is also possible to use windows of the workstations display to operate like a terminal at the CHI's and FIC's. With the so called down-loading we are able to load software from remote mounted disks. A first front-end FASTBUS testsystem was developed on this basis.

A general overview about the software structure of the Data Acquisition System will be given in a forthcoming report.

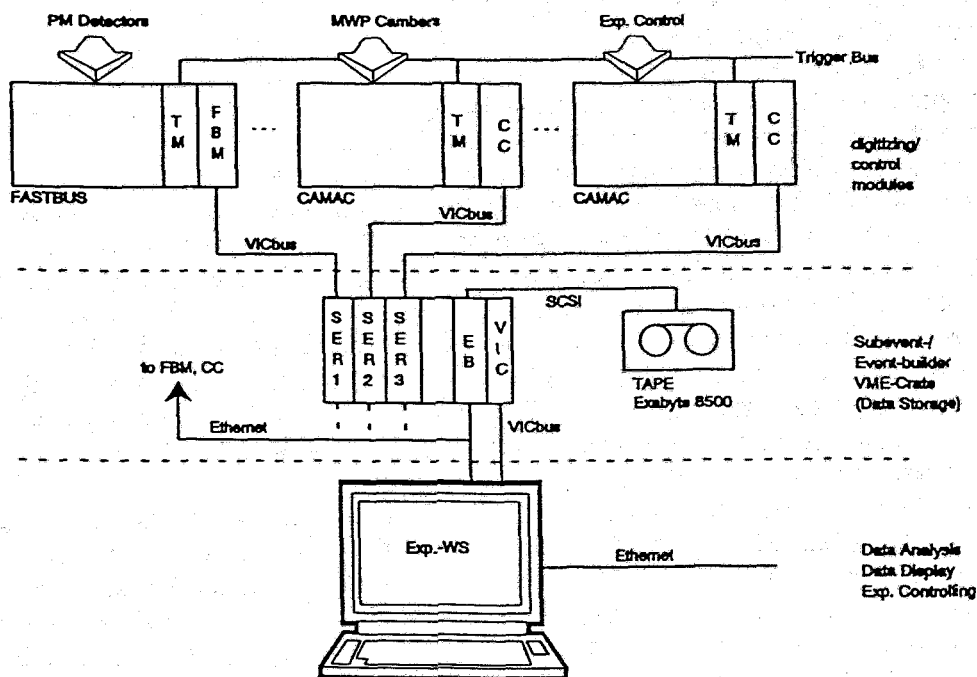


Fig.1 Basis Hardware Architecture of the Data Acquisition System of the 0° Facility

REFERENCES:

- [1] COSY-Arbeitsgemeinschaft Nordrhein-Westfälischer Universitäten CANU, Kommission Datenaufnahme COSY, "Summary of recommendations as of December 16, 1991, Internal Paper"
- [2] W. Erven, J. Holzer, H. Kopp, H.W.Loevenich, W. Meiling, K. Zvoll, M. Karnadi, R. Nellen, K.-H.Watzlawik, "COSY Data Acquisition System for Physical Experiments", Seventh Conference REAL TIME '91 on Computer Applications in Nuclear, Particle and Plasme Physics, Conference Record, June 1991, Jülich, FRG, p. 298-303
- [3] K.-H. Watzlawik, "COSY-Experiment Data Acquisition", Interne Papiere IKP-DV, Forschungszentrum Jülich
- [4] K. Zvoll, M. Drochner, W. Erven, J. Holzer, H. Kopp, P. Wüstner, "Architektur und Übersicht des Datenerfassungssystemes für COSY-Experimente", Internal Paper ZEL Forschungszentrum Jülich, 16.11.92
- [5] R. Brun et al., "PAW, Physics Analysis Workstation / HBOOK" CERN Programm Library, CERN Geneva Switzerland, 1987, 1989
- [6] W. Oehme, "COSY-Experiment Data Acquisition - Logging- and Reporting-System", Internal Paper FZ Rossendorf 30.10.92

TEST OF PHOTOMULTIPLIERS FOR THE 0° FACILITY AT COSY^B

B.PRIETZSCHK AND B.RIMARZIG

Forschungszentrum Rossendorf, Institut für Kern-und Hadronenphysik

At the 0° Facility a large number of scintillation detectors will be used. As a first step the necessary photomultipliers (PM) were tested. The amplitude and time characteristics of 60 PM's (type XP 2020 and XP 4222) to be used for the STOP detector (see Ref. [1]) were measured by using the arrangement shown in Fig. 1. A voltage divider of Philips was modified such that the voltages g_1 and d_1 could be changed continuously (see Fig. 2). As light source a green LED controlled by a pulse generator with pulse rise time of 1.2 ns and pulse amplitude of 40 V was used. In the test 8 points at a distance of 16 or 18 mm and 21 or 22 mm from the centre of the photo cathode were selected turning the PM by 45°. At each point the amplitude and rise time of the dynode pulses, the signal transit time relative to the generator time and the time resolution (FWHM) were measured. The differences of the transit times between the value for the centre of the cathode and those for the points at 16/18mm distance amounts to 220 - 450 ps and at 21/22mm distance to 250 - 600 ps, respectively. Compared to the centre of the photo cathode the amplitudes change by about 15% when measuring at a distance of 16mm from the centre and by $\leq 20\%$ at 21 mm distance. The time resolution amounts to 125 - 200 ps (FWHM).

As a result of these measurements the mechanical and electrical construction of the voltage divider could be optimized. It is important to have as small and cheap voltage dividers as possible, because of the large number of PM's to be used at the 0° Facility. Several variants of dividers were built and tested. Fig. 3 shows the mechanical construction of the developed divider with a diameter of 78mm. The electrical stability of the divider was tested at 3 kV. No deterioration of the transit time difference and time resolution has been found. Up to now 4 dividers were built and tested. The costs for the developed voltage divider amounts to about 30-40% of those for the divider from Philips GmbH [2].

PM tubes of the types XP 2972, XP 2000R and R 2076(R3478) were tested, too, because for the START detector we intend to make use of PM's with a smaller diameter of the photo cathode.

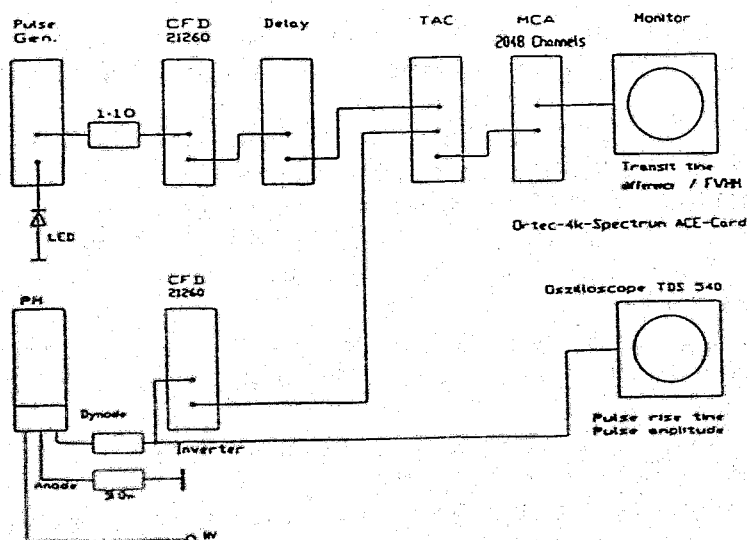


Fig.1 Set - up

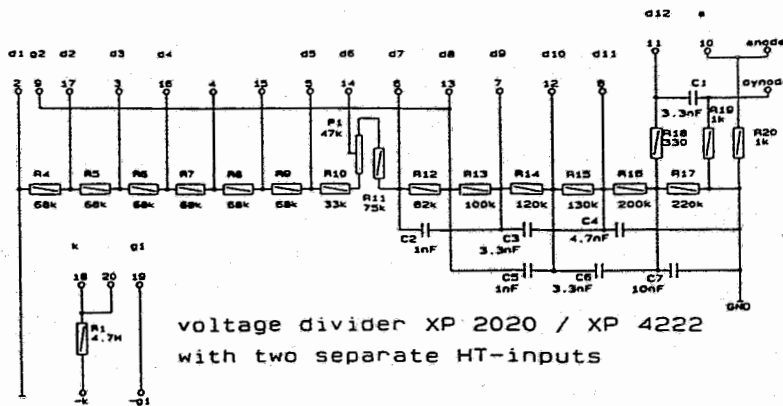


Fig.2 Electrical construction of the modified voltage divider

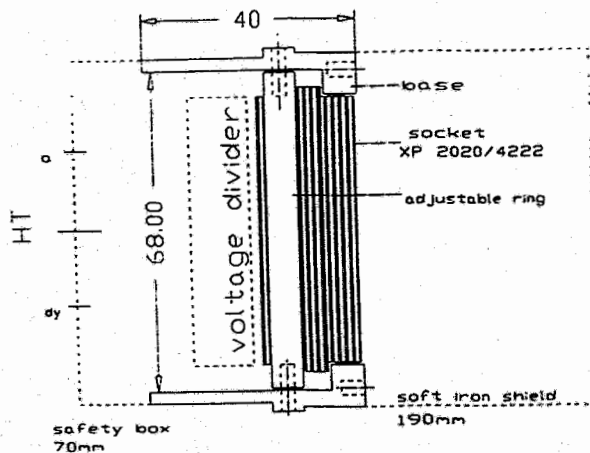


Fig.3 Mechanical construction of the voltage divider

In order to measure the signal transit time difference of the XP 2927 a suitable voltage divider had to be build. The voltage d_1 is adjustable and high voltages of 1,75 and 1,85 kV are used. The transit time difference at a distance of 11 mm from the centre of the photo cathode lays between 475 and 625 ps. The output amplitudes and the time resolution change up to 100% compared to the centre.

One PM of the type R 2076 (denoted by R 3478 with integrated voltage divider) was tested with the following result: signal transit time difference at a distance of 6.5 mm from the centre of the photo cathode amounts to 150 - 200 ps and the time resolution is $\leq 30\%$.

One part of the detector arrangement at the 0° Facility is placed in the magnetic field. Therefore, it is necessary to have shielding cylinders for the PM tubes. Some Permenorm and Mumetal shield cylinders were produced in the FZ-Rossendorf and afterwards glowed by Fa. Strömungsmaschinenbau Dresden. The shielding characteristics will be tested in the FZ-Jülich.

REFERENCES:

- [1] W. Borgs et al., COSY Proposal Nr. 18, 1991
- [2] Philips Components: Data Handbook, Photomultiplier, 1990

Development of Data Acquisition Electronics for FOBOS

K. Heidel, H.-G. Ortlepp¹

Forschungszentrum Rossendorf, Institut für Kern- und Hadronenphysik

¹ *Joint Institute for Nuclear Research Dubna, Laboratory of Nuclear Reactions*
On leave from: Forschungszentrum Rossendorf, Institut für Kern- und Hadronenphysik

Delay-line Amplifier 5027-30

The delay-line amplifier shapes the coordinate signals derived from position-sensitive avalanche counters according to the delay-line principle. It is operated in high vacuum and protected from damage caused by voltage discharges. The input impedance may be matched with different delay lines ($z_i = 200 \dots 800 \Omega$, adjustable). The linear output range is $U_A = -1.6V$ (on 50Ω load) and may be directly fed into a trigger.

The lay-out is manufactured from double layer board of the dimensions $300 \times 200 \text{ mm}^2$ designed by PCAD [1] and produced in surface-mount devices (SMD) technology.

Avalanche-Counter-Amplifier 5027-40

The avalanche-counter amplifier derives fast timing signals and spectroscopic signals from avalanche counters. It is operated in high vacuum and protected from damage caused by voltage discharges. The amplifier is isolated from high voltage (bias 1.5kV, filter time 0.5s). The linear output of the timing channel is $U_A = -1.5V$ (on 50Ω load). The timing signals may be directly fed into a trigger. The spectroscopic signals (output impedance $Z_0 = 50 \Omega$) need further amplification.

The lay-out is manufactured from double layer board of the dimensions $750 \times 300 \text{ mm}^2$ designed by PCAD and produced in SMD technology.

BRAGG Processor BDP 5385

The CAMAC 1M-module BRAGG Digital Processor (BDP) [2] was designed for the processing of digitized signals from BRAGG-ionization chambers to obtain the energy and particle information [3]. The shape of the BRAGG pulse is digitized by means of a flash ADC located in the companion module BCD 5387 [2]. The clock frequency of the ADC is 10MHz. Two arithmetic units - developed using high-performance TTL family (FAST, ALS) - determine the integral (energy E) and the smoothed maximum (nuclear charge number Z) of the signal. A digital comparator determines the threshold for pulse recognition and a pile-up inspector rejects erroneous results. The control of the working conditions and the data transfer is performed via the CAMAC-dataway.

The lay-out is manufactured from 4-layer board designed by PCAD and produced in SMD technology.

Shaper/Flash ADC BCD 5387

The CAMAC 1M-module BRAGG Curve Digitizer (BCD) was designed for the digitizing of spectroscopic signals from BRAGG ionization chambers. It includes a spectroscopic amplifier and filters (pole-zero compensated C/R differentiation and active low frequency filter) adapted to this purpose. The output signals of the amplifier are sampled with a 10MHz clock frequency generator and digitized by an 8-bit flash ADC. The control of the working conditions is performed via the CAMAC-dataway.

The lay-out is manufactured from 4-layer board designed by PCAD (mixed technology).

REFERENCE:

- [1] Heidel, K., Annual report 1991, FZR 92-09, 79
- [2] Heidel, K., Ortlepp, H.-G., Annual report 1991, FZR 92-09, 80
- [3] Ortlepp, H.-G., Romaguera, A., Nucl. Instr. and Meth. A276 (1989) 500

Complete test of the BRAGG Digital Processor BDP 5385

K. Heidel, H.-G. Ortlepp¹, A.P. Sirotin²

Forschungszentrum Rossendorf, Institut für Kern- und Hadronenphysik

¹ *Joint Institute for Nuclear Research Dubna, Laboratory of Nuclear Reactions
(On leave from: Forschungszentrum Rossendorf, Institut für Kern- und Hadronenphysik)*

² *Joint Institute for Nuclear Research Dubna, Laboratory of Neutron Research*

The BRAGG-ionization chambers of the FOBOS 4π -array [1] are read out by the special processor unit BDP 5385 [2]. In addition to the test method proposed in ref. [3] we developed a complete test procedure using a simulated near-real chamber pulse-shape.

The status word of the BRAGG Digital Processor is generated under program control interactively as follows:

- Threshold value (0-63): sets up an input threshold level
- Parameter G (1-5): sets up the number of samples used for determination of fragment charge number Z (pulse max.)
- Parameter P: sets up a time interval (pile-up) for checking the pulse-length $(0 - 255) \cdot \tau$, with $\tau = 100\text{ns}$
- Pulse-length $1.5\mu\text{s} - 3\mu\text{s}$: defines a time interval for the pulse-shape
- Pulse-shape: regime for definition of test pulse-shapes

The complete test procedure calculates the values for E and Z simultaneously. The test pulse-shape can have any form given by 72 numerical values of sample amplitudes. It will be written into the coincidence unit ZfK 5388 [3], which has been zeroed before. If the E and/or Z processing has failed the test pulse-shape can be chosen in a less complicated way and the reason of failure can easily be found.

Our complete test together with the procedure of ref. [3] gives guarantees that the BDP will work faultless under the experimental conditions of FOBOS.

The principle block-scheme of our complete BDP test arrangement is given in fig. 1. The unit ZfK 5388 is used as a program controlled generator of the simulated pulse-shape and of the START and CLEAR signals necessary. The shaper F synchronizes the test information with a takt frequency analogous to the BRAGG Curve Digitizer BCD 5387 [2] applied in experiment. The controller KK009 is a CAMAC-interface for the PC-AT.

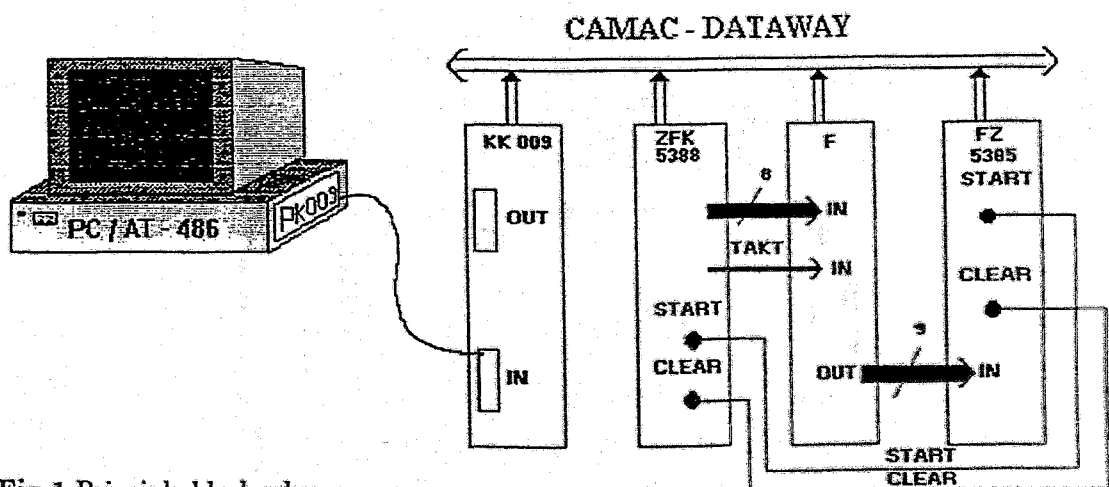


Fig.1 Principle block-scheme

REFERENCE:

- [1] Ortlepp, H.-G. et al., Proc.Int.Conf.on New Nuclear Physics with Advanced Technique Ierapetra, Crete, Greece (1991) FZR 92-11, Rossendorf, 1992
- [2] Heidel, K., Ortlepp H.-G., Annual report 1991, FZR 92-09, 80
- [3] Fromm, W.-D., Annual report 1989, ZFK-731, 119

Results of in-beam PET imaging Experiments at the Fragment Separator of the GSI Darmstadt^B

W. ENGHARDT¹, W.D. FROMM², H. GEISSEL³, H. KELLER³, G. KRAFT³, A. MAGEL³,
 P. MANFRASS⁴, G. MÜNZENBERG³, F. NICKEL³, J. PAWELKE⁴, D. SCHARDT³,
 C. SCHEIDENBERGER³, M. SOBIELLA⁴

¹ KAI e.V. im FZ Rossendorf, ² ZfK Rossendorf, ³ GSI Darmstadt,
⁴ FZ Rossendorf

In ref. [1] we presented first results of the 1991 positron emission tomography (PET) experiments with β^+ -radioactive beams obtained either from the fragment separator FRS [2] or by the nuclear interaction of a beam of stable ions with the stopping target [3].

At first we report here on an interesting byproduct of the PET measurements, namely the visualization of the fragment separator performance. For this purpose radioactive beams obtained from the fragmentation of ^{20}Ne ($E = 500$ MeV/u) in a 4 g/cm² Be target were implanted into a phantom of polymethylmethacrylate (PMMA, $\rho = 1.18$ g/cm³). The target mounted in the centre of the large area HIDAC positron camera [4] had a length of 25 cm in beam direction and of 22 cm in the x-direction of the FRS coordinate system (lateral direction). The thickness of the target amounted to 3 cm in order to reduce the influence of the scattering of the annihilation radiation to the image quality. The radioactive beams of ^{19}Ne with minor components of ^{17}F and ^{15}O had an intensity of $(1\dots 5) \times 10^5$ particles per spill. The spill repetition time was 3.5 s, the spill length amounted to 0.5 s. Annihilation data were recorded only in the pauses between the synchrotron pulses. The longitudinal tomograms were reconstructed by means of an iterative algorithm [5].

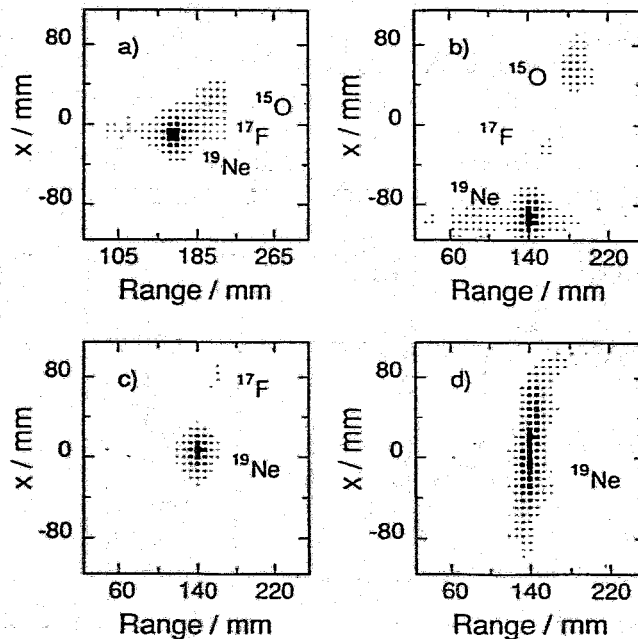


Fig. 1 Implanted β^+ -activity distributions obtained from different degraders at the central focus F_2 of the fragment separator FRS. a) without F_2 -degrader, b) homogeneous degrader, c) achromatic degrader, d) monoenergetic degrader.

In the tomograms of fig.1 representing a 2 cm thick slice of the phantom and in the widths of the ^{19}Ne distributions (tab.1) the effect of inserting differently shaped degraders at the focus F_2 of the-FRS can be clearly seen. The values of table 1 have been calculated by fitting the distributions to a Gaussian and by deconvolution with the Gaussian point response function (FWHM = 7.3 ± 0.3 mm) of the positron camera. This rather poor spatial resolution is due to the parallax error of the detectors, where two γ -electron converters at different positions are read out by one multi wire proportional chamber in between [4]. Fig. 1a shows that ions with nearly the same A/Z ratio (^{19}Ne , ^{17}F , and ^{15}O) are only poorly separated if the fragment separator is operated without a degrader at the focus F_2 . Inserting a homogeneous degrader leads to a clear separation of these beam components (fig. 1b). Figs. 1c and 1d show the effect of achromatic and monoenergetic degraders on the shape of the final focus.

F_2 -degrader	Range FWHM (mm)	Lateral FWHM (mm)
Without	11.7 ± 0.4	17.6 ± 0.5
Homogeneous	11.3 ± 0.5	20.7 ± 0.6
Achromatic	8.5 ± 0.6	19.4 ± 0.8
Monoenergetic	4.5 ± 0.7	77.5 ± 3.9

Table 1 The width (FWHM) of the implanted ^{19}Ne distribution for different F_2 -degraders

In real therapy PET range measurements using a β^+ -active beam for treatment plan verification and adjusting the therapy beam parameters should be done with low doses of radiation. Therefore, it is desirable to measure the ranges from a low number of annihilation events. Fig. 2 shows that for a beam of ^{19}Ne the centroid of the range distribution can be rather precisely calculated from several hundreds of registered annihilation events.

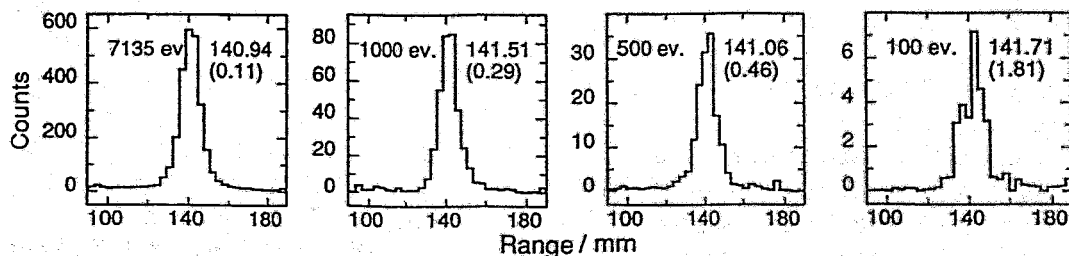


Fig. 2 Comparison of the ranges of a ^{19}Ne beam ($E = 406$ MeV/u, width: 26.9 mm FWHM) deduced from tomographic slices of 2 cm thickness which have been reconstructed from different numbers of annihilation events. The graphs have been obtained by projecting the tomograms onto the range axes. The mean ranges calculated by a Gaussian fit are given in mm with the errors in parentheses.

REFERENCES:

- [1] W. Enghardt et al., GSI Scientific Report 1991, p. 305
- [2] H. Geissel et al. Preprint GSI-91-46
- [3] W. Enghardt et al., Phys. Med. Biol. 37(1992)2127
- [4] P. Manfraß et al., Nucl. Instr. Meth. A273(1988)904
- [5] W. Enghardt, Physica Medica VII(1991)119

On the spatial Distribution of Positron-emitting Nuclei generated by relativistic light Ion Beams in organic Matter^B

W. ENGHARDT

KAI e. V. im Forschungszentrum Rossendorf

Due to their physical behaviour when penetrating matter, highly energetic light ions produce very favourable dose profiles for the radiotherapy of deeply seated tumours [1]. In order to translate these physical properties into precise, tumour conform dose profiles it is necessary to use a beam delivery which consists of a magnetic scanning system and an active energy variation [2]. Such a highly precise irradiation requires the possibility of an in-situ therapy control. The first approach to this problem was the Berkeley concept [3] of treatment plan verification by means of low-intensity beams of β^+ -active isotopes of the therapy beam.

However, nuclear fragmentation during the penetration of the therapy beam through tissue will produce a considerable amount of β^+ -active nuclei. The study of the spatial distribution of these β^+ -emitters generated by a 406 MeV/u ^{20}Ne beam in a plastic phantom by means of in-beam positron emission tomography (PET) [4] revealed that this distribution shows a pronounced maximum near the range of the ^{20}Ne particles.

In order to explain this, the nuclear fragmentation of the primary particles as well as the stopping and decay processes of the positron emitting secondaries have been calculated. For simplicity of the Monte Carlo code the following assumptions have been made:

- (i) The only processes for generating secondary radioactive isotopes are nuclear fragmentation reactions.
- (ii) Longitudinal and transverse momentum transfer in the nuclear fragmentation reactions have been neglected.
- (iii) Fragmentation cross sections have been calculated using the parametrization of ref. [5].
- (iv) Subsequent nuclear interactions of the secondaries have not been taken into account.
- (v) Range calculations have been performed using the relativistic Bethe formula.
- (vi) The distributions of the positron emitters $^{10,11}\text{C}$, ^{13}N , $^{14,15}\text{O}$, $^{17,18}\text{F}$ and $^{18,19}\text{Ne}$ have been calculated, whereas the short lived ones ^8B , ^9C , ^{12}N , ^{13}O and ^{17}Ne have not been taken into account, since their production cross sections are comparatively small and most of them have a β^+ -endpoint energy greater than 8 MeV which corresponds to maximum positron ranges in tissue of more than 4 cm [6].

The results of applying this code to β^+ -activity distributions in polymethylmethacrylate (PMMA, $\text{C}_5\text{H}_8\text{O}_2$) induced by beams of ^{20}Ne , ^{16}O and ^{12}C with a range of about 14.3 cm are shown in fig. 1. The observed β^+ -activity results from different components:

- (i) Target fragmentation gives rise to the flat, exponentially decreasing part of the spectrum, which begins at the entrance of the beam into the target and ends at a range that corresponds to the fragmentation threshold.
- (ii) Projectile fragmentation produces an activity distribution with a pronounced peak structure, where the β^+ -active isotopes of the primary nuclei have shorter ranges than the incoming beam, whereas the fragments with lower atomic numbers are found at larger ranges.

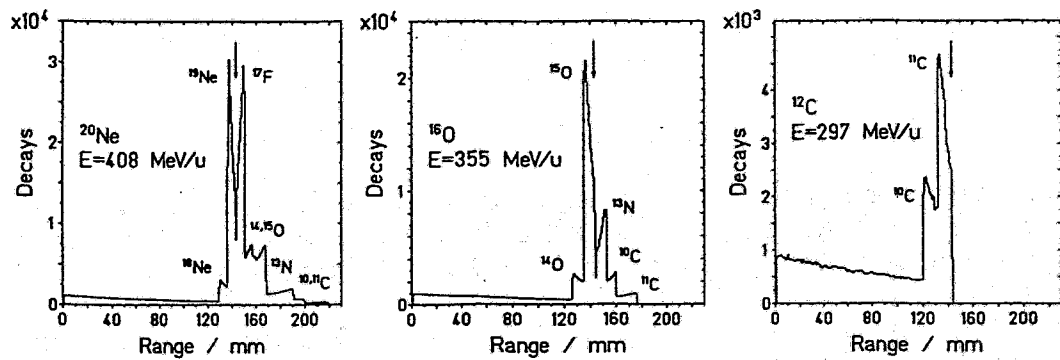


Fig. 1 Number of β^+ -decays versus the range of positron emitting fragments generated by ^{20}Ne , ^{16}O and ^{12}C beams in a PMMA phantom obtained from Monte Carlo calculations. The decays are assumed to be registered during 5 min after the irradiation with one infinitely short pulse of 10^7 primary particles. The arrows indicate the primary particle ranges as obtained from the relativistic Bethe formula.

The results show that the range distributions of the induced β^+ -emitters may involve sufficient information for extracting the range of the primary beam. This may offer the possibility of on-line monitoring light ion tumour treatment by means of PET. For proving this assumption further experiments and a refinement of the Monte Carlo code have been initialized.

REFERENCES:

- [1] G. Gademann et al., *Strahlenther. Onkol.* **166** (1990) 34
- [2] Th. Haberer et al., Report GSI-91-18
- [3] J. Llacer, *Nucl. Sci. Appl.* **3** (1988) 111
- [4] W. Enghardt et al., *Phys. Med. Biol.* **37** (1992) 2127
- [5] K. Sümmerer et al., *Phys. Rev.* **C42** (1990) 2546
- [6] ICRU Report 37

A flexible double head BGO positron camera^B

J. PAWELKE¹, W. ENGHARDT², A. FRIEDRICH³, H.G. MARTENS³,
W. MEUFELS³, K. POPPENSIEKER³, M. SOBIELLA¹

¹ FZ Rossendorf, ² KAI e.V. im FZ Rossendorf, ³ GSI Darmstadt

Positron emission tomography (PET) techniques for an in-vivo dose localization in light ion tumour therapy [1,2] requires detectors with high efficiency. Thus, bismuth germanate (BGO) is the detector material of choice for such a PET application which has to be installed at the treatment place i.e. directly at a high energy light ion beam.

For minimizing reconstruction artifacts a ring PET scanner, as it is commonly used in nuclear medicine, would be necessary. However, such a tomograph installed at the treatment position will interfere with the beam delivery.

Thus, an incomplete transaxial tomograph providing gaps for the therapy beam seems to be an adequate solution of this problem. The imaging properties of such an tomograph have to be tested at the beam-line, but a complete construction is too expensive.

Therefore two small position sensitive BGO detectors [3] were mounted on a step motor driven handling system which is capable of moving the two detectors independently on a cylindrical surface and which simulates thereby a ring tomograph with a vertically oriented axis (fig.1). The two linear tables (vertical motions) allow an increase of the axial field of view (FOV) as well as in-plane and cross-plane coincidence measurements. The turn around tables increase the transaxial FOV.

Since a correct tomographic reconstruction requires both the actual detector position and the points where the annihilation quanta hit the detectors (intrinsic detector coordinates), a real-time control for the handling system (fig. 2) had to be developed. The detector movement is controlled by a 3HE VME system [4] based on a Motorola 68020 CPU running OS9, an I/O card, floppy and hard disk drives and step motor drivers MCS1 [5] which additionally watch the end position switches.

Each step motor (VRDM 5910/50 LNC [6]) is driven by a motor driver unit (MDU) that includes the D550-04 [6] driver card, a power supply and an adapter for the end position switches.

For transferring the actual detector positions to the data acquisition system GOOSY [7] (supporting the J11 based single CAMAC crate system) the VME crate is coupled to CAMAC via the MIL bus (MIL-STD-1553B) control unit VSE1000 and a CAM1000 module. The control software has been written in C.

REFERENCES:

- [1] G. Gademann et al., *Strahlenther. Onkol.* 166(1990)34
- [2] J. Llacer, *Nucl. Sci. Appl.* 3(1988)111
- [3] J.G. Rogers et al., *IEEE Trans. Nucl. Sci.* NS-39(1992)1063
- [4] PEP Modular Computers, VME 2330-02/8 User's Manual, Kaufbeuren(1991)
- [5] ProMotion Industrie-Elektronik GmbH, *Schrittmotor-Indexer Handbuch*, Karlsruhe(1988)
- [6] Berger Lahr, *Druckschrift Nr. 3601D*, Lahr(1992)
- [7] H.G. Essel et al., *IEEE Trans. Nucl. Sci.* NS-34(1987)907

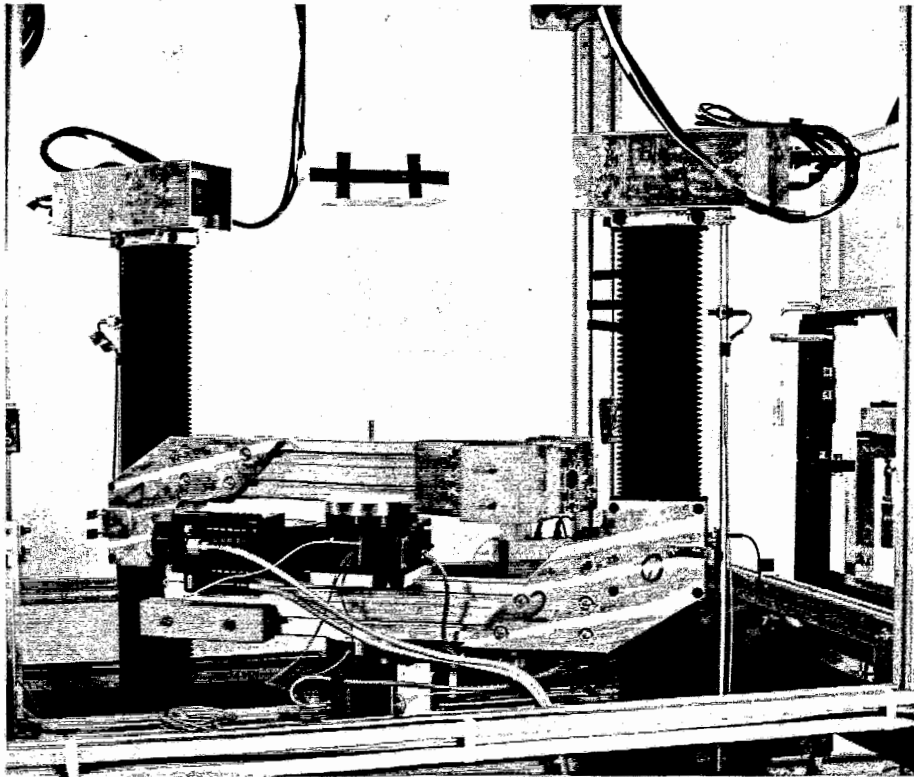


Fig. 1 The double-head BGO camera mounted at the beam line of the heavy ion synchrotron at GSI. In the centre the turn around tables are seen which bear arms with the vertically mounted linear tables with the detectors on top of it. The detectors can be moved around the phantom of plastic wherein the beam coming from the left is stopped. (Photo: Achim Zschau, GSI Darmstadt, RS-2080/11/93)

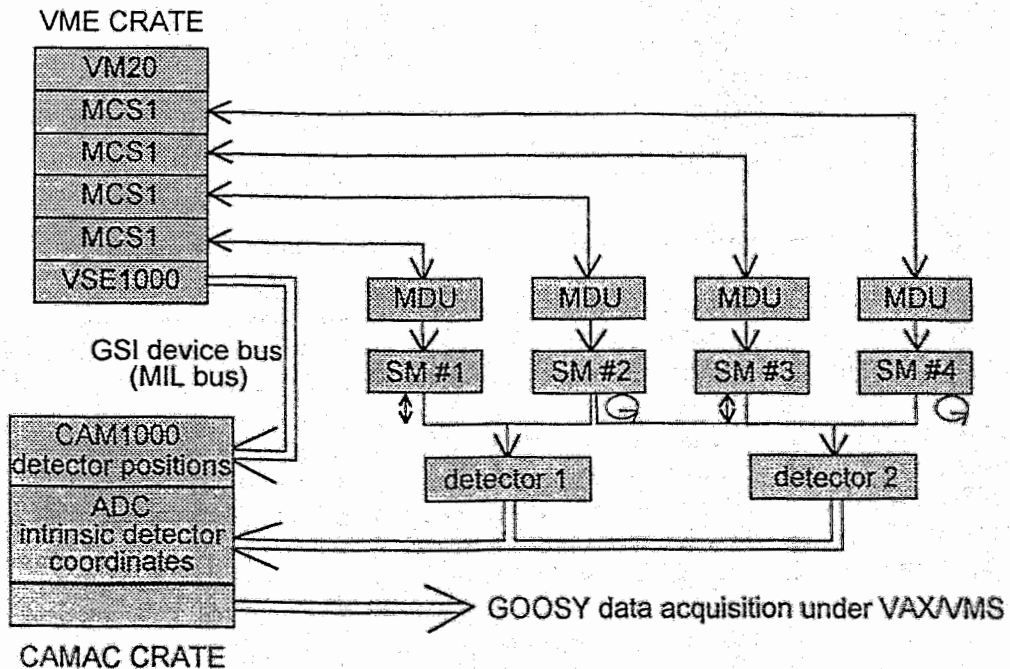


Fig. 2 Schematic drawing of the movement control of the positron camera. MDU means motor driver unit and SM means step motor.

Two different BGO detector modules for use in light ion tumour therapy^B

J. PAWELKE¹, W. ENGHARDT², P. MANFRASS¹

¹ FZ Rossendorf, ² KAI e.V. im FZ Rossendorf

In-vivo measurements of the ranges of β^+ -radioactive beams by means of positron emission tomography (PET) are regarded as an essential component for treatment plan verification in a future light ion tumour therapy [1,2]. In order to minimize the radiation dose for patient, detectors with high efficiency are required. Thus, bismuth germanate (BGO) is the detector material of choice for such a PET application.

The spatial resolution of a BGO positron camera is primarily determined by the size of the crystals. The limiting factor in decreasing the crystal size in multi detector PET scanners is the problem of one-to-one coupling between scintillators and photomultiplier tubes (PMTs). To overcome this, two dimensional arrays of crystals are coupled to PMTs, where the number of PMTs is less than the number of crystals.

On the base of the results of computer simulations of the 511 keV γ -radiation interaction in BGO scintillators 2 different multicrystal 2D BGO detectors have been investigated by measurements with an ¹⁸F flood source for an evaluation of the main properties (e.g. crystal identification, energy resolution, detector efficiency). The main properties of the detectors are:

	I) Siemens ECAT [3]	II) FZR
Scintillator	BGO block, specially cut into 8 · 8 crystals	matrix of 17 · 18 individual BGO crystals
Crystal Dimension	6.25 · 6.25 · 30 mm ³	3 · 3 · 20 mm ³
PMT	four standard PMTs (A, B, C, D)	one position sensitive cross wire anode PMT [4] coupled to x,y resistor chains
Detector Output Signals	PMT amplitudes I_A, I_B, I_C, I_D	charges divided by resistor chains Q_A, Q_B, Q_C, Q_D
Position Calculation	$X = \frac{(I_A + I_C) - (I_B + I_D)}{I_A + I_B + I_C + I_D}$ $Y = \frac{(I_A + I_B) - (I_C + I_D)}{I_A + I_B + I_C + I_D}$	$X = \frac{Q_A - Q_B}{Q_A + Q_B}$ $Y = \frac{Q_C - Q_D}{Q_C + Q_D}$
Spatial Resolution	6.25 mm	3.00 mm
Image Distortion	trapezium	none
Ratio of Max/Min of Detection Efficiency	1.8	3.0
Energy Resolution of a Crystal	about 20 % FWHM	about 37 % FWHM

In fig. 1 the position response distributions of both detector modules are compared. In both systems each crystal can be distinguished, allowing the identification of where the scintillation event took place.

The disadvantage of the FZR module is the rather great difference in the detector efficiency of a factor 3 over the sensitive detector area. To investigate the reason of this, in measurements at the KFA Jülich the PMT dynode outputs were determined, moving a blue light emission diode (LED) in front of the FZR detector module with and without crystal array in 2 dimensions [5]. A dependence of the differences in the detection efficiency on the inhomogeneous PMT efficiency was found (see fig. 2) which requires further efforts for its reduction. For a final evaluation of both detector systems, coincidence measurements (e.g. coincidence efficiency and spatial resolution of a point source) with two modules in each case and the investigation of the tomographic imaging of a tomograph using a higher number of modules in each case have to be done.

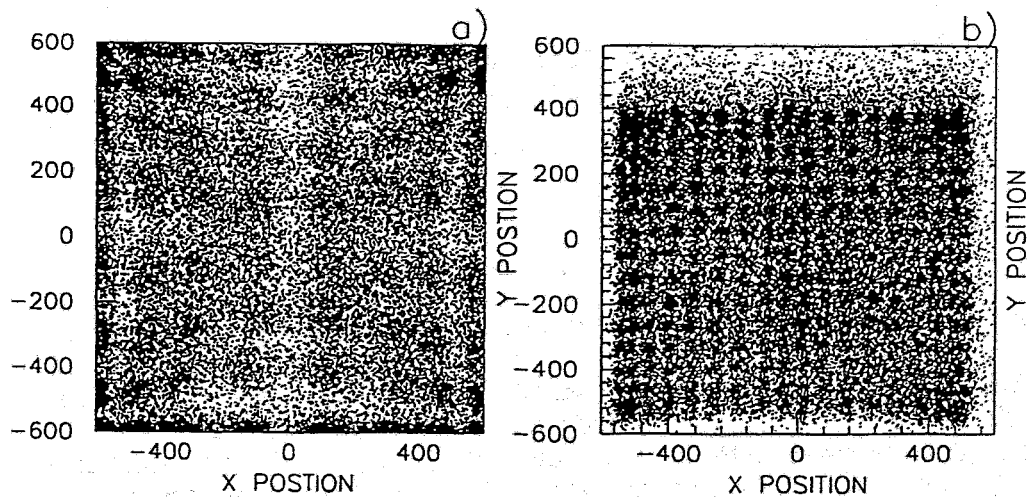


Fig. 1 Image of the X and Y position response distribution of a Siemens (fig. 1a) and of a FZR (fig. 1b) detector module formed by exposing the modules to a ^{18}F flood source.

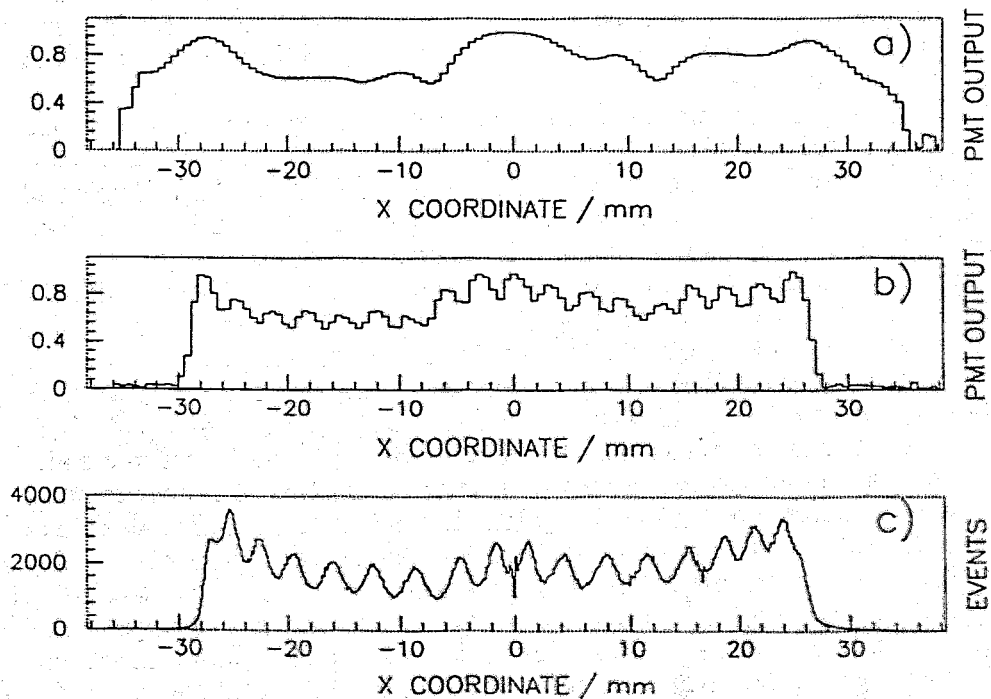


Fig. 2 Projection of the PMT dynode output, moving a LED in front of the FZR module without (fig. 2a) and with (fig. 2b) crystal array in two dimensions. Fig. 2c shows the projection of the 2-dimensional event distribution generated by irradiation with a ^{18}F flood source.

REFERENCES:

- [1] G. Gademann et al., *Strahlenther. Onkol.* 166(1990)34
- [2] J. Llacer, *Nucl. Sci. Appl.* 3(1988)111
- [3] J.G. Rogers et al., *IEEE Trans. Nucl. Sci.* NS-39(1992)1063
- [4] T. Yamashita et al., *IEEE Trans. Nucl. Sci.* NS-37(1990)589
- [5] R. Eßer, *Diplomarbeit Universität zu Köln*(1992)43

A simple and fast reconstruction algorithm suitable for on-line range measurements by means of PET in light ion tumour therapy^B

J. PAWELKE¹, W. ENGHARDT²

¹ FZ Rossendorf, ² KAI e.V. im FZ Rossendorf

In vivo measurements of the ranges of β^+ -radioactive beams by means of positron emission tomography (PET) are regarded as an essential component for treatment plan verification in a future light ion tumour therapy [1,2]. For this purpose a suitable positron camera system that considerably differs from those applied in nuclear medicine has to be used at accelerator beams. In refs. [3,4] first results of PET measurements of spatial β^+ -activity distributions were presented, when radioactive beams were implanted into organic phantoms and the following annihilation events were detected. Longitudinal tomograms were constructed from the measured data by means of backprojection and 3-dimensional iterative reconstruction [2]. In a further step the beam range was deduced from the tomograms. However, the use of the reconstruction algorithm requires a lot of computing time and the measurement has to be finished before the reconstruction can be started. Thus, an alternative algorithm for a practical use in tumour therapy is desirable. It would be worthwhile if the reconstruction can be started during data acquisition.

A 3-dimensional tomographic reconstruction starts often with a backprojection. In a second step the blurring, generated by the backprojection, is removed by means of a suitable reconstruction method. Because of the special conditions for in-beam PET imaging of implanted radioactivity (low activity, poor event statistics, limited angle and shift variant sampling) the fast Fourier space deconvolution is not applicable for reconstruction.

The 3-dimensional backprojection of a point source is a $\frac{1}{R^2}$ -function where R means the distance from the source. In this work the backprojection was replaced by an empirical method which determines the 3-dimensional distribution of pairwise intersection points of all event lines measured. In difference to the backprojection this method shows a more complex shape of blurring that depends on the spatial coordinates of the source points. However, it can be assumed that this method leads to a sufficiently low blurring for exact range calculations without the need of time consuming tomographic reconstruction. In order to check this, images were reconstructed by the crossing point scheme from simulated event data of different combinations of point and line sources. The simulation shows a general reduction of blurring in the case of simple compact activity distributions. For the purpose of range measurements in tumour therapy such source distributions are given, thus, the application of the intersection point scheme for reconstruction of PET measurements [3,4] was started. In fig. 1 the 2-dimensional radioactivity distributions in sections of 2 cm thickness with the beam in the centre calculated by the iterative scheme and the crossing point method are compared for two data sets. With both methods comparable images were obtained with the difference of a slight blurring in the distribution from the method of crossing points. In real therapy PET range measurements using a β^+ -active beam for treatment plan verification and adjusting the therapy beam parameters before the actual treatment should be done with low doses of radiation. In table 1 we compare the range values that have been extracted from tomograms reconstructed from different numbers of annihilation events. They have been calculated by projection the tomograms on the range axis and fitting the projection data to a Gaussian. Apart from the case of very low event numbers the faster crossing method calculates the same ranges as the 3-dimensional iterative reconstruction with its effective suppression of the statistical noise [2]. The possibility of starting the on-line reconstruction by calculation the intersection points of the event lines after registration of two events makes this method rather attractive for real therapy and will justify further efforts for its refinement.

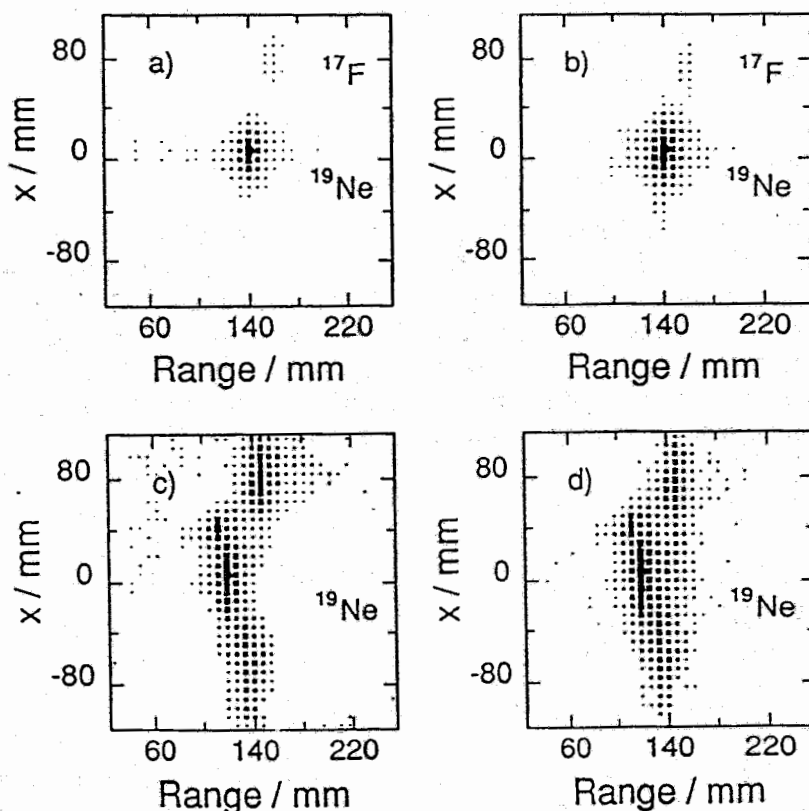


Fig. 1 Reconstructed β^+ -activity distribution obtained from 3-dimensional iterative reconstruction (fig. 1a, 1c) and the method of crossing point calculation (fig. 1b, 1d). The upper figs. show the implanted β^+ -activity distribution in the central slice of a homogeneous plastic phantom generated by implantation a ^{19}Ne beam ($E=406$ MeV/u) with a ^{17}F contamination provided by the fragment separator with an achromatic degrader. The lower figs. show the ^{19}Ne distribution in a plastic phantom with small density deviations generated by irradiation with a pure, monoenergetic ^{19}Ne beam.

Events	3D ITERATION		CROSSING	
	CPU-time / s	Range / mm	CPU-time / s	Range / mm
7130	21000	140.94±0.11	520	140.85±0.21
1000	21000	141.51±0.29	18	141.11±0.36
500	21000	141.06±0.46	9	140.60±0.49
100	21000	141.71±1.81	3	143.80±3.41

Table 1 Comparison of the 3-dimensional iteration and the crossing point method with respect to the computational labour and the accuracy of the range calculation for different numbers of annihilation events taken into account for reconstruction. The experimental data are those of figs. 1a, 1b.

REFERENCES:

- [1] J. Llacer, Nucl. Sci. Appl. 3(1988)111
- [2] W. Enghardt et al., Physica Medica VII(1991)119
- [3] W. Enghardt et al., GSI Scientific Report 1991, p. 305
- [4] W. Enghardt et al., contribution to this report

The spatial distribution of positron-emitting nuclei generated by relativistic light ion beams in organic matter
(Phys. Med. Biol. 37 (1992) 2127)

W. Enghardt, W.D. Fromm, H. Geissel, H. Keller, G. Kraft, A. Magel, P. Manfraß, G. Münzenberg, F. Nickel, J. Pawelke, D. Schardt, C. Scheidenberger and M. Sobiella

Abstract: The range distributions of positron emitters generated during the stopping process of relativistic light ions in organic matter exhibit a pronounced maximum near the range of the primary particles. The shape of this distribution can be qualitatively understood from a simple Monte Carlo approach of the stopping, fragmentation and decay processes. These results offer the possibility of beam monitoring by means of PET techniques during the tumour therapy with a light ion beam. Furthermore, a refinement of this technique may allow the actual dose distribution to be calculated from PET data.

Limited-angle 3D reconstruction of PET images for dose localization in light ion tumour therapy
(Phys. Med. Biol. 37 (1992) 791)

W. Enghardt, W.D. Fromm, P. Manfraß and D. Schardt

Abstract: In vivo dose localization in light ion tumour therapy can be performed by measuring the range distributions of β^+ active ions in tissue employing positron emission tomographic techniques. For this purpose a multiplicative iteration scheme for reconstructing three-dimensional images from shift-variant, limited-angle data is presented. In the iterative correction steps the algorithm uses the geometric means of quotients calculated from the three-dimensional Radon transforms of the backprojected measured and approximated source distributions. When sources measured with poor statistics are reconstructed, an effective noise suppression is achieved.

III. Publications and Talks

1. Publications and Conference Contributions

J.P. Alard et al., R. Kotte, J. Mösner, W. Neubert, D. Wohlfarth:
A midrapidity source of intermediate mass fragments in highly central collisions of Au + Au at 150 A MeV;
Phys. Rev. Lett. 69 (1992) 889

J.P. Alard et al., R. Kotte, J. Mösner, W. Neubert, D. Wohlfarth:
Flow and cluster formation in central Au on Au collisions at 100 to 800 A MeV;
Book of Abstracts, 1992 International Nuclear Physics Conference, Wiesbaden, Germany, Jul. 26-Aug. 1, 1992, p. 3.4.25

G. Baldisiefen, U. Birkental, H. Hübel, N. Nenoff, B.V. Thirumala Rao, P. Willsau, J. Hesse, H. Kluge, K.H. Maier, R. Schubart and S. Frauendorf:
First observation of a crossing of oblate dipole bands in the A=200 region;
Physics Letters B298 (1993) 54

M. Basler and B. Kämpfer:
Particle production during inflationary reheating;
Int. J. Mod. Phys. A7 (1992) 2033

H.W. Barz, G.F. Bertsch, P. Danielewicz, H. Schulz and G. Welke:
Pion-pion cross sections in a dense and hot pionic gas;
Phys. Lett. B275 (1992) 19

H.W. Barz, G.F. Bertsch, P. Danielewicz, H. Schulz and G.M. Welke:
Collisions in an expanding pion gas and the p_{\perp} spectrum in ultrarelativistic heavy ion collisions;
Contrib., XX Int. Workshop on Gross Properties of Nuclei and Nuclear Excitations, Hirschegg, Austria, Jan. 1992, p. 206

H.W. Barz, D.A. Cebra, H. Schulz and G.D. Westfall:
Event shape analysis of the reaction $^{40}\text{Ar} + ^{51}\text{V}$ within a prompt multifragmentation scenario;
Phys. Lett. B267 (1991) 317

H.W. Barz, P. Danielewicz, H. Schulz and G. Welke:
Thermalization of mesons in ultrarelativistic heavy ion collisions;
Phys. Lett. B287 (1992) 40

H.W. Barz, B.L. Friman, J. Knoll and H. Schulz:
Production of strangeness and vector mesons from a decaying quark-gluon plasma;
Proc. Int. Workshop on Dynamics and Correlations in Nuclear Collisions, Aussois, France, Nucl. Phys. A545 (1992) 397

H.W. Barz, J.P. Bondorf, A.S. Botwina, R. Donangelo, I.N. Mishustin, H. Schulz and K. Sneppen:
Gating in fragmentation processes?
Proc. Int. Workshop on Dynamics and Correlations in Nuclear Collisions, Aussois, France, Nucl. Phys. A545 (1992) 213

H.W. Barz, J.P. Bondorf, C.H. Dasso, R. Donangelo, G. Pollarolo,
H. Schulz and K. Sneppen:
Mechanism for nuclear disassembly of the Ar + Th and Pb + Au systems at intermediate
energies;
Phys. Rev. C46 (1992) R42

H.W. Barz, J.P. Bondorf, R. Donangelo, I.N. Mishustin, H. Schulz and K. Sneppen:
Fluctuations and intermittency in multifragmentation processes;
Phys. Rev. C45 (1992) R2541

G.G. Bunatian and B. Kämpfer:
Properties of ρ and ω mesons in dense and hot nuclear matter near the critical mode softening;
Report FZR-92-08

W. Cassing and A. Pfitzner:
Self-consistent truncation of the BBGKY hierarchy on the two-body level;
Z. Phys. A343 (1992) 161

S.Y. Chu, J.O. Rasmussen, R. Donangelo, M.A. Stoyer, S. Frauendorf and Y.R. Shimizu:
Theory of rotational population patterns in heavy-ion transfer reactions: even-even thorium
nuclei;
Proceedings of the Symposium on Nuclear Physics of our Times, Sanibel Island, USA, Nov.
17-21, 1992

F.-M. Dittes, H.L. Harney and A. Müller:
Non-exponential decay of a stochastic one-channel system;
Phys. Rev. A45 (1992) 701

F.-M. Dittes, I. Rotter and T.H. Seligman:
Chaotic behaviour of open quantum mechanical systems; in: "Quantum Chaos — Quantum
Measurement", ed. by P. Cvitanovic, I. Percival and A. Wirzba;
NATO ASI Series C - Vol. 358, Kluwer Acad. Publishers, Dordrecht 1992, p. 177

F. Dönau and S. Frauendorf:
On cranking about non-symmetry axes;
Proceeding of the Symposium on Nuclear Physics of our Times, Sanibel Island, USA, Nov.
17-21, 1992

J. Döring, G. Winter, L. Funke, B. Cederwall, F. Lidén, A. Johnson, A. Atac, J. Nyberg,
G. Sletten and M. Sugawara:
Evidence for new isomers and band structures in ^{80}Rb ;
Physical Review C46 (1992) R2127

W. Enghardt, W.D. Fromm, H. Geissel, H. Keller, G. Kraft, A. Magel, P. Manfraß, G.
Münzenberg, F. Nickel, J. Pawelke, D. Schardt, C. Scheidenberger and M. Sobiella:
The spatial distribution of positron-emitting nuclei generated by relativistic light ion beams
in organic matter;
Phys. Med. Biol. 37 (1992) 2127;
Reprint FZR-92-01

- W. Enghardt, W.D. Fromm, P. Manfraß and D. Schardt:**
 Limited-angle 3D reconstruction of PET images for dose localization in light ion tumour therapy;
 Phys. Med. Biol. 37 (1992) 791
- W. Enghardt, W.D. Fromm, P. Manfraß, J. Pawelke, M. Sobiella, D. Schardt, H. Geissel, H. Keller, G. Kraft, A. Magel, G. Münzenberg, F. Nickel and C. Scheidenberger:**
 Can the autoactivation of a stable light ion beam be employed for dose control in light ion tumour therapy?
 Particles 11 (1993) 13
- A.S. Fomichev, H.-G. Ortlepp, Yu.E. Penionshkevich, C.-M. Herbach, I. David, W. Wagner, G. Pausch, H. Sodan, V.A. Vitenko:**
 Basic features of the phoswich scintillation detectors of the 4π setup FOBOS;
 JINR Communications P15-92-15, Dubna 1992 (in Russian)
- S. Frauendorf, W. Lieberz, D. Lieberz, P. von Brentano and A. Gelberg:**
 Quenched proton-neutron coupling in $h_{11/2}$ high spin states of ^{128}Ba ;
 Physics Letters B274 (1992) 149
- A. Gobbi et al., R. Kotte, J. Mösner, W. Neubert, D. Wohlfarth:**
 One Year of Operating FOPI: Results and Status of the 4π -Detector Facility at SIS/ESR;
 GSI-Nachrichten 02-92
- A. Gobbi et al., R. Kotte, J. Mösner, W. Neubert, D. Wohlfarth:**
 A highly-segmented ΔE -time-of-flight wall as forward detector of the 4π -system for charged particles at the SIS/ESR accelerator;
 Nucl. Instr. Meth. A324 (1993) 156
- H.L. Harney, F.-M. Dittes and A. Müller:**
 Time evolution of chaotic quantum systems;
 Ann. Phys. 220 (1992) 159
- J. Hubele, P. Kreutz, V. Lindenstruth, J.C. Adloff, M. Begemann-Blaich, P. Bouissou, G. Imme, I. Iori, G.J. Kunde, S. Leray, Z. Liu, U. Lynen, R.J. Meijer, U. Milkau, A. Moroni, W.F.J. Müller, C. Ngõ, C.A. Ogilvie, J. Pochodzalla, G. Raciti, G. Rudolf, H. Sann, A. Schüttauf, W. Seidel, L. Stuttge, W. Trautmann, A. Tucholski, R. Heck, A.R. DeAngelis, D.H.E. Gross, H.R. Laqaman, H.W. Barz, H. Schulz, W.A. Friedman and R.J. Charity:**
 Statistical fragmentation of Au projectiles at $E/A = 600$ MeV;
 Phys. Rev. C46 (1992) R1577
- J. Hubele et al., W. Seidel**
 Statistical Fragmentation of Au Projectiles at $E/A = 600$ MeV;
 Book of Abstracts, 1992 International Nuclear Physics Conference, Wiesbaden, Germany, Jul. 26-Aug. 1, 1992, p. 3.4.22

J. Hubele et al., W. Seidel:
Statistical Fragmentation of Au Projectiles at $E/A = 600$ MeV;
Preprint GSI-92-17

G. Imme et al., W. Seidel:
High Energy Multifragmentation;
Italo-Japanese Colloquium, Catania, Italy, Oct. 1992;
L.N.S. Catania Report, Nov. 1992

W. Iskra, H. Müller and I. Rotter
Selforganization in the nuclear system
I: The slaving principle;
FZR Preprint 93-01

W. Iskra and I. Rotter:
Radial characteristics for nuclear states with weakly bound nucleons; in: "From Spectroscopic to Chaotic Features of Nuclear Systems", ed. by D. Seeliger;
World Scientific Singapore (1992), p. 64

W. Iskra, I. Rotter and F.-M. Dittes:
Hierarchical trapping of resonance states at high level density;
Report FZR-92-05

W. Iskra, I. Rotter and F.-M. Dittes:
Bifurcations in quantum systems;
Report FZR-92-06

L.L. Jenkovsky, B. Kämpfer and V.M. Sysoev:
Bubble free-energy in a first order phase transition;
Report ITP-92-51E

H.J. Jensen, G.B. Hagemann, P.O. Tjøm, S. Frauendorf, A. Atac, M. Bergström, A. Bracco, A. Brockstedt, H. Carlsson, P. Ekström, J.M. Espino, B. Herskind, F. Ingelbretsen, J. Jongman, S. Leoni, R.M. Lieder, T. Lönnroth, A. Maj, B. Million, A. Nordlund, J. Nyberg, M. Piiparinen, H. Ryde, M. Sugawara and A. Virtanen:
Interaction strength and shape difference of the $h_{9/2}$ and $h_{11/2}$ configurations in ^{163}Tm ;
Z. Phys. A340 (1991) 351

B. Kämpfer, et al.:
Intermediate mass fragment correlations in the reaction Au on Au at $E/A = 100, 150$ and 250 MeV;
Contrib., XX Int. Workshop on Gross Properties of Nuclei and Nuclear Excitations, Hirschegg, Austria, Jan. 1992, p. 67

B. Kämpfer, R. Kotte, J. Mösner, W. Neubert, D. Wohlfarth:
Small angle correlations of intermediate mass fragments in reactions Au + Au at $E/A = 100, 150, 250$ MeV;
Contrib., Int. Workshop on Gross Properties of Nuclei and Nuclear Excitations, Hirschegg, Austria, 1992, p. 67
Poster presentation, Int. Workshop on Dynamics and Correlations in Nuclear Collisions, Aussois, France, Mar. 1992
Poster presentation, 1992 International Nuclear Physics Conference, Wiesbaden, Germany, Jul. 26-Aug. 1, 1992

B. Kämpfer, R. Kotte, J. Mösner, W. Neubert, D. Wohlfarth:
Inclusive two-fragment velocity correlations in reactions Au + Au at $E/A = 100, 150, 250$ MeV;
Spring Meeting of the German Physical Society (Nuclear Physics), Salzburg, Austria, Feb. 24-28, 1992

B. Kämpfer, R. Kotte, J. Mösner, W. Neubert, D. Wohlfarth:
Correlations of intermediate mass fragments in reactions Au + Au at $E/A = 100, 150, 250$ MeV;
Book of Abstracts, 1992 International Nuclear Physics Conference, Wiesbaden, Germany, Jul. 26-Aug. 1, 1992, p. 3.4.21

B. Kämpfer, O.P. Pavlenko and B. Heide:
Di-Leptonen radiation from partially equilibrated parton matter;
Contrib., XX Int. Workshop on Gross Properties of Nuclei and Nuclear Excitations, Hirschegg, Austria, Jan. 1992, p. 245

B. Kämpfer and O. Pavlenko:
Kinetics of partons and pions in ultra-relativistic heavy-ion collisions probed by di-leptons;
Proc. NATO Advanced Study Institut on Particle Production (ed. H.H. Gutbrod) Plenum Press, 1993

B. Kämpfer and O. Pavlenko:
Kinetics of partons and pions in ultra-relativistic heavy-ion collisions probed by di-leptons;
Proc. Int. Workshop Budapest, Hungary (1992)

B. Kämpfer and O. Pavlenko:
Dilepton radiation from non-equilibrated parton matter produced in ultra-relativistic heavy-ion collisions;
Report FZR-92-03;
Phys. Lett. B289 (1992) 127

B. Kämpfer and H. Reinhardt:
The soliton of the effective chiral action in a heat-kernel expansion;
Report FZR-92-00;
Ann. Phys. 1 (1992) 106

B. Kämpfer, A.I. Titov and E.L. Bratkovskaya:

Estimates of dilepton production in pp and pd reactions at 1-2 GeV;

Report FZR-92-04

L.P. Kaptari, A. Yu. Umnikov and B. Kämpfer:

On the nuclear structure function F_2^A : Moments and kinematics beyond $x = 1$;

Report FZR-92-07

L.G. Kostova, W. Andrejtscheff, L.K. Kostov, L. Funke, E. Will and A.I. Vdovin:

The half-life of the 1437 keV $11/2^-$ state in ^{97}Mo ;

Z. Phys. A342 (1992) 145

P. Kreutz et al., W. Seidel:

Charge correlations as a probe of nuclear disassembly;

Preprint GSI-92-23

P. Kreutz et al., W. Seidel:

Z-bound-scaling of the charge distributions in multifragment decay;

1992 International Nuclear Physics Conference, Wiesbaden, Germany, Jul. 26-Aug. 1, 1992

U. Lynen et al., W. Seidel:

Correlations in Multi-Fragment Events;

Nucl. Phys. A545 (1992) 329c

Th. Meissner, G. Ripka, R. Wünsch, P. Sieber, F. Grümmer and K. Goetze:

Scale invariance and the stability of a hedgehog soliton;

Report RUP-TPII-30/92;

Phys. Lett. B299 (1993) 183

P. Michel, B. Miethig, K. Möller, B. Naumann, L. Naumann, W. Szczeniowski:

Hohllichtleiter zur Lichtübertragung in Szintillationsdetektoren;

Mikrowellen & HF Magazin 7 (1992) 170

H. Müller, M. Büscher and K. Sistemich:

Subthreshold production of K^+ mesons and the fragmentation of the target nucleus;

Z. Phys. A - Hadrons and Nuclei 344 (1992) 197

H.G. Ortlepp, K.D. Schilling (editors):

FOBOS-a 4π -Fragment Spectrometer for Heavy-Ion Reaction Products;

Report FZR-92-11

H.G. Ortlepp, M. Andrassy, G.G. Chubarian, L. Dietterle, A.S. Fomichev, P. Gippner, C.M. Herbach, A.I. Ivanenko, I.B. Kolesov, A. Matthies, D. May, Yu.Ts. Oganessian, Yu.E. Penionzhkevich, G. Renz, O.V. Strelakovski, V.V. Trofimov, V.M. Vasko, K. Heide, K.D. Schilling, W. Wagner, H. Sodan, W.D. Fromm, H. Fuchs, D. Hilscher, H. Homeyer, W. v. Oertzen, G. Pausch, P. Ziem:

4π -Fragment Spectrometer FOBOS;

Poster, 1992 International Nuclear Physics Conference, Wiesbaden, Germany, Jul. 26 - Aug. 1, 1992

A. Pfitzner and W. Cassing:

Unified description of nuclear damping and heavy-ion dynamics;

Proceedings 6th Int. Conf. on Nuclear Reaction Mechanisms, Varenna, Italy, 1991, p. 221

A. Pfitzner and W. Cassing:

Derivation of a nonperturbative spreading width for giant resonances;

Report UGI-90-12

J. Reif and R. Reif:

Classical phase-space structure of the single-particle motion in cranked potentials;

J. Phys. A25 (1992) L115

I. Rotter:

Formation of quantum chaos in the nuclear system;

Report FZR-92-02

I. Rotter:

Resonance phenomena at high level density and quantum chaos;

Revista Mexicana de Fisica 38, Supl. 2 (1992) 164

I. Rotter:

Formation of chaos in the nuclear system;

Book of Abstracts, 1992 International Nuclear Physics Conference, Wiesbaden, Germany, Jul. 26 - Aug. 1, 1992, p. 1.3.53

K. Sistemich, M. Büscher, V. Abaev, U. Bechstedt, P. Birien, W. Borgs, W. Cassing, S. Dienel, H. Dombrowski, S.V. Dshemuchadse, J. Ernst, R. Eßer, D. Gotta, D. Grzonka, A. Hardt, F. Hinterberger, M. Ivanov, L. Jarczyk, B. Kamys, St. Kistryn, H.R. Koch, V.I. Komarov, V. Koptev, A. Kozela, A. Krykin, K.W. Leege, H. Müller, W. Oelert, H. Ohm, R. Santo, Chr. Schneidereit, O.W.B. Schult, H. Seyfarth, V. Shelkov, J. Smyrski, A. Strzalkowski, K.-H. Watzlawik, B.Zh. Zalyhanov, N.I. Zhuravlev and P. Zolnierczuk:

Meson Studies at the 0° Facility in COSY;

Proc. Workshop on Strangeness in Nuclei, Cracow, Poland, May 5-8, 1992

W. Trautmann et al., W. Seidel:

The Rise and Fall of Multifragment Production in $^{197}\text{Au} + \text{C, Al and Cu}$ Reactions at $E/A = 600$ MeV;

Nucl. Phys. A538 (1992) 473c

G. Winter, L. Funke, R. Schwengner, H. Prade, R. Wirowski, N. Nicolay, A. Dewald, P. von Brentano:

A new sequence of high-spin states built on the $17/2^+$ isomer in ^{85}Kr ;

Z. Phys. A344 (1992) 229-230

G. Winter, L. Funke, R. Schwengner, H. Prade, R. Wirowski, N. Nicolay, A. Dewald, P. von Brentano:

High-spin states in the $N=50$ nucleus ^{86}Kr ;

Z. Phys. A343 (1992) 369-370

R. Wünsch:

Unified description of quasi-free and resonant processes of hypernuclear production and decay;

Report FZR-92-03,

Czech. J. Phys. 42 (1992) 1061

2. Lectures and Seminars

H.W. Barz:

Expansion eines relativistischen Pionen-Gases;
Seminar, TU Dresden, Jan. 1992

H.W. Barz:

Collisions in an expanding pion gas and the p_{\perp} spectrum in ultrarelativistic heavy ion collisions;
XX Int. Workshop on Gross Properties of Nuclei and Nuclear Excitations, Hirschegg, Austria, Jan. 1992

H.W. Barz:

Statistisches Modell der Multifragmentation;
Expertentreffen für Kernphysik, Schleching, Germany, Mar. 1992

H.W. Barz:

Flow and cluster production;
FOPI workshop, Bensheim, May 1992

H.W. Barz:

WS 1992/93: Moderne Entwicklungen der Kern- und Clusterphysik;
(TU Dresden, Germany)

H.W. Barz:

Low p_{\perp} enhancement in ultrarelativistic heavy-ion collisions;
Int. Workshop on Ultrarelativistic Heavy Ion Collisions, Budapest, Hungary, Aug. 1992

H.W. Barz:

Flow and cluster production;
Seminar, NBI Copenhagen, Denmark, Dec. 1992

F.M. Dittes:

Spectral properties of open quantum systems;
Seminar, The Weizmann Institute of Science, Rehovot, Israel, Jan. 28, 1992

F.M. Dittes:

Semiklassische Methoden;
Invited Lecture, Ferienkurs "Selbstorganisation und Quantenchaos", Dresden, Germany, Sep. 21 - Oct. 2, 1992

F.M. Dittes:

Breakdown of the semiclassical approximation for the spectral form factor of the Baker map;
Seminar, The Weizmann Institute of Science, Rehovot, Israel, Nov. 25, 1992

F. Dönau:

WS 1992/93: Struktur des Atomkerns;
(Uni zu Köln, Germany)

W. Enghardt:

Positronen Emissions Tomographie am Strahl leichter Ionen;
Seminar, Institut für Kern- und Hadronenphysik des FZ Rossendorf, Germany, Jun. 15,
1992

W. Enghardt:

Positron emission tomography for dose localization and beam monitoring in light ion tumour
therapy;
Int. Conf. on Biological Applications of Relativistic Nuclei, Clermont-Ferrand, Oct. 14-16,
1992

S. Frauendorf:

Tilted cranking classification of multiband spectra;
International Conference on Nuclear Structure at High Angular Momentum, Ottawa,
Canada, May 1992

S. Frauendorf:

Tilted cranking;
21st International Symposium Rapidly Rotating Nuclei 1992, Tokyo, Japan, Oct. 26-30,
1992

S. Frauendorf:

Deformation-induced splitting of the plasmon resonance;
ICW-92 on Excitations in Alkali, Michigan State University, East Lansing, USA, Jul. 29-31,
1992

S. Frauendorf:

Cluster binding energies calculated with the Strutinsky method;
Clusterworkshop, NBI Copenhagen, Denmark, Jan. 5 1993

S. Frauendorf:

Tilted cranking;
Spring Meeting of the German Physical Society (Nuclear Physics Sections), Salzburg,
Austria, Feb. 24-28, 1992

S. Frauendorf, V.V. Pashkevich:

Non-spherical shapes of sodium clusters;
Experimental Group Meeting, NBI Copenhagen, Denmark, May 30, 1992

S. Frauendorf:

Shapes and binding energies of Na clusters;
Seminar, T-Division, LANL, Los Alamos, USA, Jul. 28, 1992

S. Frauendorf:

Shapes of sodium clusters;
Physics Division Seminar, ORNL, Oak Ridge, USA, Aug. 10, 1992

S. Frauendorf:

Nuclei and alkali clusters;
Nuclear Science Division Seminar, LBL, Berkeley, USA, Sep. 14, 1992

S. Frauendorf:

Shapes of Na clusters;

Nuclear Physics Seminar, Yukawa Institute Kyoto, Japan, Oct. 20, 1992

S. Frauendorf:

Orientation of the angular momentum at high spin;

Seminar, Institut für Kern- und Hadronenphysik des FZ Rossendorf, Germany, Jan. 18, 1993

S. Frauendorf:

$\Delta I = 1$ bands in the light Pb nuclei;

Seminar, Institut of Nuclear and Radiation Physics, University Bonn, Germany, Feb. 18, 1993

S. Frauendorf:

Strutinsky calculations of the shapes and binding energies of alkali clusters;

Seminar, Institute for Theoretical Physics, University Regensburg, Germany, Feb. 16, 1993

S. Frauendorf:

Tilted cranking;

3 Lectures, LBL, Berkeley, USA, Jul. 1992

S. Frauendorf:

Physics of the Metalclusters;

Invited Lecture Ferienkurs "Selbstorganisation und Quantenchaos", Dresden, Germany, Sep. 21 - Oct. 2, 1992

B. Heide:

Velocity correlations between intermediate mass fragments;

Theorie Treffen SIS, Rauschholzhausen, Jun. 1992

B. Heide:

Beschreibung von Fragmentationsprozessen in mittlereenergetischen Schwerionenstößen im Rahmen des BUU- und des Kopenhagener Modells;

Seminar, Institut für Kern- und Hadronenphysik des FZ Rossendorf, Germany, Nov. 16, 1992

C.-M. Herbach:

First physical results of measurements using FOBOS-gas modules;

HMI Berlin, Jun. 2, 1992

B. Kämpfer:

Intermediate mass fragment correlations;

XX Int. Workshop on Gross Properties of Nuclei and Nuclear Excitations, Hirschegg, Austria, Jan. 1992

B. Kämpfer:

Dilepton radiation from non-equilibrated parton matter;

NATO Advanced Study Institute on Particle Production, II Chiocco, Italy, Jul. 1992

B. Kämpfer:

Di-lepton radiation from parton matter;

Int. Workshop on Ultrarelativistic Heavy Ion Collisions, Budapest, Hungary, Aug. 1992

B. Kämpfer:

Velocity correlation of IMF's;

Seminar, NBI Copenhagen, Denmark, Dec. 1992

B. Kämpfer:

IMF production in central Au + Au collisions;

Seminar, Institut für Theoretische Physik der Universität Heidelberg, Nov. 1992

B. Kämpfer:

WS 1991/92: Einführung in die Astrophysik

WS 1992/93: Allgemeine Relativitätstheorie

(TU Dresden, Germany)

L. Käubler:

The odd-mass valence mirror nuclei $^{113}_{50}\text{Sn}_{63}$ and $^{145}_{63}\text{Eu}_{82}$;

Spring Meeting of the German Physical Society (Nuclear Physics Sections), Salzburg, Austria, Feb. 24-28, 1992

P. Michel:

Test des COSY-TOF-Startdetektors am CERN;

TOF-Meeting, FZ Jülich, Oct. 7-8, 1992

K. Möller:

Künftige Mittelenergiephysik: Das TOF-Spektrometer am COSY Jülich;

Institut für Kern- und Atomphysik, TU Dresden, 30.4.1992

H. Müller:

Subthreshold Production of K^- Mesons;

Sitzung des COSY Program Advisory Committee in Jülich, Feb. 18.-19, 1992

H. Müller:

Correlation between K^+ Mesons and Fragment at Subthreshold Energies;

Workshop on Strangeness in Nuclei, Cracow, Poland, May 1992

H. Müller:

Results of Modified Phase-Space Model calculations;

Collaboration Meeting 0° Facility, Jülich, Nov. 24-25, 1992

M. Müller:

Selbstorganisierende Mechanismen in einem Vielteilchensystem.

I: Modellbeschreibung

II: Numerische Ergebnisse;

Seminar talks, Ferienkurs "Selbstorganisation und Quantenchaos", Dresden, Germany, Sep. 21 - Oct. 2, 1992

B. Naumann:

Programmentwicklungen zur Simulation der Proton-Proton-Bremsstrahlung am COSY-Flugzeitspektrometer;
COSY-FFE-Arbeitstreffen, FZ Jülich, Oct. 27-28, 1992

L. Naumann:

Die Mechanik des Startdetektors für die Bremsstrahlungsmessung;
TOF-Meeting, FZ Jülich, Mar. 17, 1992

L. Naumann:

Technische Anforderungen an das Flugzeitspektrometer am Kühlersynchrotron in der KFA Jülich;
Seminar, Zentralabteilung Forschungs- und Informationstechnik des FZ Rossendorf, Jun. 30, 1992

L. Naumann:

Der Status des Vakuumsystems des Startdetektors unter dem Gesichtspunkt des separaten Einsatzes ohne TOF-Tank;
TOF-Meeting, FZ Jülich, Nov. 12, 1992

W. Neubert:

Fissilities of Nuclei in the Range of Ni to U;
Systematics of Energy and Momentum Transfer in Heavy Ion Collisions;
Fission Processes in Proton-Nucleus Collisions at $E=1$ GeV;
Level Density Parameters from Excitation Functions of (HI, xn);
Seminar, University of Messina, Italy, Jun. 1992

H.-G. Ortlepp:

4π -Detector FOBOS for Experiments on Heavy Ion Beams;
Int. Workshop on Physical Experiments and First Results on Heavy Ion Storage and Cooler Rings, Smolenice, June 1-5, 1992

H.-G. Ortlepp:

The 4π Spectrometer FOBOS at Dubna;
30th Spring Meeting on Nuclear Physics, Holzgau, April 6-10, 1992

J. Pawelke:

In-beam PET imaging of implanted positron emitting ions;
Spring Meeting of the German Physical Society (Nuclear Physics Sections), Salzburg, Austria, Feb. 24-28, 1992

J. Pawelke:

PET zur in-vivo Dosislokalisierung in der Leichterionen-Tumorthherapie;
Seminar, Institut für Kern- und Hadronenphysik des FZ Rossendorf, Germany, Nov. 16, 1992

A. Pfitzner:

Correlation dynamics in nuclear matter and Landau's kinetic equation;
Lectures, TU München, Germany, Mar. 8-21, 1992

I. Rotter:

Resonance phenomena at high level density and quantum chaos;
Invited Talk, XV Nuclear Physics Symposium, Oaxtepec, Mexico, Jan. 7-10, 1992

I. Rotter:

Fluctuations of the reaction cross section and quantum chaos;
Seminar, Instituto de Fisica, UNAM, University of Mexico, Mexico-City, Jan. 17, 1992

I. Rotter:

Nuclear structure investigations at low and high level density;
Spring Meeting of the German Physical Society (Nuclear Physics Sections), Salzburg, Austria, Feb. 24-28, 1992

I. Rotter:

Quantenchaos in der Streuung;
Seminar, LMU und TU München, May 26, 1992

I. Rotter:

Resonance phenomena at high level density;
Second International Symposium on Nuclear Excited States, Lodz, Poland, Jun. 22-26, 1992

I. Rotter:

Selbstorganisation und Chaos in einem quantenmechanischen Vielteilchensystem;
Seminar, Institut für Theoretische Physik I der Universität Münster, Jun. 29., 1992

I. Rotter:

Selbstorganisation und Chaos in Atomkernen;
Invited Lecture, Ferienkurs "Selbstorganisation und Quantenchaos", Dresden, Germany, Sep. 21 - Oct. 2, 1992

I. Rotter:

Synergetik und Kernphysik;
"Chaos und Strukturbildung '92", München, Nov. 7, 1992

I. Rotter:

Nonlinear phenomena in nuclei;
"Resonant States", Workshop, GANIL, Caen, France, Nov. 19-20, 1992

I. Rotter:

Formation of quantum chaos in nuclei;
Seminar, Institut für Kernphysik des FZ Jülich, Nov. 24, 1992

R. Schwengner:

In-beam study of ^{83}Br ;
Spring Meeting of the German Physical Society (Nuclear Physics Sections), Salzburg, Austria, Feb. 24-28, 1992

R. Schwengner:

Channel selection with Si detectors;
EUROBALL Meeting on Auxiliary Detectors and Selective Devices, Berlin, Jun. 1992

W. Seidel:

Untersuchung der Multifragmentation von Atomkernen am ALADIN-Spektrometer der GSI Darmstadt;
Seminar, Institut für Kern- und Hadronenphysik des FZ Rossendorf, Germany, Mar. 2, 1992

W. Seidel:

Improvement of the MUSIC;
ALADIN-Workshop Darmstadt, Germany, May 20, 1992

W. Seidel:

Multifragmentation bei SIS-Energien;
Seminar, TU Dresden, Germany, Dec. 10, 1992

W. Wagner:

Szintillatorschale des FOBOS-Arrays;
Seminar, HMI Berlin, Germany, Jan. 20, 1992

R. Wünsch:

Peculiarities of the Nambu and Jona-Lasinio model;
Seminar, Ruhr-Universität, Bochum, Germany, Jul. 1992

R. Wünsch:

Nucleons in the Nambu & Jona-Lasinio model;
Seminar, FZ Jülich, Germany, Sep. 1992

3. Talks of Visitors

J. Speth, Jülich:

Struktur der Elementarteilchen;

Feb. 7, 1992

A. Rudchik, Kiev:

Many nucleon transfer reactions on light nuclei and cluster spectroscopy;

Mar. 9, 1992

O. Schult, Jülich:

Circulating beams - a powerful tool for medium energy physics studies;

Mar. 23, 1992

C. Toepffer, Erlangen:

Dynamik von Mehrteilchenkorrelationen in angeregten Atomkernen;

Apr. 13, 1992

H. Lenske, München:

Kovariante Reaktionstheorie für relativistische Kernreaktionen;

Apr. 27, 1992

K. Goeke, Bochum:

Hadronenmodelle im Rahmen der niederenergetischen QCD;

May. 4, 1992

D. Einfeld, Dresden:

ROSY und die Kernphysik;

May. 18, 1992

U. Schmidt-Rohr, Heidelberg:

Masse und Helizität der Neutrinos aus dem β -Zerfall;

Jun. 4, 1992

V. Herrmann, Jülich:

Off-shell Effekte in der Proton-Proton-Bremsstrahlung;

Jun. 22, 1992

O.P. Pavlenko, Kiev:

Dilepton production in ultrarelativistic heavy ion collisions;

Jun. 29, 1992

I. Ragnarsson, Lund:

Assignment of Nilsson orbitals at superdeformation - identical bands;

Jul. 6, 1992

H. Schanz, Dresden:
Quantenchaos im Modell nicht-überlappender Streuer;
Jul. 13, 1992

A. Mondragon, Mexico:
Degeneracy and crossing of resonance energy surfaces;
Aug. 5, 1992

R. Esser, Jülich:
Szintillationsdetektoren für die 0°-Facility an COSY;
Aug. 17, 1992

G. Pausch, Berlin:
Teilchenidentifikation in Halbleiterdetektoren durch Impulsformanalyse:
Experimentelle Ergebnisse und Ansätze zur quantitativen Beschreibung;
Aug. 24, 1992

A.I. Titov, Dubna:
Vector meson production within the Nambu-Jona-Lasinio model;
Sep. 7, 1992

H.L. Harney, Heidelberg:
Statistische Spektroskopie;
Sep. 14, 1992

F.M. Dittes, Rehovot:
Bericht über Arbeitsaufenthalt am Weizmann-Institut Rehovot;
Oct. 5, 1992

T. v. Egidy, München:
Antiprotonen-Annihilation an Atomkernen;
Oct. 12, 1992

U. Kaup, Köln:
Wechselwirkende Bosonen in Atomkernen;
Oct. 9, 1992

B. Lukacs, Budapest:
Anisotropic continuum models for high-energy heavy-ion collisions;
Oct. 16, 1992

D.H.E. Gross, Berlin:
Multifragmentation von Atomkernen;
Oct. 19, 1992

S. Krewald, Jülich:

Ein neuer Zugang zum Confinement-Problem;

Oct. 22, 1992

I. Kawrakow, Leipzig:

Partonenmodell zur Beschreibung hochenergetischer Kern-Kern-Stöße;

Oct. 26, 1992

Ch. Ender, Heidelberg:

Konzeptionelle Vorstellungen zur EUROBALL-Elektronik;

Nov. 6, 1992

G. Wolf, Darmstadt:

Dileptonen- und Mesonenerzeugung in Schwerionenstößen;

Nov. 9, 1992

H. Grawe, Berlin:

Struktur exotischer Kerne nahe ^{100}Sn ;

Nov. 23, 1992

G.G. Bunatian, Dubna:

Zur Nukleonenstruktur im Vakuum und in Kernmaterie;

Nov. 30, 1992

L.P. Csernai, Bergen:

Reaktionsdynamik und Hadronisation vom Quark-Gluon-Plasma in Schwerionenstößen;

Dec. 7, 1992

A. Peter, Gießen:

Einfluß der Wechselwirkung auf Nukleonenkorrelationen im Atomkern;

Dec. 10, 1992

M. Schleich, Dresden:

Baryonen im NJL-Modell;

Dec. 14, 1992

L. Kaptari, Dubna:

Nuclear effects on the quark distribution of nucleons - deep-inelastic scattering processes;

Dec. 18, 1992

IV. Personnel

Scientific Staff

M. Andrassy
Dr. H.W. Barz ¹⁾
L. Dietterle ^{2,4)}
Dr. F. Dönau
Dr. S. Dshemuchadse
Dr. W. Enghardt ¹⁾
Dr. S. Frauendorf
Dr. P. Gippner ⁴⁾
Dr. C.M. Herbach ^{2,4)}
Dr. D. Janssen ¹⁾
Dr. B. Kämpfer ¹⁾
Dr. L. Käubler ¹⁾
Dr. P. Kleinwächter
Dr. R. Kotte
Dr. P. Manfraß
Dr. A. Matthies ^{2,4)}
D. May ^{2,4)}
Dr. P. Michel
Dr. K. Möller ¹⁾
Dr. J. Mösner
Dr. H. Müller
Dr. B. Naumann ²⁾
Dr. L. Naumann
Dr. W. Neubert
Dr. H.G. Ortlepp ⁴⁾
Dr. A. Pfitzner
Dr. H. Prade
Dr. J. Reif
G. Renz ^{2,4)}
Dr. H. Richter ³⁾
Dr. H. Rotter ³⁾
Prof. I. Rotter ¹⁾
A. Schamlott ²⁾
Dr. K.D. Schilling
Dr. M. Schlett
Dr. R. Schwengner
Dr. W. Seidel
Dr. W. Wagner ⁴⁾
Dr. G. Winter
D. Wohlfarth
Dr. R. Wünsch

Technical Staff

M. Altus
H. Angermann
U. Baumann
J.U. Berlin
M. Boeck
M. Böse
J. Fiedler
R. Förster
M. Freitag
L. Göbel
K. Heidel
K.H. Hermann
J. Hutsch
J. Kerber
E. Kluge
M. Koslowsky
M. Langer
B. Prietzschk
I. Probst
B. Rimarzig
H. Römer
M. Scheinpflug
C. Schneiderei
W. Schulze
M. Sobiella
A. Uhlmann
C. Umlauf ⁴⁾

Postgraduate Students

J. Biegansky
B.G. Hasch
B. Heide
J. Krüger
T. Möhlenkamp
M. Müller
J. Pawelke
C. Schneider
A. Schülke

¹⁾ Finanzierung durch die KAI(WIP)

²⁾ Drittmittelstelle

³⁾ Finanzierung über ABM

⁴⁾ z.Z. VIK Dubna